



NTNU – Trondheim
Norwegian University of
Science and Technology

Adsorptive Hydrogen Storage: Experimental investigations on thermal conductivity in porous media

Jan Georg Henriksen

Master of Energy and Environmental Engineering

Submission date: June 2013

Supervisor: Erling Næss, EPT

Co-supervisor: Christian Schlemminger, EPT

Norwegian University of Science and Technology
Department of Energy and Process Engineering

MASTER THESIS

for

Stud.techn. Jan Georg Henriksen

Spring 2013

Thermal conductivity measurements of porous materials

*Termisk konduktiviteten for porøse materialer***Background and objective**

Hydrogen is a candidate as energy carrier for the future. The present project work efforts are focused on hydrogen storage material properties for on-board hydrogen storage technologies.

The most promising hydrogen storage methods are gas compression, liquefaction, chemical storage via metal hydrides and gas adsorption via physisorption (adsorption). Adsorption type storage systems are inexpensive alternatives that also have the potential to reach the energy density goals for on-board storage systems. Sorption type materials, like e.g. metal organic frameworks (MOFs) have been identified as a viable option. These are characterized by high porosity and high specific surface area.

However, the transient processes during charging and discharging of a storage system play an important role in the utilization of the hydrogen adsorption storage systems. Thermo-physical material properties such as thermal conductivity are crucial for determining the heat and mass transfer within the storage unit.

The main objective of this work is to install and verify a new characterization setup for thermal conductivity and specific heat capacity measurements. Furthermore, experimental investigation of porous materials provided by NTNU with an additional comparison with available literature data and prediction models.

The following tasks are to be considered:

1. A literature study on thermal conductivity of gas/solid porous media shall be performed, with emphasis on the transport mechanisms and predictive models. Also, the basic processes governing the thermal conductivity of the involved media (gases and solids) shall be presented.
2. Perform experiments to determine thermal conductivity of selected porous materials using the HotDisk transient measurement setup. The following tasks are involved:
 - a. The setup shall be described, and a set of calibration/verification measurements shall be performed.
 - b. A set of thermal conductivity measurements on selected hydrogen adsorption materials shall be performed, covering a range of temperatures and using different gases. If possible, thermal conductivity measurements shall also be performed using enhancement devices such as aluminum foam or wires.

c. An uncertainty analysis shall be performed.

The measurements shall also be compared to predictions from the literature models/correlations described in part 1. The results shall be analyzed, presented and discussed.

3. A model for heat distribution in a powdery material having aluminum foam or wires as enhancement device shall be developed. The model shall be presented and discussed. Predictions shall be compared to relevant measurements performed in section 2.
4. Suggestions for further work shall be proposed.

- " -

Within 14 days of receiving the written text on the master thesis, the candidate shall submit a research plan for his project to the department.

When the thesis is evaluated, emphasis is put on processing of the results, and that they are presented in tabular and/or graphic form in a clear manner, and that they are analyzed carefully.

The thesis should be formulated as a research report with summary both in English and Norwegian, conclusion, literature references, table of contents etc. During the preparation of the text, the candidate should make an effort to produce a well-structured and easily readable report. In order to ease the evaluation of the thesis, it is important that the cross-references are correct. In the making of the report, strong emphasis should be placed on both a thorough discussion of the results and an orderly presentation.

The candidate is requested to initiate and keep close contact with his/her academic supervisor(s) throughout the working period. The candidate must follow the rules and regulations of NTNU as well as passive directions given by the Department of Energy and Process Engineering.

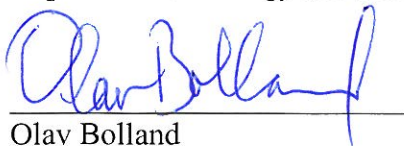
Risk assessment of the candidate's work shall be carried out according to the department's procedures. The risk assessment must be documented and included as part of the final report. Events related to the candidate's work adversely affecting the health, safety or security, must be documented and included as part of the final report. If the documentation on risk assessment represents a large number of pages, the full version is to be submitted electronically to the supervisor and an excerpt is included in the report.

Pursuant to "Regulations concerning the supplementary provisions to the technology study program/Master of Science" at NTNU §20, the Department reserves the permission to utilize all the results and data for teaching and research purposes as well as in future publications.

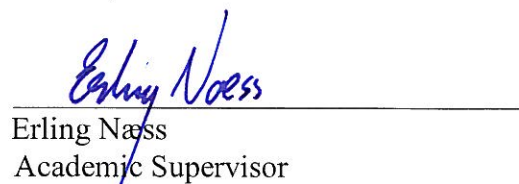
The final report is to be submitted digitally in DAIM. An executive summary of the thesis including title, student's name, supervisor's name, year, department name, and NTNU's logo and name, shall be submitted to the department as a separate pdf file. Based on an agreement with the supervisor, the final report and other material and documents may be given to the supervisor in digital format.

- Work to be done in lab (Water power lab, Fluids engineering lab, Thermal engineering lab)
 Field work

Department of Energy and Process Engineering, 14. January 2013



Olav Bolland
Department Head



Erling Næss
Academic Supervisor

Research Advisors: PhD student Christian Schlemminger, NTNU

Preface

This work is the result of my master thesis at The Norwegian University of Science and Technology (NTNU), department of Energy and Process Engineering, located in Trondheim, Norway. This study allowed me to take part in an interesting research project on advanced hydrogen adsorption materials for hydrogen storage. The thesis revolves around the issues regarding the crucial filling and discharging process of a storage tank, determining the heat transport capabilities of the adsorption materials through lab experimentations.

During my work with this project I have learned a lot about research and working in a lab environment. The installation of the brand new Hot Disk TPS experimental setup took quite a long time, and due to equipment failure and delayed equipment deliveries the preliminary tests continued through Easter. However, playing around with the setup was also a lot of fun and provided me with useful insights that helped me at the later stages of the project. Also, my Co-supervisor, Christian Schlemminger, was always around ready to lend a helping hand, making sure that we were able to perform the necessary experiments.

Even though the laboratory tasks required a great amount of time and work, I feel that I have done good and precise work, and I am pleased with the final result. I found the work both challenging and exciting, and I am very happy to have been allowed to participate in this project.

I would like to thank my supervisor Erling Næss for guiding me on how to progress my work and providing very helpful insights at the end of the thesis. I also wish to express a special thanks to Christian Schlemminger for his cheerful nature and supportive behavior. He has inspired me into moving forward with my work, always giving me good advice and coming up with creative solutions.

My fellow students and friends outside university, and especially my girlfriend Astrid also need to be thanked; for making my days generally good, and for motivating and inspiring me after long working hours.

Trondheim, June 17th, 2013



Jan Georg Henriksen

Thesis title: **Adsorptive Hydrogen Storage: Experimental investigations on thermal conductivity in porous media.**

Name: Jan Georg Henriksen

Date: 2013/06

Supervisor: Erling Næss and Ulrich Bünger

Co-supervisor: Christian Schlemminger

Abstract:

The objective of this work was to install and verify the Hot Disk TPS measurement setup for thermal conductivity measurements, and to carry out experiments on various porous materials. A literature survey on gas/solid porous media, with emphasis on the transport mechanisms and predictive models, was conducted. Special interest was taken in the widely-used Zehner/Bauer/Schlünder (ZBS) model for effective stagnant thermal conductivity of packed beds. Great care was shown in the determination of bed-properties such as porosity, because of the large effect it has on the effective thermal conductivity.

The porous materials investigated were the Metal Organic Framework (MOF) hydrogen adsorbents Cu-btc (HKUST-1) and Fe-btc-xerogel. Large ($\varnothing 1.395\text{mm}$) and smaller ($\varnothing 0.38\text{mm}$) glass beads served as a reference material for preliminary tests and setup validations. In a later stage the Cu-btc and Fe-btc was experimentally investigated. Thermal conductivity measurements were conducted on a packed bed with air, nitrogen (N_2) or helium (He) as fluid, in temperatures ranging from $243\text{K} < T < 423\text{K}$ at an absolute pressure of zero to 0.5 bar.

The smaller glass beads ($\varnothing 0.38\text{mm}$) were also tested together with an open-cell, high-porosity aluminum foam. The purpose of the metal foam in adsorption hydrogen storage is to increase the effective thermal conductivity of the bed. Experiments showed that applying the aluminum foam increased the magnitude of the effective thermal conductivity of a bed consisting of glass beads and air by a factor of 17 from $0.22 \text{ W/m}\times\text{K}$ to $3.7 \text{ W/m}\times\text{K}$ at room temperature.

The preliminary experiments revealed a calibration error in the Hot Disk software, creating a discontinuity in the effective thermal conductivity in the range of $273\text{K} < T < 283\text{K}$. Outside that range, the Hot Disk measurement setup provides accurate measurements of the effective thermal conductivity of porous materials.

Hot Disk gives a measurement uncertainty of 5%. In addition to this comes the uncertainty of the theoretical model, due to the input of measured parameters such as porosity. An uncertainty analysis on the ZBS model gave an uncertainty of approximately $\pm 10\%$ for the glass beads and $\pm 5\%$ for the MOF, respectively. Adding the uncertainty of the ZBS model to the uncertainty of the experiments gives a total uncertainty of 15% for the glass beads experiments and 10% for the MOF.

Through a least square procedure, the solid conductivity of the MOF materials were fitted to the values of the ZBS model, determining temperature dependent functions for the solid conductivity yielding for each of the MOF's. The ZBS model proved to be a reliable estimate for the effective thermal conductivity in a packed bed, differing from the measurements with less than 10%.

Opgavetittel: Adsorptiv Hydrogenlagring: Måling av termisk konduktivitet i porøse medier

Navn: Jan Georg Henriksen

Dato: 06/2013

Veileder: Erling Næss og Ulrich Bünger

Med-veileder: Christian Schlemminger

Sammendrag:

Målet med dette arbeidet var å installere og verifisere et Hot Disk TPS måleoppsett for målinger av termisk varmeledningsevne i porøse medier, og å utføre eksperimenter på ulike porøse materialer. En litteraturstudie om gassfase/faste stoff- porøse medier, med vekt på transportmekanismer og prediktive modeller, ble gjennomført. Den mye brukte Zehner/Bauer/Schlünder (ZBS)-modellen for effektiv termisk konduktivitet i porøse medier ble tillagt spesiell vekt. Stor forsiktighet ble vist ved bestemmelsen av porøsitet, på grunn av den store effekten den har på varmeledningsevnen.

De porøse materialene som ble undersøkt var Metal Organic Framework (MOF) hydrogen adsorpsjonsmidlene Cu-btc (HKUST-1) og Fe-btc-xerogel. Store ($\varnothing 1.395\text{mm}$) og mindre ($\varnothing 0.38\text{mm}$) glassperler fungerte som referansemateriale for foreløpige tester og validering av måleoppsettet. På et senere stadium ble Cu-btc og Fe-btc eksperimentelt undersøkt. Målinger av termisk konduktivitet ble utført med luft, nitrogen (N_2) eller helium (He) som fluid, ved temperaturer på $243\text{K} < T < 423\text{K}$ og med et absolutt trykk på null til 0,5 bar.

De mindre glasskulene ($\varnothing 0.38\text{mm}$) ble også testet sammen med et høyporøst aluminiumskum. Formålet med metallskum i adsorptiv hydrogenlagring er å øke den effektive termiske ledningsevnen i tanken. Eksperimenter har vist at innføring av et aluminiumskum økte størrelsen av den effektive termiske ledningsevnen i en tank fylt med glassperler og luft med en faktor på 17 fra $0,22\text{ W/m}\times\text{K}$ til $3.7\text{ W/m}\times\text{K}$ ved romtemperatur.

De første eksperimentene avslørte en kalibreringsfeil i Hot disk-programvaren som skaper en diskontinuitet i den effektive termiske ledningsevnen i området fra $273\text{K} < T < 283\text{K}$. Utenfor dette området gir den Hot Disk-måleoppsettet nøyaktige målinger av den effektive termiske ledningsevne til porøse materialer.

Hot Disk angir usikkerheten i hvert datapunkt til å være 5 %. I tillegg til dette kommer usikkerheten til den teoretiske modellen, på grunn av innføring av målte parametere slik som porøsitet. En usikkerhetsanalyse på ZBS-modellen ga en usikkerhet på omlag + -10 % for glassperler og + -5 % for MOF. Ved å summere usikkerheten i ZBS-modellen til usikkerheten gitt av forsøkene gir dette en total usikkerhet på henholdsvis 15 % for glassperler og 10 % for MOF.

Gjennom en minste-kvadrats-metode ble varmeledningsevnen til adsorbentene Cu-btc og Fe-btc bestemt. Temperaturavhengige funksjoner for begge MOF-materialene ble funnet ved sammenligning med ZBS-modellen. Denne modellen viste seg å gi gode estimater for den effektive varmeledningsevnen i porøse medier med mindre en 10 % relativt måleavvik.

Contents

Introduction	1
Part 1 - Heat transfer in porous media	3
1.1 The porous medium	3
1.1.2 Porosity	4
1.2 Heat transfer mechanisms	4
1.2.2 Conduction	5
1.2.3 Stefan Boltzmann law of radiation	8
1.3 Macroscopic transient heat conduction equations	10
1.4 Effective stagnant thermal conductivity of granular porous materials	12
1.4.1 Limiting relations	13
1.4.2 Types of models	14
1.5 Models based on the solution of the Laplace conduction equation (Type I)	15
1.6 Thermal resistance models (Type II)	16
1.7 Unit cell models (Type III)	16
1.7.1 Model of Kunii and Smith (1960)	16
1.7.2 Model of Zehner, Bauer and Schlünder (1970-1978)	21
1.7.3 Model proposed by IAEA-TECDOC-1163 (2000)	27
1.8 Effective stagnant thermal conductivity of solid matrix porous media	30
1.8.1 Hsu's phase-symmetry model (1994)	30
1.8.2 Boomsma and Poulikakos's metal foam model (2000)	31
Part 2 - Experiments	37
2.1 Transient Plane Source method (TPS)	37
2.2 Instrumentation	39
2.3 Investigated materials and their relevant properties	43
2.3.2 Density	43
2.3.3 Porosity	44
2.3.4 Particle diameter	44
2.4 Data reduction	45
2.5 Uncertainty analysis	48
Part 3 - Results and analysis	51
3.1 Reference material	51
3.2 MOF results	55
3.3 Foam effect	60

<u>Part 4 - Modified phase-symmetry model for aluminum foam</u>	<u>63</u>
4.1 Model development	63
4.2 Comparison with experimental results	66
<u>Part 5 - Conclusions</u>	<u>71</u>
5.1 Conclusion	71
5.2 Further work	73
References	75

Figures

Fig. I-1 - Map of storage capacities of different hydrogen storage options	1
Fig. 1.1 - Examples of natural porous materials	3
Fig. 1.2 - Porosity visualized	4
Fig. 1.3 - Heat transfer mechanisms in porous media.	5
Fig. 1.4 - Thermal conductivity as a function of temperature for some fluid substances	6
Fig. 1.5 - Thermal conductivity as a function of temperature for some solid substances	6
Fig. 1.6 - Thermal conductivity k_s of Aluminum Alloy-1100	7
Fig. 1.7 - Solid thermal conductivity k_s of glass	7
Fig. 1.8 - Conductivity of Air and N_2 as a function of temperature	8
Fig. 1.9 - Conductivity of He and H_2 as a function of temperature	8
Fig. 1.10 - Incident radiation on a surface.	8
Fig. 1.11 - Black body exitance at various temperatures and wavelengths	9
Fig. 1.12 - Types of models used to predict the thermal conductivity of packed beds.	14
Fig. 1.13 - Kunii and Smith's heat transfer model for a packed bed of spherical particles.	17
Fig. 1.14 - Model for heat transfer near particle contact points	17
Fig. 1.15 - Heat transfer directions for loose packing of spheres	19
Fig. 1.16 - Heat transfer directions for close packing of spheres	19
Fig. 1.17 - The unit cell from the ZBS model	21
Fig. 1.18 - The three different packing arrangements applied for the derivation of the model.	28
Fig. 1.19 - Comparison of models for a random loose packing of spherically shaped particles.	29
Fig. 1.20 - Unit cell for the phase-symmetric model	30
Fig. 1.21 - Visualization of the foam structure. To the right: the unit cell between points 1-4	32
Fig. 1.22 - The metal foam modeled in a Cartesian coordinate system	33
Fig. 1.23 - Picture of metal foam	33
Fig. 1.24 - Comparison between solid matrix models and the ZBS model	36
Fig. 2.1 - Sensor position between sample pieces	37
Fig. 2.2 - Sample holders	39
Fig. 2.3 - Vacuum cell	39
Fig. 2.4 - P&ID flow chart of the thermal conductivity experimental setup.	40
Fig. 2.5 - The Hot-Disk experimental setup.	41
Fig. 2.6 - From top left to bottom right: Cu-btc pellets, Fe-btc, aluminum foam, glass beads.	43
Fig. 2.7 - Relative undersize - small glass beads	44
Fig. 2.8 - Cumulative undersize - small glass beads	44
Fig. 2.9 - Solid conductivity of aluminium alloy 1100.	47
Fig. 2.10 - Solid conductivity of glass beads as a function of temperature	47
Fig. 3.1 - Effective thermal conductivity of six different fillings of glass beads with air as fluid.	51
Fig. 3.2 - Effective thermal conductivity of large glass beads and N_2 plotted versus temperature.	53
Fig. 3.3 - Effective thermal conductivity of two fillings of small glass beads versus temperature.	53
Fig. 3.4 - Silicon vapor seeping inside the vacuum cell.	54
Fig. 3.5 - Thermal conductivity of Cu-btc with Helium (He) gas.	56
Fig. 3.6 - Thermal conductivity of Cu-btc with Nitrogen (N_2) gas.	57
Fig. 3.7 - Thermal conductivity of Fe-btc with Helium (He) gas.	57
Fig. 3.8 - Thermal conductivity of Fe-btc with Nitrogen (N_2) gas.	58

Fig. 3.9 - The variation of solid thermal conductivity of Cu-btc and Fe-btc versus temperature	59
Fig. 3.10 - Predictions of the effective thermal conductivity of glass/foam/N ₂ .	60
Fig. 4.1 - Unit cell for the modified phase-symmetry model.	63
Fig. 4.2 - The pore structure visualized.	64
Fig. 4.3 - Actual heat transfer path and heat transfer path of the original phase-symmetry model	65
Fig. 4.4 - The modified phase symmetry model compared with the original.	66
Fig. 4.5 - New measurement setup	66
Fig. 4.6 - New foam measurements plotted versus the theoretical models.	67
Fig. 4.7 - New foam measurements.	69
Fig. 4.8 - A close-up of the aluminum foam applied in the experiments.	70

Tables

Table I-1 - Targets for hydrogen storage for light duty vehicles.	2
Table 1.1 - Total emissivity of some common materials at given temperatures	10
Table 1.2 - List of effective thermal conductivity models and their corresponding limiting relations.	15
Table 1.3 - Limiting relations and secondary parameters for Kunii and Smith's model.	16
Table 1.4 - Particle orientation.	20
Table 1.5 - Kunii and Smith model summarized	20
Table 1.6 - Zehner/Bauer/Schlünder limiting relations and secondary parameters.	21
Table 1.7 - Corresponding notations.	22
Table 1.8 - Shape factors	23
Table 1.9 - Flattening coefficients obtained by Zehner and Bauer.	26
Table 1.10 - ZBS model summarized	26
Table 1.11 - Limiting relations and secondary parameters for the IAEA-TECDOC-1163 model	27
Table 1.12 - Structural parameters for different packing of spheres.	28
Table 1.13 - IAEA-TECDOC-1163 model summarized	29
Table 2.1 - Sensor/Actuator list for the experimental setup.	42
Table 2.2 - Density.	43
Table 2.3 - Particle diameter of various materials.	45
Table 2.4 - Constants for k_f 4 th degree polynomial.	46
Table 2.5 - Constants for $k_{s,alu}$ 8 th degree polynomial.	46
Table 2.6 - Given uncertainties.	48
Table 2.7 - Comparison of fluid thermal conductivity at various pressures	50
Table 2.8 - Uncertainties.	50
Table 3.1 - Properties of glass beads experiments.	51
Table 3.2 - Optimized constants	56
Table 3.3 - The increase of the effective thermal conductivity when switching from N ₂ to He.	59
Table 4.1 - New foam approach overview.	65
Table 4.2 - Experimental data from the new foam measurements.	68
Table 4.3 - Radial and axial thermal conductivity.	69
Table 5.1 - Optimized constants	71

Appendices

Appendix A - Particle diameter	79
Appendix B - Exact composition of glass beads	81
Appendix C - Glass beads results	83
Appendix D - Cu-btc results	91
Appendix E - Fe-btc results	107
Appendix F - Mail from Hot Disk	125
Appendix G - Foam results	127
Appendix H - Risk Assessment Report	133

Nomenclature

A	Area [m ²]	l_s	Thickness of the fluid film adjacent to the contact surface of two particles [m]
a	Ligament radius [m]	l_{mfp}	Mean free path of molecular collisions [m]
a_T	Accommodation coefficient [1]	M	Molecular weight [kg/kmol]
B	Shape-/deformation factor [1]	m	Mass [kg]
b	Shape factor [1]	N	ZBS Simplification parameter [1]
C	Constant [1]	N_A	Number of particles per unit area [1]
C_p	Heat capacity at constant pressure [J/K]	N_L	Number of particles per unit length [1]
C_{el}	Electronic volumetric specific heat [J/m ³ K]	Nu_f	Radiation Nusselt number [1]
\bar{c}	Mean molecular velocity [m/s]	\mathbf{n}	Normal vector [1]
c	Specific heat capacity [J/kgK]	n	Number of contact points [1]
D	Pore diameter [m]	P_0	Sensor power output [mW]
$D(\tau)$	Function of TCT [1]	p	Pressure [Pa]
d	Diameter [m]	Q	Heat transfer [W]
\bar{d}_p	Sauter diameter [m]	R	Particle radius [m]
d_s	Equivalent spherical diameter [m]	\tilde{R}	Universal gas constant =8314 [J/kmol·K]
E	Radiation exitance [W]	R_i	Initial Nickel resistance [ohm]
E_{fuel}	Lower heating value [kJ/kg]	$R(t)$	Sensor resistance [ohm]
E_s	Young's modulus [GPa]	r	Radius [m]
E_{exp}	Expended fuel [kJ/kg]	S	Kaviany contact area parameter [1]
e	= w/L	S_F	Kaviany contact area parameter [1]
F	Function of optical properties [1]	T	Temperature [K]
f	Force exerted on particles [N]	t	Time [s]
g	= a/L	U	Simplification parameter [1]
h_c	Contact area heat transfer coefficient [W/m ² K]	V	Volume [m ³]
h_{rf}	Fluid radiation heat transfer coefficient [W/m ² K]	W_i	Any physical quantity under consideration for volume-averaging [?]
h_{rs}	Solid radiation heat transfer coefficient [W/m ² K]	w	Node width [m]
K	Solid-fluid conductivity ratio = k_s/k_f [1]	x	Direction in the Cartesian coordinate system [m]
k	Thermal conductivity [W/m·K]	x_0	Diameter of sectional area corresponding to one contact point [m]
L	Length [m]	x_r	System characteristic dimension [m]
l	Mean free path of gas molecules [m]	y	Direction in the Cartesian coordinate system [m]
l_f	Thickness of a slab of solid giving the same heat resistance as a spherical particle [m]	z	Direction in the Cartesian coordinate system [m]

Abbreviations

DOE	US Department Of Energy	P&ID	Piping and Instrumentation Diagram
IES	International Energy Summit	REV	Representative Elementary Volume
LHV	Lower Heating Value	TPS	Transient Plane Source
MOF	Metal Organic Framework	TCR	Temperature Coefficient of Resistivity
NG	Natural Gas	TCT	Ratio of Total to Characteristic Time
NTNU	Norwegian University of Science and Technology	US	United States
		ZBS	Zehner, Bauer and Schlünder

Greek letters

α	Thermal diffusivity [m ² /s]	ϑ	Temperature coefficient of resistivity (TCR) [ohm/K]
α_i	Thermal diffusivity of layer material [mm ² /s]	λ	Fluid to solid conductivity ratio = k_f/k_s [1]
β	= $\Delta L/d_p$ [1]	Λ	Dimensionless solid conductivity = $k_s/4\sigma d_p \bar{T}^3$ [1]
γ	= l_s/d_p [1]	μ_s	Poisson ratio [1]
δ	Molecular diffusivity [m ² /s]	ξ	Insulating layer thickness [mm]
Δ_p	Probing depth [mm]	π	Pi = 3.14159 [1]
ΔT_i	Initial temperature difference [K]	ρ	Density [kg/m ³]
$\Delta T(\tau)$	Sample temperature difference [K]	σ	Stephan Boltzmann constant = $5.67 \cdot 10^{-8}$ [W/m ² K ⁴]
Δt_i	Initial time difference [s]	τ	Total to characteristic time (TCT)
ΔX_i	Uncertainty of a parameter [1]	φ	ZBS contact area parameter [1]
ε	Porosity [1]	ϕ	= l_v/d_p [1]
ε_r	Emissivity [1]	χ	Reflectivity [1]
ζ	Distribution parameter [1]	ψ	Absorptivity [1]
η	Tortuosity factor [1]	ω	Transmissivity [1]
θ	Characteristic time [s]		
θ_0	Angle corresponding to the boundary of heat flow for one contact point [rad]		

Subscripts

0	Condition at 273K	i	Denoting the ith particle size fraction
a	Axial	j	Denoting the phase (fluid or solid)
alu	Aluminum	mfp	Mean free path
av	Average	n	Denoting the nth section (A,B,C or D)
b	Bed, bulk	m	Zehner and Schlünder exponential constant
bb	Black body	nc	Non-conducting
c	Core, crosssectional, contact area	p	Particle
e	Effective	ph	Phonon
el	Electron	r	Radiation, radial
exp	Expended	s	Solid, spherical
f	Fluid	uc	Unit cell
fs	Interface between fluid and solid	v	Void
g	Gas		

Superscripts

·	Quantity per unit volume
-	Average of quantity
"	Quantity per unity area
'''	Quantity per unit volume
*	Modified quantity

Other symbols

\varnothing	Diameter [mm]
---------------	---------------

Introduction

There will come a time when the fossil fuels that the world today so conveniently depends on will run out, and therefore we have to look for alternate energy sources and carriers for supporting future energy demand. The run out of fossil fuels will produce a gap that needs to be filled, and it has to be filled with sustainable renewable energy sources. Since hydrogen (H_2) can be made from electrolysis of water using renewable electricity coming from solar or wind power, hydrogen is a possible energy carrier for the future.

Recently, the European Commission conducted an extensive well-to-wheel analysis of various automotive fuels (IES, 2007). They consider the energy ratio E_{exp}/E_{fuel} , where E_{fuel} is the energy content for combustion (lower heating value, LHV) and E_{exp} is the energy expended to create the fuel. One of the most common, and short term beneficial production methods for H_2 is by steam reforming of natural gas, and this has an E_{exp}/E_{fuel} ratio of 0.75 (IES, 2007). Hydrogen thus forms a basis for an energetically viable infrastructure.

Since hydrogen can be produced from electricity, hydrogen storage allows for a more efficient utilization of the grid. In particular, the use of grid-connected intermittent energy sources such as water or wind turbines can benefit from grid energy storage. Energy derived from these energy sources is variable by nature – the amount of electrical energy produced varies with time, day of the week, season, and random factors such as the weather. Hydrogen storage thus facilitates for environmentally friendly energy sources to be utilized outside whenever, working as a grid buffer.

Hydrogen also allows for the use of high-efficiency energy conversion devices, such as fuel cells, from which the products are only water and O_2 . If H_2 made by renewable energy sources is combusted in a fuel cell, this gives a zero-emission energy chain which can be applicable for the transport sector in the future.

Compared with other fuels, H_2 has a lower heating value (LHV) of almost triple. However, there are a few challenges regarding transport and storage. Although hydrogen has a high energy density compared to other fuels, its volumetric density is only 0.084 kg/Nm^3 , compared to the 0.65 kg/Nm^3 of Methane and 4.4 kg/Nm^3 of gasoline (Ullmann, 1989).

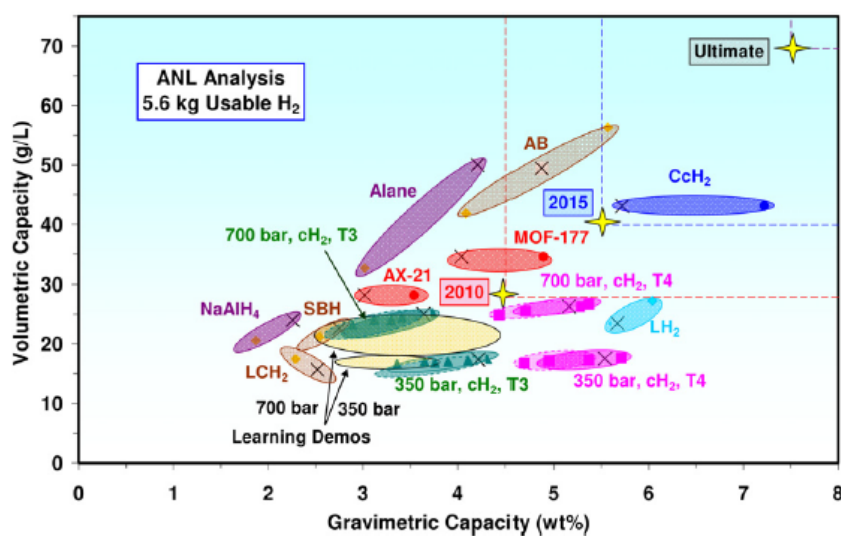


Fig. I-1 - Map of storage capacities of different hydrogen storage options (R.K. Ahluwalia, 2012).

Compression is the preferred method for hydrogen storage in automotive applications today. Fig. I-1 shows that the only storage method that meets the US Department of Energy (DOE) system targets of today is cryo-compression (C₂H₂) (R.K. Ahluwalia, 2012). Hydrogen for use in cars is mainly compressed to 35...70 MPa. This calls for expensive storage materials. Other methods for hydrogen storage are liquefaction, cryo-compression, and chemical storage via metal hydrides or adsorption via physisorption. Onboard hydrogen storage for transportation applications is proven to be one of the most technically challenging barriers to the commercialization of hydrogen fueled light-duty vehicles. The technologies today do not meet the goals set for the future. The US Department of Energy has renewed the targets for light duty transportation. Some of the goals are given in Table I-1 below.

Table I-1 - Targets for hydrogen storage for light duty vehicles
(US Department of energy, 2011).

Storage parameter	Units	2017 target	Ultimate target
System Gravimetric Capacity	kWh/kg	1.8	2.5
System Volumetric Capacity	kWh/L	1.3	2.3
Storage System Cost	\$/kWh net	12	8
System fill time (5 kg)	min	3.3	2.5
	kg H ₂ /min	1.5	2.0

Metal-Organic Frameworks (MOF), with their high porosity and large surface area, serve excellently as sorption materials for hydrogen storage. NTNU, together with Max Planck Institute for Intelligent Systems (Stuttgart) and University Dresden, participate in a research and development-project for MOF materials. In order to meet future requirements by means of storage dimension dynamics, it is important to have knowledge of the thermophysical properties of the MOF materials.

One of the key challenges is the process of charging and discharging storage systems. In order to understand transient storage behavior, and to be able to improve the storage dynamic, elemental physical properties such as thermal conductivity and permeability must be characterized. Prior to this work, reports on permeability (transport capability) of MOF materials have been conducted. (Hubert, 2011); (Henriksen, 2012). This current work follows the earlier projects on thermal conductivity conducted by Jeremy Gauthier (2011) and Rasmussen and Eithun (2011). This work will provide new experimental data on the MOF materials Cu-btc (HKUST-1) and Fe-btc-xerogel as well as further research on heat transport enhancement devices such as open-cell aluminum foams. This work is organized in five main parts:

- Part 1 – Theoretical fundamentals for heat transport through porous media, with emphasis on predictive models and transport mechanisms.
- Part 2 – Description of the measurement setup, estimate of bed properties and uncertainty analysis.
- Part 3 – Results and analysis of the experiments made on MOF materials including a detailed uncertainty analysis.
- Part 4 – A new approach for determining the quality of aluminum foam.
- Part 5 – Conclusions and suggestions for further work.

Part 1 - Heat transfer in porous media

1.1 The porous medium

A porous medium is a medium which consists of both a solid and a fluid phase. The fluid may be either gas, liquid or a combination. One may refer to porous media and mean one of two things:

- A solid structure with an interconnected void.
- A powder or a sample of particles which have a void in between them.

Both are porous. The first one can for example be a sponge-like material or porous rock. The only material described in this report which is a solid matrix is the metal-foam. The second type refers to granular porous media, like sand or powder. In this report the granular materials are glass beads or MOF (Metal Organic Framework). Both granular and solid-structure porous media are shown in Fig. 1.1. However, the MOF-particles themselves are porous, consisting of a solid structure containing extremely small pores. When hydrogen is adsorbed for storage the granular MOF-particles are packed tightly together in a packed bed (also referred to as fixed bed).

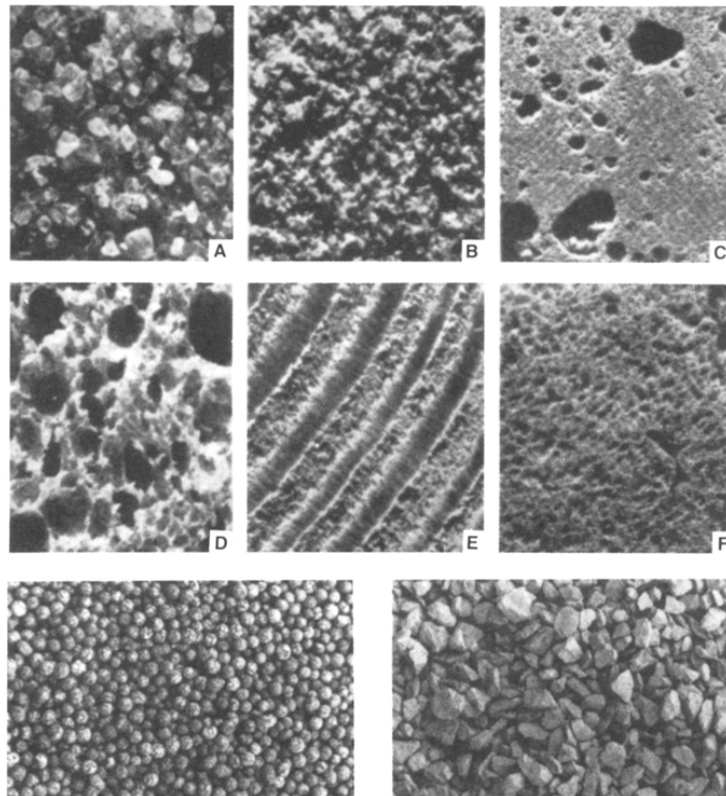


Fig. 1.1 - Top: Examples of natural porous materials: A) beach sand, B) sandstone, C) limestone, D) rye bread, E) wood, and F) human lung.

Bottom: Granular porous materials used in the construction industry, 0.5-cm-diameter Liapor spheres (left), and 1-cm-size crushed limestone (right) (Bejan 2006).

1.1.2 Porosity

The porosity is the volume fraction between the fluid and solid phase. It is described as the ratio between fluid volume and total volume, and is important to understand when conducting heat through a porous medium. For a packed bed, porosity is given as

$$\varepsilon = \frac{V_v}{V_b}. \quad (1.1)$$

Here, V_v is the volume of the void/fluid and V_b is the bulk volume, i.e. the total volume occupied by the material and the void in between. Defining the porosity this way assumes that $(1-\varepsilon)$ is the fraction of the solid.

For granular porous materials, the porosity may vary greatly with packing. For example, for equally sized spheres, the lowest porosity possible is reported to be 0.259 (Kaviany, 1995). With random packing of equally shaped spheres however, the porosity varies along 0.37 – 0.43. Preliminary tests made in this work are done with glass beads of an almost perfect-sphere shape, and the porosity is therefore expected to lie within this range.

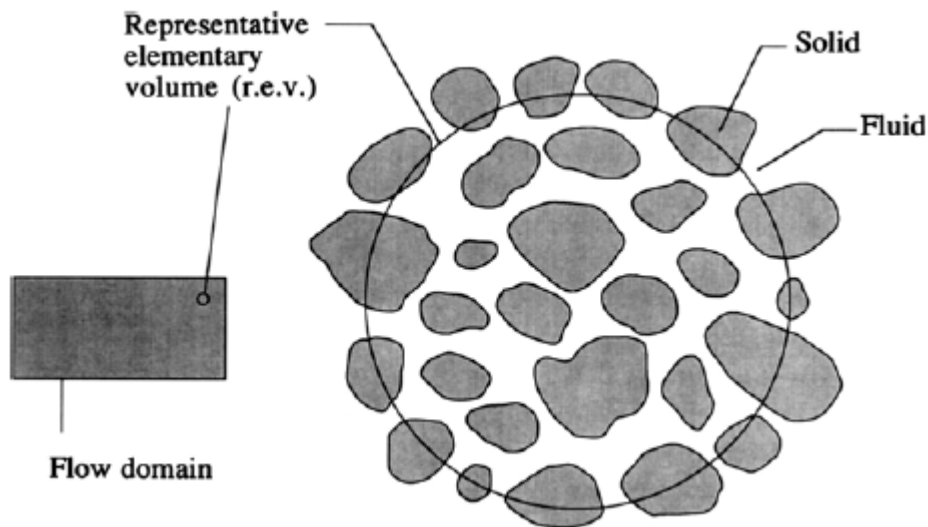


Fig. 1.2 - Porosity visualized (Bejan, 2006).

Fig. 1.2 displays a representative elementary volume (REV) of a porous medium. Since porous media is so complex in geometry, a common approach on heat transfer problems is volume averaging. This basically means to apply the basic energy and momentum equations on only a piece of the medium, a piece that within an acceptable statistical margin of error can represent the behavior of the entire medium (Tsotsas, 1987).

1.2 Heat transfer mechanisms

Heat transfer in porous media is carried out from different mechanisms. Fig 1.3 indicates the different heat transfer mechanisms in porous media. The effective thermal conductivity depends on solid and

fluid thermal conductivity, geometry of the solid medium, contact resistance between particles and the amount of heat transfer by radiation. Note that convective heat transfer will be assumed negligible throughout this work. Convection in porous media rarely occur on a notable level, because the fluid pore size between the solid structure is simply too small. All particles applied in this work have a particle diameter $\ll 1$ cm, and therefore convection will be negligible (Tavman, 1996).

1. Heat transfer through solid by heat conduction.
2. Heat transfer through the fluid by conduction.
3. Conductive heat transfer through the contact surfaces of adjacent particles.
4. Heat transfer between surfaces due to radiation.
5. Convective heat transfer (solid/gas/solid).

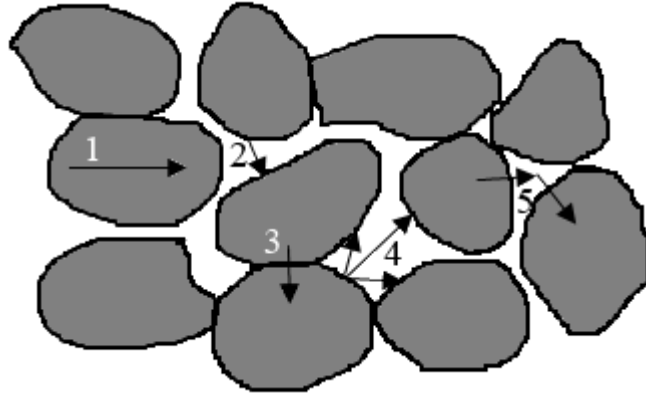


Fig. 1.3 - Heat transfer mechanisms in porous media.

As visualized in the above figure, all these processes may occur at the same time. The overall heat transported will then be a sum of the conductive heat transfer contribution both from the solid and the fluid. The radiation is expected to become increasingly significant as the temperature of the packed bed increases. In order to understand the process of heat transfer in porous media, which is a fairly complex issue, one must first begin to understand the general processes governing heat transfer.

1.2.2 Conduction

Conduction is spontaneous energy transfer from energetic particles of a medium to the adjacent less energetic ones (Cengel, 2006). These particles can be molecules, atoms, electrons or phonons. Conduction can occur in solids as well as fluids (gas or liquid). In fluids, the conduction occurs when particles collide and diffuses through the fluid during their random motion. In solids, it is due to the combination of lattice vibrations (phonons) of molecules and the energy transport by free electrons.

The magnitude of heat conduction is greater in solids than in fluids, because atoms are close together. Solids thereby allows for adjacent atoms to transfer energy to each other by lattice vibrations. In fluids, and especially gases, molecules are further away from each other, and this thus gives less conduction.

The rate of heat conduction depends on the geometry and the material of the medium, the temperature difference, as well as its thickness. This is governed by Fourier's law of heat conduction (Cengel, 2006), which yields

$$\dot{Q} = -kA_c \frac{dT}{dx} \quad (1.2)$$

Here, dT/dx is the temperature gradient with respect to the x-direction, A_c is the cross-sectional area, \dot{Q} is the rate of conduction heat transfer, and k is the thermal conductivity in $W/(m \cdot K)$.

The thermal conductivity is a thermophysical property, and the magnitude for different materials varies over a wide range. The thermal conductivity of a material depends on its state, chemical composition, and physical structure. It also varies with temperature and pressure. However, in most cases, thermal conductivity is much more dependent on temperature than on pressure. In that case, the pressure dependence can be neglected, and the thermal conductivity can be tabulated as a function of temperature only.

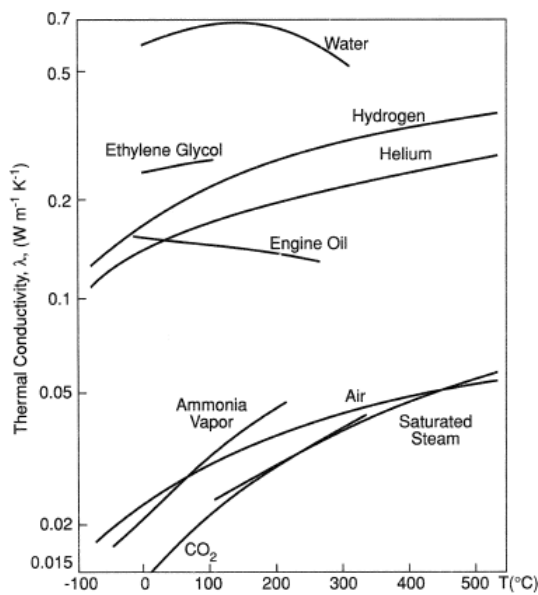


Fig. 1.4 - Thermal conductivity as a function of temperature for some fluid substances (Thermopedia.com).

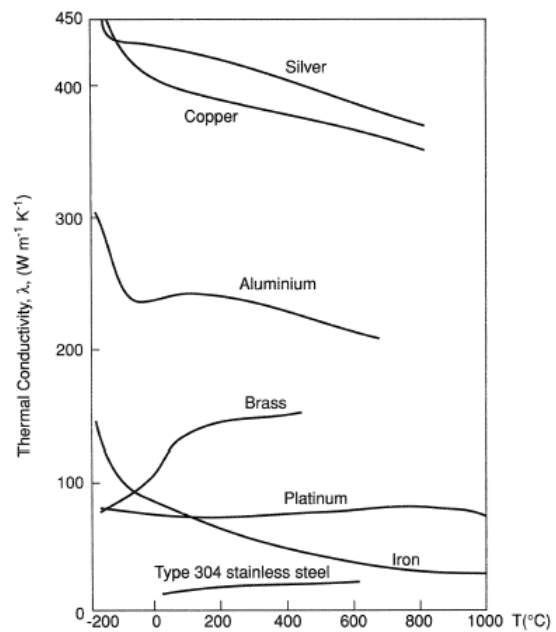


Fig. 1.5 - Thermal conductivity as a function of temperature for some solid substances (Thermopedia.com).

Fig. 1.4 and 1.5 shows the thermal conductivity as a function of temperature for various substances. As can be seen from the figure, fluids have a much lower thermal conductivity than solids.

This is the main challenge for hydrogen storage in porous materials today: Since a major part of a porous medium consists of a fluid, the thermal conductivity for the porous medium is low. Because of low thermal conductivity, porous media have difficulties transporting enough heat at a rate which allow for fast charge and discharge of a storage tank.

The physical meaning behind the solid thermal conductivity can be explained by kinetic theory. Kinetic theory gives the following expression (Incropera, 2007) for the thermal conductivity:

$$k = \frac{1}{3} C_{el} \bar{c} l_{mfp}, \quad (1.3)$$

where C_{el} is the electron specific volumetric heat, \bar{c} is mean molecular velocity, while l_{mfp} is the mean free path between molecular collisions. As mentioned earlier, transport of thermal energy

through a solid may be due to two effects: the migration of free electrons and lattice vibrational waves (phonons). For a given solid material, the thermal conductivity may therefore be expressed as a function of the electron conductivity k_{el} (for conducting solids) and the phonon thermal conductivity k_{ph} (for non-conducting solids), or $k = k_{el} + k_{ph}$.

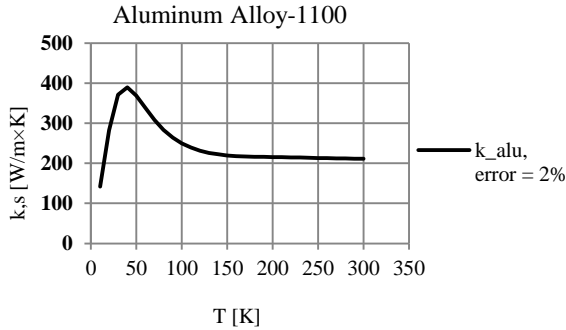


Fig. 1.6 - Thermal conductivity k_s of Aluminum Alloy-1100 (NIST Chemistry Webbook).

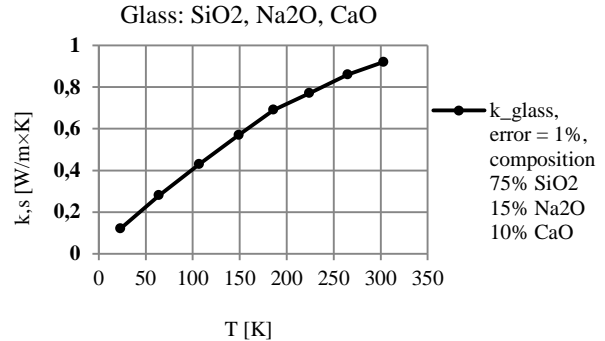


Fig. 1.7 - Solid thermal conductivity k_s of glass (Handbook of glass data, 1987).

Figures 1.6 and 1.7 above displays plots of thermal conductivity versus temperature in the range of $4K < T < 300K$. Fig 1.6 is based on data from the NIST web-book. NIST apply an 8th degree polynomial relation in their calculations which has an uncertainty of 2%. The metal foam used in this work consists of Aluminum Alloy-1100, and as can be seen from Fig. 1.6, the solid conductivity has a grand peak at approximately 390 W/m·K and 40K before flattening out at around 215 W/m·K when $150K < T < 300K$. Fig. 1.7 shows the solid conductivity of a glass melt, whose composition is quite similar to the glass beads used for reference measurements in this work.

Heat conduction in gases and vapors mainly depend on the transfer of kinetic energy from the molecular movement. The kinetic gas theory states that the temperature of a gas element is proportional to the mean kinetic energy of its constituent molecules. This suggests that the thermal conductivity of a gas should depend on its temperature. According to a simple model of kinetic theory (traffic model), an approximated relation for gases can be (W. M. Rohsenow, 1961)

$$k = \frac{1}{3} \rho c_v \bar{c} l_{mf} \quad (1.4)$$

Here, ρ is the gas density and c_v is the specific heat capacity at constant volume. The mean molecular velocity \bar{c} increases with increasing temperature and decreasing molecular weight. Hence, the thermal conductivity will also increase. The molecular weight of helium (He) is double the magnitude to that of hydrogen (H_2) and therefore the conductivity of hydrogen is higher. These trends are shown in Fig. 1.4. on the next page.

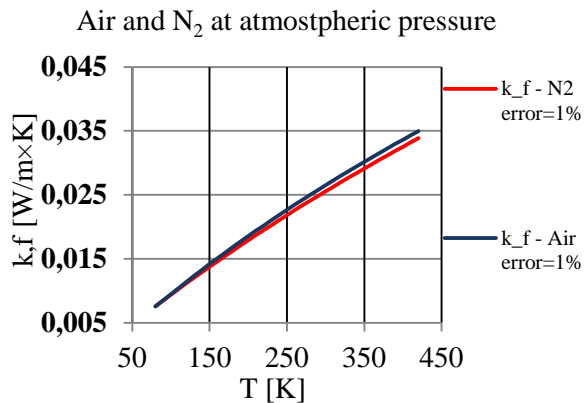


Fig. 1.8 - Conductivity of Air and N₂ as a function of temperature (VDI Heat Atlas, 2010).

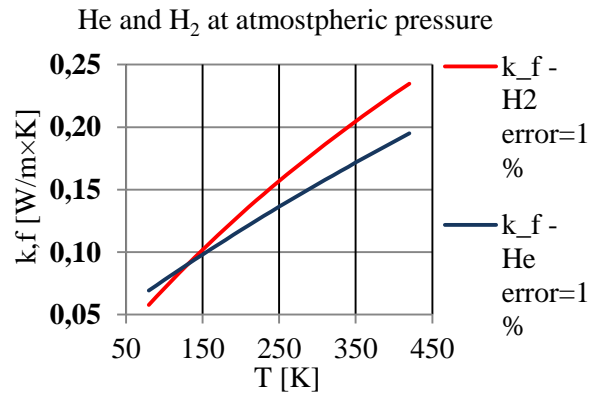


Fig. 1.9 - Conductivity of He and H₂ as a function of temperature (VDI Heat Atlas, 2010).

Fig. 1.8 and 1.9 show the fluid thermal conductivity of gases applied in this work. The plots are calculated from a 4th degree polynomial and have an uncertainty of 1%. From the figures it is clear that, at atmospheric pressure, the thermal conductivity of air and nitrogen at any given temperature between 80K and 420K are almost an order of magnitude less than helium and hydrogen thermal conductivity. Since the N₂ conductivity is almost equal to that of air, and He conductivity is almost equal to that of hydrogen, the measurements in this work were carried out with helium and nitrogen. Helium is non-flammable and a lot safer to handle than hydrogen (see the attached Risk Assessment Report).

1.2.3 Stefan Boltzmann law of radiation

Unlike conduction, where heat is transferred through a substance, energy transport can also take place without the presence of a physical medium. This process is known as thermal radiation and occurs when a substance emit electromagnetic waves. Electromagnetic waves are formed when accelerated charges or changing electric currents make an electric field in the medium (Cengel, 2006). Thermal radiation is emitted from a substance when energy in molecules, electrons and atoms is in transition. At a microscopic level, the measure of this process is temperature. Thus, thermal radiation will increase with increasing temperature. All substances are emitting electromagnetic waves; it can come from solid bodies as well as liquids and gases. All substances also possess the ability to absorb such energy.

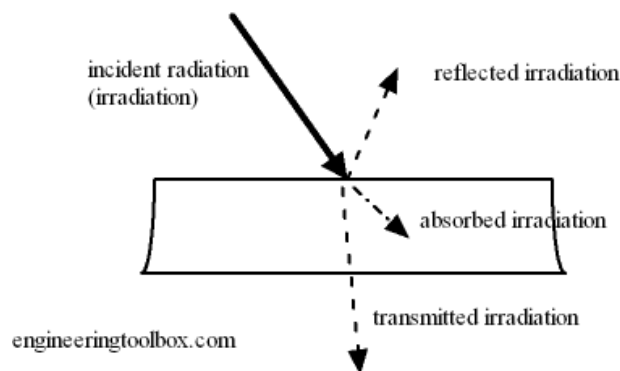


Fig. 1.10 - Incident radiation on a surface.

As seen from Fig. 1.10, when radiation is incident on a body the surface will reflect part of it. The rest is absorbed within the body or even transmitted through it. When radiation impinges on a surface, the fraction that is reflected back is defined as the *reflectivity* χ , the fraction that is absorbed is the *absorptivity* ψ , while the fraction transmitted is called the *transmissivity* ω . This gives (Cengel, 2006):

$$\chi + \psi + \omega = 1. \quad (1.5)$$

A substance which has the ability to absorb a lot of radiation is called *opaque*. In opaque bodies, the energy that penetrates the body will be absorbed and stored within a very thin layer adjacent to the surface. For an opaque body, Eq. (1.5) then reduces to $\chi + \psi = 1$. In a *transparent* body, the material thickness required to substantially absorb radiation is large compared to the thickness of the body, and then most of the radiation will pass through without being absorbed. An ideal body, which absorbs all impinging radiation energy without reflection or transmission, is called *black body*. Hence, for a black body Eq. (1.5) reduces to $\psi = 1$.

A black body is defined as a perfect emitter and absorber of radiation (R. Siegel, 2002). The total emission of radiation per surface area and per unit time E''_{bb} from a black body is related to the temperature T of the surface through the Stephan Boltzmann law of radiation. The law yields

$$E''_{bb} = \sigma T^4, \quad (1.6)$$

where $\sigma = 5.67 \cdot 10^{-8} \text{ [W/m}^2\text{K}^4\text{]}$ is the Stephan Boltzmann constant.

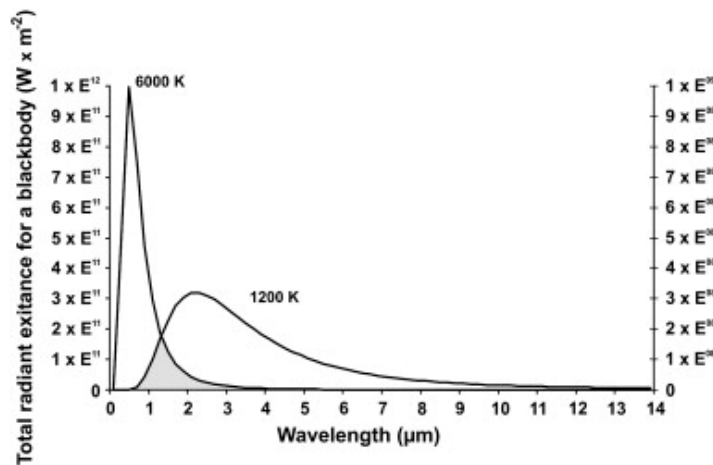


Fig. 1.11 - Black body exitance E''_{bb} at various temperatures and wavelengths (L. Spampinato, 2011).

As can be seen from Fig. 1.11, the total radiant exitance (or emittance) from a surface will increase severely with temperature. Ordinary substances do not meet the specifications of a black body; they will emit a lower rate of radiation at the same given temperature. Thus, E'' being the exited radiation flux from an ordinary body per surface area and per unit time, the emissivity ϵ_r of the surface will be

$$\epsilon_r = \frac{E''}{\sigma T^4} = \frac{E''}{E''_{bb}}. \quad (1.7)$$

Thus, for a black body, $\epsilon_r = 1$. The emissivity of a material is defined as the ratio of the radiation emitted by the surface area at a given temperature to the radiation emitted by a black body of the same temperature. It will vary with temperature and wavelength and the direction of the emitted radiation. The emissivity of some common materials is given in Table 1.1 below.

Table 1.1 - Total emissivity of some common materials at given temperatures

Material	Temperature [K]	Emissivity	Source
Aluminum Alloy-1100	366-700	0.05	(Monarchserver.com)
Aluminum foil	300	0.04	(engineeringtoolbox.com)
Aluminum oxidized	472	0.11	(Monarchserver.com)
Aluminum unoxidized	298-373	0.02-0.03	(Monarchserver.com)
Glass	293	0.94	(Stephan Kabelac, 2010)
Glass, smooth	273-473	0.95	(Berkely Engineering Division)
Quartz glass	300	0.93	(engineeringtoolbox.com)
Steel oxidized	300	0.79	(engineeringtoolbox.com)
Steel polished	300	0.07	(engineeringtoolbox.com)
Styrofoam insulation	N/A	0.6	(Thermoworks.com)

As seen from Table 1.1, the emissivity will increase when substances become more oxidized, and when temperature increases. The aluminum foam in this work consists of aluminum Alloy-1100 and clearly has a very low emissivity (0.05). Since the foam is cut and stored in ambient moist air in the lab, the edges will be somewhat oxidized, so an emissivity up until 0.1 could be closer to the real value. The glass beads one the other hand, is expected to have a very high emissivity, close to a black body (>0.9).

In order to understand the role that the effective thermal conductivity plays in porous media, one must take a closer look at the basic conduction heat transfer equations. The following section will address the basis for how the effective stagnant thermal conductivity can describe heat conduction in porous media.

1.3 Macroscopic transient heat conduction equations

As mentioned in section 1.1.2, heat transfer problems in porous media are most commonly approached macroscopically by averaging the microscopic heat transfer process over a representative elementary volume (REV). By assuming local thermal equilibrium within the fluid and solid phases one can describe the heat transfer process in two-phase media by a single conduction equation. Then the problem comes down to construction of a correct correlation for describing the effective stagnant thermal conductivity of the whole mixture.

Assume a pack of solid particles surrounded by a fluid, as described in Fig. 1.2. The particles are considered to be spherical and of uniform size with particle diameter d_p . By assuming that d_p is much larger than the typical molecule size, one can treat the fluid and solid both as macroscopically continuous, thus the macroscopic transient heat conduction equations are (Hsu, 1999)

$$\rho_f c_{pf} \frac{\partial T_f}{\partial t} = \nabla \cdot (k_f \nabla T_f), \quad (1.8)$$

for the fluid and

$$\rho_s c_{ps} \frac{\partial T_s}{\partial t} = \nabla \cdot (k_s \nabla T_s), \quad (1.9)$$

for the solid, respectively. In the above equations, the subscripts f and s refer to the fluid and the solid phase, ρ is the material density, k is the thermal conductivity, and c_p is the specific heat capacity at constant pressure. All properties are assumed constant. Furthermore, on the interface between the fluid and solid phases A_{fs} the temperatures T_f and T_s will be equal. Hence,

$$\mathbf{n}_{fs} \cdot k_f \nabla T_f = \mathbf{n}_{fs} \cdot k_s \nabla T_s \quad \text{on } A_{fs}, \quad (1.10)$$

where \mathbf{n}_{fs} is the normal vector from fluid to solid. Solving equations (1.8) - (1.10) in detail when the number of particles is large requires extensive numerical modeling; therefore it is more practical to apply the volume averaging-method. Now introducing the REV of volume V and with W_j denoting any physical quantity under consideration, the procedure of volume averaging can then be defined as

$$\bar{W}_j = \frac{1}{V_j} \iiint_{V_j} W_j dV. \quad (1.11)$$

Here, V_j is the volume of the j -phase (thus either fluid or solid). The phase-averaged quantity W_j can be considered continuous by assuming that the volume of the REV is much larger than the volume of a single particle yet much smaller than the entire flow domain volume. Defining $V = V_s + V_f$ then gives the opportunity to define the porosity as $\varepsilon = V_f/V$. Then, by averaging equations (1.8) and (1.9) over the REV and applying the divergence theorem, the volumetric phase averaged equations are (Hsu, 1999)

$$\rho_f c_{pf} \frac{\partial \varepsilon \bar{T}_f}{\partial t} = \bar{\nabla} \cdot [k_f \bar{\nabla}(\varepsilon \bar{T}_f)] + \bar{\nabla} \cdot (k_f \bar{A}_{fs}) + Q_{fs}''', \quad (1.12)$$

and

$$\rho_s c_{ps} \frac{\partial [(1-\varepsilon)\bar{T}_s]}{\partial t} = \bar{\nabla} \cdot \{k_s \bar{\nabla}[(1-\varepsilon)\bar{T}_s]\} - \bar{\nabla} \cdot (k_s \bar{A}_{fs}) - Q_{fs}''', \quad (1.13)$$

where $\bar{\nabla}$ is the gradient in the macroscopic coordinate system. In equations (1.12) and (1.13), the contribution due to thermal tortuosity is

$$\bar{A}_{fs} = \frac{1}{V} \iint_{A_{fs}} T_f d\mathbf{s} = \frac{1}{V} \iint_{A_{fs}} T_s d\mathbf{s}, \quad (1.14)$$

and the interfacial heat transfer contribution Q_{fs}''' is

$$Q_{fs}''' = \frac{1}{V} \iint_{A_{fs}} k_f \nabla T_f d\mathbf{s} = \frac{1}{V} \iint_{A_{fs}} k_s \nabla T_s d\mathbf{s} \quad (1.15)$$

with $d\mathbf{s} = \mathbf{n}_{fs} dA_{fs}$ as described in Eq. (1.10). The term on the left hand side of Eq. (1.12) and (1.13) represents the rate of thermal energy stored in the REV. On the right hand side, the first term represents the conductive heat transfer rate entering the fluid (1.12) and solid (1.13) phase through the REV boundary. The second term associates with the thermal tortuosity effect – an elongation in the thermal path travel due to the presence of solid particles. Note that magnitude of the tortuosity term in (1.12) differs from that in (1.13), due to the fact that the thermal conductivities of solid and fluid are

different. However, the magnitude of the interfacial heat transfer is the same. (This is obvious, since one can only assume that all heat transferred from the solid to the fluid is also gained in the fluid, and vice versa). Finally, the last term represents the heat transfer rate between the fluid and solid phases. The last two terms in both equations (1.12) and (1.13) have opposite signs because the source terms in (1.12) have to be sink terms in (1.13).

The assumption of having local thermal equilibrium has been proven not to be mathematically valid (Hsu, 1999), however, for any practical purposes it will suffice. Then, by assuming local thermal equilibrium, the local temperatures

$$\bar{T}_f = \bar{T}_s = \bar{T}. \quad (1.16)$$

Inserting Eq. (1.16) into the phase averaged equations (1.12) and (1.13) then gives the transient heat conduction equation for stagnant porous media (Hsu, 1999)

$$(\rho_f c_{pf} + \rho_s c_{ps}) \frac{\partial \bar{T}}{\partial t} = \bar{\nabla} \cdot [k_e \bar{\nabla} \bar{T}], \quad (1.17)$$

where k_e is the effective stagnant thermal conductivity of the mixture given by

$$k_e = \varepsilon k_f + (1 - \varepsilon) k_s + (1 - K)^2 \eta. \quad (1.18)$$

In (1.18), K is the solid- to fluid thermal conductivity ratio, while η is the thermal tortuosity parameter. The effective thermal conductivity then only depends on the interfacial geometry and the thermal properties of solid and fluid. Solutions to Eq. (1.17) has been extensively presented and debated in open literature. The problem then comes down to obtaining the correct value for the effective stagnant thermal conductivity.

1.4 Effective stagnant thermal conductivity of granular porous materials

Determining the effective stagnant thermal conductivity has been examined thoroughly for more than a century (Maxwell, 1873). Early experiments for measuring the effective thermal conductivity have been carried out in the late 60s (Kunii and Smith, 1960) (Krupiczka, 1967) along with theoretical predictive models. Most of these measurements were carried out in the range of $1 < K < 10^3$. Later, experiments with higher (Nozad et al, 1985) and lower (Prasad et al, 1989) values of K were published. The predictive models for determining k_e have been reviewed by Tsotsas (1987), and more recent by van Antwerpen et al. (2010). Over the years, several analytical composite-layer models have been proposed for k_e (Kunii and Smith, 1960) (Zehner and Schlünder, 1970). Recently, Hsu et al. (1994) extended the Zehner-Schlünder model for spherical particles by introducing a particle touching parameter. Newer experiments on open-cell materials like metal foams were conducted by Boomsma and Poulikakos (2001).

According to the simpler models for effective stagnant thermal conductivity, k_e depends on the geometry of the porous medium and the thermal conductivity of the fluid and solid phases. The overall conductivity can consequently be described as (VDI Heat Atlas, 2010)

$$k_e = k_e(\varepsilon, k_f, k_s) \quad (1.19)$$

Parameters listed above are so-called primary parameters, and most predictive models depend only on these three main parameters. However, as previously described, other parameters might also need to be taken into account, depending on the physical state of the medium (Tsotsas, 1987):

1. According to the kinetic gas theory, the thermal conductivity of unconfined, dilute gas is pressure-independent. However, with the presence of a solid medium the thermal conductivity of gas will decrease with decreasing pressure.
2. Chances of radiation heat transfer occurring increases with increasing temperature. This means that the effective thermal conductivity becomes a function also of optical properties (like emissivity ε_r), the relation between void and particles (which corresponds to the particle diameter d_p) of the media involved, as well as their temperature T .
3. Particles subjected to a force f as a result of the pressure caused by their own weight pressing down on each other, will lead to an increase in heat transfer between particles since the contact area of the particles are enlarged (larger contact area means that the solid conductivity $k_s > k_f$ will transfer more heat between particles if $K > 1$). Deformation of particles depends mainly on the mechanical properties of the solid and the morphology of particle surface.
4. Heat transfer by free convection will occur in very large voids, and with sufficient solid-fluid temperature difference.

In experiments conducted in this work the pressure is maintained constant, it is therefore reasonable to state that one can neglect the pressure dependence when processing these data. As stated in section 1.2, convective heat transfer can be neglected. For this study, points 1 and 4 are therefore irrelevant. However, adding the secondary parameters to the list given in Eq. (1.19) gives the following functional dependence:

$$k_e = k_e \left(\begin{array}{c} \varepsilon, k_f, k_s, T, \varepsilon_r, d_p, \\ \text{particle shape and size distribution,} \\ \text{particle mechanical and optical properties,} \\ \text{fluid thermodynamic and optical properties,} \\ \text{flattening of contact points} \end{array} \right) \quad (1.20)$$

1.4.1 Limiting relations

Predictive models need to describe the functional relationship in Eq. (1.19) or (1.20) in a general way, and in order to result in the most accurate solution they should take into account the primary parameters and as many of the secondary ones as possible. A good model should also be mathematically concise and be valid for a large range of both fluid and solid substances. It should also possess some flexibility by allowing for parameter-fitting regarding shape and size, and if possible be easy to apply. Furthermore, taking into account the primary parameters from Eq. (1.19), it should fulfill the following limiting physical relations (Shcumann, 1934):

1. $\varepsilon = 0 \quad \Rightarrow \quad k_e = k_s$; the system consists of solid only.
2. $\varepsilon = 1 \quad \Rightarrow \quad k_e = k_f$; the system consists of fluid only.
3. $k_s = k_f \quad \Rightarrow \quad k_e = k_s = k_f$; all phases have the same thermal conductivity.
4. $k_f \rightarrow \infty \quad \Rightarrow \quad k_e \rightarrow \infty$; particles can be bypassed for an infinitely good conducting

- continuous phase.
5. $k_s \rightarrow \infty \Rightarrow k_e \rightarrow \infty$; if particles touch each other.
 6. $k_f \rightarrow 0 \Rightarrow k_e \rightarrow 0$; valid if particles touch each other, or has point contact.
 7. $k_s \rightarrow 0 \Rightarrow k_e/k_f = \delta_e/\delta$; the reduced thermal conductivity of a mixture of non-conducting particles should be equal to the effective diffusion coefficient δ_e divided by the molecular diffusivity δ .

Most of the above limitations are evident and do not require further explanation. However, regarding limiting relation 7, the conductivity of a substance containing a non-conducting dispersed phase is not actually *known*, though it is a definite function of its structure and of the conductivity of the continuous phase (Tsotsas, 1987).

1.4.2 Types of models

In order to keep track of all the models determining the effective thermal conductivity in porous media, one might feel the need to classify them on the basis of from which method they were obtained. Almost all models predicting the thermal conductivity of packed beds can then be divided into three different categories (Tsotsas, 1987):

Type I) - In type one models, the Laplace equation for heat conduction is solved analytically or numerically in order to make an exact computation of the temperature field in and around the solid substance.

Type II) - Second type models are represented by thermal resistances for conduction in the solid and fluid phases. The limiting relations are also represented by the limiting theoretical correlations *parallel* and *series* arrangement, which are the simplest forms of the thermal resistance type models.

Type III) - Employing a unit cell as a basis for calculation, type three models set the thermal conductivity in the unit cell equal to the conductivity of the whole mixture. This implies that the specific unit cell must be representative for an average of all the other unit cells in the mixture. If it is indeed so, these types of models give a very precise prediction of the effective thermal conductivity. In order to ensure easy calculation, either parallel heat flux lines (type IIIa) or parallel isotherms (type IIIb) are assumed.

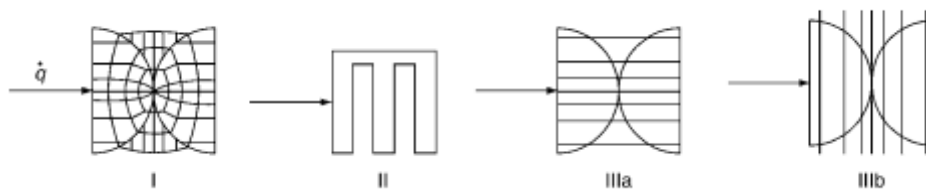


Fig. 1.12 - Types of models used to predict the thermal conductivity of packed beds. Type I: Exact analytical or numerical computation of the temperature field. Type II: Combination of resistances. Type IIIa: Unit cell with parallel heat flux lines. Type IIIb: Unit cell with parallel isotherms.

The above figure visualizes the three model types. For comparison purposes, Table 1.2 lists a selection of models along with their limiting relations and the secondary parameters they include. Regarding the limiting relation 7 (non-conducting solid particles), the value of k_e/k_f is given. It is calculated with $\varepsilon = 0.4$ and $k_f = 0.25$ at 273K and atmospheric pressure. Values for limiting relation 7 for the Bauer and

Schlünder and IAEA-TECDOC models are from this work. Values for other models are taken from Tsotsaas (1987).

Table 1.2 - List of effective thermal conductivity models and their corresponding limiting relations.

Author	Year	Type	Limiting relations							Secondary parameters					Source
			1	2	3	4	5	6	7	Press.	Rad.	Form	Distr.	Cont.	
Maxwell	1873	Ia	Y	Y	Y	Y	N	Y	0.308	N	N	N	N	N	Tsotsaas
Kuuni and Smith	1960	IIIa	N	Y	Y	Y	Y	Y	0.400	N	Y	N	N	Y	Tsotsaas
Krupiczka	1967	Ia	N	N	Y	Y	Y	Y	0.0	N	N	N	N	N	Tsotsaas
Zehner and Schlünder	1970	IIIa	Y	Y	Y	Y	Y	Y	0.225	N	N	Y	Y	N	Tsotsaas
Bauer and Schlünder	1978	IIIa	Y	Y	Y	Y	Y	Y	0.294	Y	Y	Y	Y	Y	This work
IAEA-TECDOC-1163	2000	IIIa	Y	Y	Y	Y	Y	Y	0.250	N	Y	Y	Y	Y	This work

Y = Yes, N = No. Cont.=Contact area heat transfer (not to be mistaken for point contact heat transfer)

The model of Krupiczka has been shown to give good estimations in fluidized beds when $K < 1$ (Prasad et al, 1989). The Zehner and Schlünder model tends to underestimate the effective thermal conductivity because it does not take into account the possibility of enlarged contact area between particles. This is however fixed in the upgraded Bauer-Schlünder model. This fix also accounts for radiation. This model is more commonly known as the Zehner-Bauer-Schlünder (hereby ZBS) model. Also, note that the ZBS model is not valid in the near-wall region, thus one need to ensure that the bulk is sufficiently large compared to the particle size when applying this model. Both the model proposed by the IAEA-TECDOC-1163 and the ZBS model have been proven to correlate well with experimental data (van Antwerpen et al, 2010).

As one can see from the Table 1.2, the type III models clearly provide a larger spectrum of applicability. The Models of type I and II will therefore be discussed briefly, while the type III models will be given a more detailed review.

1.5 Models based on the solution of the Laplace conduction equation (Type I)

The oldest and simplest analytical solution has been provided by Maxwell in 1873. This solution is

$$\frac{k_e}{k_f} = \frac{2\varepsilon + K(3 - 2\varepsilon)}{3 - \varepsilon + K\varepsilon}. \quad (1.21)$$

The Maxwell equation is valid for $\varepsilon \rightarrow 1$, because of the assumption that the solid particles are so far apart that they do not have contact with each other. In Eq. (1.21), K denotes the solid to fluid conductivity ratio k_s/k_f . Since most granular porous media usually have porosities ranging from 0.3 to 0.5, this model may not be particularly applicable for this work.

Another model of type one is the Krupiczka (1967) correlation. He solved a set of two-dimensional heat conduction equations with no temperature-drop at the solid-fluid interface. He then applied these results in a spherical lattice and came up with the following model for stagnant thermal conductivity:

$$\frac{k_e}{k_f} = \lambda^{-a}, \quad (1.22)$$

with

$$a = 0.28 - 0.757 \log_{10}(\varepsilon) + 0.057 \log_{10} \lambda, \quad (1.23)$$

where $\lambda = k_f/k_s$ is the fluid to solid conductivity ratio. Prasad et al. (1989) reviewed this correlation for liquid fluid substances and found that it gave good results.

1.6 Thermal resistance models (Type II)

With the solid-fluid conductivity ratio $K = k_s/k_f$, the parallel and series arrangement resistance models yields:

$$\frac{k_e}{k_f} = \varepsilon + (1 - \varepsilon)K, \quad (1.24)$$

and

$$\frac{k_e}{k_f} = \frac{1}{\varepsilon + (1 - \varepsilon)/K}, \quad (1.25)$$

respectively. The maximum effective thermal conductivity for a two-phase system is given by a unidirectional heat flow through parallel layers of solid and fluid phases, while the minimum is given by a series arrangement (Dressler and Boegli, 1958). The two models from Eq. (1.24) and (1.25) act as the boundaries for the other thermal conductivity models.

1.7 Unit cell models (Type III)

Unit cell models seem to be the most applicable ones, and they also take in many of the secondary parameters from Eq. 1.18. The model of Kunii and Smith was obtained in 1960. They obtained the model by discretizing the solid and fluid phase into different modes acting in series and parallel.

1.7.1 Model of Kunii and Smith (1960)

Table 1.3 shows the limits for this model. Note that particle form and distribution is not taken into account. Hence, the model is only applicable for beds of mono-sized spherical particles.

Table 1.3 - Limiting relations and secondary parameters for Kunii and Smith's model.

Author	Year	Type	Limiting relations							Secondary parameters				
			1	2	3	4	5	6	7	Press.	Rad.	Form	Distr.	Cont.
Kuuni and Smith	1960	IIIa	N	Y	Y	Y	Y	Y	0.400	N	Y	N	N	Y

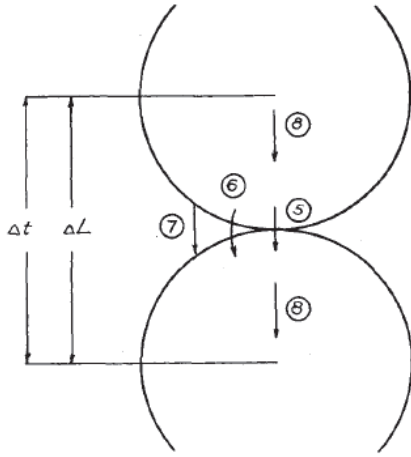


Fig. 1.13 - Kunii and Smith's heat transfer model for a packed bed of spherical particles.

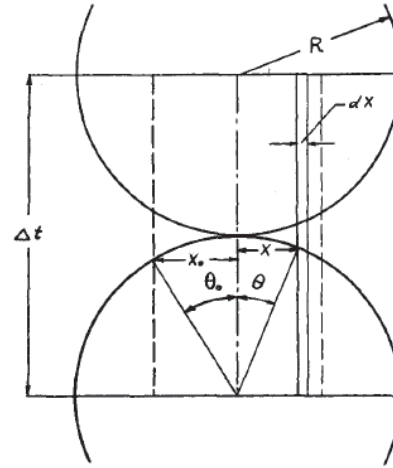


Fig. 1.14 - Model for heat transfer near particle contact points (Kunii and Smith, 1960). Note that they use t for temperature instead of T (this work).

In figures and above are Kunii and Smith's general model for heat transfer in a packed bed (Fig. 1.13) and their model for heat transfer near particle contact points (Fig. 1.14). They presume that the heat transfer occurs in the vertical direction by the following mechanisms:

1. Heat transfer through the fluid in the void space by conduction and by radiation between adjacent voids.
2. Heat transfer through solid:
 - a. Conduction through contact area between adjacent particles.
 - b. Conduction through the stagnant fluid near the contact surface.
 - c. Radiation heat transfer between solid surfaces.
 - d. Conduction through the solid phase.

According to figure 1.13, they then state that if the length between the center of the two spheres is ΔL , then the effective thermal conductivity is given by $-k_e(\Delta T)/(\Delta L) = [\text{heat flux in void space}] + [\text{heat flux through solid}] = [\text{mechanism 1}] + [\text{mechanism 2}]$. This yield

$$-k_e \frac{\Delta T}{\Delta L} = -k_f \varepsilon \frac{\Delta T}{\Delta L} + h_{rs} \cdot \varepsilon \cdot (-\Delta T) + \dot{Q}_s'' \quad (1.26)$$

where h_{rs} is the thermal radiation heat transfer coefficient between solid surfaces and \dot{Q}_s'' is the heat flux rate through the solid per surface area. They then assume that the temperature drop in a particle equals the sum of the temperature drop in the solid phase and the temperature near the contact surface, or

$$\Delta T = \Delta T_s + \Delta T_{fs} \quad (1.27)$$

The temperature drops ΔT_s in solid and ΔT_{fs} near the contact surface may be written in terms of

$$\Delta T_s = -\frac{\dot{Q}_s''}{(k_s/l_s)(1-\varepsilon)} \quad (1.28)$$

and

$$\Delta T_{fs} = -\frac{\dot{Q}_s''}{(h_c + h_{rs} + k_f/l_f)(1 - \varepsilon)}. \quad (1.29)$$

In the above equations (1.28) and (1.29) the thickness of a slab of material which would give the same heat resistance as a spherically shaped particle is denoted l_s , while l_f is the thickness of a slab of stationary fluid which would offer the same resistance as the filaments of fluid near the particle contact points. In Eq. (1.29), h_c is the heat transfer coefficient representing the heat transfer through the contact area of adjacent particles. Combining Eq. (1.26) through (1.29) and then dividing by the fluid conductivity k_f and inserting the quantities $\beta = \Delta L/d_p$, $\phi = l_f/d_p$ and $\gamma = l_s/d_p$ gives the expression

$$\frac{k_e}{k_f} = \varepsilon \left(1 + \beta \frac{h_{rf} \cdot d_p}{k_f} \right) + \frac{\beta(1 - \varepsilon)}{\left[\frac{1}{(1/\phi) + (d_p/k_f)(h_c + h_{rs})} + \frac{\gamma}{K} \right]}, \quad (1.30)$$

where h_{rf} and h_{rs} is the radiation heat transfer coefficient in the void space (fluid) and solid, respectively. The numerical values of β , ϕ , and γ will be discussed further down. By neglecting the heat transfer through contact area h_c (a valid assumption for every use except extremely low pressures (Kunii and Smith, 1960)), the above equation can also be written as

$$\frac{k_e}{k_f} = \varepsilon \left(1 + \beta \frac{(2 - \varepsilon_r)}{\varepsilon_r + \frac{\varepsilon(1 - \varepsilon_r)}{2(1 - \varepsilon)}} Nu_f \right) + \frac{\beta(1 - \varepsilon)}{\left[\frac{1}{(1/\phi) + Nu_f} + \frac{\gamma}{K} \right]}, \quad (1.31)$$

with the radiation Nusselt number (Vortmeyer, 1980)

$$Nu_f = \left[4\sigma T^3 \cdot \frac{\varepsilon_r}{(2 - \varepsilon_r)} \right] \cdot \frac{d_p}{k_f} = h_{rs} \frac{d_p}{k_f} \quad (1.32)$$

By combining Eq. (1.30) through (1.32) one can obtain the relations for the radiation heat transfer coefficients

$$h_{rf} = \frac{4\sigma T^3}{\left[1 + \frac{\varepsilon}{2(1 + \varepsilon)} \cdot \frac{(1 - \varepsilon_r)}{\varepsilon_r} \right]}, \quad (1.33)$$

and

$$h_{rs} = 4\sigma T^3 \cdot \frac{\varepsilon_r}{(2 - \varepsilon_r)}. \quad (1.34)$$

Now, one need to find the numerical values of the quantities β , ϕ , and γ . Fig. 1.15 and 1.16 below visualizes Kunii and Smith's model for heat transfer directions through loose- and close-packed beds.

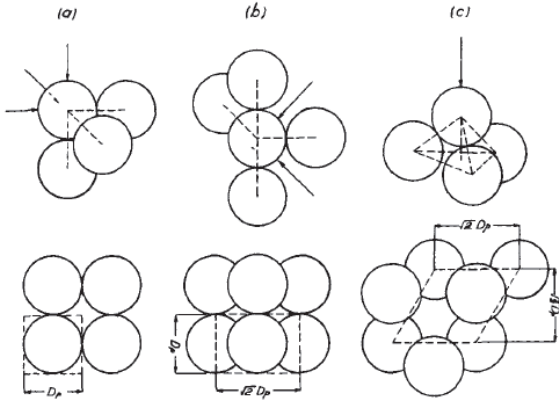


Fig. 1.15 - Heat transfer directions for loose packing of spheres (Kunii and Smith, 1960).

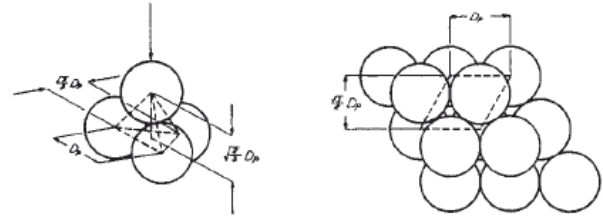


Fig. 1.16 - Heat transfer directions for close packing of spheres (Kunii and Smith, 1960).

The value of β for close spherical packing as shown in Fig. 1.16 above is then

$$\beta = \frac{\Delta L}{d_p} = \frac{1}{d_p} \cdot \frac{1}{3} \left[\left(\frac{2}{9} \right)^{\frac{1}{2}} + 1 + \left(\frac{3}{2} \right)^{\frac{1}{2}} \right] d_p = 0.895. \quad (1.35)$$

For the loosest packing the value of β should be unity, since the spheres are very far apart from one another. Hence, for loose packing, $\beta=1$. The value of γ depends upon l_s , and Kunii and Smith assume that it is a length of a cylinder having the same size as a spherical particle. Hence,

$$\gamma = \frac{l_s}{d_p} = \frac{1}{d_p} \cdot \left[\frac{\left(\frac{\pi}{6} d_p^2 \right)}{\left(\frac{\pi}{4} d_p^2 \right)} \right] = \frac{2}{3}. \quad (1.36)$$

In order to obtain the ϕ value ($\phi=l_f/d_p$), they state that the fraction of the total heat flux through the fluid near one contact point is given by

$$\frac{1}{n} = \frac{\pi x_0^2}{\pi R^2} = \sin^2 \theta_0. \quad (1.37)$$

with the parameters explained in Fig. 1.14. With this in mind, the one can derive the following expression for the heat flux

$$Q'' = \int_0^{\theta_0} dQ'' = \pi R k_f \Delta T \left(-\frac{K}{K-1} \right)^2 \left\{ \ln [K - (K-1) \cos \theta_0] - \frac{K-1}{K} (1 - \cos \theta_0) \right\}. \quad (1.38)$$

Equation (1.38) includes heat transfer through solid and filaments of fluid in series, thus the heat flux can also be described through the resistance of two steps:

$$Q'' = \frac{\pi (R \sin \theta_0)^2 \Delta T}{\frac{2R \left(\frac{2}{3} \right)}{k_s} + \frac{l_f}{k_f}}, \quad (1.39)$$

where $2R(2/3)=l_s$. Since $l_f=d_p \phi$ and $d_p=2R$, combining equations (1.38) and (1.39) gives

$$\phi_{tight\ or\ loose} = \frac{1}{2} \cdot \frac{\left(\frac{K-1}{K}\right)^2 \sin^2 \theta_0}{\ln[K - (K-1) \cos \theta_0] - \left(\frac{K-1}{K}\right) (1 - \cos \theta_0)} - \frac{2}{3K} \quad (1.40)$$

The above equation, however only applies for one single contact point. They argue (based on Fig. 1.15) that the number of contact points can be assumed as stated in Table 1.4 below.

Table 1.4 - Particle orientation (Kunii and Smith, 1960).

Orientation (ref. Fig. 1.15)	a)	b)	c)
Contact point	1	2	3
Area corresponding to one particle	$2d_p^2$	$2^{1/2}d_p^2$	$3^{1/2}d_p^2$
Number of directions	3	2	4

The cases of the loosest and tightest packing available should then be considered. As shown in Fig. 1.14, the derivation of Eq. (1.40) is based upon case a). Therefore, the approximate average number of contact points $n_{loose} = (n_a + n_b + n_c)$ for a loose bed of spherical particles should be

$$n_{loose} = \frac{1}{3} \left[1 + \left(2 \cdot \frac{d_p^2}{\sqrt{2}d_p^2} \cdot \frac{2}{3} \right) + \left(3 \cdot \frac{d_p^2}{\sqrt{3}d_p^2} \cdot \frac{4}{3} \right) \right] \approx 1.5. \quad (1.41)$$

The equivalent number of contact points for tight packing is then obtained in the same manner (ref. Fig. 1.16):

$$n_{tight} = \left(6 \cdot \frac{d_p^2}{\sqrt{3}/2 \cdot d_p^2} \right) \approx 4\sqrt{3}. \quad (1.42)$$

The most dense packing available is $\varepsilon=0.26$ and the most loose is $\varepsilon=0.476$ (Kaviany, 1995). Kunii and Smith (1960) argue that a packed bed can be considered a composite of these two extremes. They then approximate ϕ as

$$\phi = \phi_{tight} + (\phi_{loose} + \phi_{tight}) \frac{\varepsilon - 0.26}{0.476 - 0.26}; 0.26 < \varepsilon < 0.476. \quad (1.43)$$

To sum up the effective thermal conductivity model by Kunii and Smith (1960), the equations and parameters needed are given in Table 1.5 below.

Table 1.5 - Kunii and Smith model summarized

Effective thermal conductivity k_e	Eq. (1.30)
Radiation heat transfer h_{rr} and h_{rs}	Eq. (1.33) and (1.34)
Point contact ϕ	Eq. (1.43) and (1.40)
Contact area (flattening) h_c	N/A
Packing structure	Loose Dense

β	1	0.895
γ	2/3	0.67
n	1.5	$4\sqrt{3}$

Note that the heat transfer h_c due to flattening of particles (contact area) is neglected. The Kunii and Smith model should give good predictions of the effective thermal conductivity, but due to the neglecting of flattened contact area heat transfer, the values might be lower than the real case. Another popular type III model which takes this into consideration however, is the Zehner-Bauer-Schlünder model.

1.7.2 Model of Zehner, Bauer and Schlünder (1970-1978)

The model of Zehner and Schlünder (1970), which takes into consideration a unit cell of either perfectly spherically shaped or deformed particles, is widely used within literature and has been verified to give good estimations of the effective thermal conductivity for a wide range of solid-fluid conductivity ratios (Kandula, 2011). This model was later extended by improving the deformation factor for spheres (Hsu et al, 1994) and by adding heat transfer expressions related to contact area and radiation (Bauer and Schlünder, 1978). The combination of above mentioned models are more commonly known as the Zehner-Bauer-Schlünder (ZBS) model. As seen from Table 1.6 the model looks very promising; it takes in to account a lot of parameters, and is as previously mentioned valid for a large range of conductivity ratios.

Table 1.6 - Zehner/Bauer/Schlünder limiting relations and secondary parameters.

Author	Year	Type	Limiting relations							Secondary parameters				
			1	2	3	4	5	6	7	Press.	Rad.	Form	Distr.	Cont.
Zehner/Bauer/Schlünder	1970-1978	IIIa	Y	Y	Y	Y	Y	Y	0.294	Y	Y	Y	Y	Y

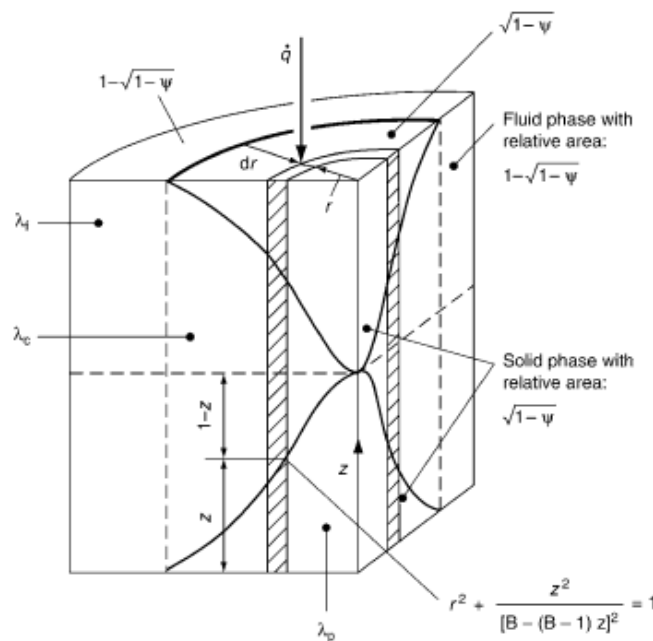


Fig. 1.17 - The unit cell from the ZBS model (VDI Heat Atlas, 2010).

Fig. 1.17 shows the unit cell as proposed by the ZBS model. Note that the notations from the figure differ from the notations used in this work. To avoid any misconception, the equivalent parameters are listed in Table 1.7 below.

Table 1.7 - Corresponding notations.

Zehner/ Bauer /Schlünder		This work
Ψ	→	ε
λ_f	→	k_f
λ_p	→	k_s
λ_c	→	k_c
\dot{q}	→	\dot{Q}_s''

The main idea of this model is to repair the incorrect assumption of parallel heat flux lines by using fictitious non-spherical particles to simulate the thermal behavior of spherical ones. The main characteristic is thus the deformation factor B which is modeled according to the equation (ref. Fig. 1.17) (Zehner and Schlünder, 1970)

$$r^2 = \frac{z^2}{[B - (B - 1)z]^2}, \quad (1.44)$$

With r and z as the radius and z -axis in the cylindrical coordinate system. For $B=1$, Eq. (1.44) describes the surface of a sphere. $B < 1$ gives something like prolonged needles, and with $B > 1$ one obtains cylinder-like bodies. The deformation factor gives the opportunity to change the width of the voids in the area around contact points. In this manner, the error caused by the assumption of parallel heat flux lines can be compensated for (to a certain extent). From Fig. 1.17, one can define the porosity of the unit cell as (Zehner and Schlünder, 1970)

$$\varepsilon = 1 - \frac{V_p}{V_{uc}} \sqrt{1 - \varepsilon}, \quad (1.45)$$

where V_p is the volume of the deformed particle and V_{uc} is the volume of the cylinder wrapped in the unit cell. Rearranging Eq. (1.45) gives

$$\varepsilon = 1 - \left(\frac{V_p}{V_{uc}} \right)^2. \quad (1.46)$$

It is then possible to compute V_p/V_{uc} from Eq. (1.44) by a volume integral, thus giving the following relationship between porosity ε and the deformation factor B :

$$\varepsilon = 1 - \left\{ \frac{B}{(B - 1)^3} [3 - 4B + B^2 + 2 \ln B] \right\}^2. \quad (1.47)$$

B can be explicitly computed from the porosity, and a good approximation of Eq. (1.46) is then given by (Zehner and Schlünder, 1970)

$$B = C \left(\frac{1 - \varepsilon}{\varepsilon} \right)^m, \quad (1.48)$$

with $m=10/9$ and the shape-factor $C=1.25$. The parameters C and m allows for fitting of particles other than spherical ones. They gave parameters for spheres, cylinders and broken particles from experimental data given in Table 1.8.

Table 1.8 - Shape factors

Particle shape	C
Spheres	1.25
Broken particles	1.4
Cylinders	2.5

It can be discussed whether Eq. (1.48) gives an accurate approximate for Eq. (1.47), and this was pointed out by Hsu et al. (1994). Based on a least square procedure the found that Eq. (1.48) with $C=1.364$ and $m=1.055$ resulted in a more accurate prediction for spherical particles.

That aside; with the deformation factor known, the conductivity of the core of the unit cell k_c can be calculated from integrating over the parallel heat flux lines. By setting the conductivity of the whole mixture equal to that of the unit cell, one can thus obtain the formula for the ratio of the effective stagnant thermal conductivity to fluid conductivity (see Fig. 1.17)

$$\frac{k_e}{k_f} = 1 - \sqrt{1 - \varepsilon} + \sqrt{1 - \varepsilon} K_c \quad (1.49)$$

with $K_c = k_c/k_f$. The core-fluid conductivity ratio K_c is then given by (Zehner and Schlünder, 1970)

$$K_c = \frac{2}{N} \left[\frac{B}{N^2} \cdot \frac{K-1}{K} \cdot \ln\left(\frac{K}{B}\right) - \frac{B+1}{2} - \frac{B-1}{N} \right], \quad (1.50)$$

where

$$N = \left(1 - \frac{B}{K}\right). \quad (1.51)$$

Equations (1.48) through (1.51) are together known as the Zehner and Schlünder model. It does not account for secondary parameters and is a function of only the primary parameters (ε, k_s and k_f) and the deformation factor B . The given model was then extended, accounting for the secondary parameters presented in Eq. (1.20). The extension based on the figure of the unit cell (Fig. 1.17) is given as (Zehner and Schlünder, 1972); (Bauer and Schlünder, 1978):

$$\frac{k_e}{k_f} = (1 - \sqrt{1 - \varepsilon}) \varepsilon \left[\frac{1}{\left(\varepsilon - 1 + \frac{1}{K_g}\right)} + K_r \right] + \sqrt{1 - \varepsilon} [\varphi K + (1 - \varphi) K_c], \quad (1.52)$$

with

$$K_c = \frac{2}{N} \left(\frac{B(K + K_r - 1)}{N^2 K_g K} \cdot \frac{K - 1}{K} \cdot \ln \frac{K + K_r}{B[K_g + (1 - K_g)(K + K_r)]} \right. \\ \left. + \frac{B + 1}{2B} \left[\frac{K_r}{K_g} - B \left(1 + \frac{1 - K_g}{K_g} K_r \right) \right] - \frac{B - 1}{N K_g} \right), \quad (1.53)$$

$$N = \frac{1}{K_g} \left(1 + \frac{K_r - B K_g}{K} \right) - B \left(\frac{1}{K_g} - 1 \right) \left(1 + \frac{K_r}{K} \right), \quad (1.54)$$

and

$$B = C \left(\frac{1 - \varepsilon}{\varepsilon} \right)^{10/9} \cdot f(\zeta). \quad (1.55)$$

The contribution due to radiation is

$$K_r = \frac{k_r}{k_f} = \frac{4\sigma T^3 d_p}{\left(\frac{2}{\varepsilon_r} - 1 \right)} \cdot \frac{1}{k_f}, \quad (1.56)$$

while the gaseous conduction related to the Knudsen regime is given by:

$$K_g = \frac{k_g}{k_f} = \frac{1}{(1 + l/d_p)}. \quad (1.57)$$

For beds packed with particles of various sizes, a mean particle size

$$\bar{d}_p = \left[\sum_{i=1}^n \left(\frac{V_i}{V} \cdot \frac{1}{d_{pi}} \right) \right]^{-1}, \quad (1.58)$$

should be used. In Eq. (1.58), V_i/V is the volume of the i th particle size fraction V_i referred to the total analyzed particle volume V . The letter d_{pi} is the average particle diameter of fraction i . In the case of non-spherical particles, the diameter of a sphere of equal volume as the particle should be used (neglecting inner porosity), in place of d_p and d_{pi} . The effective conductivity of thermal radiation k_r , or in dimensionless form K_r , is given by equation (1.56). This is a general Damköhler radiation term (Damköhler, 1937)

$$k_r = 4\sigma F \bar{T}^3 x_r, \quad (1.59)$$

where F is a function the optical properties of the surfaces in the mixture (in this case the emissivity ε_r of the solid), σ is the Stefan Boltzmann constant, \bar{T} is the average bed temperature and x_r is some characteristic dimension of the system (in this case the porosity ε and particle diameter d_p). The temperature \bar{T} is actually a result of an averaging assumption that $((T_1^4 - T_2^4)/(T_1 - T_2)) \approx 4\bar{T}^3$, which is only valid as long as the steady state temperature drop ΔT across the unit cell is much smaller than the average bed temperature, i.e. $\Delta T \ll \bar{T}$.

The local version of Eq. (1.56) has been integrated over the unit cell, in order to account for the variation in distance between particles. Hence, this includes a correction for the thermal radiation exchange between adjacent particles. The section of the unit cell representing the void (fluid) is $1 - \sqrt{1 - \varepsilon}$. In order to give a true estimate of the radiation paths through the void, the particle diameter d_p has been divided by the bed porosity ε (Zehner and Schlünder, 1972).

Equation (1.57) denotes the pressure dependence. It relates the thermal conductivity of a gas-filled gap k_g to the fluid conductivity k_f . In reduced form this gives $K_g = k_g/k_f$, hence, if the fluid is not a gas, $K_g \rightarrow 1$. In Eq. (1.57), l/d_p is the Knudsen number, with l being the modified mean free path of gas molecules. The gap size between particles is here represented by the particle diameter d_p . In order to account for the change in distance between particles, the local version Eq. (1.57) was integrated over the particle radius (Schlünder, 1981). The mean free path of the molecules l is calculated from the following formula (Möllenkopf and Martin, 1982):

$$l = 2 \frac{2 - a_t}{a_t} \left(\frac{2\pi\tilde{R}T}{M_g} \right)^{1/2} \cdot \frac{k_f}{p(2C_{pf} - \tilde{R}/M_g)} \quad (1.60)$$

where the thermal accommodation coefficient a_t , which is a measure of the effectiveness of energy transfer when gas molecules collide with the solid surface, is best given by (Song and Yovanovich, 1987)

$$a_t = \exp \left[-0.57 \left(\frac{T_s - T_0}{T_0} \right) \right] \left(\frac{M^*}{6.8 + M^*} \right) + \frac{2.4M}{(1 + M)^2} \left\{ 1 - \exp \left[-0.57 \left(\frac{T - T_0}{T_0} \right) \right] \right\} \quad (1.61)$$

with

$$M^* = \begin{cases} M_g & \text{for monoatomic gases} \\ 1.4M_g & \text{for diatomic gases} \end{cases} \quad (1.62)$$

$$M = M_g/M_s$$

In equations (1.60) through (1.62), T_s is the temperature of the solid surface, $T_s = 273,15\text{K}$, p is the pressure of the gas, \tilde{R} is the universal gas constant, C_{p_g} is the gas thermal heat capacity under constant pressure, while M_g and M_s is the molecular weight of gas and solid, respectively.

In order to describe the influence of particle shape, the deformation factor B from Eq. (1.48) has been corrected with a distribution factor $f(\zeta)$ (see Eq. (1.55)). This distribution function is then

$$f(\zeta) = 1 + 3\zeta, \quad (1.63)$$

with the distribution parameter

$$\zeta = \left\{ \frac{\sum_{i=1}^n \left(\frac{V_i}{V} \cdot \frac{1}{d_{pi}^2} \right)}{\left(\sum_{i=1}^n \left(\frac{V_i}{V} \cdot \frac{1}{d_{pi}} \right) \right)^2} - 1 \right\}^{1/2} \quad (1.64)$$

However, experimental investigations on beds packed with poly-dispersed media show that the thermal conductivity can be calculated accurately with a distribution function equal to unity (Tsotsas and Schlünder, 1991), i.e.

$$f(\zeta) = 1. \tag{1.65}$$

In Eq. (1.52), φ is the flattening coefficient modeling the heat transfer through flattened contact areas between adjacent particles, and values for this are given in Table 1.9 below.

Table 1.9 - Flattening coefficients obtained by Zehner and Bauer (Schlünder, 1981).

Particle shape	φ	Material
Spheres	0.0013	Steel
	0.0077	Ceramic
	0.0253	Copper
Broken particles	0.001	
Cylinders	?	

Summing up the model of Zehner, Bauer and Schlünder, it takes into account particle distribution and shape, as well as heat transfer through flattening of contact points. This shows promise regarding the experimental investigations of this work. This study will make use of both broken and cylindrically shaped particles as well as spheres (glass beads) and it is therefore expected that the ZBS model gives a very precise prediction of the effective thermal conductivity. A brief summary of the model is shown in Table 1.10 below.

Table 1.10 - ZBS model summarized

Total effective thermal conductivity k_e	Eq. (1.52)		
Core thermal conductivity K_c	Eq. (1.53) and (1.54)		
Radiation heat transfer K_r	Eq. (1.56)		
Pressure dependence K_g	Eq. (1.57), (1.60), (1.61) and (1.62)		
Particle deformation factor B	Eq. (1.55)		
Particle diameter d_p	Eq. (1.58)		
Particle distribution $f(\zeta)$	Eq. (1.65)		
Particle shape and contact area (flattening)	C	φ	Material
Spheres	1.5	0.0013	Steel
		0.0077	Ceramic
		0.0253	Copper
Broken	1.4	0.001	
Cylinders	2.5		

The ZBS model was, among other models, recently compared with a newer model (van Antwerpen et al, 2010) proposed by the IAEA-TECDOC-1163 (2000). This new model is based on the ZBS model and will be explained in the next section.

1.7.3 Model proposed by IAEA-TECDOC-1163 (2000)

The IAEA-TECDOC-1163 (2000) model utilizes the unit cell of the original Zehner and Schlünder (1970) model (Fig. 1.17; Eqs. (1.48)-(1.51)) and combines this with other models for contact area (Kaviany, 1995) and radiation (Breitbach and Barthels, 1980) heat transfer.

Table 1.11 - Limiting relations and secondary parameters for the IAEA-TECDOC-1163 model

Author	Year	Type	Limiting relations							Secondary parameters				
			1	2	3	4	5	6	7	Press.	Rad.	Form	Distr.	Cont.
IAEA-TECDOC-1163	2000	IIIa	Y	Y	Y	Y	Y	Y	0.250	N	Y	Y	Y	Y

Table 1.11 shows the parameter inputs of this model. Fulfilling every limiting relation and accounting for all secondary parameters except one shows that this might be a model applicable for various purposes. The dimensionless effective thermal conductivity (k_e/k_f) is given by the Zehner and Schlünder model from equations (1.48) through (1.51) with the following terms added (IAEA-TECDOC-1163, 2000):

The radiation heat transfer given by

$$K_r = \frac{k_r}{k_f} = \frac{4\sigma T^3 d_p}{k_f} \left\{ \varepsilon \cdot [1 - \sqrt{1 - \varepsilon}] + \frac{\sqrt{1 - \varepsilon}}{\frac{2}{\varepsilon_r} - 1} \cdot \frac{B + 1}{B} \cdot \frac{1}{1 + \frac{1}{(2/\varepsilon_r - 1)\Lambda}} \right\}, \quad (1.66)$$

where the dimensionless solid conductivity is $\Lambda = k_s/4\sigma\bar{T}^3 d_p$ and the heat transfer due to contact area flattening is

$$\frac{k_c}{k_f} = K \left[\frac{3(1 - \mu_s^2)}{4E_s} fR \right]^{1/3} \cdot \frac{1}{0.531 \cdot S} \left(\frac{N_A}{N_L} \right), \quad (1.67)$$

with the external collinear force f related to the external pressure through (Kaviany, 1995)

$$f = p \frac{S_F}{N_A}. \quad (1.68)$$

Equations (1.67) and (1.68) were obtained on the basis of three different spherical arrangements (Table 1.12; Fig. 1.18), and are a function of the solid elastic properties Poisson ratio, μ_s , and Young's modulus, E_s . N_A and N_L are the number of particles per unit area and length, respectively. S_F is also given in Table 1.12.

Table 1.12 - Structural parameters for different packing of spheres (Kaviany, 1995).

Parameter	Simple cubic	Body-centered cubic	Face-centered cubic
ε	0.476	0.32	0.26
N_L	$\frac{1}{2R}$	$\frac{\sqrt{3}}{2R}$	$\frac{\sqrt{3/8}}{R}$
N_A	$\frac{1}{4R^2}$	$\frac{3}{16R^2}$	$\frac{1}{2\sqrt{3}R^2}$
S	1	0.25	$\frac{1}{3}$
S_F	1	$\frac{\sqrt{3}}{4}$	$\frac{1}{\sqrt{6}}$
Number of contact points	6	8	12
Points used in the heat flow analysis	2	8	6

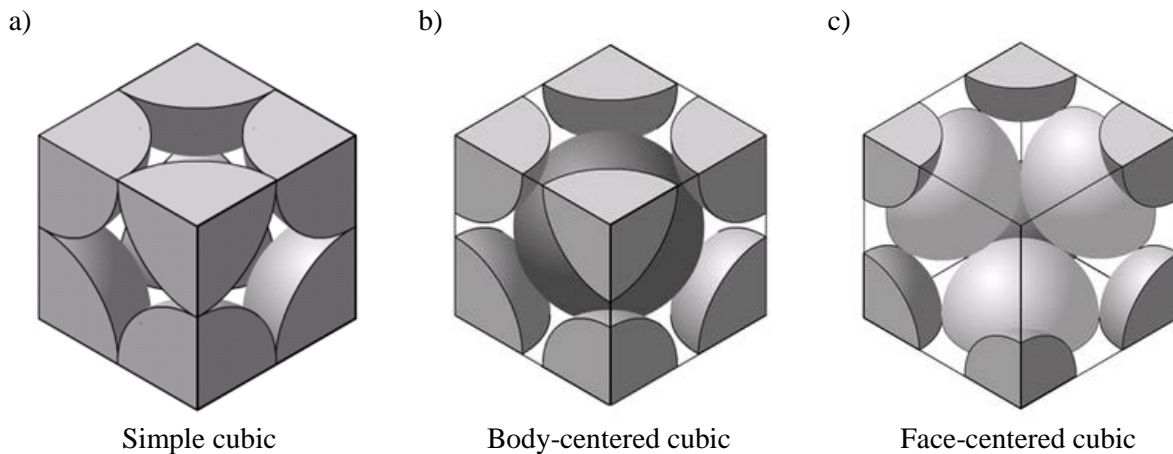


Fig. 1.18 - The three different packing arrangements applied for the derivation of the model.

The IAEA model should give good results when applied for spherical packing. If the contact area equation also manages to predict accurately with broken or cylindrical particles, it is expected that this model should perform well; it takes into account all secondary parameters from Eq. (1.20) except pressure dependence and distribution. For this study, pressure dependence is not really relevant, since all experiments are to be performed at constant pressure. The distribution function (1.65) can be set equal to unity, and as previously discussed in section 1.7.2, and the model will still perform well.

A summary of the IAEA-TECDOC-1163 model is given in Table 1.13.

Table 1.13 - IAEA-TECDOC-1163 model summarized

Total effective thermal conductivity k_e	Eq. (1.49)
Core thermal conductivity K_c	Eq. (1.50) and (1.51)
Radiation heat transfer K_r	Eq. (1.66)
Pressure dependence	N/A
Contact area heat transfer k_c	Eq. (1.67) ^A and (1.68) ^A
Particle deformation factor B	Eq. (1.48)
Particle diameter d_p	Eq. (1.58)
<hr/>	
Particle shape coefficients	C
Spheres	1.25
Broken	1.4
Cylinders	2.5

^AWith structural parameters given in Table 1.12

All models may prove to give good results for different applications. The ZBS - and IAEA models are expected to perform well over a large range of fluid to conductivity ratios. The model by Kunii and Smith should also perform well, although it does not account for all secondary parameters. Non-radiation models such as those by Maxwell and Krupiczka may give good predictions when the temperature is sufficiently low and radiation heat transfer can be neglected. It is the goal of this work to generate as much experimental data as possible, in order to find a model that will accurately predict the effective thermal conductivity of various hydrogen adsorption substances filled with different gases. All previously described models are now compared together (Fig. 1.19) for a bed filled with spherical particles with a porosity ε of 0.4 and air as the fluid medium.

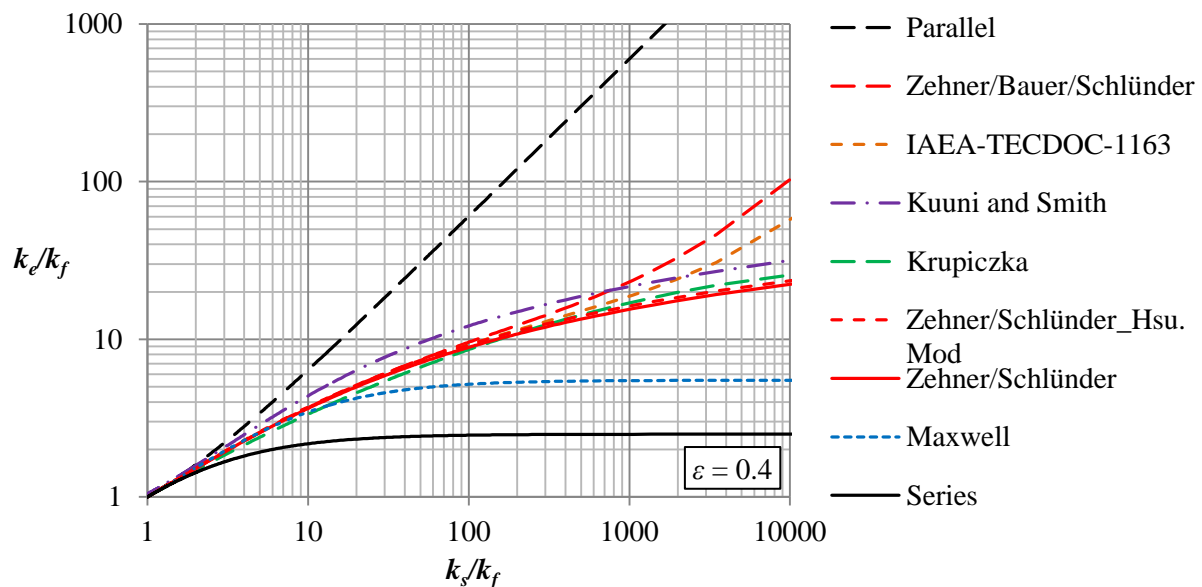


Fig. 1.19 - Comparison of models for a random loose packing of spherically shaped particles.

As Fig. 1.19 displays, all models go through the point 1.1, thus satisfying the limiting relation number three ($k_s = k_f = k_e$; Eq. (1.20)). The lower and upper bound is provided by the series and parallel

arrangement, as it should. If one considers the original Zehner and Schlünder model to be the most accurate, the model of Maxwell gives low values for $k_s/k_f > 10$. The Kunii and Smith model on the other hand, seems to slightly overpredict the thermal conductivity throughout the whole spectrum plotted. This may be due to their radiation term not working correctly. As can be seen from the figure (1.19) the radiation term of the IAEA-TECDOC-1163 and ZBS models starts to become apparent at approximately $k_s/k_f = 120$. This is because a solid-fluid conductivity-ratio $K > 100$ only occurs at very high temperatures, and thus the radiation starts to come into effect.

For applications with solid-matrix porous media, however, the above mentioned models will not suffice. Relatively recent, some new models concerning continuously connected solid structure media (like metal foam) have been developed (Hsu et al, 1994); (Boomsma and Poulikakos, 2000). These models will be presented in the next section.

1.8 Effective stagnant thermal conductivity of solid matrix porous media

A solid matrix structure, like open cell metal foam, can make a significant contribution to the effective thermal conductivity of a packed bed, thus allowing for more efficient charging and discharging of a hydrogen-filled tank. Not many models exist for foam-like materials, and it remains to be seen if the models can give a good enough prediction for metal foam filled with granular porous media. If not, a new model shall be developed.

1.8.1 Hsu's phase-symmetry model (1994)

The phase-symmetry model by Hsu et al. (1994) is based on the method of Zehner and Schlünder (1970). However, in this approach both the solid and fluid phase is assumed continuously connected and having a phase-symmetry. For this reason, the Zehner and Schlünder equation for effective thermal conductivity (Eq. (1.49)) cannot be used because the expression is not symmetric with respect to the two phases. Hsu et al. (1994) therefore sketch a new unit cell given in Fig. 1.20 below.

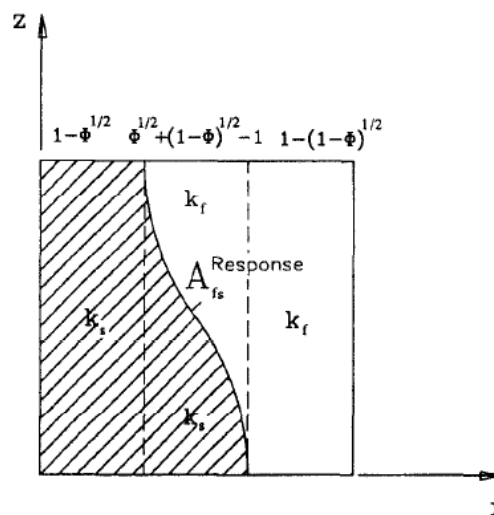


Fig. 1.20 - Unit cell for the phase-symmetric model (Hsu et al, 1994).

Note that they use Φ for porosity instead of ε (this work). As displayed by the figure, Hsu et al. (1994) divides the unit cell into three layers: layer one consisting of pure solid, layer two consisting of a

symmetric solid-fluid composition, and layer three which is pure fluid. They then give a new function for the reduced effective thermal conductivity k_e based on Eq. (1.49) and Fig. 1.20:

$$\frac{k_e}{k_f} = (1 - \sqrt{1 - \varepsilon}) + (1 - \sqrt{\varepsilon})K + (\sqrt{1 - \varepsilon} + \sqrt{\varepsilon} - 1)K_{sf}, \quad (1.69)$$

where K_{sf} is the dimensionless equivalent thermal conductivity of the composite layer, which can be expressed as

$$K_{sf} = \frac{k_{sf}}{k_f} = \frac{b(1 - \lambda)}{(1 - \lambda b)^2} \ln\left(\frac{1}{\lambda b}\right) - \frac{b - 1}{1 - \lambda b}, \quad (1.70)$$

with $\lambda = k_f/k_s$. The solid-fluid interface, as a function of the coordinate system parameters z and x and the deformation factor b , is given as

$$x + \frac{z}{b - (b - 1)z} = 1. \quad (1.71)$$

By setting the volumetric fraction of the solid in the sandwiched layer equal to the integral over Eq. (1.70) the obtained the following relationship between ε and b

$$\frac{\sqrt{\varepsilon} - \varepsilon}{\sqrt{1 - \varepsilon} + \sqrt{\varepsilon} - 1} = \frac{b}{(1 - b)}(b - 1 - \ln b). \quad (1.72)$$

They then found a good approximation of the new deformation factor b , which can be expressed as

$$b = C \left(\frac{1 - \varepsilon}{\varepsilon} \right)^m \quad (1.73)$$

like before, but with $C=1$ and $m=0.9676$ giving the best fit with Eq. (1.72). Equation (1.73) satisfies the constraints of Eq. (1.72), $\varepsilon \rightarrow 0 \rightarrow b \rightarrow \infty$, and $\varepsilon \rightarrow 1 \rightarrow b \rightarrow 0$. Also, if $C=1$, then the constraint of ε being 0.5 when $b=1$ (sphere) is satisfied as well.

1.8.2 Boomsma and Poulikakos's metal foam model (2000)

The model for effective stagnant thermal conductivity inside metal foam (Boomsma and Poulikakos, 2000) showed that the phase-symmetry model of Hsu et al. (1994) gave somewhat high predictions, while the predictions of Boomsma-Poulikakos model were quite accurate, compared with various measurements. However, they later released a corrigendum-paper (Boomsma and Poulikakos, 2011) where they altered their model.

Their model is based on modeling the foam as a tetrakaidecahedron with cylindrical ligaments and cubic nodes, as visualized in figures 1.21 through 1.23 (Boomsma and Poulikakos, 2000).

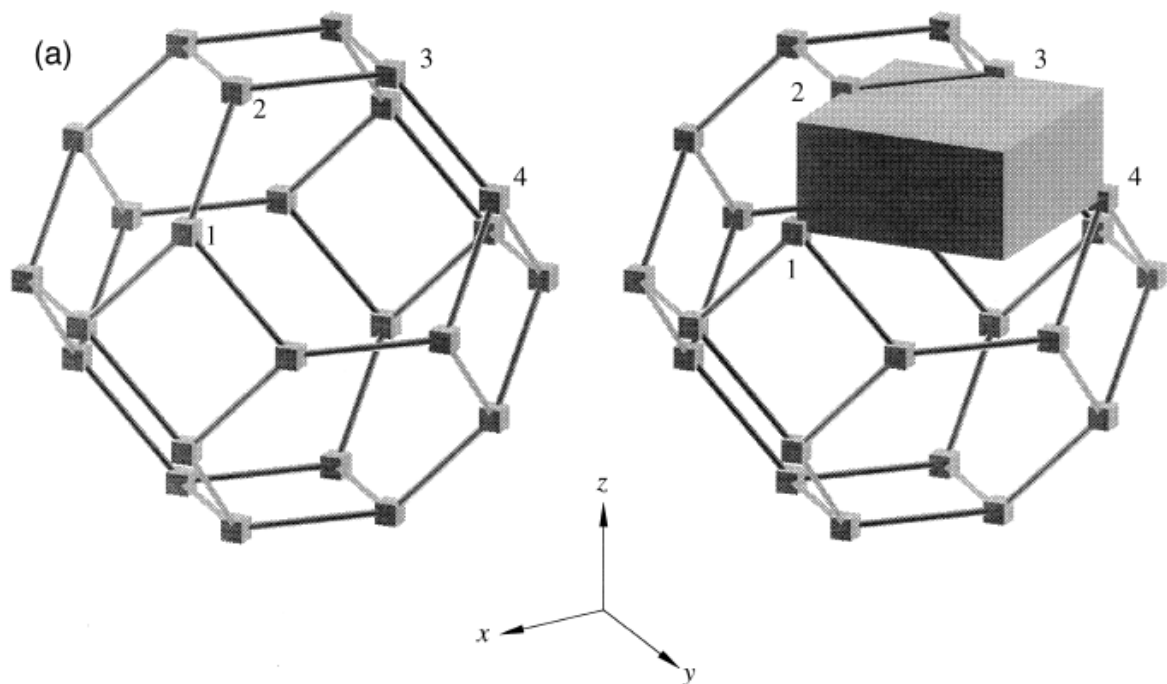


Fig. 1.21 - Their visualization of the foam structure. To the right: the unit cell between points 1-4 (Boomsma and Poulikakos, 2000)

Fig. 1.21 displays the foam structure, fig 1.23 displays the unit cell in relation to the image at the right side in Fig. 1.21, and Fig. 1.22 shows a photo of their metal foam. In Fig. 1.21, the Cartesian coordinate system is shown in order to explain the technical modeling of the foam shown in Fig. 1.23. In Fig 1.23, they denote the width of the node to r . However, this work will denote the node with w instead, so that it is not mistaken for radius. Furthermore, the length of each ligament L is denoted with subscripts A , B , C and D for each subsection of the unit cell (Fig 1.23). The radius of the ligaments is a . The unit cell consists of six squares and eight hexagons. This shape is the most likely shape that the foam will attain from the foam manufacturing process (Thompson, 1995), and selecting this as an approximate for the foam structure thus gives a good approximate on how the foam will look like as a whole.

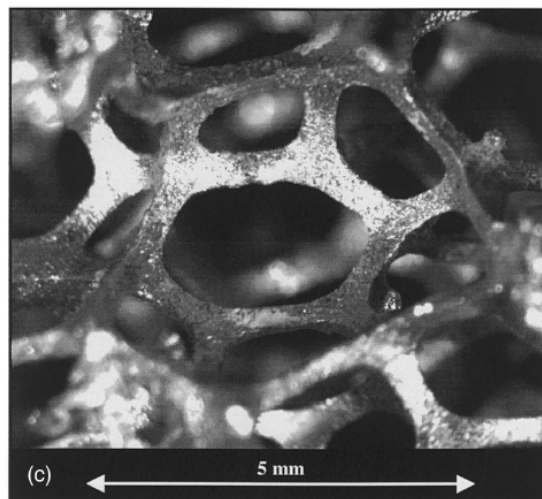


Fig. 1.22 - Picture of metal foam (Boomsma and Poulikakos, 2000).

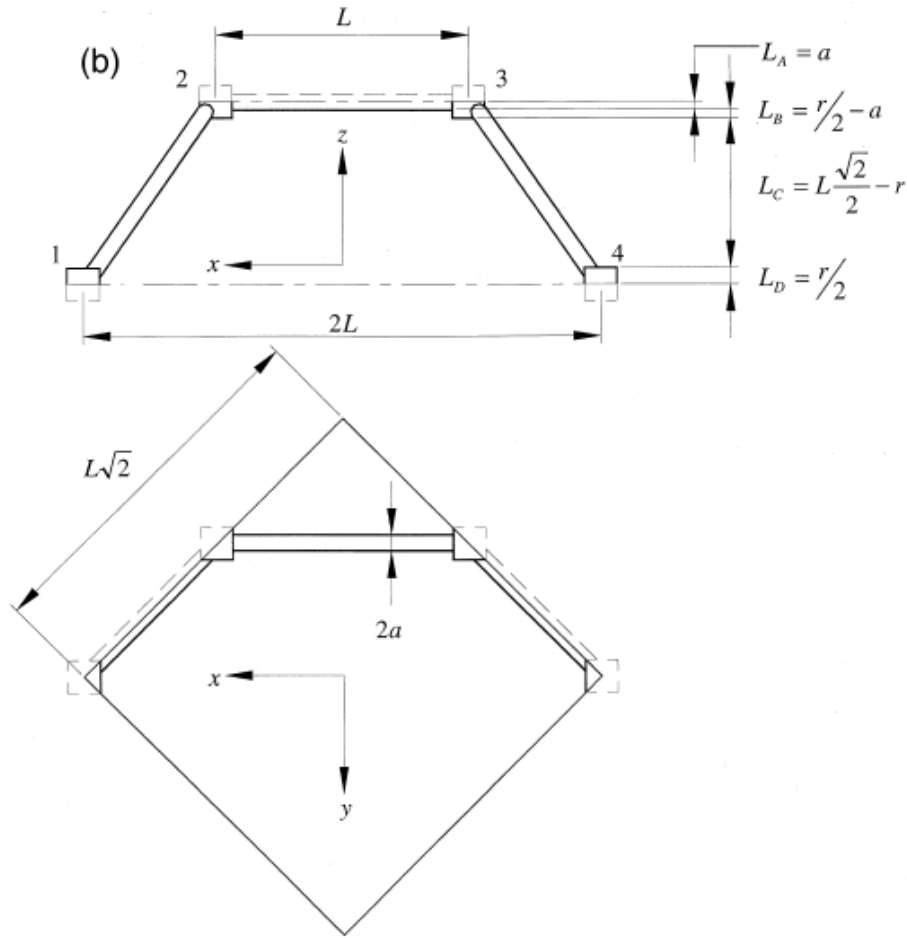


Fig. 1.23 - The metal foam modeled in a Cartesian coordinate system (Boomsma and Poulikakos, 2000).

Boomsma and Poulikakos (2000) choose one sixteenth of the tetrakaidecahedron as their unit cell, because this feature holds all geometric information on the structure. From Fig. 1.23, the length of the rectangular unit cell in the z -direction is

$$L_{uc} = L \frac{\sqrt{2}}{2}, \quad (1.74)$$

The two other variables, a and w , divide the cell into four different sections from top to bottom (z -direction). The first section, A , have a height of a . This is because the other half of this ligament belongs to the unit cell above. Further down, in the B -section, the height of this section is $w/2 - a$. Proceeding to section D , the height is the half of one node, $w/2$, because half the node belong to the unit cell below. Finally, the height for section C is the difference between the total unit cell height (Eq. 1.74) and sum of all the other sections. Hence,

$$L_C = L_{uc} - (L_A + L_B + L_D), \quad (1.75)$$

and

$$L_C = L \frac{\sqrt{2}}{2} - \left[a + \left(\frac{r}{2} - a \right) + \frac{r}{2} \right] = L \frac{\sqrt{2}}{2} - r. \quad (1.76)$$

Having defined these heights for the different subsections one can simply multiply the area of each section in the x-y-plane (see Fig. 1.22, bottom) by their respective heights in order to find the volume V of each section :

$$V_A = 2aL^2. \quad (1.77)$$

$$V_B = (w - 2a)L^2. \quad (1.78)$$

$$V_C = 2 \left(\frac{1}{2} L \sqrt{2} - w \right) L^2. \quad (1.79)$$

$$V_D = rL^2. \quad (1.80)$$

They then introduce a set of non-dimensional parameters. With the dimensionless parameters $e=w/L$ and $g=a/L$, they then calculate the volume of the unit cell occupied by solid as (Boomsma and Poulikakos, 2000); (Boomsma and Poulikakos, 2011)

$$V_{A,s} = \left[e^2 + \frac{1}{2} g \pi (1 - e) \right] g L^3. \quad (1.81)$$

$$V_{B,s} = \left(\frac{1}{2} e - g \right) e^2 L^3. \quad (1.82)$$

$$V_{C,s} = (1 - e\sqrt{2}) \pi g^2 L^3. \quad (1.83)$$

$$V_{D,s} = \frac{1}{4} e^3 L^3. \quad (1.84)$$

By substituting the dimensionless parameters e and g also into equations (1.77) through (1.80), one can define the porosity by

$$\varepsilon = 1 - \frac{V_s}{V} = 1 - \left(\frac{\sum_{n=A}^{n=D} V_{n,s}}{\sum_{n=A}^{n=D} V_n} \right) = \quad (1.85)$$

$$1 - \frac{\sqrt{2}}{2} \left[g e^2 + \frac{1}{2} \pi g^2 (1 - e) + e^2 \left(\frac{1}{2} e - g \right) + \pi g^2 (1 - e\sqrt{2}) + \frac{1}{4} e^3 \right]$$

Solving Eq. (1.85) in terms of g gives (Boomsma and Poulikakos, 2011)

$$g = \sqrt{\frac{\sqrt{2} [2 - (3\sqrt{2}e^3/4) - 2e]}{\pi(3 - 2e\sqrt{2} - e)}}. \quad (1.86)$$

In order to determine the effective conductivity of the unit cell, the thermal conductivity is then averaged over each section as

$$k_n = \frac{V_{n,s}k_s + (V_n - V_{n,s})k_f}{V_n} \quad (1.87)$$

where n denotes the sections A , B , C or D , respectively. Based on the Fourier law of heat conduction (Eq. 1.2) in the z -direction, through a series of four sections, the effective thermal conductivity of the unit cell yields

$$k_e = \frac{L_A + L_B + L_C + L_D}{(L_A/k_A) + (L_B/k_B) + (L_C/k_C) + (L_D/k_D)}. \quad (1.88)$$

One can then obtain the effective thermal conductivity by substituting for section lengths L_n , each of the thermal conductivities k_n , and the positive solution for g , and then fitting the parameter e on the basis of experimental data. However, this expression will be rather long and untidy. Therefore, it seems more appropriate to introduce the simplifying notations (Boomsma and Poulikakos, 2000); (Boomsma and Poulikakos, 2011)

$$U_A = \frac{4g}{2e^2 + \pi g(1-e)k_s + [4 - 2e^2 - \pi g(1-e)]k_f}. \quad (1.89)$$

$$U_B = \frac{(e-2g)^2}{e^2(e-2g)k_s + [2e-4g-e^2(e-2g)]k_f}. \quad (1.90)$$

$$U_C = \frac{\sqrt{2} - 2e}{\sqrt{2}\pi g^2 k_s + (2 - \sqrt{2}\pi g^2)k_f}. \quad (1.91)$$

$$U_D = \frac{2e}{e^2 k_s + (4 - e^2)k_f}. \quad (1.92)$$

Then, the solution for the effective thermal conductivity yields

$$k_e = \frac{\sqrt{2}}{2(U_A + U_B + U_C + U_D)}. \quad (1.93)$$

The parameter e , which is actually equal to the radius of a node divided by the radius of a ligament, now works as a fitting parameter. This means that it can be applied for other types of foams having the same structure (i.e. smaller voids; same structure), by fitting the curve to the experimental data. Plotting this model versus the phase-symmetry model of Hsu et al. (1994) and the ZBS-model gives the predictions showed in Fig. 1.24 on the next page.

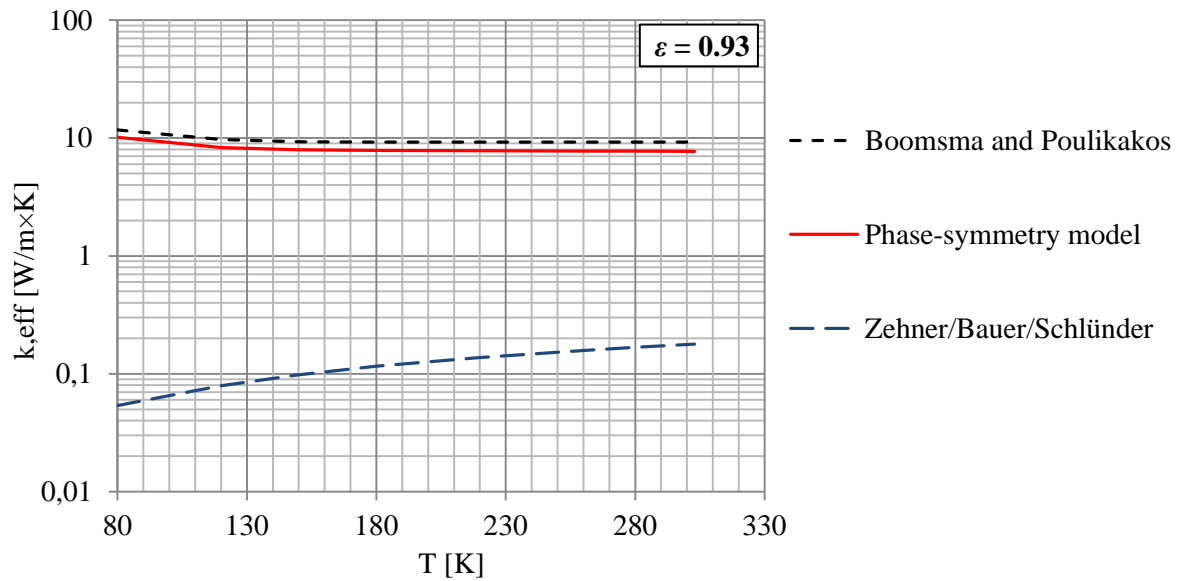


Fig. 1.24 - Comparison between solid matrix models and the ZBS model

In Fig. 1.24, the ZBS model is applied on spherical glass beads with air as fluid. The Boomsma-Poulikakos and phase-symmetry models are applied to aluminum foam filled with the same air and glass beads as applied with the ZBS model. The foam (aluminum Alloy 1100) has a porosity of 0.93. As seen from Fig. 1.24, both foam models suggest that a high-porosity aluminum foam should increase the magnitude of the effective thermal conductivity of a bed with glass beads with about a 100 times. This is a severe improvement and should be worth the reduction in permeability that the foam causes. This increase comes from the thermal conductivity of aluminum which is in the magnitude of $200 W/m \cdot K$ (NIST Chemistry Webbook) in room temperature compared to approximately $1 W/m \cdot K$ of the glass beads (Handbook of glass data, 1987).

Part 2 - Experiments

The experiments aim to determine the effective stagnant thermal conductivity of MOF material filled with gases such as nitrogen (N₂) and helium (He) as a function of temperature. Measurements were performed in the range of 243K < T < 423K, and 1bar < p < 1.5bar (absolute). In order to ensure the repeatability of measurements, each data point is measured three times, and each experiment (filling) was also repeated at least three times.

Effective stagnant thermal conductivity experiments were first conducted on glass beads, which worked as a reference material, with air and N₂ as the fluid phase. Second, experiments on the MOF materials Cu-btc (HKUST-1) and Fe-btc-xerogel were performed with both N₂ and He. Then, the glass beads were measured together with a high-porosity aluminum foam in order to examine the effect of the foam. The thermal conductivity of helium is quite similar to that of hydrogen, and thus the results with He will give a good read on what to expect when hydrogen is applied. The experiment setup used is a Hot Disk TPS 2500s.

2.1 Transient Plane Source method (TPS)

Measurements of thermal conductivity by the means of the TPS-method have previously been documented elsewhere (M. Gustavsson, 1994). This method is based on the use of a transiently heated plane sensor, which consists of an electrically conducting pattern in the shape of a double spiral, and this has been etched out of a thin nickel foil. This spiral is sandwiched between two thin samples of insulating material (Kapton/Mica). During a measurement, the sensor is placed carefully between two sample pieces, as Fig. 2.1 depicts.

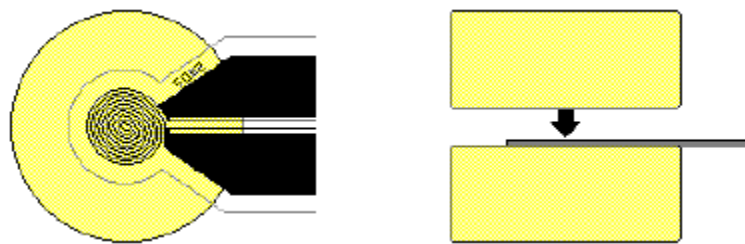


Fig. 2.1 - Sensor position between sample pieces

The solution of the thermal conductivity equation is based on the assumption that the Hot Disk sensor is located in an infinite medium, which means that the transient recording must be interrupted as soon as any influence from the outside boundaries of the two sample pieces is recorded by the sensor. Hence, the thermal penetration depth must not reach the outside boundaries of the sample pieces during transient recording. An estimation of how far this thermal wave has proceeded through the sample is called the probing depth. The probing depth is thus very important, and it is defined as (M. Gustavsson, 1994)

$$\Delta_p = 2\sqrt{\alpha t}, \quad (2.1)$$

where $\alpha = k/(\rho \cdot C_p)$ is the thermal diffusivity of the sample and t is the measuring time of the experiment. A consequence of this equation is that the distance from any point of the sensor to any point on the surface of the two sample pieces must exceed Δ_p if the total measuring time is t .

The theory of the TPS-method is developed under the assumption that the Hot Disk sensor consists of a certain number of concentric ring heat sources located in an infinitely large sample. A constant electric power is supplied to the sensor, creating an increase in temperature which is related to the sensor resistance $R(t)$ through the relation (M. Gustavsson, 1994)

$$R(t) = R_0\{1 + \vartheta[\Delta T_i + \Delta T_{av}(\tau)]\}. \quad (2.2)$$

In Eq. (2.2), R_i is the initial nickel resistance at the beginning of a recording, ϑ is the temperature coefficient of resistivity (TCR) of the nickel foil, and ΔT_i is the constant temperature difference that develops momentarily over the thin insulating layers covering the two sides of the sensor material. $\Delta T_{av}(\tau)$ is the temperature increase of the sample of the other side of the insulating layer. From Eq. (2.2), the temperature increase recorded by the sensor can be described by

$$\Delta T_i + \Delta T_{av}(\tau) = \frac{1}{\vartheta} \left[\frac{R(t)}{R_i} - 1 \right]. \quad (2.3)$$

The instant temperature difference ΔT_i becomes constant after a very short time (Δt_i). Then, Δt_i can be estimated as (M. Gustavsson, 1994)

$$\Delta t_i = \frac{\xi^2}{\alpha_i}, \quad (2.4)$$

where ξ is the thickness of the insulating layer and α_i is the thermal diffusivity of the layer material. The spatial average can be obtained through the equation (M. Gustavsson, 1994)

$$\Delta T_{av}(\tau) = \frac{P_0}{\pi^{3/2}(r \cdot k)} D(\tau). \quad (2.5)$$

In Eq. (2.5), P_0 is the power output from the sensor, r is the radius of the disk, k is the thermal conductivity of the sample and $D(\tau)$ is a dimensionless time dependent function defined

$$D(\tau) = \sqrt{\frac{t}{\theta}}; \theta = \frac{r^2}{k}. \quad (2.6)$$

In this equation (2.6), t is the time measured from the start of the transient recording, and θ is the characteristic time. The ratio total to characteristic time (TCT) need to be between 0.3 and 0.9 in order for the thermal diffusivity to be estimated correctly. Furthermore, the total temperature increase should be between 2K and 5K (M. Gustavsson, 1994). It is important that all measurements are kept within these constraints as well as the probing depth boundaries. In order to ensure that all measurement values for the effective thermal conductivity are kept within the given uncertainty range of 5% (M. Gustavsson, 1994), the above constraints must be satisfied. The thermal conductivity can be obtained by fitting the experimental data to the linear curve in Eq. (2.5).

2.2 Instrumentation

The Hot Disk TPS 2500S is supplied by the Swedish company Hot-Disk AB. It utilizes a small electrical power ($<2\text{W}$) to heat up a special shaped resistance, which is used as a temperature sensor simultaneously. The transient temperature rise of the sensor is recorded and analyzed by the TPS2500S. As result the material thermal diffusivity, specific heat capacity and thermal conductivity are determined. Different material types e.g. solid materials or powders can be measured. In this particular case different sorts of powders are used for the measurements.

Porous media is poured in to a sample holder, and a Hot Disk sensor is placed in between the samples.

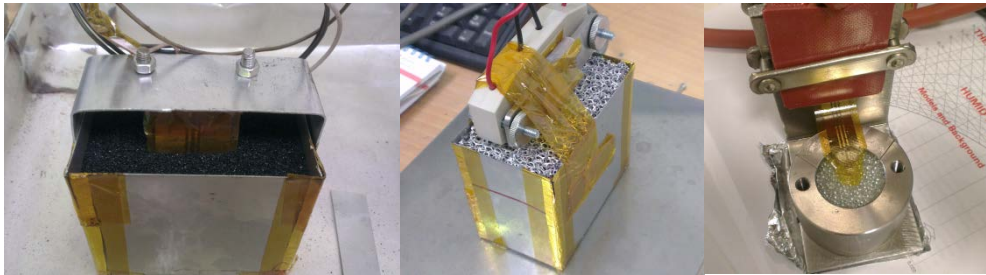


Fig. 2.2 - Sample holders

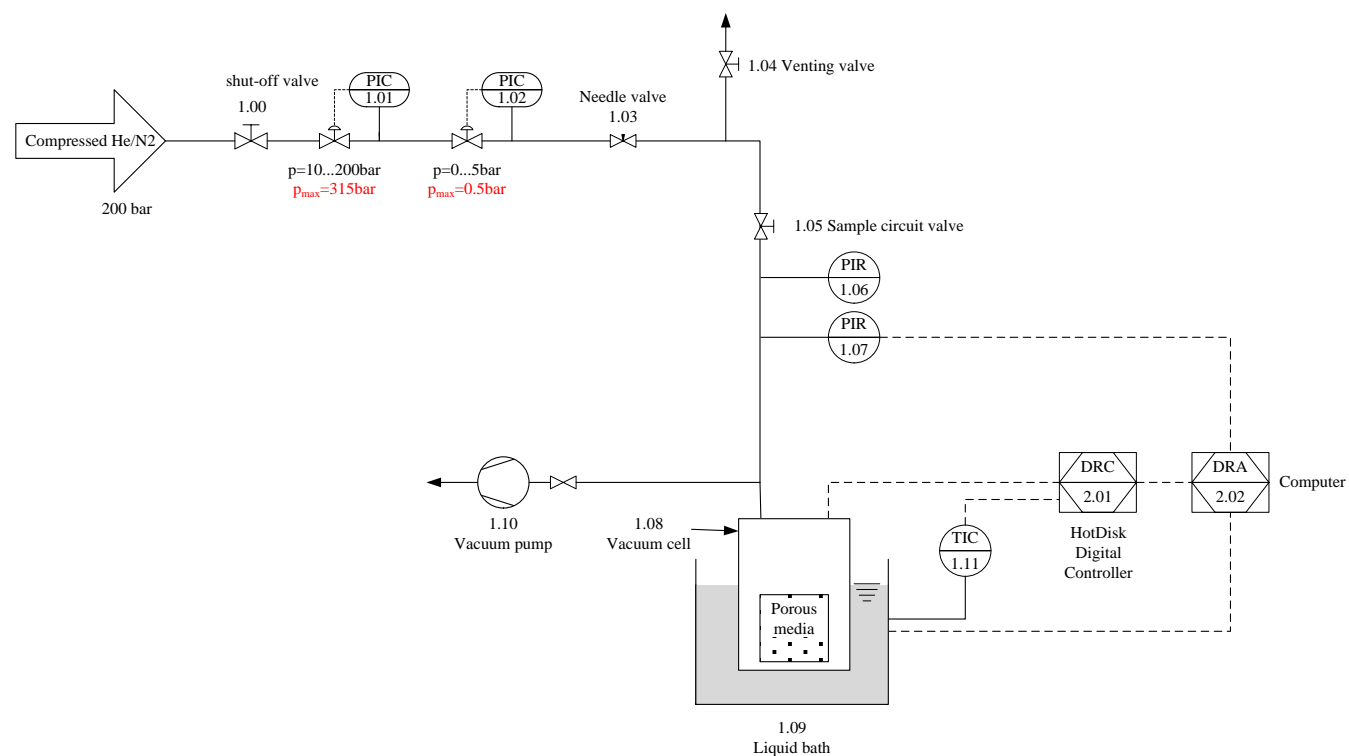
Different sample holders are used for different types of porous media. Graphic examples are given in Fig. 2.2. If room-temperature measurements with air are conducted, measurements can start as soon as the wires are connected to the sensor.



Fig. 2.3 - Vacuum cell

Most measurements however, are conducted at a range of $-30\text{ }^{\circ}\text{C} < T < 150\text{ }^{\circ}\text{C}$ with pressurized gas (He/N₂, at 0.1 ...0.4 bar relative). In order to do this, the sample holder, or sometimes the porous media itself, is lowered into the vacuum / pressure cell. This pressure cell is provided by Hot Disk AB as well and can withstand pressures of 1 bar relative and 200°C (see attachment B, in the Risk Assessment Report). Wires are then connected to the vacuum / pressure cell itself (from inside and outside), as shown in Figure 2.3. The lid is then sealed with a silicone gasket and if necessary with silicon vacuum grease and lowered into a thermal bath. The oil bath can stabilize at any given temperature between -35 and +200 degrees Celsius. After connecting the vacuum suction line with pressure sensors and the gas supply (Figure 2.4 or 2.5, next page) a final leakage test is necessary to guaranty safe and reliable measurements. Once thermal bath has stabilized, measurements can start.

2.2 Instrumentation



reference DIN EN ISO 10628



 NTNU – Trondheim Norwegian University of Science and Technology	P&ID conductivity rig			
	nr.	title	date	reference person
	1	P&ID conductivity rig	14.05.2013	Jan Georg Henriksen
DATUM	KOMPLETTER PFAD			
DATEINAME				
VISIODOCUMENT				
- confidential document -		Page	1 from 1	

Fig. 2.4 - P&ID flow chart of the thermal conductivity experimental setup.

As shown in Fig. 2.4 and Fig. 2.5, compressed gas (N₂ or He at approximately 200 bar) from a gas bottle is supplied after opening the shut-off valve (1.00). A maximal allowed pressure is set with the pressure regulators (max 1.4 bar (absolute)) (1.01) and (1.02). Experiments are performed usually at 1.2...1.4 bar (absolute). Next follows a needle valve (1.03) for extra security, and a venting valve (1.04). The venting valve is there in order to ensure that pressure can be released if it is too high, or for venting before gas change. By turning the pressure regulator (1.02) up, or turning it down and venting through (1.04) one can regulate the pressure. By opening up the sample circuit valve (1.05) the system is supplied with gas.

The porous medium is located inside the pressure cell (1.08), which again is lowered in the liquid bath (1.09). Before one starts any measurements the porous medium must be evacuated. This is because the porous powder contains humid air which can interfere with the measurement. Evacuation is monitored through the vacuum pressure indicators (1.06) and (1.07). In order to evacuate, the sample circuit valve (1.05) is closed, the vacuum pump (1.10) is started and its valve is opened. When vacuum reaches 10^{-2} torr (0.13 bar), the valve on the vacuum pump (1.10) is closed and the sample circuit valve (1.05) is opened. Gas is then purged into the system. The Hot Disk Digital Controller TPS2500S (2.01) governs the measurements together with a timetable set up on the computer (2.02).

To ensure that all humidity is gone, the porous medium must also be activated. In order to heat it, the liquid bath controller (1.11) is then set to 150 degrees Celsius. The evacuation process is then repeated five times over.

A “Procedure for running experiments” summarizes all important steps for carrying out safe measurements and is added in the Risk Assessment Report at the very end of the document.

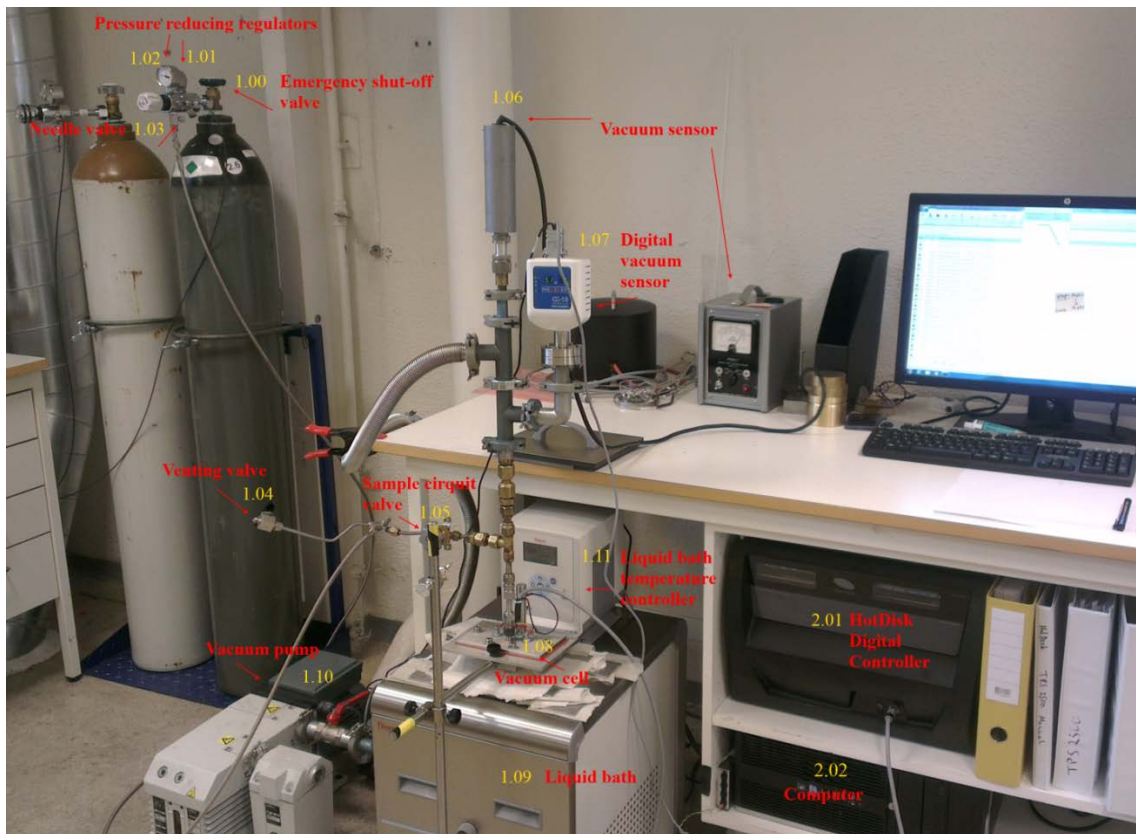




Fig. 2.5 - The Hot-Disk experimental setup.

Table 2.1 - Sensor/Actuator list for the experimental setup.

 											
Lfd. Nr.	P&ID Nr.	measurement position		measure-/actuating variable			device specification			signal	comments
		medium	position	sensor / device	S/A	EMSR	device type	measure-/control value	Unit	range	
							(z.B. producer, name.)				
1	1.00	compressed N2/He	gas bottle	shut-off valve	A		Yara Praxair	200bar	bar		
2	1.01	compressed N2/He	gas bottle	Pressure reducing regulator	A/S	PIC	Yara Praxair	200bar	bar	p_max=315 bar	
3	1.02	compressed N2/He	gas bottle	Pressure reducing regulator	A/S	PIC	Yara Praxair	operating @ < 0.5 bar	bar	p_max=5 bar	
4	1.03	compressed N2/He	gas bottle	Needle valve	A		Yara Praxair	operating @ 0.2/0.4 bar	bar	p_max= 60 bar	
5	1.04	compressed N2/He	between gas bottle/sample circuit	Venting valve	A		Swagelok SS 43GS 6mm	operating @ 0.2/0.4 bar	bar	0.5bar	
6	1.05	compressed or evacuated N2/He	between venting valve/sample holder	Sample circuit valve	A		Danfoss	operating @ 0.2/0.4 bar	bar	0.5bar	
7	1.06	compressed or evacuated N2/He	above sample holder	Vacuum pressure indicator	S	PIR	SPEEDIVAC	0.005...1 torr	torr	0.005...1 torr	1 torr =0.013 bar
8	1.07	compressed or evacuated N2/He	above sample holder	Vacuum pressure indicator	S	PIR	TELEVAC CC-10	10 ⁻⁹ ...10 ⁻³ torr 10 ⁻³ ...10 ⁻¹ torr 10 ⁻¹ ...10 ¹ torr 10 ¹ ...10 ³ torr	torr	10 ⁻⁹ ...10 ³ torr	can log to pc
9	1.08	compressed or evacuated N2/He	in liquid bath	Vacuum pressure cell (sample inside)	-		HotDisk Vacuum cell 11502	operating @ 0.2/0.4 bar	bar	Tmax =200°C p_max=2.5 bar	
10	1.09	Oil	floor	Liquid bath	-		AC200				
11	1.10	compressed or evacuated N2/He	floor next to liquid bath	Vacuum pump	A		Oerlikon AF-16-25	p=10 ³ ...5·10 ⁻³	torr	p=10 ³ ...5·10 ⁻³ torr	<=10 ⁻⁴ mbar (given from producer)
12	1.11		on top of liquid bath	liquid bath temperature controller	A/S	TIC	Thermo Scientific AC 200	T=243...423	K	T=238...473K	
13	2.01		in desk next to liquid bath	Hotdisk digital measurement controller	A/S	DRC	HotDisk Th. Const. Analyser TPS 2500S				Bridge: Keithley 2400, Off balance: Keithley 2700 (6.5 digits resolution)
14	2.02		in desk next to liquid bath	Computer	A/S	DRA	HotDisk Th. Const. Ana. Version 7.0.16	Thermal conductivity k	W/mK	0.005-500 W/mK	Repeatability ±0.5%, Thermal conductivity uncertainty=±5%

2.3 Investigated materials and their relevant properties

As mentioned before, different reference materials are tested, as well as the Cu-btc and Fe-btc-particles. The small glass beads are almost the same size as the Fe-btc, and can therefore give a good assumption for the magnitude of the effective thermal conductivity when applying Fe-btc.

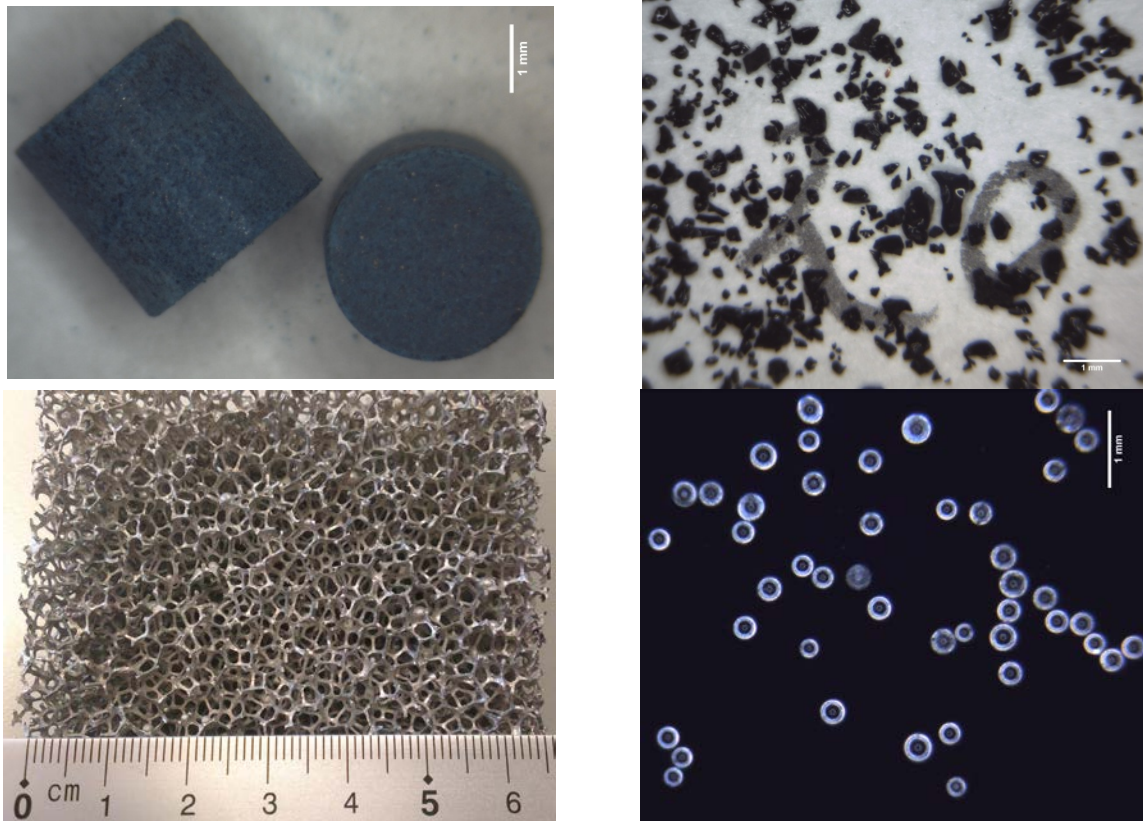


Fig. 2.6 - From top left to bottom right: Cu-btc pellets, Fe-btc, aluminum foam, glass beads.

2.3.2 Density

The density of glass beads was obtained by dividing measured volume by measured mass. The respective Cu-btc and Fe-btc densities were obtained by bathing a significant amount of them in ethanol, measuring the volume before and after. The densities given are in dry (activated) condition. This means that the porosity inside the particle is also taken into account. The density of each material is given in Table 2.2 below:

Table 2.2 - Density.

Material	Particle density ρ_p [kg/m ³]	Source
Glass	2602	(Henriksen, 2012)
Fe-btc	1085.4	(Schlemminger, 2013)
Cu-btc	946.9	(Schlemminger, 2013)
Foam	2700	(NIST Chemistry Webbook)

The bulk densities were obtained by dividing the measured mass m_b by the bulk volume V_b :

$$\rho_b = \frac{m_b}{V_b}. \quad (2.7)$$

When conducting experiments with MOF, there is a chance that the particles contain moisture. In order to determine the correct porosity, the mass and volume of the bed was measured before and after each experiment.

2.3.3 Porosity

Rearranging Eq. (1.1, part 1), the porosity of a bed of granular porous media can be defined also as

$$\varepsilon = 1 - \frac{\rho_b}{\rho_p} \quad (2.8)$$

Here, ρ_p is the density of the solid particles and ρ_b is the total bulk density. The porosity is determined individually for each bed. The bulk density is obtained by weighing the powder before it is put into the cylinder, and then measuring the height H_b inside the sample holder. The porosity of the aluminum foam is obtained from the relation

$$\varepsilon_{foam} = 1 - \frac{V_{foam}}{V_b} = 1 - \frac{(m/\rho)_{foam}}{V_b}. \quad (2.9)$$

2.3.4 Particle diameter

The glass beads and the Fe-btc particles are too small to measure by hand. In addition, the Fe-btc particles are of arbitrary shape, and it is therefore best to determine the diameter from a mass distribution. The sieving analysis was done in accordance with the ISO-2591-1 and ISO-9276-1 standards for sieving and representation of sieving results. Distribution is given in Fig. 2.6 and 2.7.

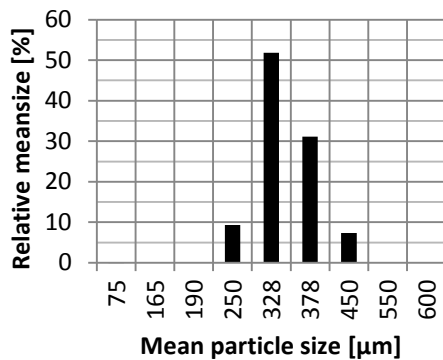


Fig. 2.7 - Relative undersize – glass beads

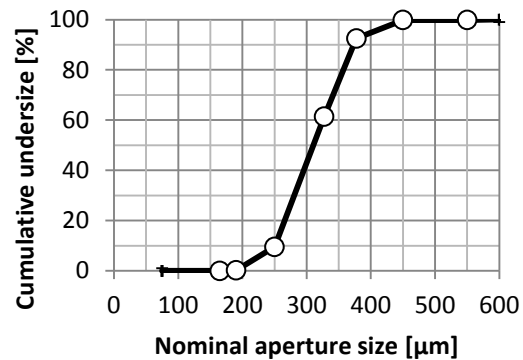


Fig. 2.8 - Cumulative undersize – glass beads

At first sieves were weighed individually before putting them together and pouring powders in the top sieve. The sieves were then shaken using a mechanical shaker. The glass beads were shaken for 20 minutes. Because the Fe-btc is so light and small, the particles have great difficulty coming through

the sieves. Sieving time were therefore 3×20 minutes, pounding them lightly with the palm in between. Afterwards, the sieves were weighed once again, to determine the mass of solids. The process is then repeated five times over. The sieving results are presented in full in Appendix A.

Distributions obtained are cumulative mass distribution, and particle diameter is computed modifying Eq. (1.50, Part 1). Since the particle density ρ_{pi} for the i th fraction is the same as the total particle density ρ_p , becomes

$$\bar{d}_p = \left[\sum_{i=1}^n \left(\frac{V_i}{V} \cdot \frac{1}{d_{pi}} \right) \right] = \left[\sum_{i=1}^n \left(\frac{V_i/\rho_p}{V/\rho_p} \cdot \frac{1}{d_{pj}} \right) \right] = \left[\sum_{i=1}^n \left(\frac{V_i/\rho_{pi}}{V/\rho} \cdot \frac{1}{d_{pi}} \right) \right] = \left[\sum_{i=1}^n \left(\frac{m_i}{m} \cdot \frac{1}{d_{pi}} \right) \right]. \quad (2.10)$$

An average particle diameter for the large glass beads were obtained by hand measurement (Henriksen, 2012).

The Cu-btc particles are of cylindrical shape, and a different particle diameter must be applied. Loreline Hubert (2011), whose report also covered Cu-btc, estimated the length L_p and diameter d_p to be respectively 3.04 mm and 3.09 mm. The equivalent spherical particle diameter d_s is given by (Kaviany, 1995)

$$d_s = \sqrt{\frac{A_p}{\pi}}, \quad (2.11)$$

where A_p is the surface area of the particle. The particle diameters used in measurements are then given in Table 2.3 below.

Table 2.3 - Particle diameter of various materials.

Material	Distribution diameter d_p [mm]	Spherical diameter d_s [mm]	Source
Glass beads – small	0.338		This work
Glass beads - large	1.395		(Henriksen, 2012)
Fe-btc, fillings 1-2	0.456		This work
Fe-btc, fillings 3-5	0.440		This work
Cu-btc		3.764	(Hubert, 2011)
Foam	N/A		

2.4 Data reduction

In order to determine the effective thermal conductivity correctly, the solid conductivity k_s and the fluid conductivity k_f as a function of temperature need to be known. The fluid conductivity of air, He and N₂ can be expressed as (VDI Heat Atlas, 2010)

$$k_f = C_1 + C_2T + C_3T^2 + C_4T^3 + C_5T^4, \quad (2.12)$$

with the constants given in Table 2.4.

Table 2.4 - Constants for k_f 4th degree polynomial.

Medium	$10^3 \cdot C_1$	$10^3 \cdot C_2$	$10^6 \cdot C_3$	$10^9 \cdot C_4$	$10^{12} \cdot C_5$	Eq. range	Eq. error
Air	-0.908	0.112	-0.084333	0.056964	-0.015631	223K<T<773K	1%
N ₂	-0.133	0.101	-0.060650	0.033610	-0.007100	223K<T<773K	1%
He	34.00	0.457	-0.214890	0.100710	-0.019140	223K<T<773K	1%

The solid conductivity of glass beads and the aluminum foam also need to be known. The MOF conductivities are found by fitting theoretical models to the experimental data. However, in order to know which of the theoretical models to apply, all the properties for the reference material must be known. Conductivity of Aluminum Alloy 1100 is given as (NIST Chemistry Webbook) by the relation

$$\log_{10} k_{s,alu} = C_1 + C_2 \log_{10} T + C_3 \log_{10} T^2 + C_4 \log_{10} T^3 + C_5 \log_{10} T^4 + C_6 \log_{10} T^5 + C_7 \log_{10} T^6 + C_8 \log_{10} T^7 + C_9 \log_{10} T^8 \quad (2.13)$$

Table 2.5 - Constants for $k_{s,alu}$ 8th degree polynomial.

C_1	23.39172
C_2	-148.5733
C_3	422.1917
C_4	-653.6664
C_5	607.0402
C_6	-346.152
C_7	118.4276
C_8	-22.2781
C_9	1.770187
Range	4K<T<300K
Eq. error	2%

Constants for Eq. (2.13) is given in Table 2.5. As seen from the Table, the range is not wide enough. Experiments are done in the range of 243<T<423K. Therefore the rest of the range is covered by an extrapolation equation. Fig. 2.8 displays this function graphically. The equation is given as

$$k_{s,alu} = 8 \cdot 10^{-5} \cdot T^2 - 0.0803 \cdot T + 228.55. \quad (2.14)$$

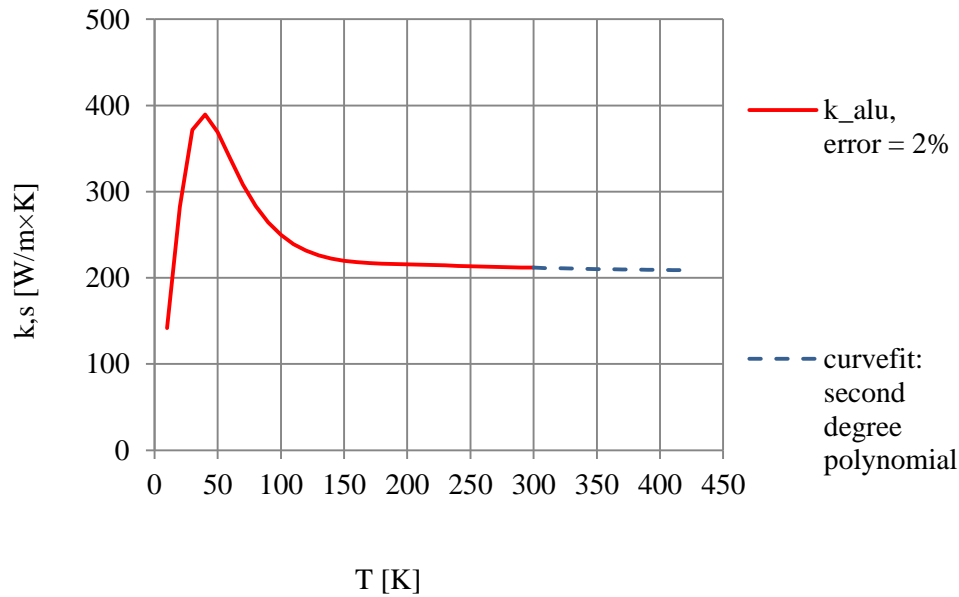


Fig. 2.9 - Solid conductivity of aluminum alloy 1100.

The solid conductivity of glass beads is also an extrapolation, based on data from the Handbook of Glass Data (1987) and an algorithm developed by glassproperties.com. The computation of the thermal conductivity with the exact composition of the glass beads is given in Appendix B. The equation, with $C=1.2$, is expressed as

$$k_{s, \text{glass}} = C \cdot (-4.8502 \cdot 10^{-8} \cdot T^2 + 4.4634 \cdot 10^{-3} \cdot T + 1.5825 \cdot 10^{-2}). \quad (2.15)$$

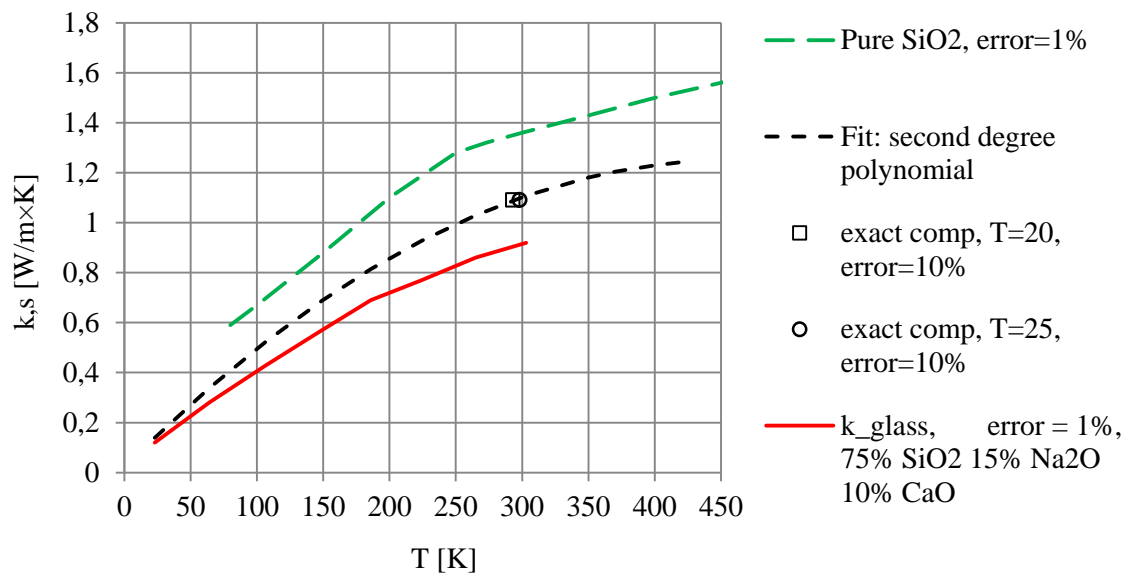


Fig. 2.10 - Solid conductivity of glass beads as a function of temperature (Handbook of glass data, 1987); (Glassproperties.com).

The exact composition of the glass beads is (KarlRoth.com):

- SiO₂ 72.5 %
- Na₂O 13.0 %
- K₂O 0.2 %
- CaO 9.6 %
- MgO 4.22 %
- Al₂O₃ 0.58 %
- Fe₂O₃ 0.11 %.

As seen in Fig. 2.9 above, the thermal conductivity of the curve-fit equation follows the same trend as the thermal conductivity of a glass-melt (red line; (Handbook of glass data, 1987)) with almost the exact same composition as glass beads. The extrapolated equation (Eq. 2.15) is actually the second order polynomial for the near-exact composition (red line) in Fig. 2.10 multiplied by the constant $C=1.2$. This constant was inserted into the equation in order to fit the curve to the thermal conductivity magnitude for the exact composition (which is $k=1.086$, at room temperature, i.e. $293\text{K}<T<298\text{K}$). The thermal conductivity for pure SiO₂ (Ed. James, 2001) also follows this same trend.

2.5 Uncertainty analysis

The producer of the Hot Disk system gives the uncertainties on the effective thermal conductivity rendered in Table 2.6.

Table 2.6 - Given uncertainties (M. Gustavsson, 1994).

	Effective thermal conductivity k_e
Uncertainty	5%
Reproducibility	2%

The effective stagnant thermal conductivity that comes out of the software is given with 5% uncertainty. But each data point is also given with some parameters not affected by the Hot Disk program. These include:

- The porosity of the bed ε , which is a function of the bed mass m_b and bed volume V_b .
- Temperature at a given data point, T .
- Pressure at a given data point, p .

The uncertainty of a variable

$$R = R(X_1, X_2, X_3, \dots, X_N), \quad (2.16)$$

depending on the calculated or measured values (X_1, \dots, X_N) , can be expressed as (Moffat, 1988):

$$\delta R = \left\{ \sum_{i=1}^N \left(\frac{\delta R}{\delta X_i} \delta X_i \right)^2 \right\}^{\frac{1}{2}}. \quad (2.17)$$

Rewriting Eq. (2.8), and the porosity is expressed as

$$\varepsilon = 1 - \frac{m_b/V_b}{\rho_s} = 1 - \frac{m_b/h_b l_b w_b}{\rho_s}, \quad (2.18)$$

where h_b , l_b and w_b is the height, length and width of the bed, respectively. Then

$$\varepsilon = \varepsilon(m_b, H_b, l_b, w_b, \rho_s). \quad (2.19)$$

Rewriting Eq. (2.17) in terms of ε then gives the uncertainty equation for the porosity

$$\delta \varepsilon = \left\{ \left(\frac{\delta \varepsilon}{\delta m_b} \Delta m_b \right)^2 + \left(\frac{\delta \varepsilon}{\delta H_b} \Delta H_b \right)^2 + \left(\frac{\delta \varepsilon}{\delta l_b} \Delta l_b \right)^2 + \left(\frac{\delta \varepsilon}{\delta w_b} \Delta w_b \right)^2 + \left(\frac{\delta \varepsilon}{\delta \rho_s} \Delta \rho_s \right)^2 \right\}^{\frac{1}{2}}, \quad (2.20)$$

or in terms of relative uncertainty

$$\frac{\Delta \varepsilon}{\varepsilon} = \left\{ \left(\frac{\Delta m_b}{m_b} \right)^2 + \left(\frac{\Delta H_b}{H_b} \right)^2 + \left(\frac{\Delta l_b}{l_b} \right)^2 + \left(\frac{\Delta w_b}{w_b} \right)^2 + \left(\frac{\Delta \rho_s}{\rho_s} \right)^2 \right\}^{\frac{1}{2}}. \quad (2.21)$$

The temperature is controlled by the liquid bath controller, which has an uncertainty of $\Delta T = \pm 0.1\text{K}$. The pressure is controlled by the pressure regulator. All Experiments are done at constant pressure. However, the pressure may vary as much as $\Delta p = \pm 0.2$ bar.

Since the experiments on MOF are to be fitted with the theory, an uncertainty analysis on the parameters affecting the theoretical models was conducted. The parameters making an impact on the theoretical models are:

- Porosity, ε .
- Temperature, T .
- Pressure, p .
- Solid conductivity, k_s
- Fluid conductivity, k_f

The solid and fluid conductivities are mainly a function of temperature. The temperatures calculated from the liquid bath controller are very accurate.

The conductivity of glass of solids varies greatly with pressure when the pressure is low, however, conductivity of solids will level out and become constant in the vicinity of 1000 hPa (=1 bar) (E. S. Huetter, 2008). As all measurements were carried out in ambient-like pressures, the relative error of solid conductivity of MOF is assumed constant at 2%. The curve-fit for glass beads is on the other hand based on experimental data with 1% uncertainty as well as theoretical correlations with 10%

uncertainty. Therefore, the relative conductivity error of the thermal conductivity of glass beads is assumed to be 15%.

The conductivity of fluids as a function of temperature has a given (Table 2.4) relative error of 1%. The fluid conductivity variation due to pressure is examined in Table 2.7 (NIST Chemistry Webbook).

Table 2.7 - Comparison of fluid thermal conductivity at various pressures

	Temp.	Thermal conductivity		Increase ($p_n \rightarrow p_{n+1}$)	
		N ₂	He	N ₂	He
p ₁ =1 bar	240	0.02168	0.13372		
	420	0.03341	0.19692		
p ₂ =1.2 bar	240	0.02168	0.13374	0.032 %	0.015 %
	420	0.03342	0.19694	0.015 %	0.010 %
p ₃ =1.4 bar	240	0.02169	0.13375	0.032 %	0.007 %
	420	0.03342	0.19695	0.015 %	0.005 %

Table 2.7 shows that it is acceptable to assume that the relative error on fluid conductivity is <0.05%.

Uncertainties will be given as a lower and upper band for the theoretical models. The experimental result uncertainties are visualized as error bars around the experimental data points. Note that the uncertainty of a data point most likely is > 5%, due to the effect of the parameters that the computer software does not take into account (porosity variation, temperature variation, pressure variation).

The density of glass beads was estimated manually on a set of larger glass beads (ø4.9mm) (Henriksen, 2012) to be 2602 kg/m³. However, the producer states that the density is approximately 2500 kg/m³ (KarlRoth.com). This gives a discrepancy of approximately 5%. A 5% discrepancy from the given value indicates that the actual density may even be as low as 2400 kg/m³. Therefore the total density uncertainty will be assumed to be 10%.

The constant relative uncertainty of each variable is given in Table 2.8

Table 2.8 - Uncertainties.

Parameter	Uncertainty [ΔX_i]	Rel. uncertainty [$\Delta X_i/X_i$]
ε		Eq. (2.10)
m_b	0.1g	
H_b	1 mm	
l_b	1 mm	
w_b	1 mm	
ρ_s		10 %
T	0.1 K	
p	0.2 bar	
k_s		MOF: 2% Glass: 15%
k_f		0.05%

Part 3 - Results and analysis

Experiments were performed on large ($\phi 1.395$ mm) and smaller ($\phi 0.38$ mm) glass beads as well as Fe-btc and Cu-btc MOF. Last, some experiments were performed on aluminum foam filled with the small glass beads and N_2 or air as fluid. All graphs presented in this section show the measured effective stagnant thermal conductivity (y-axis, $W/m\cdot K$) plotted versus temperature (x-axis, K) plotted versus theoretical models. Experiments with N_2 or He are performed at a constant absolute pressure of 1.2 bar, if another pressure is not specified. A selection results will be presented and discussed in this chapter. All results for the glass beads, Cu-btc, Fe-btc and aluminum foam are shown in Appendix C, D, E, and G, respectively. These Appendices also contain the data from which the plots are produced.

3.1 Reference material

In order to find a theoretical model which can be used to determine the MOF solid conductivity (k_s), experiments were first conducted on glass beads of various sizes. Some of the results are displayed in Fig. 3.1 - 3.3. The rest of the glass beads results are given in Appendix C. Preliminary results for the effective thermal conductivity of glass beads with air as fluid are shown in Fig. 3.1 with properties given in Table 3.1 below.

Table 3.1 - Properties of glass beads experiments.

material	m_bulk m,b [mg]	H_bulk H [m]	D_bulk D [m]	Volume V,b [m ³]	Density ρ_{bulk} [kg/m ³]	Porosity ϵ [1]	Uncertainty $d\epsilon/\epsilon$
glass_1.395mm	13261	0,0174	0,025	8,5E-06	1556	0,40	12,24 %
glass_1.395mm	13614	0,0186	0,025	9,1E-06	1493	0,43	12,06 %
glass_1.395mm	12742	0,0172	0,025	8,5E-06	1506	0,42	12,26 %
glass_0.38mm	12992	0,0168	0,025	8,2E-06	1575	0,39	12,33 %
glass_0.38mm	13923	0,0181	0,025	8,9E-06	1566	0,40	12,12 %
glass_0.38mm	14684	0,0189	0,025	9,3E-06	1584	0,39	12,02 %

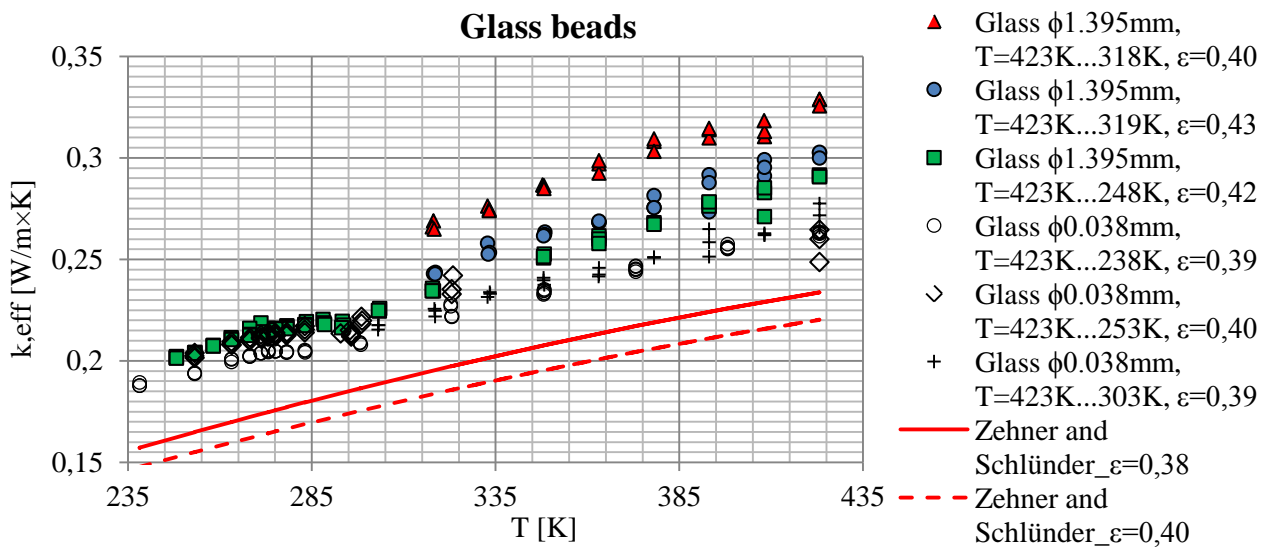


Fig. 3.1 - Effective thermal conductivity of six different fillings of glass beads with air as fluid.

The figure (3.1) shows that the effective thermal conductivity has an ascending curve from low to high temperature. The conductivity of the larger glass beads (colored, filled markers) has a higher magnitude than the small glass beads (black, non-filled markers). The large glass beads have as well a difference of approximately 11% from the lower (green squares) measurement series to the lower (red triangles) measurement series. This could be due to a change in porosity. As seen from the two lines for the Zehner and Schlünder model (Fig. 3.1; red stapled and red solid line), changing the porosity from 0.38 to 0.4 (5%), results in a reduction of the effective conductivity of a little less than 5%. Summing up the porosity uncertainties and the TPS measurement device uncertainties then gives an uncertainty of approximately $\pm 10\%$ which can explain the variation between experiments performed on the same material.

Furthermore, the results do not match the theoretical models at a given porosity. Each measurement point has an uncertainty of 5%, but repeated measurements show that the effective thermal conductivity consequently is approximately 15% higher in magnitude than suggested by the theoretical models. However, the porosity errors (displayed in Table 3.1) are quite high, and this could explain some of this behavior. As an example, take the top red triangles from Fig 3.1 (glass $\varnothing 1.395\text{mm}$, $\varepsilon=0.4$): With the porosity error of 12.24%, this series could actually have porosity as low as 0.35. As stated in the uncertainty analysis in part two, the porosity error affects both measurements and the theoretical model. The porosity error, which is mainly due to the particle density error (10%) may be responsible for some of this behavior. Though, the most likely scenario is that the humidity (20% relative humidity for all measurements) in the air causes an increase in the effective thermal conductivity due to the formation of water droplets at the vicinity of contact points between particles, thus increasing the effective conductivity of the bed (as shown in Fig. 1.4, the thermal conductivity of water is severely higher than that of air).

Last, Fig 1.3 show a trend of discontinuity in the magnitude of the effective thermal conductivity in the range of $265 < T < 295\text{K}$. At these temperatures, the effective thermal conductivity of the bed seems to flatten out. This discontinuity could be due to icing, and the issue may remove itself when experiments with evacuated material flushed with nitrogen gas are performed.

The figures 3.2 and 3.3 show the effective thermal conductivity of glass beads filled with N_2 gas. A lower and upper band for the ZBS-model is added in these figures. This is the upper and lower relative uncertainty bounds of this model due to the parameters discussed in the uncertainty analysis (sect. 2.5). The error bars represent the 5% error for each data point given by Hot Disk.

Figure 3.2 shows the effective stagnant thermal conductivity of a packed bed filled with large glass beads ($\varnothing 1.395\text{mm}$) with N_2 gas at 1.2 bar absolute pressure. The figure clearly shows a resemblance with the theoretical models: The conductivity of the experimental results increases with increasing temperature, following the ascending trend of the theoretical models. The results follow the high uncertainty bound of the ZBS-model. The model of Kunii and Smith and the Maxwell model predict high and low, respectively. The model from IAEA-TECDOC-1163 predict slightly lower than the ZBS-model. All these trends also show in the comparison from part 1 (Fig. 1.19). The figures 3.2 and 3.3 show that the ZBS model gives the best prediction for the effective thermal conductivity. However, due to the large uncertainties of the porosity and solid conductivity, the ZBS-model has a relative uncertainty of about $\pm 10\%$. The 5% uncertainty for each measurement point also needs to be taken into account. Generally, a relative uncertainty over 10% is not acceptable, and therefore it is somewhat problematic that the uncertainties of the solid conductivity and porosity are so large. For

future applications, the choice of glass beads as a reference material should therefore be reconsidered. For effective thermal conductivity experiments, the most important properties of a reference material are density (for calculation of the porosity) and solid thermal conductivity (as input parameter in the theoretical models). The thermophysical properties of a reference material should be well-known.

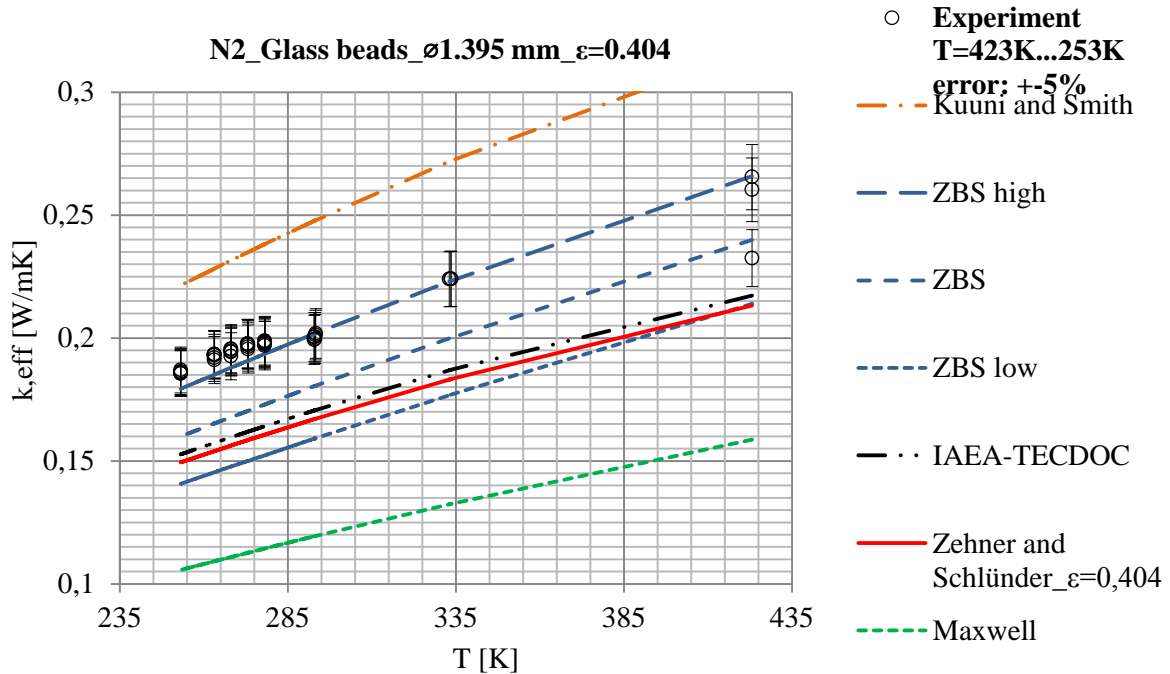


Fig. 3.2 - Effective thermal conductivity of large glass beads and N₂ plotted versus temperature.

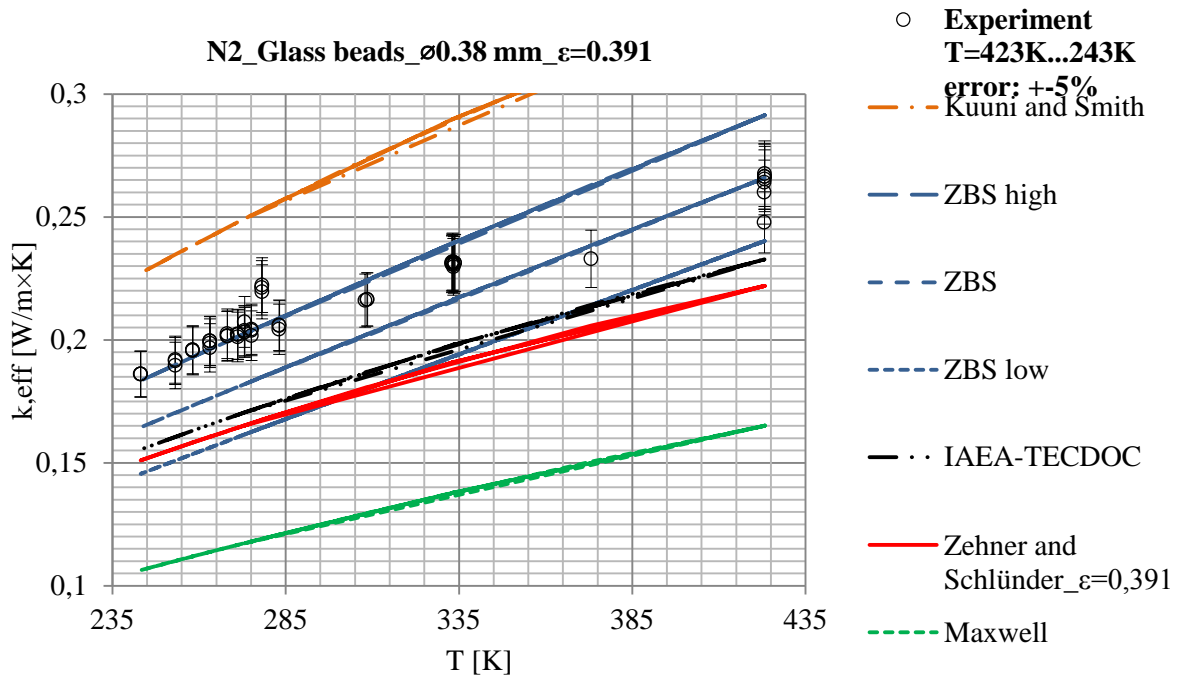


Fig. 3.3 - The effective thermal conductivity of small glass beads with N₂ gas.

Fig. 3.3 shows the effective thermal conductivity of a bulk filled with small glass beads ($\varnothing 0.38$ mm) and nitrogen gas. These measurements were done at temperatures ranging from $T_{\text{high}}= 243\text{K}$ down to $T_{\text{low}}= 243\text{K}$. Then, the measurements were repeated from T_{low} and up to T_{high} again. The repeatability is very good; the figure shows that all data points are almost identical. All results keep within the ZBS relative uncertainty bounds, except for the values at approximately 277 K. What caused this is uncertain. It could be some disturbance in the measurement environment, or a computational or calibration-related error in the Hot Disk software. The latter issue is addressed further down on this page.

By comparing the small glass beads experiments conducted with N_2 gas (Fig. 3.3) with the ones conducted with air (Fig. 3.1), one can see that the magnitude of the thermal conductivity seems to be about the same compared to their respective Zehner and Schlünder curves. This indicates that it might not be any humidity-effect on the thermal conductivity, but perhaps rather a miscalculation of the particle density (which can lead to a large miscalculation of the porosity).

A major concern is that the discontinuity of the effective thermal conductivity shown in Fig. 3.2 through 3.4 around $T=273\text{K}$ is still present, even though the experiments were conducted with pure N_2 as fluid. This behavior is clearly not supported by the theoretical models, which give ascending, almost linear, curves for thermal conductivity from $T=243\text{K}$ to $T=423\text{K}$. Since the bulk material may contain moisture from the setup mantling process, a possible explanation is that this was due to the formation of ice around $T=273\text{K}$. However, this is not the case, since the air has been evacuated prior to experiment startup. Another possible scenario is that the system had a leakage. After performing several measurements, the conclusion was that this was indeed the case. The silicon grease used for sealing the pressure cell was seeping through and into the pressure cell during measurements. A photo taken after an experiment is displayed below (Fig. 3.2).

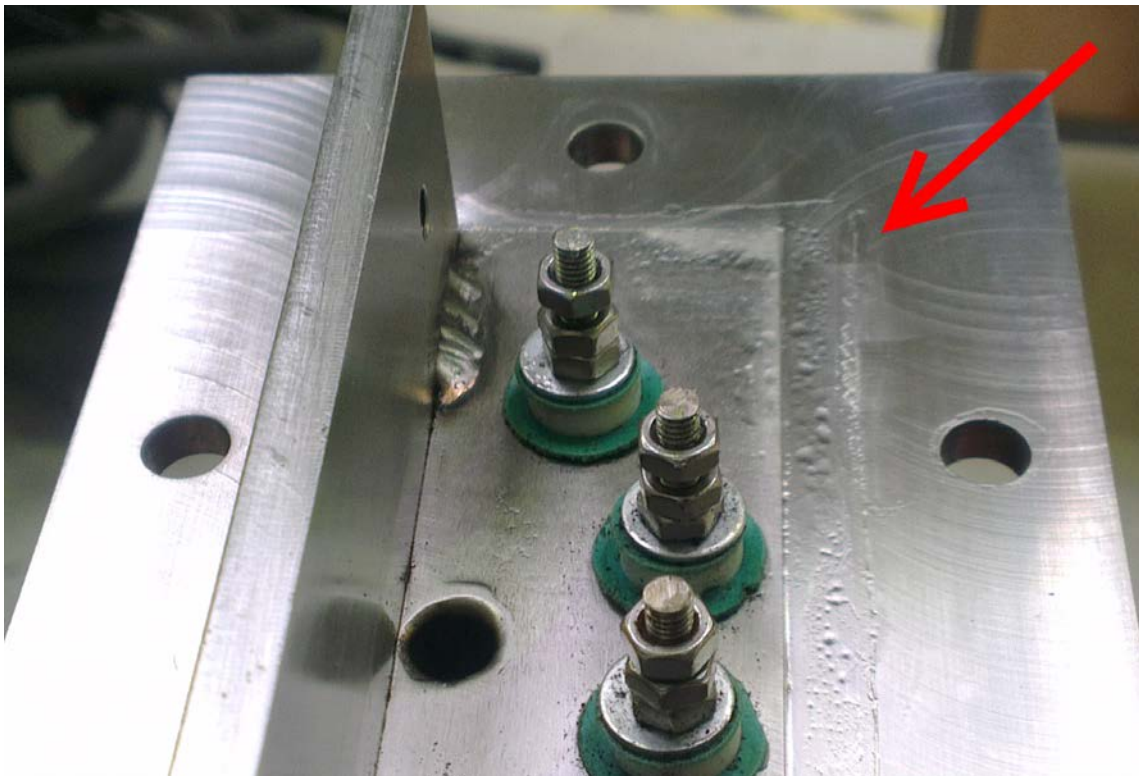


Fig. 3.4 - Silicon vapor seeping inside the pressure/vacuum cell.

The photo (Fig. 3.4) clearly shows that silicon vapor has been seeping inside the container through the sealing. If this affects the measurements around $T=273\text{K}$, it would most likely also affect the measurements at other temperatures as well, so this being the cause of the problem is unlikely.

Another proposal is that the Hot Disk TPS software is unable to compute the thermal conductivity correctly in the area around $T=273\text{K}$, due to some calibration error. After checking with the producer (mail attached in Appendix F), the conclusion was that a calibration error is most likely to have caused this behavior. Since there was no time to address this concern at the time of this discovery, the results in the range of $263\text{K}<T<283\text{K}$ were not taken into account during the fitting of MOF solid conductivities.

Summarizing the glass beads experiments, it is clear that the theoretical model that is best fit to use for determining the solid conductivity of the MOF materials is the ZBS model. The Hot Disk setup have a very good repeatability, and measures the effective thermal conductivity of a granular porous bed of glass beads in the temperature range of $243\text{K}<T<263\text{K}$ and $283\text{K}<T<423\text{K}$ within 15% accuracy. However, in order to confirm the validity of this experimental setup within 10% accuracy, more experiments with a different reference material should be carried out.

3.2 MOF results

The MOF materials Cu-btc and Fe-btc were measured in the range of $243<T<423\text{K}$. Some of the results from these experiments are given in visual form further down. All of the plots, as well as the produced data, are given in Appendix D (Cu-btc) and Appendix E (Fe-btc). The results for the effective thermal conductivity k_s were fitted to the ZBS model through the temperature-dependent relation

$$k_s = k_{s0} \left(\frac{T}{T_0} \right)^n, \quad (3.1)$$

where $T_0=273\text{K}$, k_{s0} is the solid thermal conductivity at T_0 , and n is an exponential coefficient. The ZBS model was chosen on the basis of it providing the most accurate predictions, and as well because it is a versatile model which takes into account all of the secondary parameters given in Eq. 1.20. The fit for the solid thermal conductivity can thus be applied for prediction of larger storage systems as well. The optimal values for k_{s0} and n were found setting the absolute of the sum of all effective thermal conductivity differences (Δk_e) between the ZBS model and the measured values to a minimum. This gives

$$k_{s0} \Big|_{n \text{ optimal}} = \text{MIN} \left\{ \left| \sum_{i=1}^N \Delta k_e \right| \right\} = \text{MIN} \left\{ \sqrt{\sum_{i=1}^N (k_{e,ZBS} - k_{e,measured})^2} \right\}. \quad (3.2)$$

The solution to equations (3.1) and (3.2) were obtained using Solver in Excel. These values are displayed in Table 3.2.

Table 3.2 - Optimized constants

	Cu-btc	Fe-btc
k_{s0}	0.33	0.28
n	0.11	0.26
$ \sum \Delta k_e / \sum k_{ZBS}$	5.01%	5.44%

Table 3.2 also shows that using Eq. (3.1) to approximate the solid thermal conductivity gives a deviance from the ZBS model of approximately 5 %.

Fig 3.5 and 3.6 shows the measured effective thermal conductivity of two fillings of Cu-btc MOF filled with helium and nitrogen, respectively. In these figures, the error bars represents the 5% error that comes with the measurements. The measurements are performed at a constant pressure of 1.2 bar, except the Cu-btc experiment with He, which is at 1.4 bar. The difference between the measurements at 1.2 bar and 1.4 bar is much lower than the uncertainty of the measurement itself (see Appendix D), and it should therefore not be a problem comparing N₂ and He experiments performed at 1.2 bar and 1.4 bar, respectively. All theoretical models in Fig. 3.5 through Fig. 3.8 are based on the solid conductivity obtained from the fitting (Eq. (3.1) and (3.2); Table 3.2).

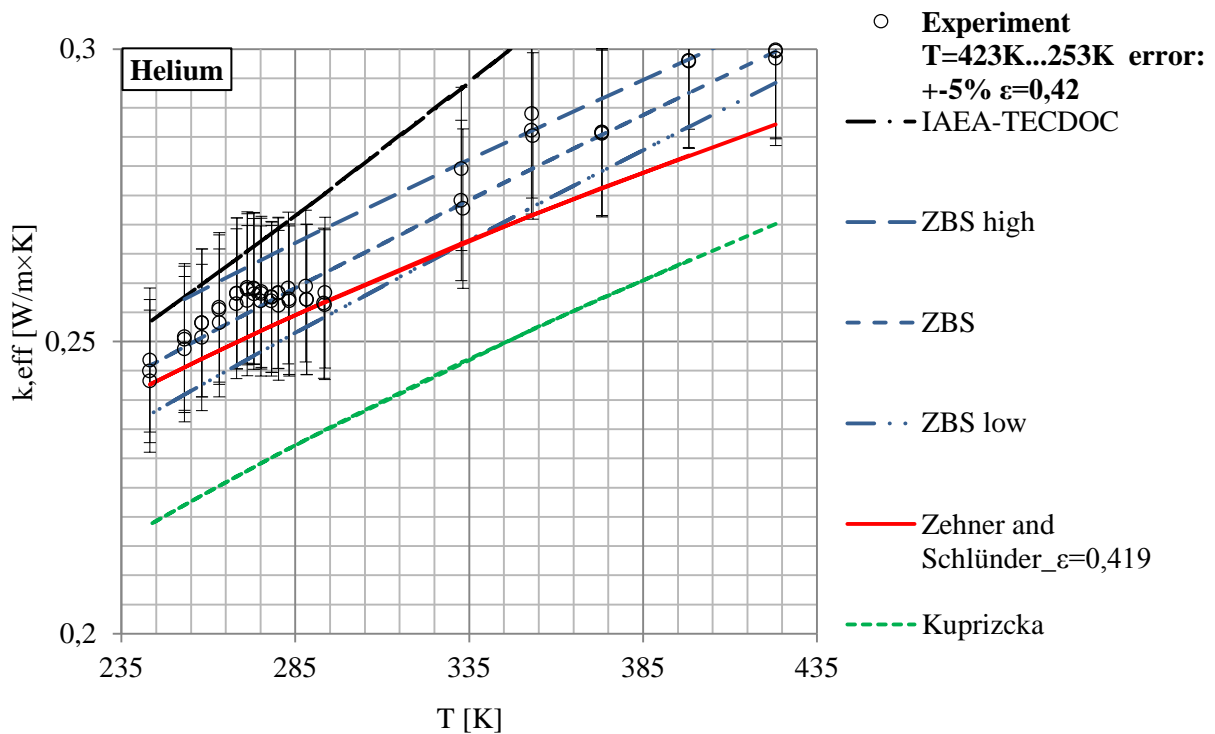


Fig. 3.5 - Effective thermal conductivity of Cu-btc with helium (He) gas at 1.4 bar absolute pressure.

In figures 3.5 and 3.6, all the measured values of the effective thermal conductivity are within the relative uncertainty bounds of the ZBS model. The figures show a discrepancy between the effective thermal conductivity of the bulk filled with helium and the one filled with nitrogen. This is to be expected, since the thermal conductivity of helium is so much larger than nitrogen (ref. Fig. 1.4).

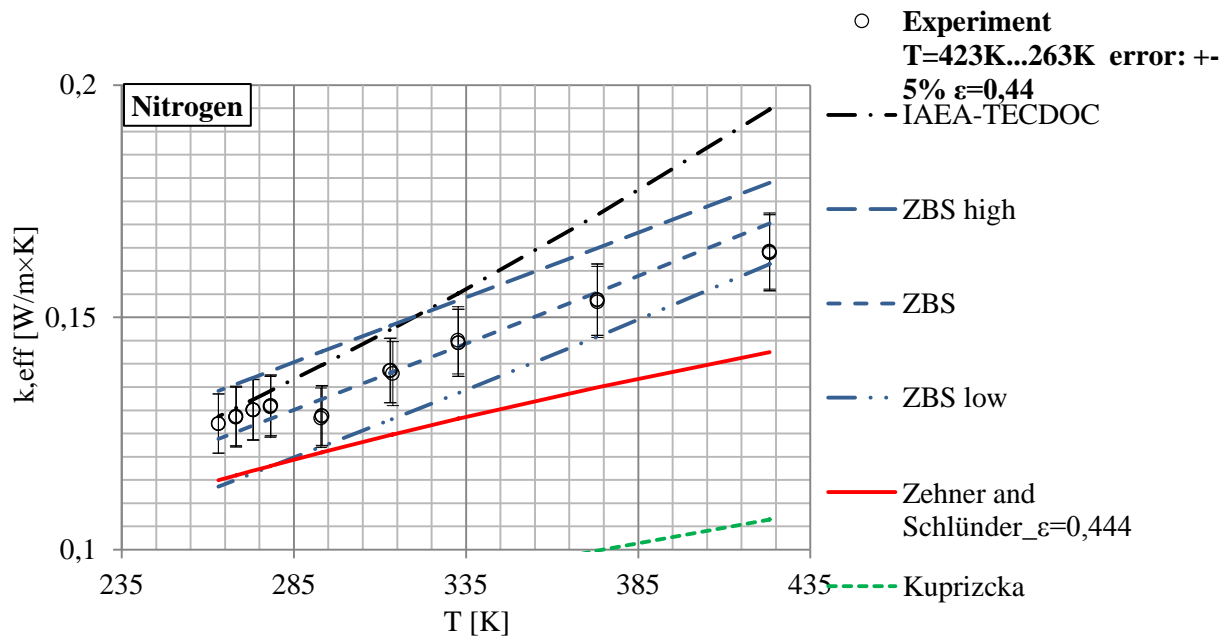


Fig. 3.6 - Effective thermal conductivity of Cu-btc with nitrogen (N_2) gas at 1.2 bar absolute pressure.

Fig. 3.5 and 3.6 also show that the experimental data correspond very well with the slope of the ZBS-model curve. This indicates that the temperature dependent function for the solid conductivity has a correct relation between the solid thermal conductivity k_{so} at 273K and the temperature T .

Furthermore, the discontinuity of the effective thermal conductivity around $T=273\text{K}$ is still there. This continuity showing up in all measurements indicates that it is in fact due to a computational error from the TPS Hot Disk software. The results from the Fe-btc also show this same behavior.

Figures 3.7 and 3.8 show the results for the effective thermal conductivity of Fe-btc with helium and nitrogen gas, respectively.

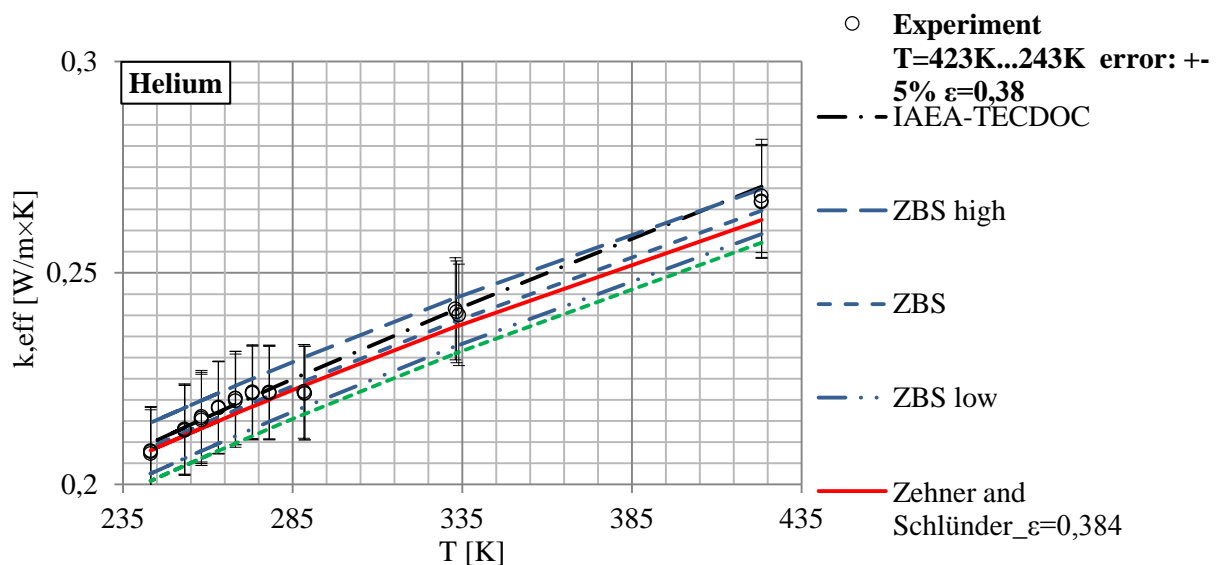


Fig. 3.7 - Thermal conductivity of Fe-btc with helium (He) gas.

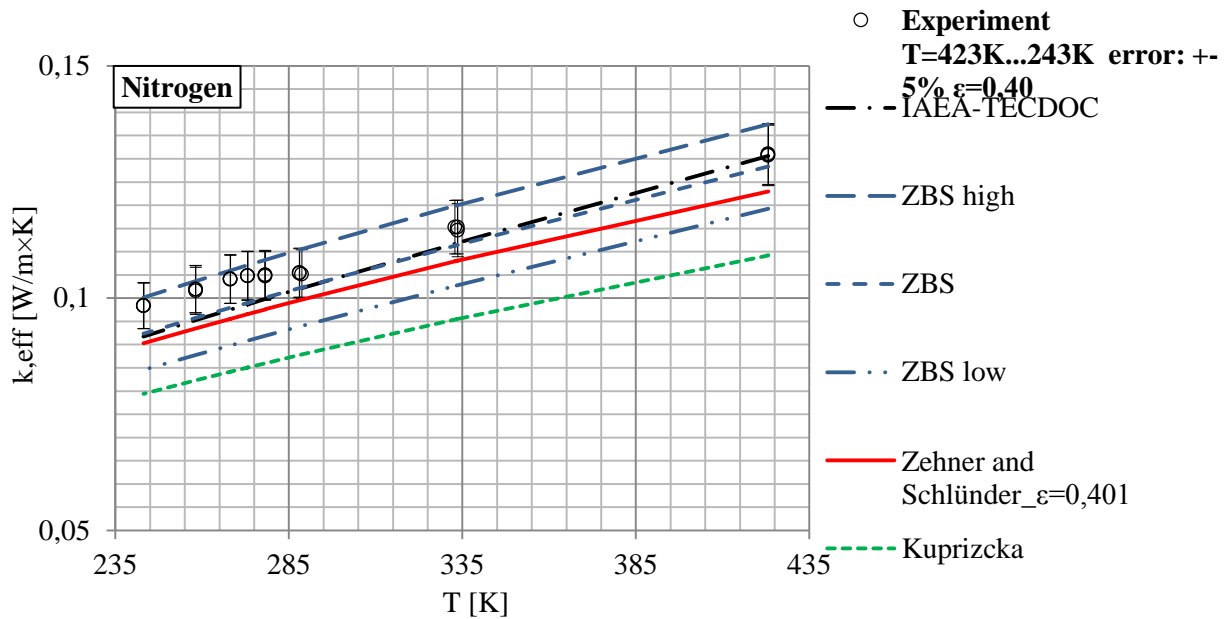


Fig. 3.8 - Thermal conductivity of Fe-btc with nitrogen (N_2) gas.

As for the Cu-btc, the measured effective thermal conductivities of Fe-btc shown in Figures 3.7 and 3.8 are also within the relative uncertainty bounds of the ZBS model. The slope of the experimental data fits very well with the ZBS model for Fe-btc as well.

However, comparing the predictions for the effective thermal conductivity of Cu-btc and N_2 (Fig. 3.6) with the predictions of Fe-btc with N_2 in (Fig. 3.8) shows that Cu-btc predictions has a greater discrepancy between the ZBS and the IAEA-TECDOC model as the temperature increases. The trend is also shown when comparing the predictions with helium gas. The fact that the gas does not affect this tendency suggests that it is due to the difference in material structure. Also, the fact that the discrepancy increases with temperature suggests that it is due to the radiation term of each of the models being different. Looking at the equations for the respective models (part 1, section 1.7.2 and 1.7.3) gives a perfectly good explanation:

Both models require the use of the deformation factor B from Eq. (1.55). However, the constant C in the deformation factor term is 2.5 for cylindrical particles (Cu-btc), 1.4 for broken particles (Fe-btc) and 1.25 for spherical particles. Investigating the works on the IAEA-TECDOC radiation term (Eq. (1.66)) from the original author reveals that the term was derived under the assumption that the particles are spherically shaped (Breitbach and Barthels, 1980). Hence, they only allow for C to be equal to 1.25. With the deformation factor being larger for Cu-btc particles, the last term inside the bracket of the IAEA-TECDOC radiation term will result in a radiation term of greater magnitude than that of the ZBS model (Eq. 1.56). The particle diameter of Cu-btc is approximately $3.76/0.43 \approx 8$ times greater than that of Fe-btc. Since the IAEA-TECDOC radiation term is multiplied with the particle diameter d_p and T^3 this effect will increase with temperature. This shows that this model is actually not applicable for the purpose of this work. The ZBS model however, provide accurate predictions for both broken and cylindrically shaped particles.

A comparison of the predictions for the effective thermal conductivity from the ZBS model at 285K and 385K, for both Cu-btc (Fig. 3.5 and 3.6) and Fe-btc (Fig. 3.7 and 3.8), is shown in Table 3.3.

Table 3.3 - The increase of the effective thermal conductivity when switching from N₂ to He.

	Cu-btc			Fe-btc		
	N ₂	He	Increase	N ₂	He	Increase
k_{ZBS} at 285K	0,13	0,26	100 %	0,102	0,22025	116 %
k_{ZBS} at 385K	0,16	0,29	81 %	0,132	0,2504	90 %

As shown in the above table, a bulk of Fe-btc receives a higher increase in thermal conductivity than a bulk of Cu-btc when the gas is switched. This is the result of their respective solid conductivities having a different temperature variation as well as a different magnitude. The solid conductivity of Cu-btc is already much higher than that of Fe-btc, and this is why the effect of changing to a more conductive gas will not provide the same effect for the Cu-btc. The temperature variation of the solid thermal conductivity of both MOF materials is shown in Fig. 3.9 below.

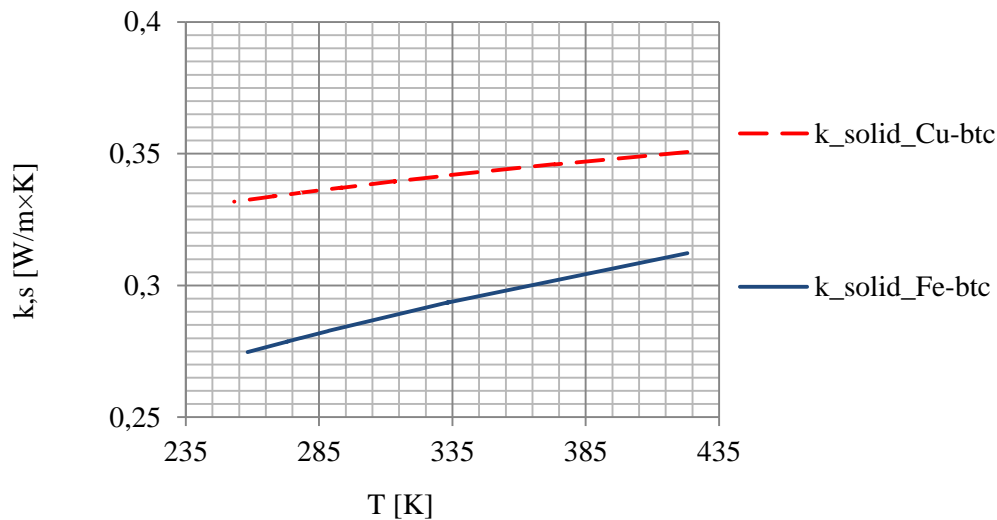


Fig. 3.9 - The variation of solid thermal conductivity of Cu-btc and Fe-btc as a function of temperature (Based on Eq. (3.1) and (3.2) with values from Table 3.2).

In Fig 3.9, the increase of solid thermal conductivity of Fe-btc is almost linear, while the Cu-btc thermal conductivity has a slight descending increase over the temperature range. The solid thermal conductivities of both Cu-btc and Fe-btc are fitted values from the ZBS model. The conductivity of Cu-btc is higher than Fe-btc. This is to be expected, since Cu-btc is copper-based and thus generally should have better heat transfer capabilities than an iron-based substance. However, confirming that the obtained relations give the true values for the thermal conductivity requires more experimental data from various gases.

The magnitude of the effective thermal conductivity of a packed bed of MOF material is not very large. Even though changing gas from nitrogen to helium provides approximately a 100% increase, the aluminum foam supposedly increases the effective thermal conductivity by two orders of magnitude.

At the time of writing this, there was not enough time available to test the performance of the aluminum foam together with a MOF material. However, experiments were made on foam filled with glass beads and nitrogen gas.

3.3 Foam effect

Experiments on an aluminum open-cell foam were conducted with nitrogen and glass beads. The results are given in full in Appendix G. The effective thermal conductivity of a packed bed with glass beads is in the magnitude of 0.2. According to the predicted values of the Phase-symmetry model (1994) and the model of Boomsma and Poulikakos (2000) showed in Fig 1.24, the magnitude of the effective thermal conductivity of the bed should increase approximately 50 times when applying a high-porosity aluminum foam. The experiments conducted by this work, plotted in Fig. 3.10, shows that this is not the case.

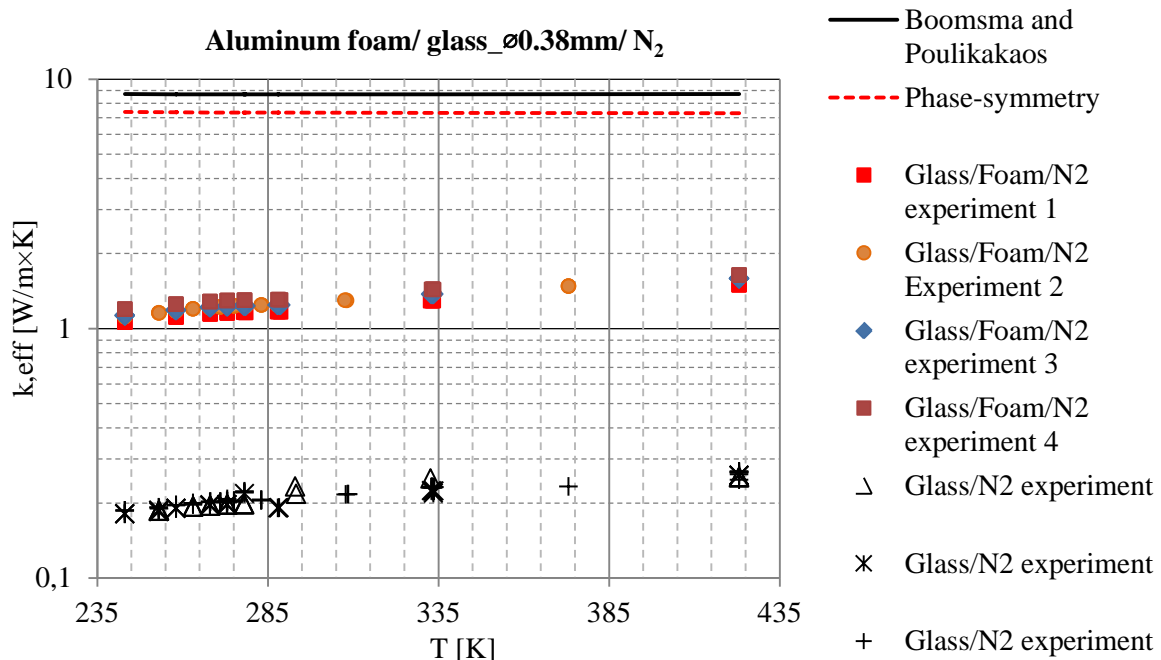


Fig. 3.10 - Top: Predictions of the effective thermal conductivity of glass/foam/N₂.
Middle: Measured effective thermal conductivity of glass/foam/N₂.
Bottom: Measured effective thermal conductivity of glass/N₂.

In Fig. 3.10, the middle placed colored markers show the results for the effective thermal conductivity of a bulk containing a high-porosity aluminum foam filled with small glass beads ($\varnothing 0.38\text{mm}$) and nitrogen gas. The bottom results (black, non-filled markers) show the effective thermal conductivity of glass beads with nitrogen only. At the top the model of Boomsma and Poulikakos (2000) (with shape-parameter $e=0.18$) predict a thermal conductivity of approximately constant magnitude of 9 W/m·K. The Phase-symmetry-model of Hsu et al. (1994) predict a little lower, the effective thermal conductivity being constant at approximately 7 W/m·K. The conductivity of aluminum is descending from 235 to 435 K, contrary to other substances such as the glass beads and nitrogen. The theoretical models show that the descending conductivity of aluminum counteracts the ascending conductivities of the other substances, creating almost linear predictions for the effective thermal conductivity.

Fig. 3.10 clearly shows that both the experiments with and without foam have the same ascending tendency over the temperature range, suggesting that in reality the foam does not affect the thermal conductivity to the same extent as predicted in theory.

Regarding the experimental results, Fig. 3.10 shows that the use of this particular aluminum foam only increases the effective thermal conductivity about 6 times, compared to approximately 50 times for the theoretical models. The magnitude of the effective thermal conductivity of the foam with small glass beads and nitrogen gas ranges from 0.18 to 0.25 W/m·K over the temperature range. Previous experiments performed on aluminum-based foam (AlSi₇Mg, $k_s \approx 160$ W/m·K) also show this same magnitude for the effective thermal conductivity (Inger-Anne Rasmussen, 2011).

What is now clear is that the theoretical models are not able to predict the effective thermal conductivity correctly for these particular foams. This could be the result of two different scenarios:

1. The theoretical models do not give an accurate prediction for foam-like structures.
2. The measurements are wrongly executed.

According to other authors, the effective thermal conductivity of pure-aluminum foam ($\varepsilon=0.937$) filled with air should be in the magnitude of 4.5 W/m·K (Valmirdi, 1999). This indicates that both of the above scenarios are likely to be true. On this basis the decision was made, to modify the phase-symmetry model of Hsu et al. (1994) and compare this to a new set of foam experiments. This model will be presented in part 4.

Part 4 - Modified phase-symmetry model for aluminum foam

In this part, a modification to the phase-symmetry model of Hsu et al. (1994) described in section 1.8.1 will be presented. The original model only assumes phase symmetry and a continuous solid and fluid phase, and does not take into account the extra distance that the heat must travel due to the structure of the foam. In the present approach, this effect will be included by the introduction of a dimensionless geometrical tortuosity factor.

A new set of experiments on the same aluminum foam ($\varepsilon=0.93$) with $\varnothing 0.38\text{mm}$ glass beads and air as fluid were performed. These experiments were carried out with an external force exerted on the foam in order to ensure good contact between the foam and the Hot Disk sensor. In addition, the surfaces of the foam parts in contact with the sensor were finished using a wide belt finishing machine.

4.1 Model development

The unit cell from the original phase-symmetry model is pictured in Fig. 1.20. The unit cell of the new modified model is depicted below.

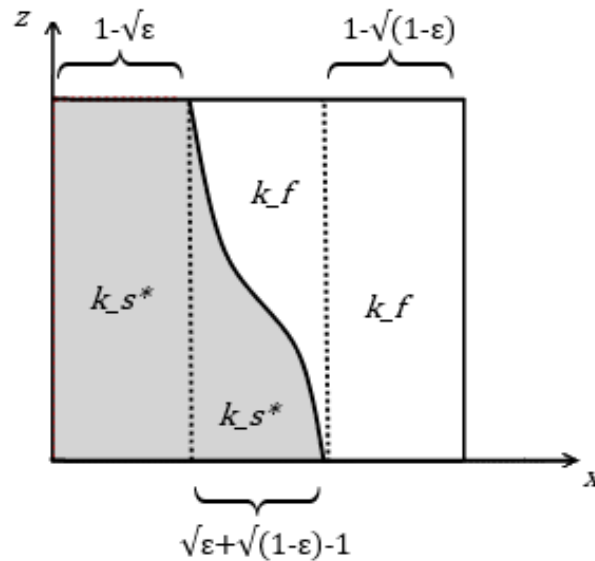


Fig. 4.1 - Unit cell for the modified phase-symmetry model.

Fig 4.1 shows the unit cell for the modified phase symmetry model. In the figure, k_s^* is the solid conductivity to be modified. The phase symmetry model can then be expressed as follows (Hsu et al, 1994):

$$k_e = (1 - \sqrt{1 - \varepsilon})k_f + (1 - \sqrt{\varepsilon})k_s^* + (\sqrt{1 - \varepsilon} + \sqrt{\varepsilon} - 1)k_{sf}, \quad (4.1)$$

where k_{sf} is the equivalent thermal conductivity of the composite layer, which can be expressed as

$$k_{sf} = k_f \left[\frac{b(1-\lambda)}{(1-\lambda b)^2} \ln\left(\frac{1}{\lambda b}\right) - \frac{b-1}{1-\lambda b} \right], \quad (4.2)$$

with $\lambda = k_f/k_s^*$. The shape factor b is the same as before (Eq. 1.73).

The path of heat transfer in the solid phase is then modified by a dimensionless tortuosity factor η . The relation between the modified solid conductivity and the regular solid conductivity can be described by the relation

$$k_s^* = \eta \cdot k_s, \quad (4.3)$$

where

$$\eta = \frac{\text{pore diameter [m]}}{\text{actual heat transfer path [m]}}. \quad (4.4)$$

In order to find the value of the tortuosity factor, one must take a look at the actual structure of the foam. The Hot Disk sensor measures the heat transfer in the axial and radial direction. As demonstrated in Fig 4.2 below, the 2-dimensional pore structure in the radial and axial direction has the shape of a hexagon and pentagon, respectively.

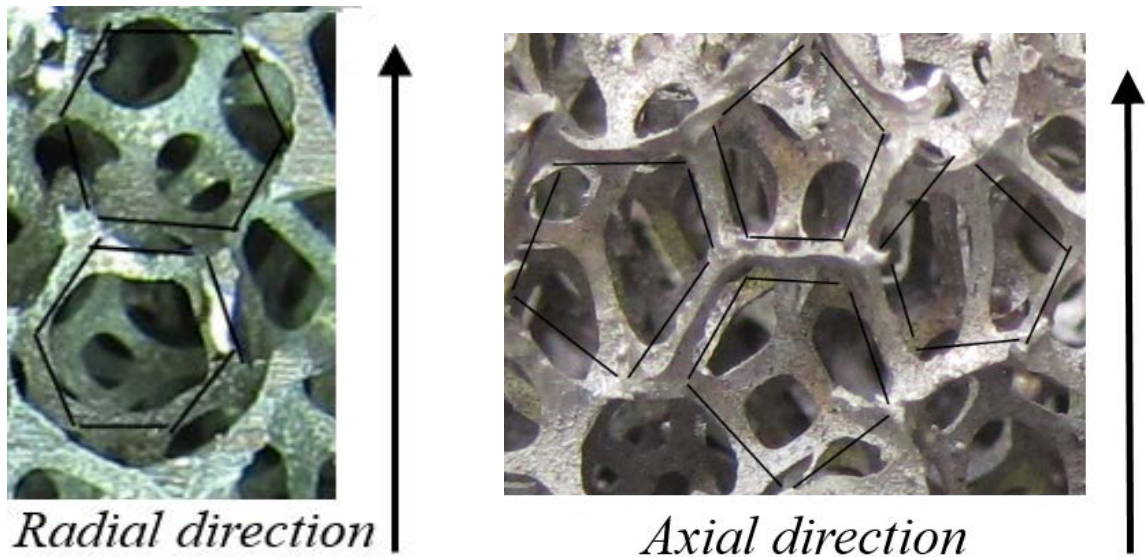


Fig. 4.2 - The pore structure visualized.

Hence, the ratio of the pore diameter to the actual heat transfer path in 2 dimensions can be approximated as shown in Fig. 4.3 below. The original phase symmetry model does not take into account the path of heat transfer, it only accounts for the ratio between the respective phases.

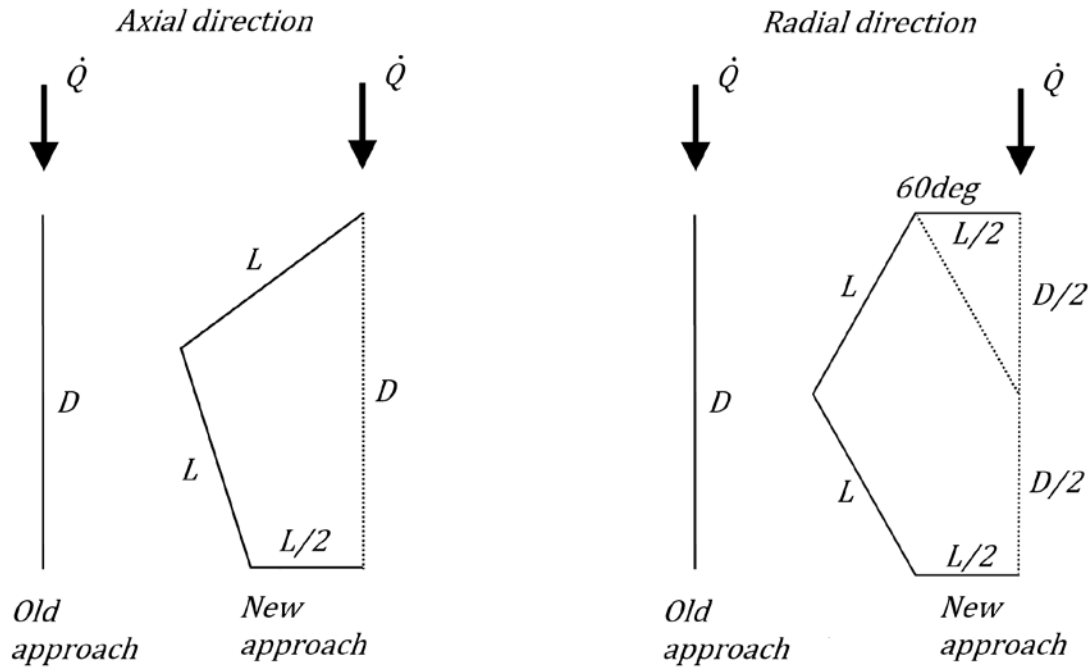


Fig. 4.3 - Actual heat transfer path and the heat transfer path of the original phase-symmetry model.

In Fig. 4.3, D is the pore diameter, and L is the length of the side of the pentagon and hexagon. The influence of the pore size diameter can be neglected due to the fact that the ratio of the pore diameter to the actual heat transfer path will be the same regardless of a change in the pore diameter. The heat transfer path in the axial direction will be half of a pentagon circumference, while the path in the radial direction will be the circumference of half a hexagon. Thus, the tortuosity factor in the axial direction can be expressed as

$$\eta_{high} = \frac{D}{2.5L} = \frac{\frac{L}{2}(\sqrt{5} + 1)}{2.5L} = \frac{1}{5}(\sqrt{5} + 1) \approx 0.647, \quad (4.5)$$

while the tortuosity factor in the radial direction is

$$\eta_{low} = \frac{D}{3L} = \frac{1}{3}\tan(60^\circ) \approx 0.557. \quad (4.6)$$

These values for η will provide a lower and upper band for the new phase symmetry model. Note that this approach involves the use of the ZBS model on the glass beads and the air, in order to gain an effective thermal conductivity for the *phase* that the foam is filled with. An overview of this approach is given in Table 4.1 below.

Table 4.1 - New foam approach overview.

Model applied	Effective thermal conductivity	Input parameters		
		porosity	fluid	solid
Phase-symmetry	k_e	ϵ_{foam}	k_{ZBS}	$k_s^* = \eta k_s$
Zehner/Bauer/Schlünder	k_{ZBS}	ϵ_{glass}	k_{air}	k_{glass}

A comparison with the original phase symmetry model and the model of Boomsma and Poulikakaos (2000) ($\epsilon=0.18$) is given in Fig. 4.4 below.

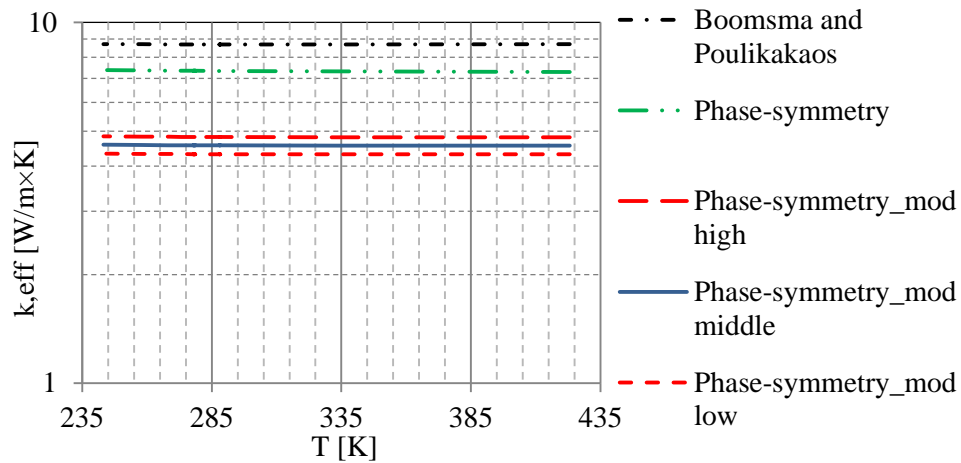


Fig. 4.4 - The modified phase symmetry model compared with the original.

Fig. 4.4 shows the prediction for the effective thermal conductivity of various theoretical models plotted versus temperature at 1.2 bar absolute pressure. The bed consists of aluminum foam ($\epsilon=0.93$) with glass beads and air as fluid. The figure shows that the modified phase-symmetry model predicts the effective thermal conductivity to be in the magnitude of 4.7 W/m·K. This is very close to the experiments of Valmirdi (1999), which had a thermal conductivity of 4.5 W/m·K ($\epsilon=0.937$, 1 bar, air).

4.2 Comparison with experimental results

In a late stage of this study, experiments were performed on foam with small glass beads and air as fluid. The experiments were performed at 298 K and ambient pressure. Pictures of the setup are provided in Fig. 4.5.

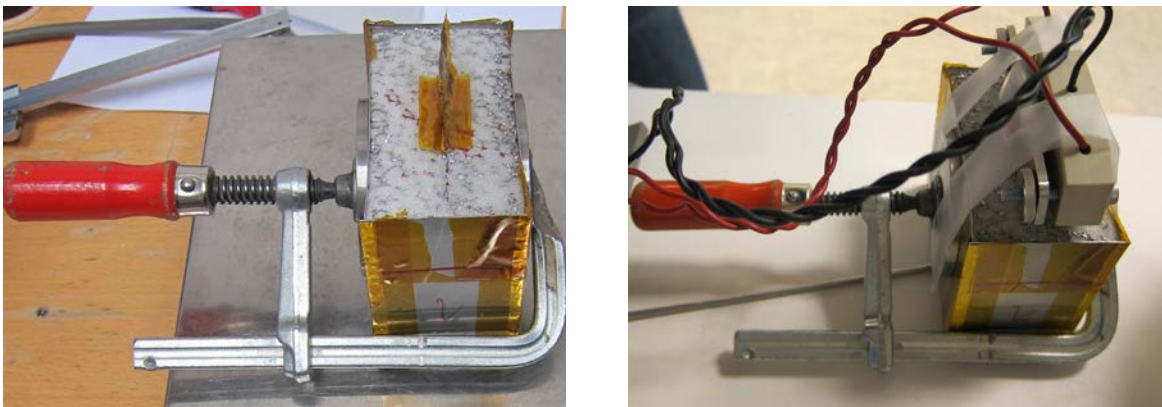


Fig. 4.5 - New measurement setup

The new experiments were conducted due to a suspicion that the previous experiments gave low values for the effective thermal conductivity, as shown in Fig. 3.10. Fig. 4.5 gives a visualization of the new experimental setup, and shows that the foam is subjected to compression in the axial direction, in order to reach an acceptable contact surface between the foam and the sensor.

The Hot Disk software enables both isotropic and anisotropic measurements. The anisotropic measurement module provides values for the effective thermal conductivity in both the radial and axial directions. The effective thermal conductivity of an anisotropic measurement is then given as (M. Gustavsson, 1994)

$$k_e = \sqrt{k_a \cdot k_r}, \quad (4.7)$$

where k_a and k_r is the measured thermal conductivity of the bed in the axial and radial direction, respectively. Contrary to the isotropic method, the anisotropic measurement method requires the input of the bed volumetric specific heat capacity ρc_p [MJ/m³K]. This was estimated to be 1.35 MJ/(m³K).

The experiments were performed once, and then the pressure was increased. This process was then repeated two times over. The experimental data are given in Table 4.2. Some of these data are plotted in Fig. 4.6 and 4.7.

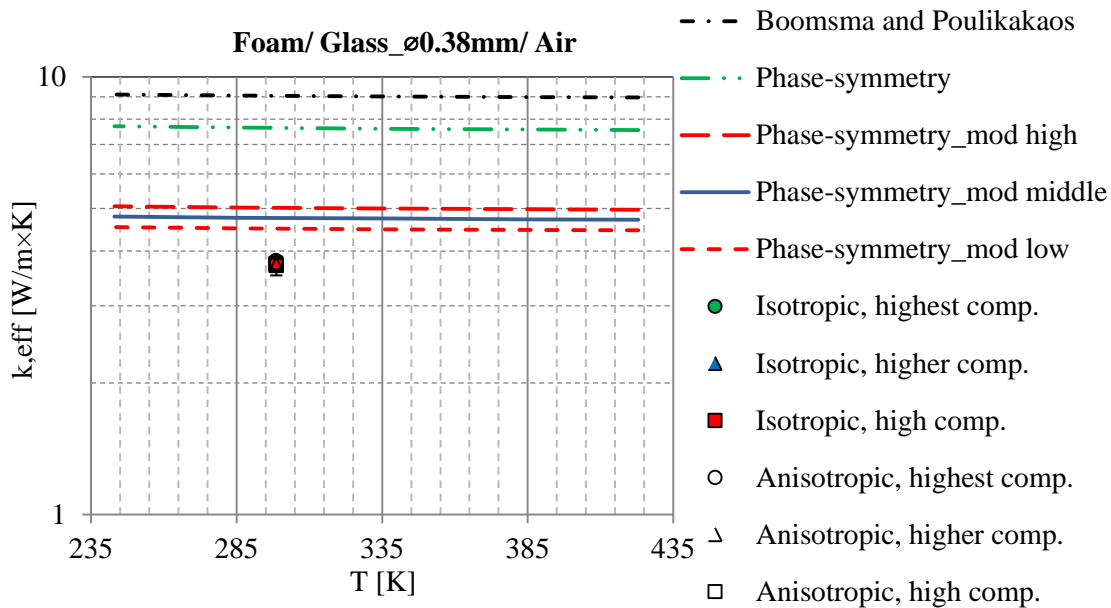


Fig. 4.6 - New foam measurements performed at 298K plotted versus the theoretical models.

Fig 4.6 shows the theoretical models plotted over the whole temperature range, and the experimental results from both isotropic and anisotropic measurements performed at 298K. A more close-up plot is given in Fig. 4.7. The magnitudes of the exerted pressure on the foam were not known, and therefore the exerted force is denoted as from high to the highest compression available. Fig. 4.6 show however little difference between the measurements, and according to Table 4.2 the variation from the lowest to the highest measured effective thermal conductivity is as little as 3%. The experimental data is approximately 20% lower than the middle bound of the new modified phase-symmetry model (blue, solid line). The reason for this will be discussed further down.

4.2 Comparison with experimental results

Table 4.2 - Experimental data from the new foam measurements.

Aluminum foam/Glass_ø0.38mm/ Air													
ε_{tot}	0,36309	R	8314	e	0,174667								
ε_{spec}	0,39	Cp_gas	1009	η_{high}	0,647214								
ε_{foam}	0,931	dp	0,00038	η_{low}	0,57735								
T	Cp_mes.	k_measured			k_f	k_s_glass	k_ZBS	k_s_alu	k_phase-sym_mod			Exp.	Compression.
		Effective	Axial	Radial					High bound	Low bound	Middle	method	
[K]	[MJ/m ³ K]	[W/m·K]	[W/m·K]	[W/m·K]	[W/m·K]	[W/m·K]	[W/m·K]	[W/m·K]	[W/m·K]	[W/m·K]	[W/m·K]		
298,65	1,348217	3,70654	3,162517	4,344148	0,0263	1,099465	0,189279	211,7847	5,024172	4,504187	4,764185	Aniso.	High
298,65	1,348217	3,728154	3,241302	4,288132	0,0263	1,099465	0,189279	211,7847	5,024172	4,504187	4,764185	Aniso.	Higher
298,65	1,348217	3,753695	3,361703	4,191396	0,0263	1,099465	0,189279	211,7847	5,024172	4,504187	4,764185	Aniso.	Highest
298,55	1,134521	3,733641	-	-	0,0263	1,099277	0,189265	211,7847	5,024154	4,50417	4,764168	Iso.	High
298,55	1,160301	3,766763	-	-	0,0263	1,099277	0,189265	211,7847	5,024154	4,50417	4,764168	Iso.	Higher
298,55	1,155828	3,78877	-	-	0,0263	1,099277	0,189265	211,7847	5,024154	4,50417	4,764168	Iso.	Highest
298,55	1,162978	3,798265	-	-	0,0263	1,099277	0,189265	211,7847	5,024154	4,50417	4,764168	Iso.	Highest
298,55	1,145366	3,792659	-	-	0,0263	1,099277	0,189265	211,7847	5,024154	4,50417	4,764168	Iso.	Highest
298,55	1,15525	3,790111	-	-	0,0263	1,099277	0,189265	211,7847	5,024154	4,50417	4,764168	Iso.	Highest
298,55	1,162441	3,788542	-	-	0,0263	1,099277	0,189265	211,7847	5,024154	4,50417	4,764168	Iso.	Highest
298,55	1,142308	3,779273	-	-	0,0263	1,099277	0,189265	211,7847	5,024154	4,50417	4,764168	Iso.	Highest
298,55	1,149854	3,802789	-	-	0,0263	1,099277	0,189265	211,7847	5,024154	4,50417	4,764168	Iso.	Highest
298,55	1,153614	3,793865	-	-	0,0263	1,099277	0,189265	211,7847	5,024154	4,50417	4,764168	Iso.	Highest
298,55	1,163294	3,790825	-	-	0,0263	1,099277	0,189265	211,7847	5,024154	4,50417	4,764168	Iso.	Highest
298,55	1,159858	3,80246	-	-	0,0263	1,099277	0,189265	211,7847	5,024154	4,50417	4,764168	Iso.	Highest

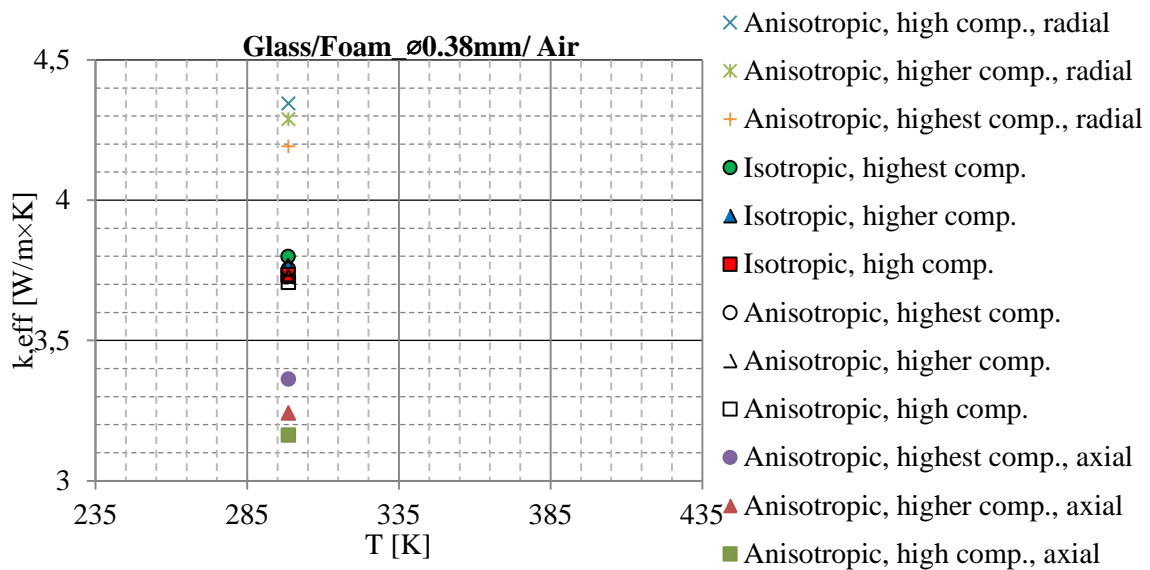


Fig. 4.7 - Anisotropic and isotropic effective thermal conductivity measurements of aluminum foam at 298K and ambient pressure. The foam porosity is $\varepsilon=0.93$.

Fig 4.7 shows the same experimental data as Fig. 4.6, and in addition it shows the axial and radial components of the anisotropic measurements. The Fig. 4.7 shows, that if the compression is increased (from high \rightarrow highest) the thermal conductivity increases. This is to be expected, since the thermal contact between the sensor and the foam will be increased, and thus increasing the quality of the measurement and thereby also the conductivity. Beside this, two conclusions can be drawn from this plot:

1. The radial component of the thermal conductivity (Fig. 4.7, Top three markers) does not increase when compression is increased. Due to the improvement in contact area between the sensor and the foam, the thermal conductivity should therefore increase when applying higher compression. However, this was not the case. A possible explanation is that the compression that is exerted on the foam in the axial direction will *increase* the heat transfer path in the radial direction, and thus decreasing the thermal conductivity in the radial direction. In the axial direction it will be the other way around.
2. The magnitude of the axial thermal conductivity component should, according to the new modified phase-symmetry model, be higher than the radial thermal conductivity. An example is given in Table 4.3.

Table 4.3 - Radial and axial thermal conductivity.

Compression	k_Experiment [W/m \cdot K]		k_Phase-sym_mod [W/m \cdot K]	
	Axial	Radial	High	Low
High	3,163	4,344	5,024	4,504
Higher	3,241	4,288	5,024	4,504
Highest	3,362	4,191	5,024	4,504

The values for the thermal conductivity given in Table 4.3 suggest that the axial component should be in the magnitude of approximately 5 W/m·K. This implies that either the pentagon is not a satisfactory way to model the pore structure in the axial direction, or the contact area between the sensor and the aluminum foam needs to be improved even further. Either way, this is an issue that needs to be examined through further experimental investigations. The reduction in axial conductivity could also be due to bubble-like structures inside the foam, as shown in Fig. 4.8 below.

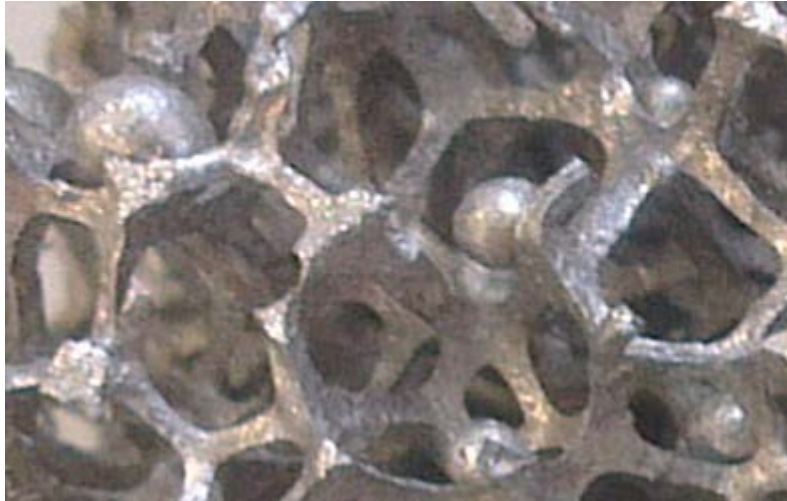


Fig. 4.8 - A close-up of the aluminum foam applied in the experiments.

Fig. 4.8 also shows signs of damage on the ligaments. Some of them may be broken, and thus extending the path of heat transfer by conduction through the foam. The foam consists of pure aluminum, whose solid conductivity is very high in ambient conditions (211.79 W/m·K at 298K; (NIST Chemistry Webbook)). The bubbles in Fig. 4.8 may have been formed during the foam production process, and although the bubbles consist of pure aluminum, they do not contribute to heat transfer in either direction. The bubbles are in fact only taking up space inside the bed, and this can be modeled theoretically with the introduction of a non-conducting foam porosity ϵ_{nc} which can be related to the conducting foam porosity ϵ_{cond} through the relation

$$\epsilon_{foam} = \epsilon_{nc} + \epsilon_{cond}. \quad (4.8)$$

This introduction implies that $\epsilon_{foam} < \epsilon_{nc}$. At the moment of this discovery there was not enough time to address this issue, however it is an issue that needs to be investigated further.

Summing up the experiments conducted on aluminum foam, the conclusion is that with the current measurement techniques one can expect an increase in thermal conductivity at 298 K and ambient pressure from 0.22 W/m·K to approximately 3.7 W/m·K with the use of a high porosity ($\epsilon=0.93$) aluminum foam. The magnitude increases by a factor of 17. However, the new theoretical model which was developed suggests that the thermal conductivity should be in the magnitude of 4.7 W/m·K. The discrepancy between theory and experimental results therefore needs to be addressed in future works.

Part 5 - Conclusions

5.1 Conclusion

The goal of this work was to determine the effective stagnant thermal conductivity of the MOF materials Cu-btc and Fe-btc, and as well examine the effect of introducing heat transfer enhancement structures such as aluminum foam or wires. Furthermore, it was important to confirm the validity of the Hot Disk TPS measurement setup.

First, experiments were performed on glass beads ($\varnothing 0.38\text{mm}$ and $\varnothing 1.395\text{mm}$), which served as a reference material, in order to understand the setup and find a suitable correlation for determining the solid conductivity of the MOF. The model of Zehner/Bauer/Schlünder (ZBS) was chosen for this task because of its best fit with the glass beads experimental data.

In addition to the 5% uncertainty on each measured data point come the uncertainties of the ZBS model, due to the input of measured parameters such as porosity. The uncertainty analysis revealed that the experimental data fitted within the uncertainty bounds of the ZBS model, which were approximately $\pm 10\%$. Adding the uncertainty of the ZBS model to the uncertainty of the experiments gives a total uncertainty of 15% from the glass beads experiments.

Solid conductivity of MOF materials Fe-btc and Cu-btc were then successfully determined. Temperature dependent functions for the solid conductivity were obtained through a least square procedure with the ZBS model. The obtained solid conductivity can be expressed by the function

$$k_s = k_{s0} \left(\frac{T}{T_0} \right)^n, \quad (5.1)$$

with the values given in Table 5.1 below. This function is valid in the range of $240\text{K} < T < 420\text{K}$.

Table 5.1 - Optimized constants

	Cu-btc	Fe-btc
k_{s0}	0.33	0.28
n	0.11	0.26
$ \sum \Delta k_e / \sum k_{ZBS}$	5.01%	5.44%

Also, a modified phase-symmetry model for determination of the effective stagnant thermal conductivity for high-porosity metal foams was developed. The model was obtained by modifying the model of Hsu et al. (1994) with the introduction of a dimensionless tortuosity factor accounting for extended heat transfer path through the solid structure. The effective stagnant thermal conductivity is given as

$$k_e = (1 - \sqrt{1 - \varepsilon})k_f + (1 - \sqrt{\varepsilon})k_s^* + (\sqrt{1 - \varepsilon} + \sqrt{\varepsilon} - 1)k_{sf}, \quad (5.2)$$

with

$$k_{sf} = k_f \left[\frac{b(1-\lambda)}{(1-\lambda b)^2} \ln\left(\frac{1}{\lambda b}\right) - \frac{b-1}{1-\lambda b} \right], \quad (5.3)$$

where

$$b = \left(\frac{1-\varepsilon}{\varepsilon} \right)^{0.9676}, \quad (5.4)$$

$$\lambda = k_f/k_s^*, \quad (5.5)$$

and

$$k_s^* = \eta \cdot k_s. \quad (5.6)$$

The tortuosity factor η is given to be

$$\eta = \begin{cases} 0.647; & \text{axial direction} \\ 0.557; & \text{radial direction} \end{cases} \quad (5.7)$$

The η -value in the axial and radial direction result in a high and low band for the effective thermal conductivity. The middle bound of this model is expressed as

$$k_e = \sqrt{k_{e,a} \cdot k_{e,r}}, \quad (5.8)$$

where $k_{e,a}$ and $k_{e,r}$ is the effective thermal conductivity of the bed in the axial and radial direction, respectively. This modified phase-symmetry model is applicable for high porosity metal foams, and gives values for the effective thermal conductivity in the magnitude of 4.5 W/m·K at 298 K and ambient pressure.

Experimental investigations on aluminum foam filled with glass beads and air (298K, 1 bar) show that the foam increases the effective thermal conductivity of the bed from 0.22 W/m·K to 3.7W/m·K. According to the newly developed model, as well as other authors (Valmirdi, 1999), this value should be ~4.5 W/m·K for this type of foam. This therefore needs to be investigated further.

Overall, the Hot Disk measurement setup provides accurate measurements of the effective thermal conductivity of porous materials. However, due to a calibration error, the setup show a discontinuity in the effective thermal conductivity in the range of $273 < T < 283$ K. Moreover, during measurements of heat distribution structures, it was discovered that the contact between the structure and the sensor needs to be as high as possible.

5.2 Further work

Conducting measurements with glass beads as a reference material proved somewhat problematic, because no data existed on the thermophysical properties of the exact composition of the glass melt applied. In order to ensure a total uncertainty below 10%, a pure substance whose thermophysical properties are well-known should be applied in future investigations.

Furthermore, the following improvements should be made of the measurement setup:

- The reason for the silicon seepage into the vacuum/pressure cell should be investigated. A new sealing or another type of vacuum grease should be applied.
- The discontinuity in the effective thermal conductivity in the range of $263\text{K} < T < 283\text{K}$ needs to be investigated further.
- A cryo-probe should be installed and calibrated, in order to perform experiments on MOF and aluminum foam in temperatures below 240K – the actual working range of a cryo-adsorption hydrogen storage.

Also, further experiments, both isotropic and anisotropic, should be performed on various metal foams. The measurement techniques used in this work gave values for the foam effective thermal conductivity up to $\sim 3.7 \text{ W/m}\cdot\text{K}$. The theory suggests that it should be in the magnitude of $4.7 \text{ W/m}\cdot\text{K}$. Anisotropic measurements show that the axial thermal conductivity component is only $\sim 3 \text{ W/m}\cdot\text{K}$, while the model suggests that this value should be in the vicinity of $5 \text{ W/m}\cdot\text{K}$. In order to find the reason for this discrepancy, new foam experiments with emphasis on improving the thermal contact between the Hot Disk sensor and the sample should be performed. Moreover, a larger sensor can be applied to reduce the structural influences of the foam. However, this may also require that the sample size needs to be increased.

References

- Bauer and Schlünder. 1978.** Part I: Effective radial thermal conductivity of packings in gas flow. Part II: Thermal conductivity of the packing fraction without gas flow. *Int. Chem. Eng.* 1978, 18, ss. 189-204.
- Bejan, Donald A. Nield and Adrian. 2006.** *Convection in porous media*. New York : Springer, 2006. ss. 3,4.
- Berkely Engineering Division.** Table Of Emissivity Of Various Surfaces. [Internet] http://www-eng.lbl.gov/~dw/projects/DW4229_LHC_detector_analysis/calculations/emissivity2.pdf.
- Boomsma and Poulikakos. 2011.** Corrigendum for the paper: "On the effective thermal conductivity of a three-dimensionally structured fluid-saturated metal foam". *Journal of Heat and Mass Transfer*. 2011, 54, ss. 746-748.
- Boomsma and Poulikakos. 2000.** On the effective thermal conductivity of a three-dimensionally structured fluid-saturated metal foam. *Int Journal of Heat and Mass transfer*. 2000, 44, ss. 827-836.
- Breitbach and Barthels. 1980.** The radiant heat transfer in the high temperature reactor core after failure of the afterheat removal systems. *Nuclear Techn.* 1980, 49, ss. 392-399.
- Cengel, Yunus A. 2006.** *Heat and Mass Transfer - A practical approach*. s.l. : McGraw Hill, 2006. s. 18.
- Chapman, J. A. 1984.** *Heat transfer*. 4th. s.l. : MacMillan, 1984.
- Damköhler, G. 1937.** *Der Chemie-Ingenieur*. 1937, Vol. 3.
- Dressler and Boegli. 1958.** An investigation of effective thermal conductivities of powders in various gases. *ASME Transactions*. 1958, 80, ss. 1417-1425.
- E. S. Huetter, N. I. Koemle, G. Kargl, E. Kaufmann. 2008.** Determination of the effective thermal conductivity. *Journal fo geophysical research*. 2008, Vol. 113, E12004, ss. 1-11.
- Ed. James, F. Shackelford, W. Alexander. 2001.** Thermal properties of materials. *Materials Science and Engineering Handbook*. s.l. : CRC Press LCC, 2001, 5.
- engineeringtoolbox.com.** Emissivity coefficients of some common materials. [Internet] http://www.engineeringtoolbox.com/emissivity-coefficients-d_447.html.
- Glassproperties.com.** Calculation of phonon thermal conductivity of glass melts. [Internet] <http://www.glassproperties.com/thermal-conductivity/>.
- Handbook of glass data. 1987.** Part C. s.l. : Elsevier, 1987, s. 212.
- Henriksen, Jan Georg. 2012.** *Experimental investigations on pressure drop effects in various packed beds*. Trondheim : NTNU, 2012. ss. 1-138.
- Hsu et al. 1994.** Modified Zehner-Schlünder models for stagnant thermal conductivity of porous media. *Int J of Heat and Mass transfer*. 1994, 37, ss. 2751-2759.
- Hsu, C. T. 1999.** A Closure Model for Transient Heat Conduction in Porous Media. *Journal of Heat Transfer*. 1999, Vol. 121, 3, ss. 733-739.
- Hubert, Loreline. 2011.** *Experimental study of permeability effects in porous media in order to implement hydrogen storage*. Trondheim : NTNU, 2011. s. 36.
- IAEA-TECDOC-1163. 2000.** Vienna : IAEA, 2000. ss. 301-303.
- IES. 2007.** Well-to-wheels analysis of future automotive fuels and powertrains in the European context. *Institute for Environment and Sustainability*. [Internet] 2007. http://ies.jrc.ec.europa.eu/uploads/media/WTW_Report_010307.pdf.
- Incropera, DeWitt, Bergmann, Lavine. 2007.** *Fundamentals of heat and mass transfer*. New York : Wiley, 2007. ss. 60-68.
- Inger-Anne Rasmussen, Camilla Foyn Eithun. 2011.** *Hydrogen storage Development of a setup for thermal conductivity measurements of porous materials*. Trondheim : NTNU, 2011. ss. 1-95.

- Kandula, M. 2011.** On the effective thermal conductivity of porous packed beds with uniform spherical particles. *Journal of Porous Media*. 2011, Vol. 14, ss. 919-926.
- KarlRoth.com.** Glass Beads. [Internet]
<http://www.carlroth.com/catalogue/catalogue.do?favOid=00000000000334c600070023&act=showBookmark&lang=en-com&market=COM>.
- Kaviany, M. 1995.** *Principles of heat transfer*. 2nd edition. New York : Springer, 1995. 119-156.
- Krupiczka, R. 1967.** Analysis of thermal conductivity in granular materials. *Int Chem Eng*. 1967, 7, ss. 122-144.
- Kunii and Smith. 1960.** Heat transfer characteristics of porous rocks. *AIChE Journal*. 1960, 6, ss. 71-78.
- L. Spampinato, S. Calvari, C. Oppenheimer, E. Boschi. 2011.** Volcano surveillance using infrared cameras. *Earth Science Reviews*. May 2011, Vol. 106, 1-2, s. 68.
- M. Gustavsson, E. Karawacki, S. E. Gustafsson. 1994.** Thermal conductivity, thermal diffusivity, and specific heat of thin samples from transient measurements with Hot Disk sensors. *Rev. Sc. Instrum.* 1994, Vol. 12, 65.
- Maxwell, J. C. 1873.** A Treatise on Electricity and Magnetism. *Clarendon Press*. 1873, s. 365.
- Moffat, R. J. 1988.** *Describing uncertainties in experimental results*. New York : Exp. Therm. & fluid Sci, 1988. ss. 3-17.
- Monarchserver.com.** Table Of Total Emissivity. [Internet]
<http://www.monarchserver.com/TableofEmissivity.pdf>.
- Möllenkopf and Martin. 1982.** Zur Theorie des Wärmeübergangs an bewegte Kugelschüttungen bei kurzfristigem kontakt. *Vt-Verfahrenstechnik*. 1982, 16, ss. 701-706.
- NIST Chemistry Webbook.** Material Properties: 1100 Aluminum (UNS A91100). [Internet]
http://cryogenics.nist.gov/MPropsMAY/1100%20Aluminum/1100%20Aluminum_rev.htm.
- NIST Chemistry Webbook.** Thermophysical Properties of Fluid Systems. [Internet]
<http://webbook.nist.gov/chemistry/fluid/>.
- Nozad et al. 1985.** Heat conduction in multiphase systems. 1: Theory and experiments for two-phase systems. *Chem Eng Sci*. 1985, 40, ss. 843-855.
- Prasad et al. 1989.** Evaluation of correlations for stagnant thermal conductivity of liquid-saturated porous beds of spheres. *International Journal of Heat and Mass transfer*. 1989, 32, ss. 1793-1796.
- R. Siegel, J. R. Howell. 2002.** *Thermal Radiation Heat Transfer*. s.l. : Taylor and Francis, 2002.
- R.K. Ahluwalia, T.Q. Hua, J.K. Peng. 2012.** On-board and Off-board performance of hydrogen storage options for light-duty vehicles. *Int. Journal of Hydrogen Energy*. 2012, 37, s. 2899.
- Schlemminger, Christian. 2013.** *Work in progress*. Trondheim : NTNU, 2013.
- Schlünder, E. U. 1981.** *Einführung in die Wärmeübertragung*. 3. Brunswick : Vieweg Verlag, 1981.
- Schlünder, E. U. 1981.** Über den Stand der wissenschaftlichen Grundlagen zur Auslegung von Kontaktrocknern für grobkörniges, rieselfähiges Trocknungsgut. *Chem Ing Tech*. 1981, Vol. 53, 12, s. 930.
- Shcumann, T. E. W. 1934.** Heat flow through granulated material. *Fuel*. 1934, 13, ss. 249-256.
- Song and Yovanovich. 1987.** Correlation of thermal accommodation coefficient for engineering surfaces. *Nat. Heat Transfer Conference*. 1987.
- Stephan Kabelac, Dieter Vortmeyer. 2010.** K1 Radiation Of Surfaces. *VDI Heat Atlas*. s.l. : Springer, 2010.
- Tavman, I.H. 1996.** Effective thermal conductivity of granular porous materials. *Communications in Heat and Mass Transfer*. 1996, Vol. 23, 2, ss. 169-176.
- Thermopedia.com.** A-to-Z Guide to Thermodynamics, Heat & Mass Transfer, and Fluids Engineering. [Internet] <http://www.thermopedia.com/content/1187/?tid=110&sn=24>.
- Thermoworks.com.** Emissivity table. [Internet] http://www.thermoworks.com/emissivity_table.html.

- Thompson, D'Arcy. 1995.** *On growth and form*. Cambridge : Canto, 1995. s. 121.
- Tsotsas and Schlünder. 1991.** The impact of particle size dispersity on the thermal conductivity of packed beds: Measurement, numerical simulation, prediction. *Chem. Eng. Technol.* 1991, 14, ss. 421-427.
- Tsotsas, E. 1987.** Thermal Conductivity of Packed Beds: A Review. *Chem Eng Process.* 1987, 22, ss. 19-37.
- Ullmann. 1989.** Encyclopedia of Industrial Chemistry, 5th ed. [Internet] 1989.
- US Department of energy. 2011.** *Targets for Onboard Hydrogen Storage Systems for Light-Duty Vehicles*. 2011.
- Valmidi, Mahajan,. 1999.** The effective thermal conductivity of high porosity fibrous metal foams. *Journal of Heat Transfer.* 1999, Vol. 121, s. 467.
- van Antwerpen et al. 2010.** A review of correlations to model the packing structure and effective thermal conductivity in packed beds of mono-sized spherical particles. *Nuclear Engineering and Design.* 2010, 240, ss. 1803-1818.
- VDI Heat Atlas. 2010.** D6.3. s.l. : Springer, 2010, ss. 571-579.
- VDI Heat Atlas. 2010.** Section D3. s.l. : Springer, 2010, s. 344.
- Vortmeyer, D. 1980.** Radiation in packed solids. *Ger. Chem. Eng. Journal.* 1980, s. 127.
- W. M. Rohsenow, H. Choi. 1961.** *Heat, Mass and Momentum Transfer*. s.l. : Prentice-Hall, 1961.
- Zehner and Schlünder. 1972.** Einfluß der Wärmestrahlung und des Druckes auf den Wärmetransport in nicht durchströmten Schüttungen. *Chem. Ing. Tech.* 1972, Vol. 44, 23, ss. 1303-1308.
- Zehner and Schlünder. 1970.** Thermal conductivity of granular materials at moderate temperatures. *Chem Ing-Tech.* 1970, 42, ss. 933-941.

Appendix A - Particle diameter

Particle diameter of small glass beads are given in Fig- A-1. This particle diameter was used for all measurements with the small glass beads. This also applies for the larger glass beads, whose sieving results are displayed in Fig. A-2 The particle diameter for Fe-bc in fillings one and two is shown in Fig A-3, and the one in fillings three, four and five, is shown in Fig. A-4.

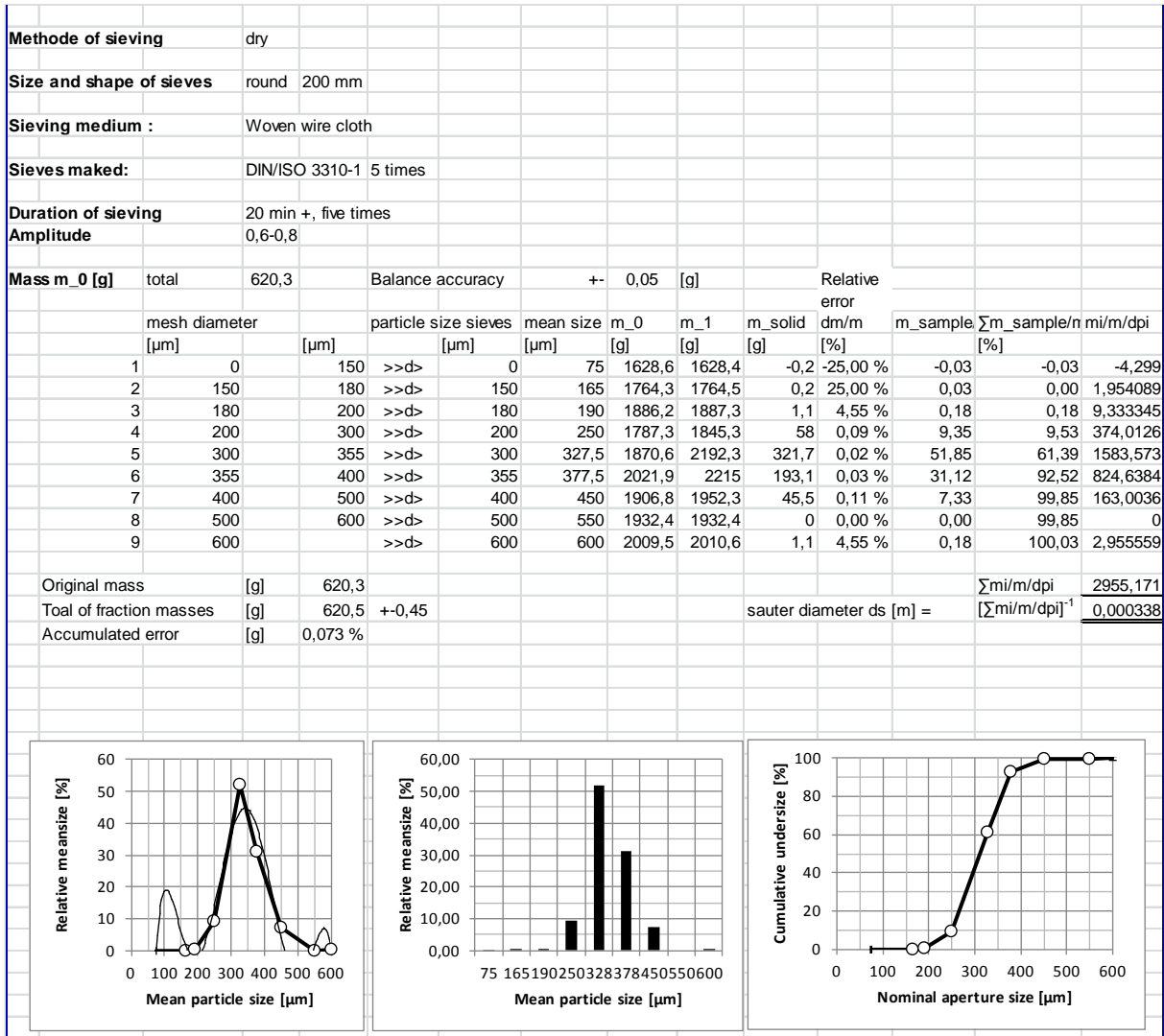


Fig. A-1 Particle diameter of small glass beads.

sieving analysis 08.05.2013 glass beads ROTH-A555.1 1.25<dp<1.65													
m tot	407,2												
siev				mean	m_o_siev	m_1_siev	mbed	mi/m/dpi					
	1	0	>>	1000	500	381,3	381,3	0	0				
	2	1000	>>	1250	1125	433,2	433,3	0,1	0,218292949				
	3	1250	>>	1400	1325	387,6	415,6	28	51,89605961				
	4	1400	>>	1400	1400	479,4	858,4	379	664,8189728				
								$\sum mi/m/dpi$	716,9333253				
								particle diameter	$(\sum mi/m/dpi)^{-1}$				0,0013948 m

Fig. A-2 Particle diameter of the larger glass beads.

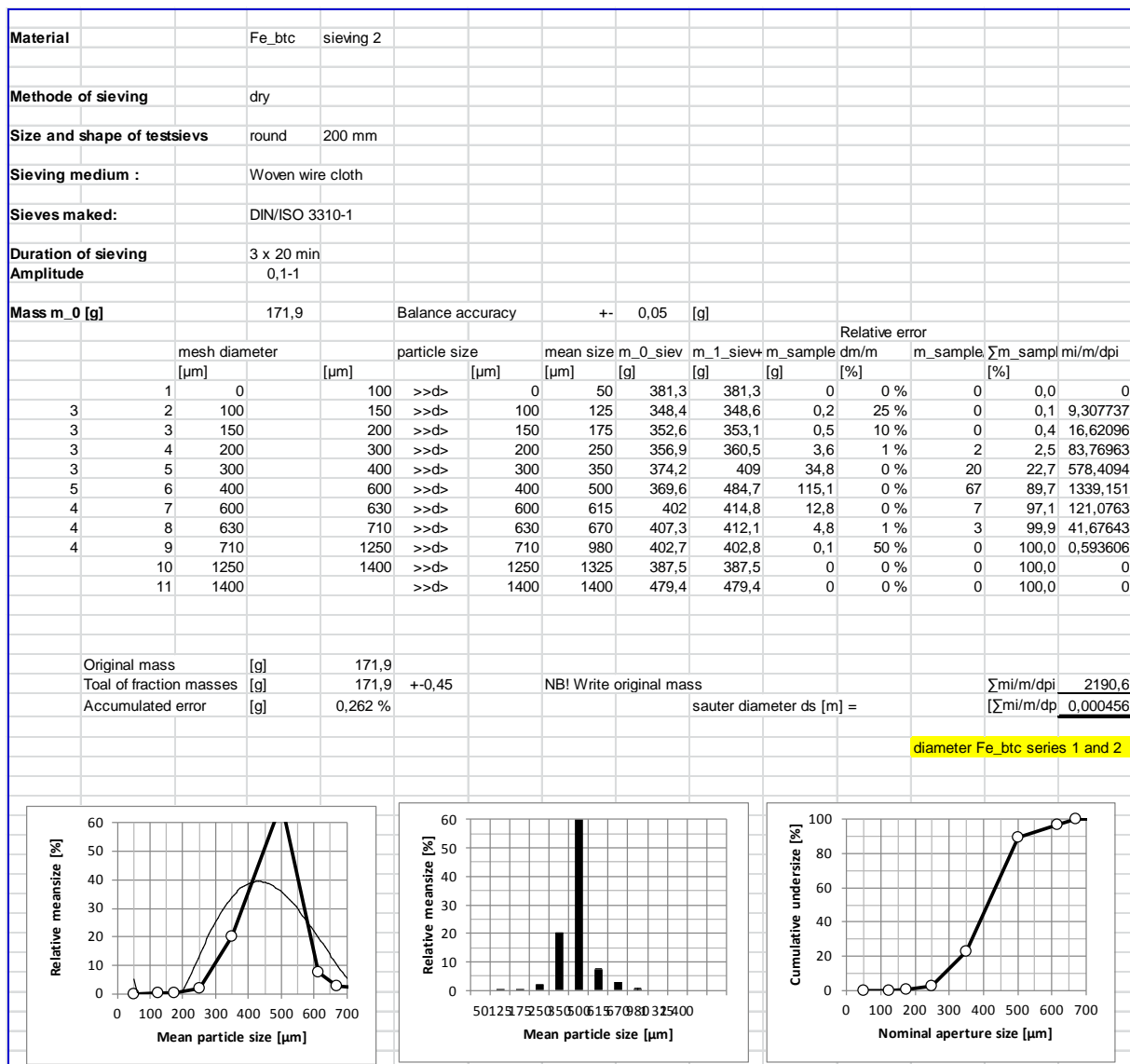


Fig. A-3 Particle diameter of Fe-btc used for measurement series 1 and 2.

container	mean size	m_sample	mi/m/dpi
3..	125	0,3	13,913043
3..	175	0,6	19,875776
3..	250	4,5	104,34783
3..	350	39,4	652,58799
3..	500	127,7	1480,5797
m		172,5	2271,3043
		[Σmi/m/dpi] ⁻¹	0,000440
diameter fe_btc series 3, 4 and 5			
5..	500	71,5	amount of 5

Fig. A-4 Particle diameter of Fe-btc used for measurement series 3 through 5.

Appendix B - Exact composition of glass beads

Source: (Glassproperties.com). The source claim that this applies for room temperature. This indicates that the data is valid between 293K and 298K.

Calculation of the thermal (phonon) conductivity of glass at room temperature

M. K. Choudhary, R. M. Potter: "Heat Transfer in Glass-Forming Melts"; Chapter 9 in: "Properties of Glass-Formation Melts" edited by D. L. Pye, A. Montenegro, I. Joseph; CRC Press, Boca Raton, Florida, May 2005, ISBN: 1-57444-662-2
 Excel file designed by Alexander Fluegel, November 2007, info@glassproperties.com, http://glassproperties.com/thermal-conductivity/

Glass composition in wt%	
SiO ₂	72,290
B ₂ O ₃	0,000
Al ₂ O ₃	0,580
Li ₂ O	0,000
Na ₂ O	13,000
K ₂ O	0,200
Cs ₂ O	0,000
MgO	4,220
CaO	9,600
SrO	0,000
BaO	0,000
PbO	0,000
Fe ₂ O ₃	0,110
TiO ₂	0,000
MnO	0,000
ZnO	0,000
CoO	0,000
NiO	0,000
CuO	0,000
Bi ₂ O ₃	0,000
Sb ₂ O ₃	0,000
F	0,000

Thermal conductivity in W / (m · K)
1,086

The error of the prediction is about 10% of the predicted value.

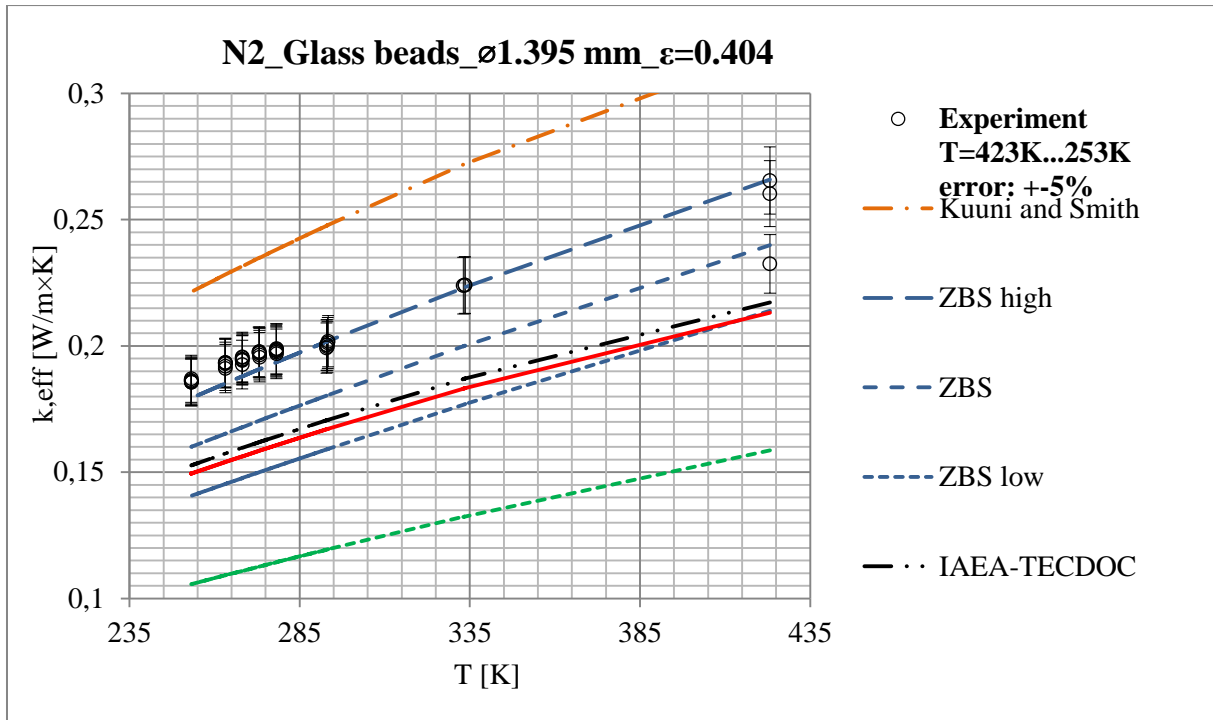
Glass composition in mol%	
SiO ₂	70,886
B ₂ O ₃	0,000
Al ₂ O ₃	0,335
Li ₂ O	0,000
Na ₂ O	12,358
K ₂ O	0,125
Cs ₂ O	0,000
MgO	6,169
CaO	10,086
SrO	0,000
BaO	0,000
PbO	0,000
Fe ₂ O ₃	0,041
TiO ₂	0,000
MnO	0,000
ZnO	0,000
CoO	0,000
NiO	0,000
CuO	0,000
Bi ₂ O ₃	0,000
Sb ₂ O ₃	0,000
F	0,000

Appendix C - Glass beads results

Glass beads with N₂, filling 1, measurement error =5% ϵ_{bulk} 0,404064 ρ_{bulk} 1550,03 kg/m³ d_p 0,001395 m

T [K]	k [W/m·K]	Cp_gas [J/kgK]	k_f [W/m·K]	k_s [W/m·K]	K=k_s/k_f	k_ZBS [W/m·K]	$\Delta k_{\text{ZBS}}/k_{\text{ZBS}}$
423,164	0,232	1046,360	0,034	1,243	36,497	0,240	11 %
423,146	0,260	1046,358	0,034	1,243	36,498	0,240	11 %
423,137	0,265	1046,357	0,034	1,243	36,498	0,240	11 %
333,071	0,224	1040,026	0,028	1,157	41,430	0,200	12 %
333,605	0,224	1040,045	0,028	1,158	41,402	0,200	12 %
333,515	0,224	1040,042	0,028	1,158	41,407	0,200	12 %
292,879	0,199	1039,143	0,025	1,088	43,472	0,180	12 %
293,104	0,200	1039,146	0,025	1,089	43,461	0,180	12 %
293,165	0,200	1039,146	0,025	1,089	43,458	0,181	12 %
278,138	0,198	1039,056	0,024	1,058	44,199	0,173	12 %
278,110	0,198	1039,056	0,024	1,058	44,200	0,173	12 %
278,126	0,198	1039,056	0,024	1,058	44,199	0,173	12 %
273,178	0,196	1039,049	0,024	1,048	44,441	0,170	12 %
273,164	0,197	1039,049	0,024	1,048	44,442	0,170	12 %
272,998	0,198	1039,049	0,024	1,047	44,450	0,170	12 %
268,147	0,194	1039,053	0,023	1,037	44,686	0,168	12 %
268,153	0,195	1039,053	0,023	1,037	44,685	0,168	12 %
268,114	0,196	1039,053	0,023	1,037	44,687	0,168	12 %
263,137	0,192	1039,065	0,023	1,025	44,928	0,165	12 %
263,112	0,193	1039,065	0,023	1,025	44,929	0,165	12 %
263,135	0,193	1039,065	0,023	1,025	44,928	0,165	12 %
253,140	0,186	1039,114	0,022	1,002	45,408	0,160	12 %
253,129	0,186	1039,114	0,022	1,002	45,408	0,160	12 %
253,146	0,187	1039,114	0,022	1,002	45,408	0,160	12 %
253,157	0,186	1039,114	0,022	1,002	45,407	0,160	12 %
253,138	0,186	1039,114	0,022	1,002	45,408	0,160	12 %
253,159	0,186	1039,114	0,022	1,002	45,407	0,160	12 %
263,178	0,191	1039,065	0,023	1,025	44,926	0,165	12 %
263,141	0,193	1039,065	0,023	1,025	44,928	0,165	12 %
263,148	0,193	1039,065	0,023	1,025	44,927	0,165	12 %
268,111	0,193	1039,053	0,023	1,037	44,687	0,168	12 %
268,162	0,195	1039,053	0,023	1,037	44,685	0,168	12 %
268,151	0,194	1039,053	0,023	1,037	44,685	0,168	12 %
273,208	0,196	1039,049	0,024	1,048	44,440	0,170	12 %

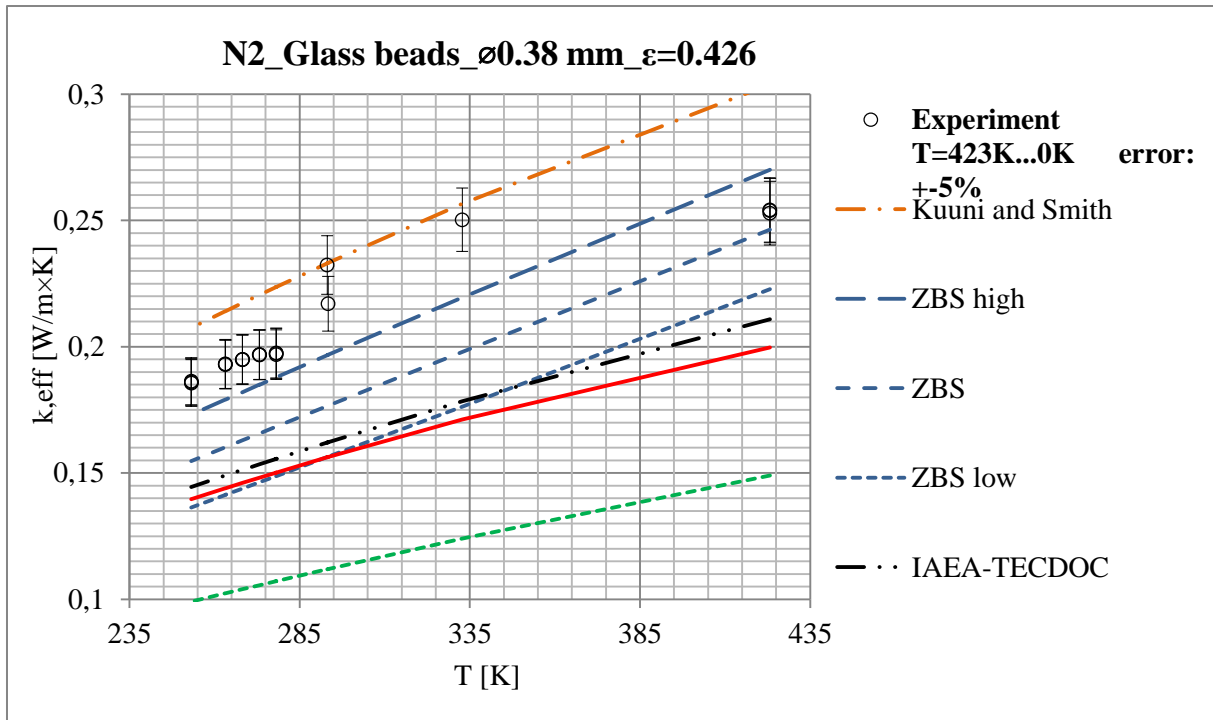
273,148	0,197	1039,049	0,024	1,048	44,443	0,170	12 %
273,120	0,198	1039,049	0,024	1,048	44,444	0,170	12 %
278,159	0,197	1039,056	0,024	1,059	44,198	0,173	12 %
278,195	0,199	1039,056	0,024	1,059	44,196	0,173	12 %
278,170	0,199	1039,056	0,024	1,059	44,197	0,173	12 %
292,883	0,200	1039,143	0,025	1,088	43,472	0,180	12 %
293,225	0,201	1039,147	0,025	1,089	43,455	0,181	12 %
293,340	0,202	1039,148	0,025	1,089	43,449	0,181	12 %



Glass beads with N₂, filling 1, measurement error =5%

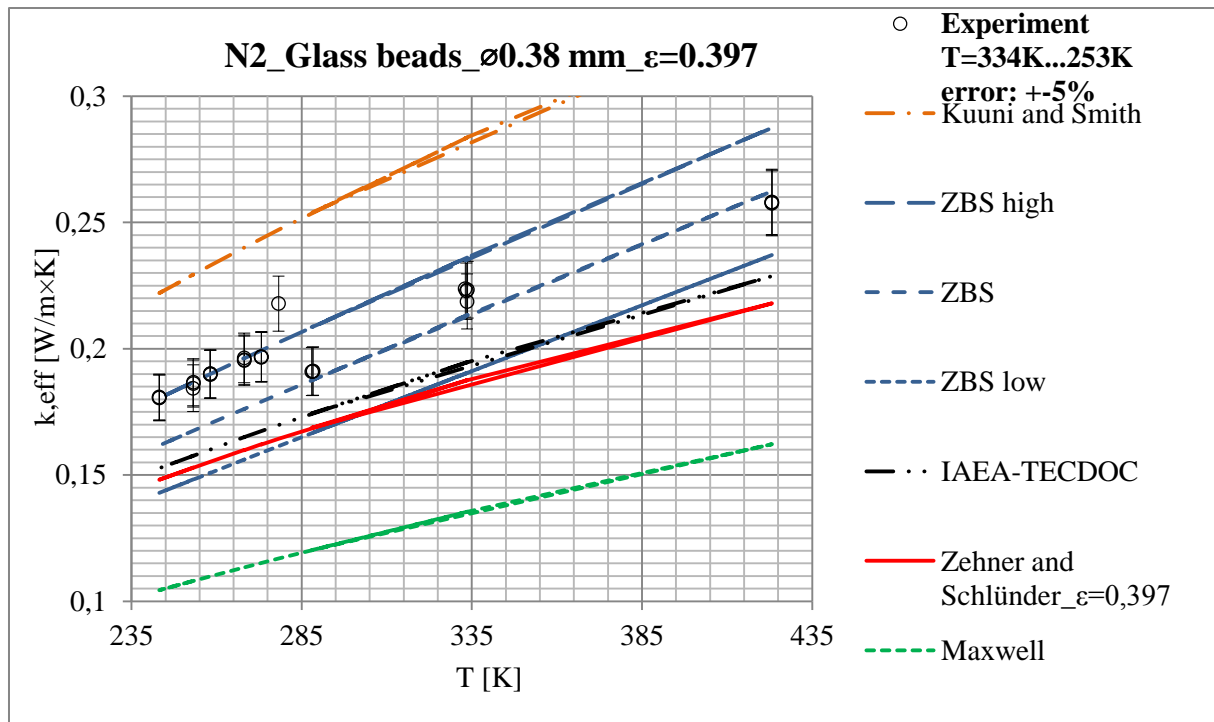
ϵ_{bulk} 0,425965
 ρ_{bulk} 1493,06 kg/m³
 d_p 0,00038 m

T [K]	k [W/m×K]	Cp _{gas} [J/kgK]	k _f [W/m×K]	k _s [W/m×K]	K=k _s /k _f	k _{ZBS} [W/m×K]	$\Delta k_{\text{ZBS}}/k_{\text{ZBS}}$
423,170	0,253	1046,360	0,034	1,243	36,496	0,246	10 %
423,160	0,254	1046,359	0,034	1,243	36,497	0,246	10 %
423,144	0,254	1046,358	0,034	1,243	36,498	0,246	10 %
332,757	0,250	1040,015	0,028	1,157	41,446	0,198	11 %
293,060	0,232	1039,145	0,025	1,089	43,463	0,176	11 %
293,364	0,217	1039,148	0,025	1,089	43,448	0,177	11 %
278,126	0,197	1039,056	0,024	1,058	44,199	0,168	12 %
278,097	0,197	1039,056	0,024	1,058	44,201	0,168	12 %
278,121	0,197	1039,056	0,024	1,058	44,200	0,168	12 %
273,144	0,197	1039,049	0,024	1,048	44,443	0,166	12 %
273,191	0,197	1039,049	0,024	1,048	44,440	0,166	12 %
273,174	0,197	1039,049	0,024	1,048	44,441	0,166	12 %
268,150	0,195	1039,053	0,023	1,037	44,685	0,163	12 %
268,201	0,195	1039,052	0,023	1,037	44,683	0,163	12 %
268,214	0,195	1039,052	0,023	1,037	44,682	0,163	12 %
263,196	0,193	1039,065	0,023	1,026	44,925	0,160	12 %
263,157	0,193	1039,065	0,023	1,025	44,927	0,160	12 %
263,138	0,193	1039,065	0,023	1,025	44,928	0,160	12 %
253,168	0,186	1039,114	0,022	1,002	45,407	0,155	12 %
253,147	0,186	1039,114	0,022	1,002	45,408	0,155	12 %
253,156	0,186	1039,114	0,022	1,002	45,407	0,155	12 %



Glass beads with N₂, filling 2, measurement error =5% $\varepsilon_{\text{bulk}}$ 0,396707583 ρ_{bulk} 1569,16 kg/m³ d_p 0,00038 m

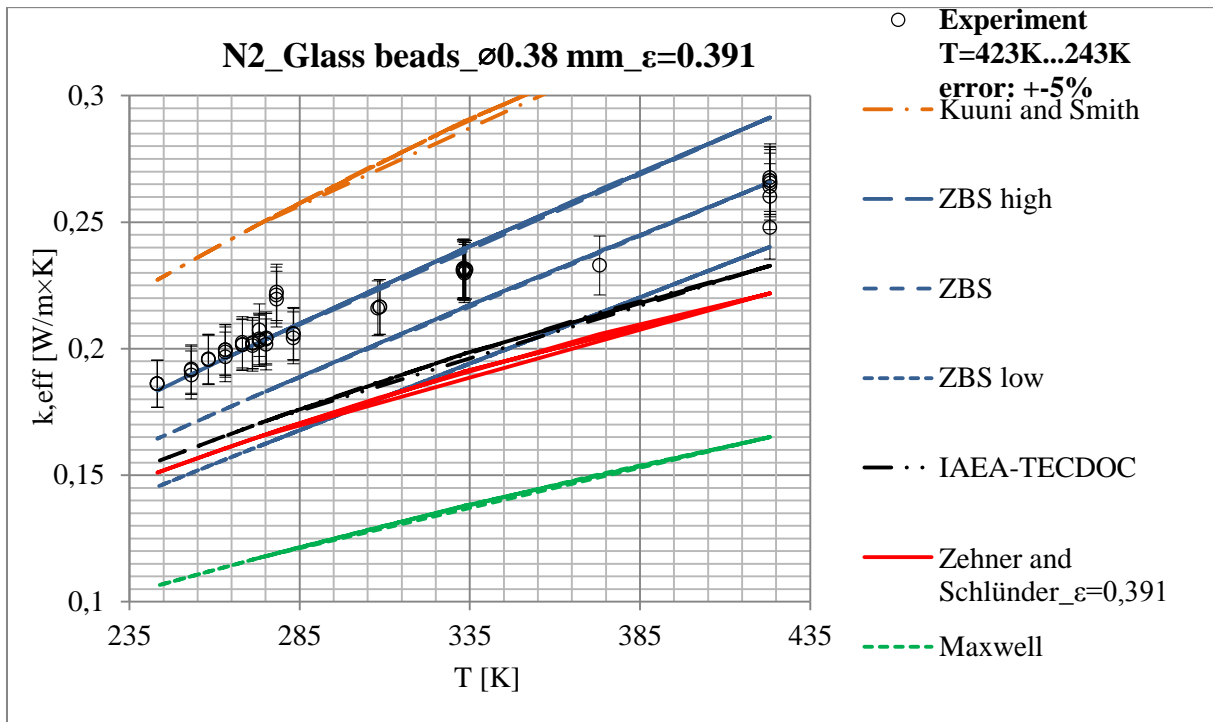
T [K]	k [W/m×K]	Cp_gas [J/kgK]	k _f [W/m×K]	k _s [W/m×K]	K=k _s /k _f	k_ZBS [W/m×K]	$\Delta k_{\text{ZBS}}/k_{\text{ZBS}}$
333,599	0,219	1040,045	0,028	1,158	41,402	0,213	11 %
287,958	0,191	1039,102	0,025	1,079	43,716	0,188	11 %
288,328	0,191	1039,105	0,025	1,079	43,697	0,188	11 %
288,286	0,191	1039,105	0,025	1,079	43,700	0,188	11 %
423,160	0,258	1046,359	0,034	1,243	36,497	0,262	10 %
423,143	0,258	1046,358	0,034	1,243	36,498	0,262	10 %
423,144	0,258	1046,358	0,034	1,243	36,498	0,262	10 %
333,732	0,223	1040,049	0,028	1,158	41,395	0,213	11 %
333,049	0,224	1040,025	0,028	1,157	41,431	0,213	11 %
333,367	0,223	1040,036	0,028	1,158	41,414	0,213	11 %
278,200	0,218	1039,056	0,024	1,059	44,196	0,182	11 %
273,123	0,197	1039,049	0,024	1,048	44,444	0,179	11 %
273,125	0,197	1039,049	0,024	1,048	44,444	0,179	11 %
273,155	0,197	1039,049	0,024	1,048	44,442	0,179	11 %
268,102	0,196	1039,053	0,023	1,037	44,688	0,176	11 %
268,145	0,196	1039,053	0,023	1,037	44,686	0,176	11 %
268,123	0,195	1039,053	0,023	1,037	44,687	0,176	11 %
258,133	0,190	1039,086	0,022	1,014	45,169	0,170	11 %
258,146	0,190	1039,086	0,022	1,014	45,168	0,170	11 %
258,132	0,190	1039,086	0,022	1,014	45,169	0,170	11 %
243,142	0,181	1039,188	0,021	0,977	45,884	0,162	12 %
243,168	0,181	1039,188	0,021	0,977	45,883	0,162	12 %
243,147	0,181	1039,188	0,021	0,977	45,884	0,162	12 %
253,134	0,184	1039,114	0,022	1,002	45,408	0,168	12 %
253,149	0,186	1039,114	0,022	1,002	45,407	0,168	12 %
253,146	0,187	1039,114	0,022	1,002	45,408	0,168	12 %



Glass beads with N₂, filling 3, measurement error =5% ϵ_{bulk} 0,390662 ρ_{bulk} 1584,89 kg/m³ d_p 0,00038 m

T [K]	k [W/m×K]	Cp _{gas} [J/kgK]	k _f [W/m×K]	k _s [W/m×K]	K=k _s /k _f	k _{ZBS} [W/m×K]	$\Delta k_{\text{ZBS}}/k_{\text{ZBS}}$
423,135	0,248	1046,357	0,034	1,243	36,498	0,266	10 %
333,210	0,232	1040,031	0,028	1,157	41,422	0,216	11 %
333,758	0,231	1040,050	0,028	1,158	41,394	0,217	11 %
332,998	0,231	1040,023	0,028	1,157	41,433	0,216	11 %
278,224	0,222	1039,056	0,024	1,059	44,195	0,185	11 %
273,145	0,207	1039,049	0,024	1,048	44,443	0,182	11 %
423,117	0,260	1046,355	0,034	1,243	36,500	0,266	10 %
423,159	0,268	1046,359	0,034	1,243	36,497	0,266	10 %
423,128	0,264	1046,356	0,034	1,243	36,499	0,266	10 %
333,832	0,231	1040,053	0,028	1,158	41,390	0,217	11 %
333,234	0,231	1040,032	0,028	1,158	41,421	0,216	11 %
333,561	0,230	1040,043	0,028	1,158	41,404	0,217	11 %
278,200	0,220	1039,056	0,024	1,059	44,196	0,185	11 %
273,168	0,203	1039,049	0,024	1,048	44,442	0,182	11 %
273,078	0,204	1039,049	0,024	1,048	44,446	0,182	11 %
273,194	0,203	1039,049	0,024	1,048	44,440	0,182	11 %
268,171	0,203	1039,053	0,023	1,037	44,684	0,179	11 %
268,205	0,202	1039,052	0,023	1,037	44,683	0,179	11 %
268,143	0,201	1039,053	0,023	1,037	44,686	0,179	11 %
258,207	0,196	1039,086	0,022	1,014	45,165	0,173	11 %
258,155	0,196	1039,086	0,022	1,014	45,168	0,173	11 %
258,190	0,196	1039,086	0,022	1,014	45,166	0,173	11 %
243,165	0,186	1039,188	0,021	0,977	45,883	0,164	12 %
243,147	0,186	1039,188	0,021	0,977	45,884	0,164	12 %
243,162	0,186	1039,188	0,021	0,977	45,883	0,164	12 %
253,153	0,190	1039,114	0,022	1,002	45,407	0,170	11 %
253,133	0,191	1039,114	0,022	1,002	45,408	0,170	11 %
253,140	0,192	1039,114	0,022	1,002	45,408	0,170	11 %
263,145	0,197	1039,065	0,023	1,025	44,927	0,176	11 %
263,163	0,199	1039,065	0,023	1,025	44,927	0,176	11 %
263,137	0,200	1039,065	0,023	1,025	44,928	0,176	11 %
263,158	0,200	1039,065	0,023	1,025	44,927	0,176	11 %
271,142	0,201	1039,049	0,023	1,043	44,540	0,181	11 %
271,214	0,202	1039,049	0,023	1,044	44,537	0,181	11 %
271,125	0,202	1039,049	0,023	1,043	44,541	0,181	11 %
275,134	0,202	1039,051	0,024	1,052	44,346	0,183	11 %
275,141	0,204	1039,051	0,024	1,052	44,345	0,183	11 %
275,143	0,204	1039,051	0,024	1,052	44,345	0,183	11 %

283,125	0,204	1039,074	0,024	1,069	43,954	0,188	11 %
283,194	0,206	1039,074	0,024	1,069	43,951	0,188	11 %
283,122	0,206	1039,074	0,024	1,069	43,954	0,188	11 %
307,927	0,216	1039,354	0,026	1,116	42,718	0,202	11 %
308,487	0,216	1039,364	0,026	1,117	42,690	0,202	11 %
308,588	0,216	1039,366	0,026	1,118	42,684	0,202	11 %
373,131	0,233	1042,050	0,031	1,207	39,299	0,239	10 %
423,152	0,266	1046,359	0,034	1,243	36,498	0,266	10 %
423,197	0,265	1046,363	0,034	1,243	36,495	0,266	10 %
423,162	0,266	1046,360	0,034	1,243	36,497	0,266	10 %
332,987	0,232	1040,023	0,028	1,157	41,434	0,216	11 %
333,021	0,231	1040,024	0,028	1,157	41,432	0,216	11 %
333,396	0,230	1040,037	0,028	1,158	41,413	0,216	11 %
278,106	0,221	1039,056	0,024	1,058	44,200	0,185	11 %

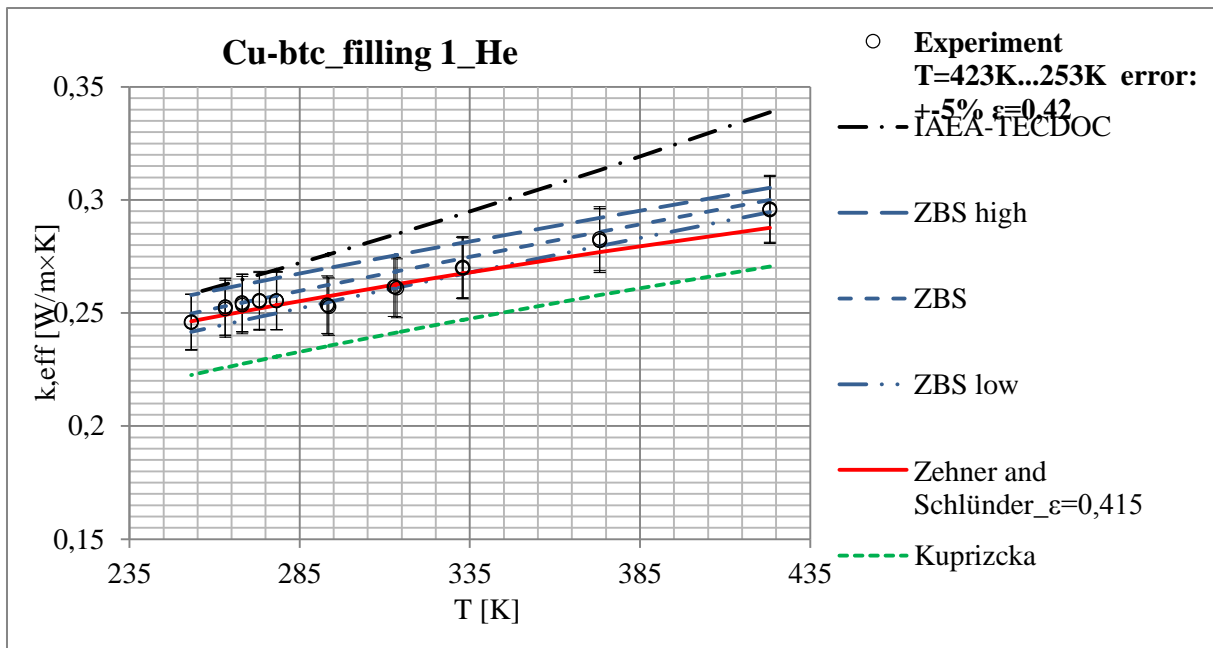


Appendix D - Cu-btc results

Cu-btc with He, filling 1, measurement error =5%

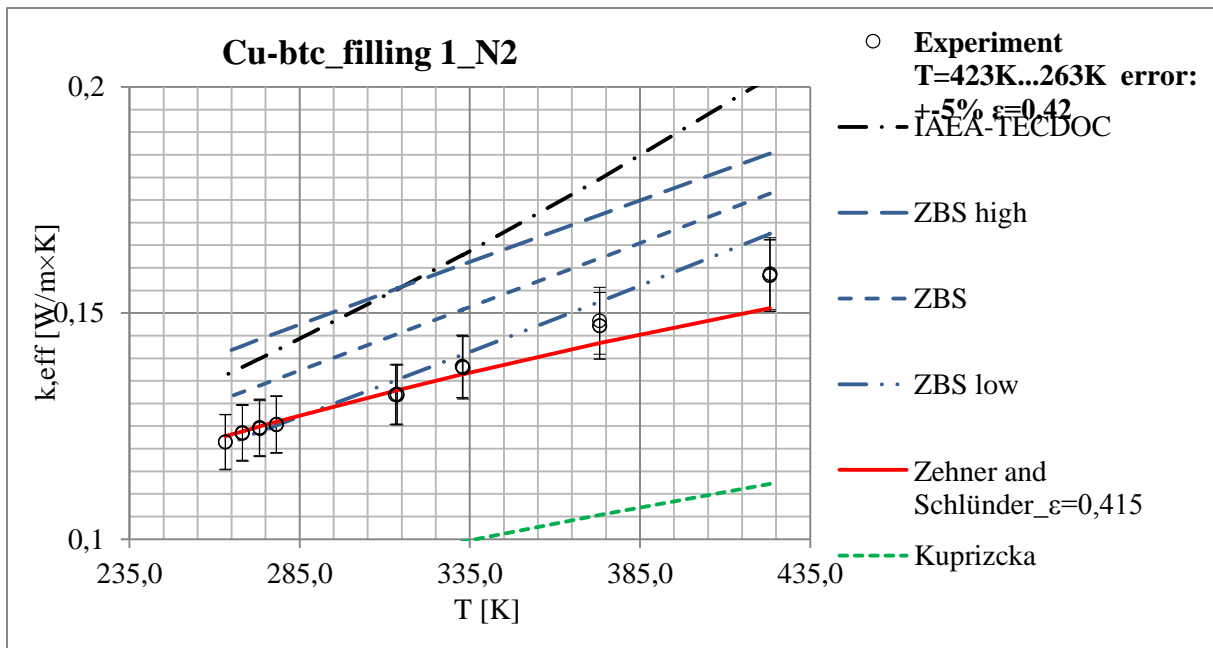
$\varepsilon_{\text{bulk}}$ 0,415206
 ρ_{bulk} 553,16 kg/m³
 d_p 0,00376 m
 p 1,2 bar

T [K]	k [W/m×K]	Cp_gas [J/kgK]	k_f [W/m×K]	k_s [W/m×K]	K=k_s/k_f	k_ZBS [W/m×K]	$\Delta k_{\text{ZBS}}/k_{\text{ZBS}}$
423,141	0,296	5196,250	0,196	0,351	1,790	0,300	2 %
423,131	0,296	5196,250	0,196	0,351	1,790	0,300	2 %
423,136	0,296	5196,250	0,196	0,351	1,790	0,300	2 %
373,125	0,283	5196,250	0,179	0,346	1,928	0,286	2 %
373,142	0,282	5196,250	0,179	0,346	1,928	0,286	2 %
373,166	0,282	5196,250	0,179	0,346	1,928	0,286	2 %
332,898	0,270	5196,250	0,166	0,342	2,061	0,274	3 %
333,047	0,270	5196,250	0,166	0,342	2,061	0,274	3 %
332,708	0,270	5196,250	0,166	0,342	2,062	0,274	3 %
313,066	0,262	5196,250	0,159	0,339	2,136	0,268	3 %
313,562	0,261	5196,250	0,159	0,340	2,134	0,268	3 %
312,679	0,262	5196,250	0,159	0,339	2,138	0,268	3 %
293,328	0,253	5196,250	0,152	0,337	2,218	0,262	3 %
293,045	0,254	5196,250	0,152	0,337	2,220	0,262	3 %
293,596	0,253	5196,250	0,152	0,337	2,217	0,262	3 %
278,228	0,255	5196,250	0,147	0,335	2,287	0,258	3 %
278,131	0,255	5196,250	0,147	0,335	2,287	0,258	3 %
278,225	0,255	5196,250	0,147	0,335	2,287	0,258	3 %
273,176	0,255	5196,250	0,145	0,335	2,311	0,256	3 %
273,125	0,256	5196,250	0,145	0,335	2,311	0,256	3 %
273,196	0,255	5196,250	0,145	0,335	2,311	0,256	3 %
268,134	0,254	5196,250	0,143	0,334	2,336	0,255	3 %
268,079	0,255	5196,250	0,143	0,334	2,336	0,255	3 %
268,159	0,254	5196,250	0,143	0,334	2,336	0,255	3 %
263,128	0,253	5196,250	0,141	0,333	2,361	0,253	3 %
263,147	0,253	5196,250	0,141	0,333	2,361	0,253	3 %
263,146	0,252	5196,250	0,141	0,333	2,361	0,253	3 %
253,128	0,246	5196,250	0,137	0,332	2,414	0,250	3 %
253,153	0,246	5196,250	0,137	0,332	2,413	0,250	3 %
253,143	0,246	5196,250	0,137	0,332	2,413	0,250	3 %



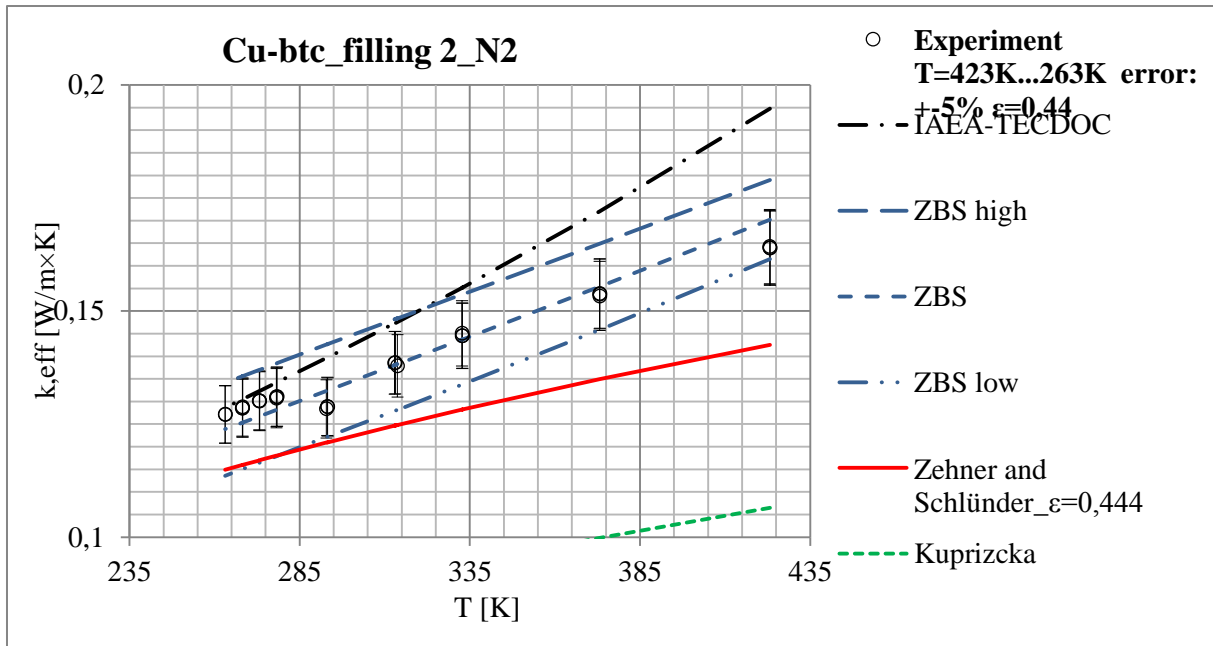
Cu-btc with N2, filling 1, measurement error =5%

T [K]	k [W/m×K]	Cp_gas [J/kgK]	k_f [W/m×K]	k_s [W/m×K]	K=k_s/k_f	k_ZBS [W/m×K]	Δk_ZBS/kZBS
ε_bulk	0,415206						
ρ_bulk	553,16	kg/m ³					
d_p	0,00376	m					
p	1,2	bar					
423,183	0,159	1046,362	0,034	0,351	10,295	0,176	5 %
423,128	0,158	1046,356	0,034	0,351	10,296	0,176	5 %
423,147	0,158	1046,358	0,034	0,351	10,296	0,176	5 %
373,126	0,148	1042,050	0,031	0,346	11,263	0,162	6 %
373,136	0,147	1042,051	0,031	0,346	11,263	0,162	6 %
373,167	0,147	1042,053	0,031	0,346	11,263	0,162	6 %
332,755	0,138	1040,015	0,028	0,342	12,243	0,151	7 %
332,849	0,138	1040,018	0,028	0,342	12,241	0,151	7 %
333,022	0,138	1040,024	0,028	0,342	12,236	0,151	7 %
313,556	0,132	1039,468	0,027	0,340	12,793	0,145	7 %
313,694	0,132	1039,471	0,027	0,340	12,789	0,145	7 %
313,107	0,132	1039,458	0,027	0,339	12,807	0,145	7 %
278,170	0,125	1039,056	0,024	0,335	13,995	0,135	8 %
278,186	0,125	1039,056	0,024	0,335	13,994	0,135	8 %
278,108	0,125	1039,056	0,024	0,335	13,997	0,135	8 %
273,265	0,124	1039,049	0,024	0,335	14,185	0,134	8 %
273,211	0,125	1039,049	0,024	0,335	14,187	0,134	8 %
273,210	0,125	1039,049	0,024	0,335	14,187	0,134	8 %
268,169	0,123	1039,053	0,023	0,334	14,389	0,133	8 %
268,171	0,123	1039,053	0,023	0,334	14,389	0,133	8 %
268,141	0,124	1039,053	0,023	0,334	14,390	0,133	8 %
263,146	0,121	1039,065	0,023	0,333	14,598	0,131	8 %
263,162	0,122	1039,065	0,023	0,333	14,597	0,131	8 %



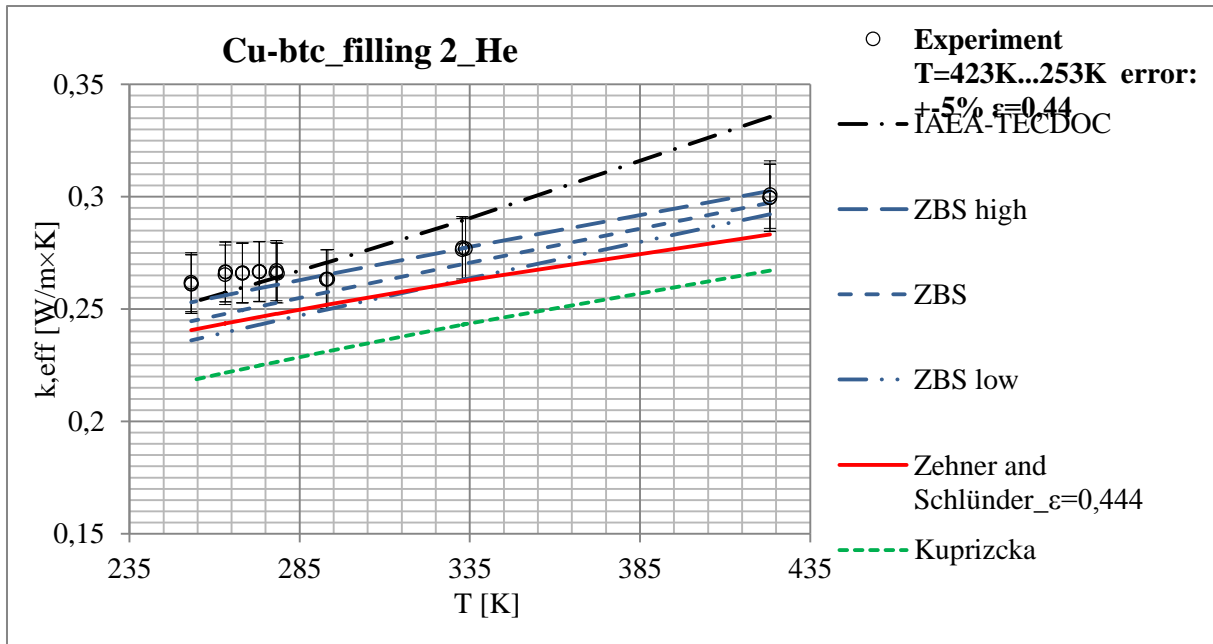
Cu-btc with N2, filling 2, measurement error =5%

T [K]	k [W/m×K]	Cp_gas [J/kgK]	k_f [W/m×K]	k_s [W/m×K]	K=k_s/k_f	k_ZBS [W/m×K]	Δk_ZBS/kZBS
ε_bulk	0,444422						
ρ_bulk	525,52	kg/m ³					
d_p	0,00376	m					
p	1,2	bar					
423,141	0,164	1046,357	0,034	0,351	10,296	0,170	5 %
423,173	0,164	1046,361	0,034	0,351	10,295	0,170	5 %
423,147	0,164	1046,358	0,034	0,351	10,296	0,170	5 %
373,165	0,154	1042,053	0,031	0,346	11,263	0,155	6 %
373,138	0,154	1042,051	0,031	0,346	11,263	0,155	6 %
373,150	0,153	1042,052	0,031	0,346	11,263	0,155	6 %
332,703	0,145	1040,013	0,028	0,342	12,245	0,144	7 %
332,815	0,145	1040,017	0,028	0,342	12,242	0,144	7 %
332,743	0,145	1040,014	0,028	0,342	12,244	0,144	7 %
313,091	0,139	1039,457	0,027	0,339	12,807	0,138	7 %
312,888	0,139	1039,453	0,026	0,339	12,813	0,138	7 %
313,736	0,138	1039,472	0,027	0,340	12,788	0,138	7 %
293,124	0,129	1039,146	0,025	0,337	13,453	0,132	8 %
293,200	0,129	1039,147	0,025	0,337	13,451	0,132	8 %
292,866	0,128	1039,143	0,025	0,337	13,462	0,132	8 %
278,347	0,131	1039,056	0,024	0,335	13,988	0,128	8 %
278,227	0,131	1039,056	0,024	0,335	13,992	0,128	8 %
278,191	0,131	1039,056	0,024	0,335	13,994	0,128	8 %
273,215	0,130	1039,049	0,024	0,335	14,187	0,127	8 %
273,182	0,130	1039,049	0,024	0,335	14,188	0,127	8 %
273,132	0,130	1039,049	0,024	0,335	14,190	0,127	8 %
268,177	0,129	1039,052	0,023	0,334	14,389	0,125	8 %
268,240	0,129	1039,052	0,023	0,334	14,386	0,125	8 %
268,189	0,129	1039,052	0,023	0,334	14,388	0,125	8 %
263,116	0,127	1039,065	0,023	0,333	14,599	0,124	8 %
263,111	0,127	1039,065	0,023	0,333	14,599	0,124	8 %



Cu-btc with He, filling 2, measurement error =5%

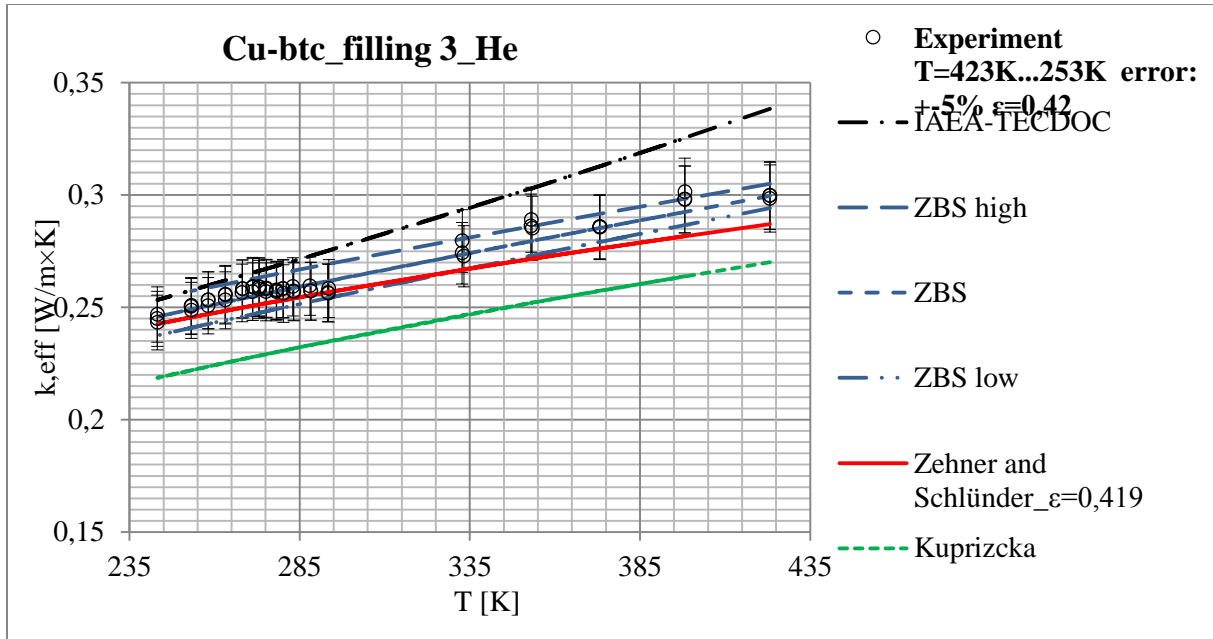
T [K]	k [W/m×K]	Cp_gas [J/kgK]	k_f [W/m×K]	k_s [W/m×K]	K=k_s/k_f	k_ZBS [W/m×K]	Δk_ZBS/kZBS
ε_bulk	0,444422						
ρ_bulk	525,52	kg/m ³					
d_p	0,00376	m					
p	1,2	bar					
423,177	0,301	5196,250	0,196	0,351	1,790	0,297	2 %
423,165	0,300	5196,250	0,196	0,351	1,790	0,297	2 %
423,149	0,300	5196,250	0,196	0,351	1,790	0,297	2 %
332,812	0,277	5196,250	0,166	0,342	2,061	0,270	3 %
332,772	0,276	5196,250	0,166	0,342	2,062	0,270	3 %
333,692	0,277	5196,250	0,166	0,342	2,058	0,270	3 %
293,269	0,263	5196,250	0,152	0,337	2,219	0,258	3 %
292,899	0,263	5196,250	0,152	0,337	2,220	0,258	3 %
292,865	0,263	5196,250	0,152	0,337	2,220	0,257	3 %
278,440	0,266	5196,250	0,147	0,335	2,286	0,253	3 %
278,168	0,267	5196,250	0,147	0,335	2,287	0,253	3 %
278,046	0,266	5196,250	0,147	0,335	2,288	0,253	3 %
273,202	0,267	5196,250	0,145	0,335	2,311	0,251	3 %
273,142	0,267	5196,250	0,145	0,335	2,311	0,251	3 %
273,103	0,267	5196,250	0,145	0,335	2,311	0,251	3 %
268,204	0,266	5196,250	0,143	0,334	2,335	0,250	3 %
268,148	0,266	5196,250	0,143	0,334	2,336	0,250	3 %
268,187	0,266	5196,250	0,143	0,334	2,335	0,250	3 %
263,165	0,267	5196,250	0,141	0,333	2,361	0,248	3 %
263,102	0,265	5196,250	0,141	0,333	2,361	0,248	3 %
263,223	0,267	5196,250	0,141	0,333	2,360	0,248	3 %
253,121	0,261	5196,250	0,137	0,332	2,414	0,245	3 %
253,115	0,262	5196,250	0,137	0,332	2,414	0,245	3 %
253,174	0,261	5196,250	0,137	0,332	2,413	0,245	3 %



Cu-btc with He, filling 3, measurement error =5%

T [K]	k [W/m×K]	Cp_gas [J/kgK]	k_f [W/m×K]	k_s [W/m×K]	K=k_s/k_f	k_ZBS [W/m×K]	Δk_ZBS/kZBS
ε_bulk	0,419108						
ρ_bulk	549,47	kg/m ³					
d_p	0,00376	m					
p	1,4	bar					
423,144	0,300	5196,250	0,196	0,351	1,790	0,300	2 %
423,148	0,298	5196,250	0,196	0,351	1,790	0,300	2 %
423,150	0,300	5196,250	0,196	0,351	1,790	0,300	2 %
373,186	0,286	5196,250	0,179	0,346	1,928	0,285	2 %
373,159	0,286	5196,250	0,179	0,346	1,928	0,285	2 %
373,160	0,286	5196,250	0,179	0,346	1,928	0,285	2 %
332,767	0,280	5196,250	0,166	0,342	2,062	0,274	3 %
332,713	0,274	5196,250	0,166	0,342	2,062	0,274	3 %
333,232	0,273	5196,250	0,166	0,342	2,060	0,274	3 %
293,551	0,258	5196,250	0,152	0,337	2,217	0,262	3 %
293,463	0,256	5196,250	0,152	0,337	2,218	0,262	3 %
293,230	0,257	5196,250	0,152	0,337	2,219	0,262	3 %
282,991	0,259	5196,250	0,148	0,336	2,265	0,259	3 %
283,255	0,257	5196,250	0,148	0,336	2,263	0,259	3 %
283,218	0,257	5196,250	0,148	0,336	2,264	0,259	3 %
278,139	0,257	5196,250	0,147	0,335	2,287	0,257	3 %
278,140	0,258	5196,250	0,147	0,335	2,287	0,257	3 %
278,221	0,258	5196,250	0,147	0,335	2,287	0,257	3 %
273,094	0,258	5196,250	0,145	0,335	2,311	0,255	3 %
273,093	0,259	5196,250	0,145	0,335	2,311	0,255	3 %
273,065	0,259	5196,250	0,145	0,335	2,312	0,255	3 %
268,070	0,256	5196,250	0,143	0,334	2,336	0,254	3 %
268,196	0,258	5196,250	0,143	0,334	2,335	0,254	3 %
268,196	0,258	5196,250	0,143	0,334	2,335	0,254	3 %
263,159	0,253	5196,250	0,141	0,333	2,361	0,252	3 %
263,120	0,255	5196,250	0,141	0,333	2,361	0,252	3 %
263,139	0,256	5196,250	0,141	0,333	2,361	0,252	3 %
253,144	0,249	5196,250	0,137	0,332	2,413	0,249	3 %
253,155	0,251	5196,250	0,137	0,332	2,413	0,249	3 %
253,119	0,250	5196,250	0,137	0,332	2,414	0,249	3 %
243,182	0,243	5196,250	0,134	0,330	2,469	0,246	3 %
243,180	0,247	5196,250	0,134	0,330	2,469	0,246	3 %
243,160	0,245	5196,250	0,134	0,330	2,469	0,246	3 %
258,117	0,251	5196,250	0,139	0,332	2,387	0,251	3 %
258,108	0,253	5196,250	0,139	0,332	2,387	0,251	3 %
258,168	0,253	5196,250	0,139	0,332	2,387	0,251	3 %
271,181	0,257	5196,250	0,144	0,334	2,321	0,255	3 %
271,212	0,259	5196,250	0,144	0,334	2,321	0,255	3 %

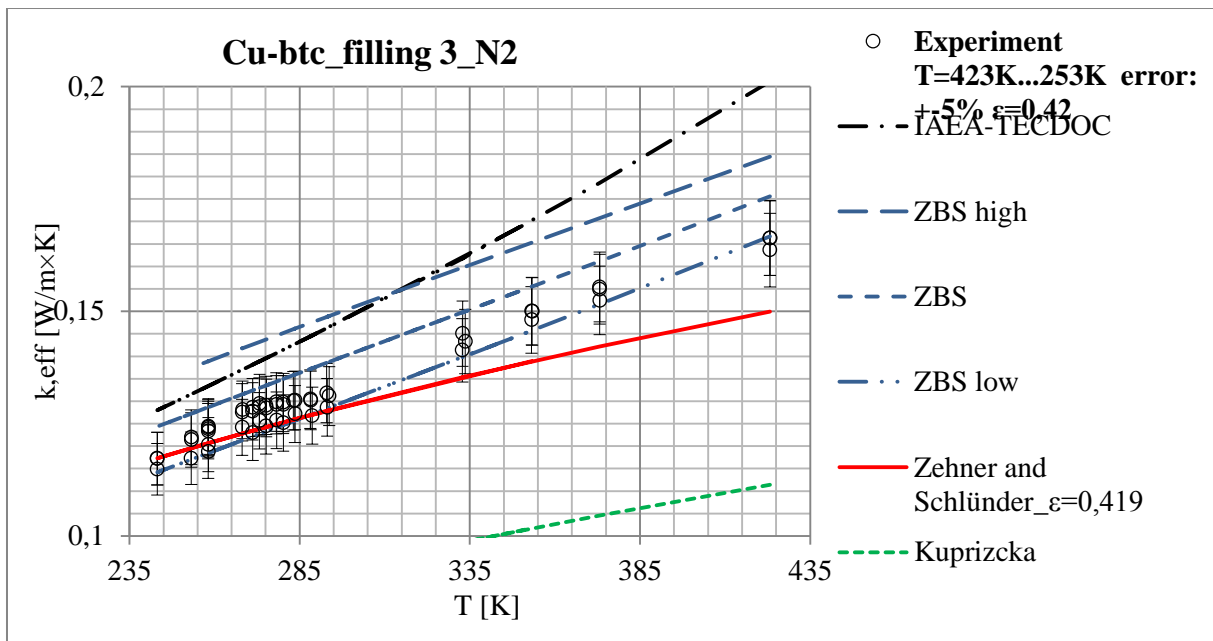
271,198	0,259	5196,250	0,144	0,334	2,321	0,255	3 %
275,108	0,257	5196,250	0,145	0,335	2,302	0,256	3 %
275,229	0,258	5196,250	0,145	0,335	2,301	0,256	3 %
275,213	0,258	5196,250	0,145	0,335	2,301	0,256	3 %
280,204	0,256	5196,250	0,147	0,335	2,278	0,258	3 %
280,113	0,258	5196,250	0,147	0,335	2,278	0,258	3 %
280,119	0,258	5196,250	0,147	0,335	2,278	0,258	3 %
288,016	0,259	5196,250	0,150	0,336	2,242	0,260	3 %
288,273	0,257	5196,250	0,150	0,336	2,241	0,260	3 %
288,262	0,257	5196,250	0,150	0,336	2,241	0,260	3 %
353,042	0,289	5196,250	0,173	0,344	1,992	0,280	2 %
353,322	0,285	5196,250	0,173	0,344	1,991	0,280	2 %
352,927	0,286	5196,250	0,173	0,344	1,992	0,280	2 %
398,164	0,301	5196,250	0,188	0,348	1,856	0,293	2 %
398,136	0,298	5196,250	0,188	0,348	1,856	0,293	2 %
398,177	0,298	5196,250	0,188	0,348	1,856	0,293	2 %



Cu-btc with N2, filling 3, measurement error =5%

T [K]	k [W/m×K]	Cp_gas [J/kgK]	k_f [W/m×K]	k_s [W/m×K]	K=k_s/k_f	k_ZBS [W/m×K]	Δk_ZBS/kZBS
ε_bulk	0,419108						
ρ_bulk	549,47	kg/m ³					
d_p	0,00376	m					
p	1,4	bar					
423,150	0,164	1046,358	0,034	0,351	10,296	0,176	5 %
423,180	0,166	1046,362	0,034	0,351	10,295	0,176	5 %
423,141	0,166	1046,357	0,034	0,351	10,296	0,176	5 %
373,142	0,152	1042,051	0,031	0,346	11,263	0,161	6 %
373,134	0,155	1042,051	0,031	0,346	11,263	0,161	6 %
373,123	0,155	1042,050	0,031	0,346	11,263	0,161	6 %
332,783	0,141	1040,016	0,028	0,342	12,243	0,150	7 %
333,645	0,143	1040,046	0,028	0,342	12,219	0,150	7 %
332,853	0,145	1040,018	0,028	0,342	12,241	0,150	7 %
293,073	0,129	1039,145	0,025	0,337	13,455	0,139	7 %
293,658	0,131	1039,151	0,025	0,337	13,435	0,139	7 %
292,921	0,132	1039,144	0,025	0,337	13,460	0,139	7 %
283,612	0,127	1039,076	0,024	0,336	13,791	0,136	8 %
283,142	0,130	1039,074	0,024	0,336	13,809	0,136	8 %
283,630	0,130	1039,076	0,024	0,336	13,791	0,136	8 %
278,220	0,126	1039,056	0,024	0,335	13,993	0,134	8 %
278,155	0,129	1039,056	0,024	0,335	13,995	0,134	8 %
278,144	0,130	1039,056	0,024	0,335	13,996	0,134	8 %
273,179	0,126	1039,049	0,024	0,335	14,188	0,133	8 %
273,166	0,129	1039,049	0,024	0,335	14,188	0,133	8 %
273,205	0,129	1039,049	0,024	0,335	14,187	0,133	8 %
268,108	0,124	1039,053	0,023	0,334	14,391	0,132	8 %
268,102	0,128	1039,053	0,023	0,334	14,392	0,132	8 %
268,201	0,128	1039,052	0,023	0,334	14,388	0,132	8 %
258,167	0,120	1039,086	0,022	0,332	14,812	0,129	8 %
258,125	0,124	1039,086	0,022	0,332	14,814	0,129	8 %
258,172	0,124	1039,086	0,022	0,332	14,812	0,129	8 %
253,123	0,117	1039,114	0,022	0,332	15,038	0,127	8 %
253,150	0,121	1039,114	0,022	0,332	15,037	0,127	8 %
253,143	0,122	1039,114	0,022	0,332	15,037	0,127	8 %
243,163	0,115	1039,188	0,021	0,330	15,510	0,124	8 %
243,162	0,117	1039,188	0,021	0,330	15,510	0,124	8 %
243,161	0,117	1039,188	0,021	0,330	15,510	0,124	8 %
258,134	0,119	1039,086	0,022	0,332	14,814	0,129	8 %
258,140	0,123	1039,086	0,022	0,332	14,813	0,129	8 %
258,130	0,124	1039,086	0,022	0,332	14,814	0,129	8 %
271,171	0,123	1039,049	0,023	0,334	14,268	0,132	8 %
271,166	0,128	1039,049	0,023	0,334	14,268	0,132	8 %

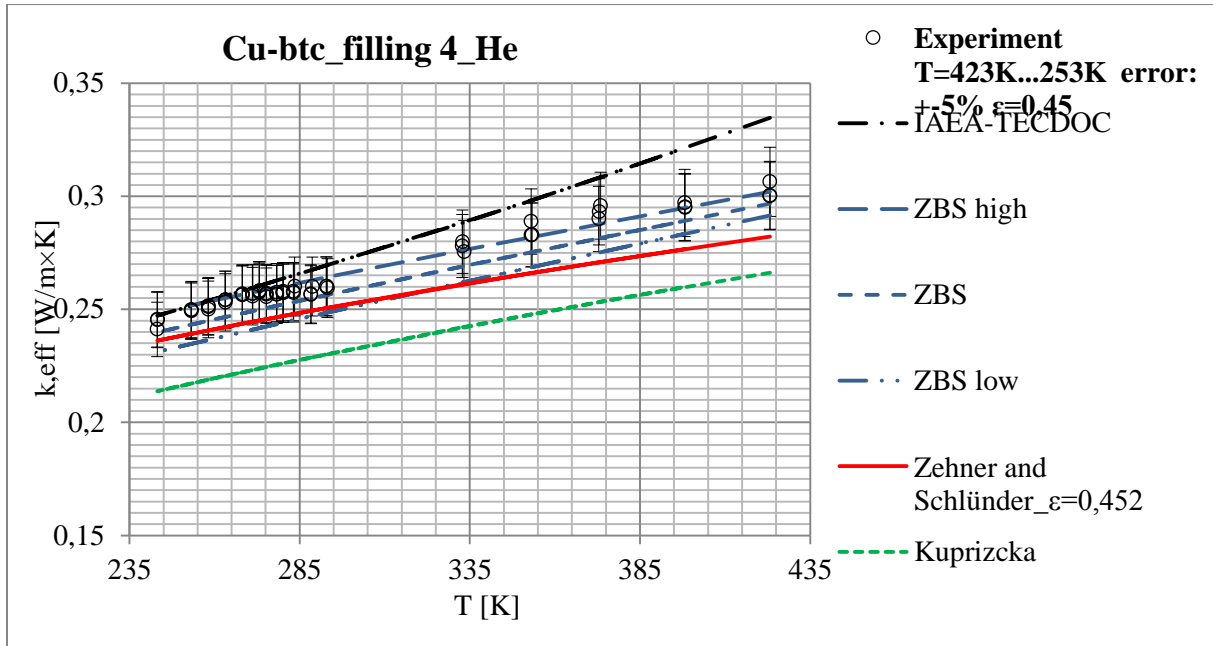
271,148	0,129	1039,049	0,023	0,334	14,269	0,132	8 %
275,118	0,124	1039,051	0,024	0,335	14,112	0,134	8 %
275,195	0,128	1039,051	0,024	0,335	14,109	0,134	8 %
275,138	0,129	1039,051	0,024	0,335	14,111	0,134	8 %
280,181	0,125	1039,062	0,024	0,335	13,919	0,135	8 %
280,155	0,129	1039,062	0,024	0,335	13,920	0,135	8 %
280,206	0,130	1039,062	0,024	0,335	13,918	0,135	8 %
288,677	0,127	1039,107	0,025	0,337	13,609	0,137	7 %
288,226	0,130	1039,104	0,025	0,336	13,625	0,137	7 %
288,124	0,130	1039,103	0,025	0,336	13,628	0,137	7 %
353,128	0,148	1040,885	0,029	0,344	11,722	0,155	6 %
353,141	0,150	1040,886	0,029	0,344	11,722	0,155	6 %
353,307	0,150	1040,894	0,029	0,344	11,718	0,156	6 %



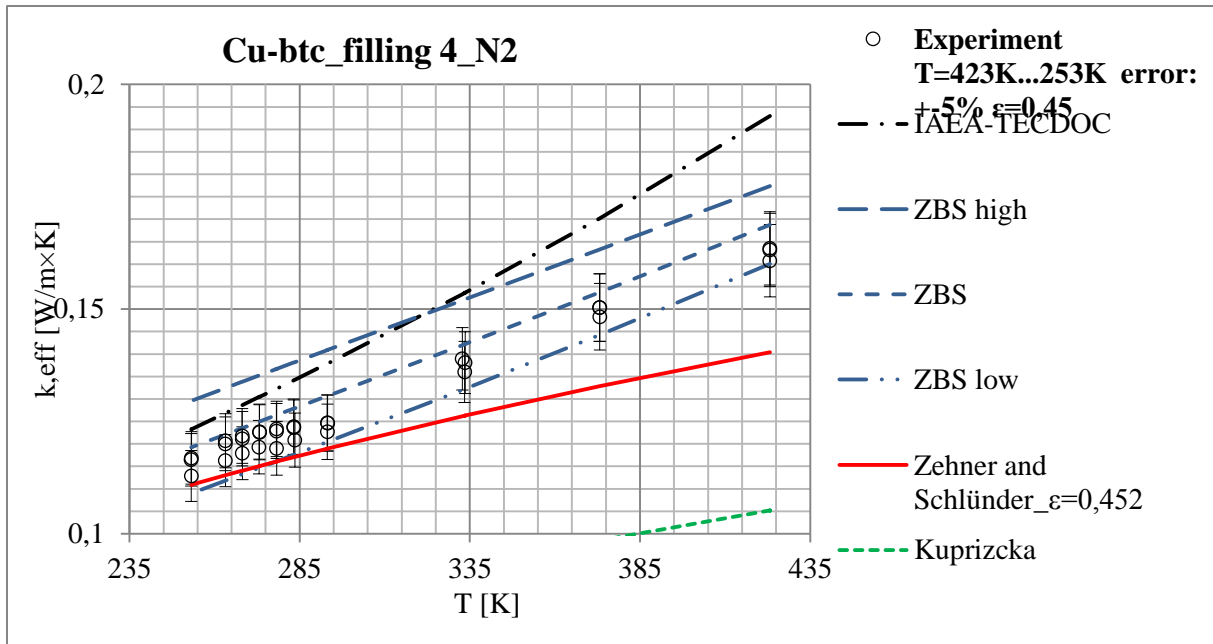
Cu-btc with He, filling 4, measurement error =5%

T [K]	k [W/m×K]	Cp_gas [J/kgK]	k_f [W/m×K]	k_s [W/m×K]	K=k_s/k_f	k_ZBS [W/m×K]	Δk_ZBS/kZBS
ε_bulk	0,451856						
ρ_bulk	518,49	kg/m ³					
d_p	0,00376	m					
p	1,2	bar					
423,163	0,306	5196,250	0,196	0,351	1,790	0,297	2 %
423,139	0,300	5196,250	0,196	0,351	1,790	0,297	2 %
423,152	0,300	5196,250	0,196	0,351	1,790	0,297	2 %
372,955	0,293	5196,250	0,179	0,346	1,928	0,281	2 %
373,409	0,296	5196,250	0,180	0,346	1,927	0,282	2 %
372,883	0,290	5196,250	0,179	0,346	1,929	0,281	2 %
332,836	0,280	5196,250	0,166	0,342	2,061	0,269	3 %
332,782	0,278	5196,250	0,166	0,342	2,062	0,269	3 %
333,305	0,275	5196,250	0,166	0,342	2,060	0,269	3 %
292,842	0,260	5196,250	0,152	0,337	2,220	0,256	3 %
293,146	0,259	5196,250	0,152	0,337	2,219	0,256	3 %
292,846	0,260	5196,250	0,152	0,337	2,220	0,256	3 %
283,533	0,260	5196,250	0,148	0,336	2,262	0,253	3 %
283,106	0,258	5196,250	0,148	0,336	2,264	0,253	3 %
283,198	0,257	5196,250	0,148	0,336	2,264	0,253	3 %
278,211	0,257	5196,250	0,147	0,335	2,287	0,252	3 %
278,262	0,257	5196,250	0,147	0,335	2,287	0,252	3 %
278,238	0,257	5196,250	0,147	0,335	2,287	0,252	3 %
273,124	0,258	5196,250	0,145	0,335	2,311	0,250	3 %
273,152	0,258	5196,250	0,145	0,335	2,311	0,250	3 %
273,093	0,258	5196,250	0,145	0,335	2,311	0,250	3 %
268,092	0,256	5196,250	0,143	0,334	2,336	0,248	3 %
268,214	0,257	5196,250	0,143	0,334	2,335	0,248	3 %
268,146	0,257	5196,250	0,143	0,334	2,336	0,248	3 %
263,161	0,253	5196,250	0,141	0,333	2,361	0,247	3 %
263,134	0,254	5196,250	0,141	0,333	2,361	0,247	3 %
263,128	0,254	5196,250	0,141	0,333	2,361	0,247	3 %
253,137	0,249	5196,250	0,137	0,332	2,413	0,243	4 %
253,179	0,250	5196,250	0,137	0,332	2,413	0,243	4 %
253,129	0,250	5196,250	0,137	0,332	2,413	0,243	4 %
243,141	0,241	5196,250	0,134	0,330	2,469	0,240	4 %
243,183	0,245	5196,250	0,134	0,330	2,469	0,240	4 %
243,173	0,246	5196,250	0,134	0,330	2,469	0,240	4 %
258,179	0,250	5196,250	0,139	0,332	2,387	0,245	3 %
258,142	0,251	5196,250	0,139	0,332	2,387	0,245	3 %
258,148	0,251	5196,250	0,139	0,332	2,387	0,245	3 %
271,149	0,256	5196,250	0,144	0,334	2,321	0,249	3 %
271,139	0,257	5196,250	0,144	0,334	2,321	0,249	3 %

271,148	0,257	5196,250	0,144	0,334	2,321	0,249	3 %
275,195	0,256	5196,250	0,145	0,335	2,301	0,251	3 %
275,200	0,257	5196,250	0,145	0,335	2,301	0,251	3 %
275,190	0,257	5196,250	0,145	0,335	2,301	0,251	3 %
280,106	0,258	5196,250	0,147	0,335	2,278	0,252	3 %
280,109	0,257	5196,250	0,147	0,335	2,278	0,252	3 %
280,117	0,257	5196,250	0,147	0,335	2,278	0,252	3 %
288,716	0,260	5196,250	0,150	0,337	2,239	0,255	3 %
288,290	0,257	5196,250	0,150	0,336	2,241	0,255	3 %
288,277	0,257	5196,250	0,150	0,336	2,241	0,255	3 %
352,989	0,289	5196,250	0,173	0,344	1,992	0,275	2 %
353,276	0,283	5196,250	0,173	0,344	1,991	0,275	2 %
353,004	0,283	5196,250	0,173	0,344	1,992	0,275	2 %
398,130	0,297	5196,250	0,188	0,348	1,856	0,289	2 %
398,172	0,295	5196,250	0,188	0,348	1,856	0,289	2 %
398,164	0,295	5196,250	0,188	0,348	1,856	0,289	2 %



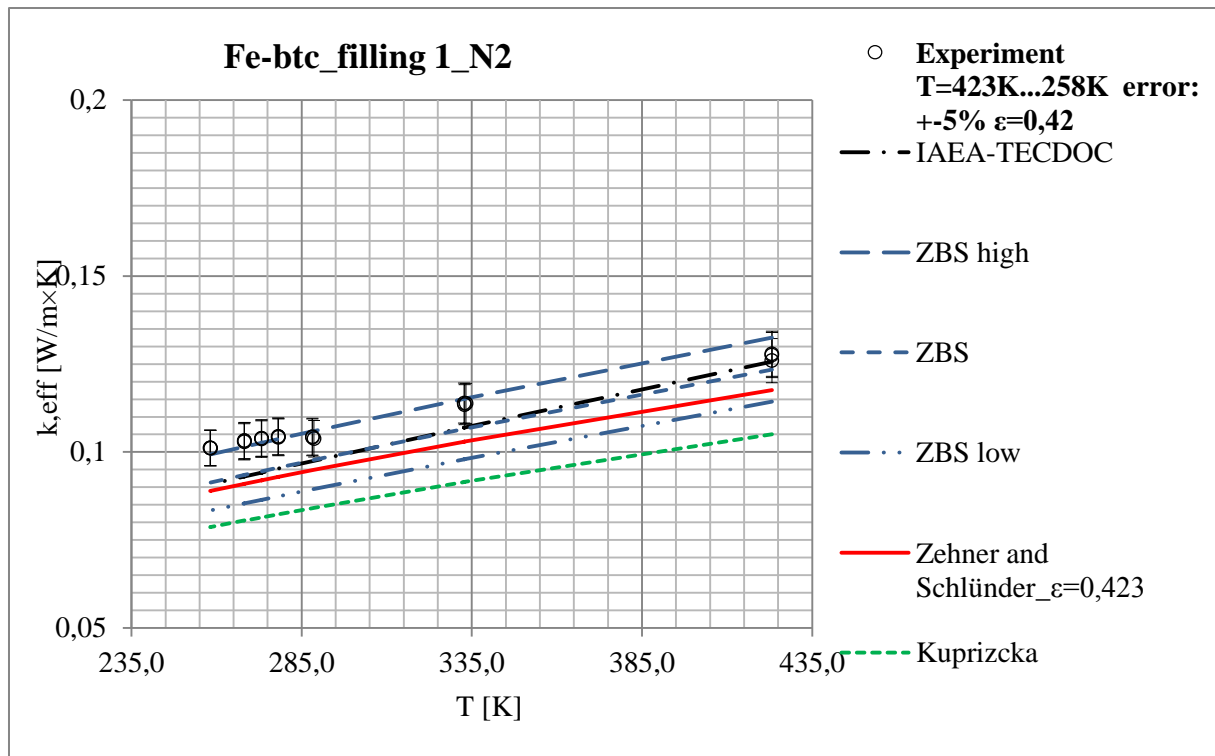
Cu-btc with N2, filling 4, measurement error =5%							
$\varepsilon_{\text{bulk}}$	0,451856						
ρ_{bulk}	518,49	kg/m ³					
d_p	0,00376	m					
p	1,2	bar					
T [K]	k [W/m×K]	Cp_gas [J/kgK]	k_f [W/m×K]	k_s [W/m×K]	K=k_s/k_f	k_ZBS [W/m×K]	$\Delta k_{\text{ZBS}}/k_{\text{ZBS}}$
423,152	0,161	1046,359	0,034	0,351	10,296	0,169	5 %
423,147	0,164	1046,358	0,034	0,351	10,296	0,169	5 %
423,162	0,163	1046,360	0,034	0,351	10,295	0,169	5 %
373,163	0,148	1042,053	0,031	0,346	11,263	0,154	6 %
373,153	0,150	1042,052	0,031	0,346	11,263	0,154	6 %
373,131	0,150	1042,050	0,031	0,346	11,263	0,154	6 %
333,468	0,136	1040,040	0,028	0,342	12,224	0,142	7 %
333,604	0,138	1040,045	0,028	0,342	12,220	0,142	7 %
332,773	0,139	1040,015	0,028	0,342	12,243	0,142	7 %
293,142	0,123	1039,146	0,025	0,337	13,453	0,131	8 %
293,117	0,125	1039,146	0,025	0,337	13,453	0,131	8 %
293,205	0,125	1039,147	0,025	0,337	13,450	0,131	8 %
283,595	0,121	1039,076	0,024	0,336	13,792	0,128	8 %
283,282	0,124	1039,074	0,024	0,336	13,803	0,128	8 %
283,245	0,124	1039,074	0,024	0,336	13,805	0,128	8 %
278,228	0,119	1039,056	0,024	0,335	13,992	0,126	8 %
278,188	0,123	1039,056	0,024	0,335	13,994	0,126	8 %
278,232	0,123	1039,056	0,024	0,335	13,992	0,126	8 %
273,029	0,119	1039,049	0,024	0,334	14,194	0,125	8 %
273,203	0,123	1039,049	0,024	0,335	14,187	0,125	8 %
273,182	0,123	1039,049	0,024	0,335	14,188	0,125	8 %
268,173	0,118	1039,053	0,023	0,334	14,389	0,124	8 %
268,129	0,121	1039,053	0,023	0,334	14,391	0,124	8 %
268,112	0,122	1039,053	0,023	0,334	14,391	0,124	8 %
263,155	0,116	1039,065	0,023	0,333	14,597	0,122	8 %
263,152	0,120	1039,065	0,023	0,333	14,597	0,122	8 %
263,176	0,121	1039,065	0,023	0,333	14,596	0,122	8 %
253,157	0,113	1039,114	0,022	0,332	15,036	0,119	9 %
253,120	0,116	1039,114	0,022	0,332	15,038	0,119	9 %
253,188	0,117	1039,114	0,022	0,332	15,035	0,119	9 %



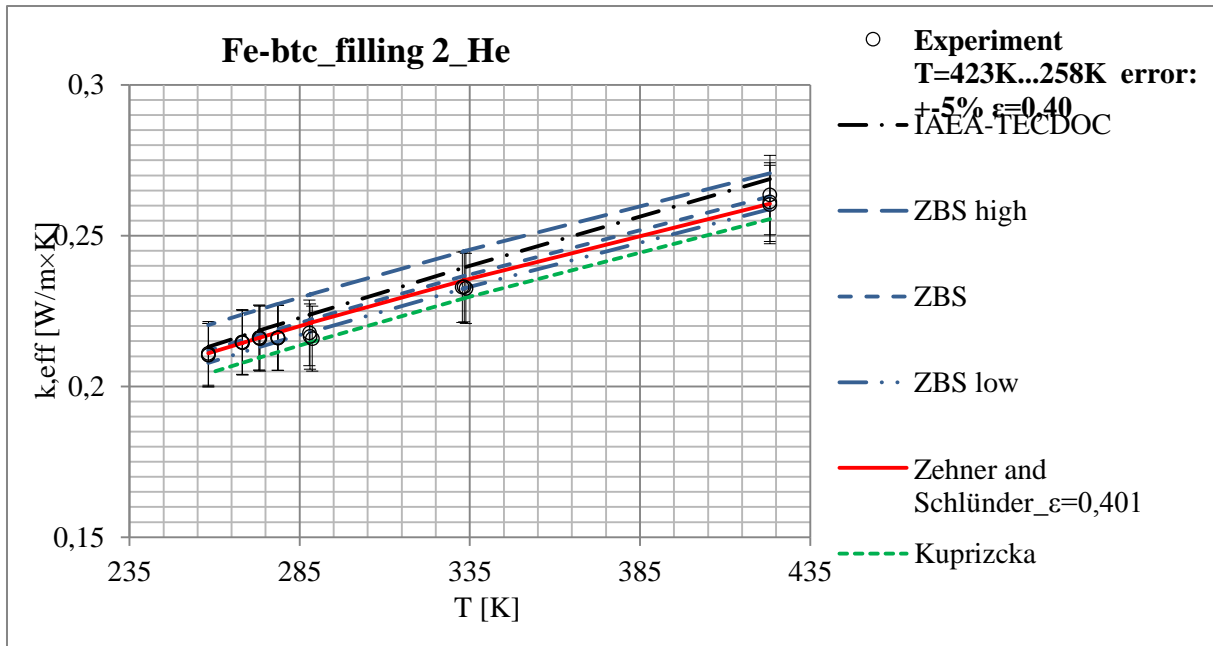
Appendix E - Fe-btc results

Fe-btc with N2, filling 1, measurement error =5%

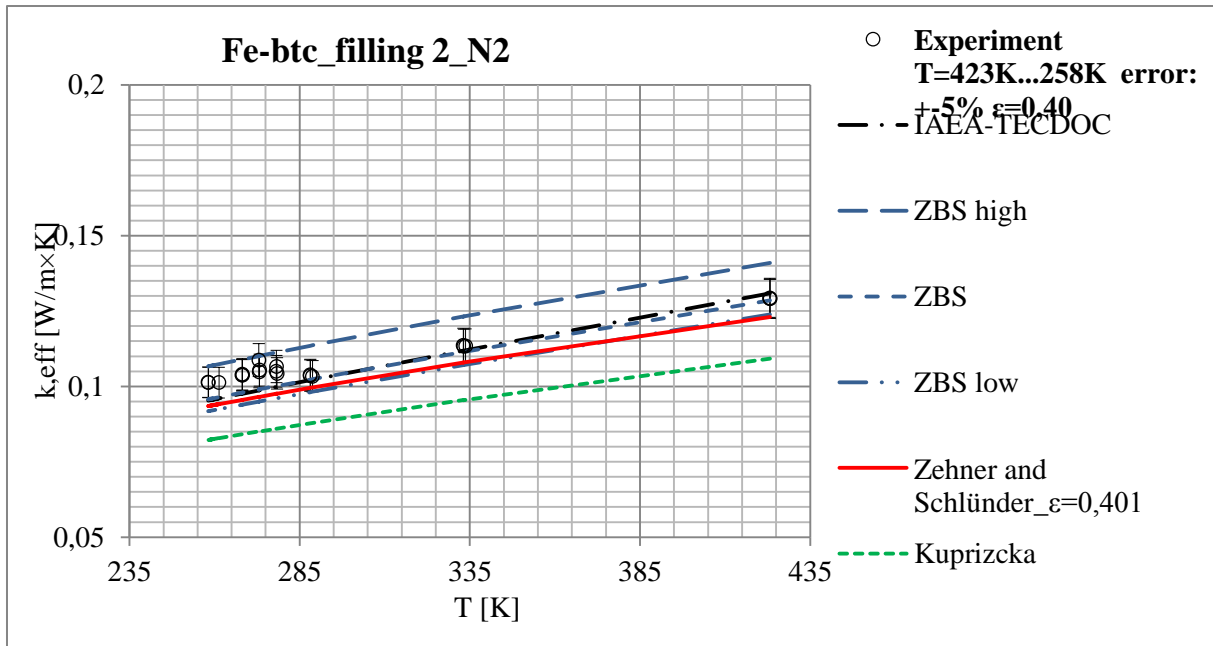
$\varepsilon_{\text{bulk}}$	0,423						
ρ_{bulk}	730,15	kg/m ³					
d_p	0,00046	m					
p	1,2	bar					
T [K]	k [W/m×K]	Cp_gas [J/kgK]	k_f [W/m×K]	k_s [W/m×K]	K=k_s/k_f	k_ZBS [W/m×K]	$\Delta k_{\text{ZBS}}/k_{\text{ZBS}}$
423,147	0,126	1046,358	0,034	0,312	9,168	0,123	7 %
423,167	0,128	1046,360	0,034	0,312	9,168	0,123	7 %
423,150	0,128	1046,358	0,034	0,312	9,168	0,123	7 %
333,270	0,114	1040,033	0,028	0,294	10,503	0,107	8 %
332,712	0,114	1040,013	0,028	0,293	10,514	0,107	8 %
332,884	0,113	1040,019	0,028	0,293	10,510	0,107	8 %
288,635	0,104	1039,107	0,025	0,283	11,437	0,098	8 %
288,162	0,104	1039,104	0,025	0,283	11,448	0,098	8 %
288,130	0,104	1039,103	0,025	0,283	11,449	0,098	8 %
278,191	0,104	1039,056	0,024	0,280	11,694	0,096	9 %
278,069	0,104	1039,056	0,024	0,280	11,697	0,096	9 %
278,147	0,104	1039,056	0,024	0,280	11,695	0,096	9 %
273,175	0,104	1039,049	0,024	0,279	11,824	0,095	9 %
273,216	0,104	1039,049	0,024	0,279	11,823	0,095	9 %
273,184	0,104	1039,049	0,024	0,279	11,824	0,095	9 %
268,107	0,103	1039,053	0,023	0,277	11,959	0,093	9 %
268,189	0,103	1039,052	0,023	0,277	11,957	0,093	9 %
268,165	0,103	1039,053	0,023	0,277	11,958	0,093	9 %
258,113	0,101	1039,086	0,022	0,275	12,240	0,091	9 %
258,132	0,101	1039,086	0,022	0,275	12,240	0,091	9 %
258,216	0,101	1039,086	0,022	0,275	12,237	0,091	9 %



Fe-btc with He, filling 2, measurement error =5%							
$\varepsilon_{\text{bulk}}$	0,401						
ρ_{bulk}	668,32	kg/m ³					
d_p	0,00046	m					
p	1,2	bar					
T [K]	k [W/m×K]	Cp_gas [J/kgK]	k_f [W/m×K]	k_s [W/m×K]	K=k_s/k_f	k_ZBS [W/m×K]	$\Delta k_{\text{ZBS}}/k_{\text{ZBS}}$
423,147	0,260	5196,250	0,196	0,312	1,594	0,263	2 %
423,147	0,261	5196,250	0,196	0,312	1,594	0,263	2 %
423,151	0,263	5196,250	0,196	0,312	1,594	0,263	2 %
333,330	0,233	5196,250	0,166	0,294	1,769	0,237	3 %
332,754	0,233	5196,250	0,166	0,293	1,770	0,236	3 %
333,830	0,233	5196,250	0,166	0,294	1,768	0,237	3 %
287,847	0,218	5196,250	0,150	0,283	1,884	0,222	3 %
288,035	0,217	5196,250	0,150	0,283	1,883	0,222	3 %
288,702	0,216	5196,250	0,150	0,283	1,881	0,222	3 %
278,669	0,216	5196,250	0,147	0,280	1,910	0,219	3 %
278,529	0,216	5196,250	0,147	0,280	1,910	0,219	3 %
278,554	0,216	5196,250	0,147	0,280	1,910	0,219	3 %
273,077	0,216	5196,250	0,145	0,279	1,926	0,217	3 %
273,345	0,216	5196,250	0,145	0,279	1,925	0,217	3 %
273,106	0,216	5196,250	0,145	0,279	1,926	0,217	3 %
268,228	0,214	5196,250	0,143	0,277	1,941	0,215	3 %
268,042	0,215	5196,250	0,143	0,277	1,941	0,215	3 %
268,167	0,215	5196,250	0,143	0,277	1,941	0,215	3 %
258,181	0,211	5196,250	0,139	0,275	1,972	0,212	3 %
258,167	0,210	5196,250	0,139	0,275	1,972	0,212	3 %
258,151	0,210	5196,250	0,139	0,275	1,972	0,212	3 %

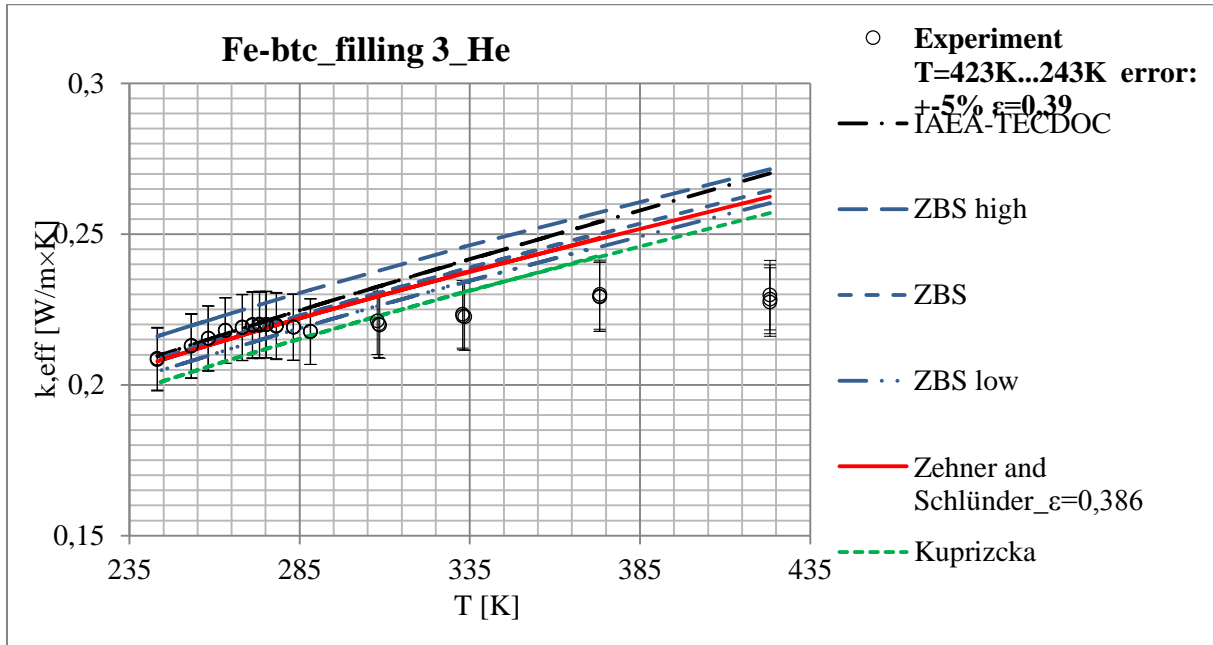


Fe-btc with N2, filling 2, measurement error =5%							
$\varepsilon_{\text{bulk}}$	0,401						
ρ_{bulk}	668,32	kg/m ³					
d_p	0,00046	m					
p	1,2	bar					
T [K]	k [W/m×K]	Cp_gas [J/kgK]	k_f [W/m×K]	k_s [W/m×K]	K=k_s/k_f	k_ZBS [W/m×K]	$\Delta k_{\text{ZBS}}/k_{\text{ZBS}}$
423,144	0,129	1046,358	0,034	0,312	9,168	0,128	6 %
423,134	0,129	1046,357	0,034	0,312	9,168	0,128	6 %
423,173	0,129	1046,361	0,034	0,312	9,168	0,129	6 %
333,773	0,113	1040,051	0,028	0,294	10,494	0,112	7 %
333,064	0,114	1040,026	0,028	0,293	10,507	0,111	7 %
333,207	0,113	1040,031	0,028	0,294	10,504	0,111	7 %
288,762	0,103	1039,108	0,025	0,283	11,434	0,102	7 %
288,114	0,104	1039,103	0,025	0,283	11,450	0,102	7 %
288,074	0,104	1039,103	0,025	0,283	11,450	0,102	7 %
278,187	0,107	1039,056	0,024	0,280	11,694	0,100	7 %
278,144	0,105	1039,056	0,024	0,280	11,695	0,100	7 %
278,346	0,104	1039,056	0,024	0,280	11,690	0,100	7 %
272,990	0,109	1039,049	0,024	0,279	11,829	0,099	7 %
273,208	0,105	1039,049	0,024	0,279	11,823	0,099	7 %
273,125	0,105	1039,049	0,024	0,279	11,825	0,099	7 %
268,051	0,104	1039,053	0,023	0,277	11,961	0,098	7 %
268,141	0,104	1039,053	0,023	0,277	11,958	0,098	7 %
268,189	0,104	1039,052	0,023	0,277	11,957	0,098	7 %
258,177	0,101	1039,086	0,022	0,275	12,238	0,096	7 %
261,279	0,101	1039,072	0,023	0,276	12,149	0,096	7 %
258,075	0,101	1039,086	0,022	0,275	12,241	0,096	7 %



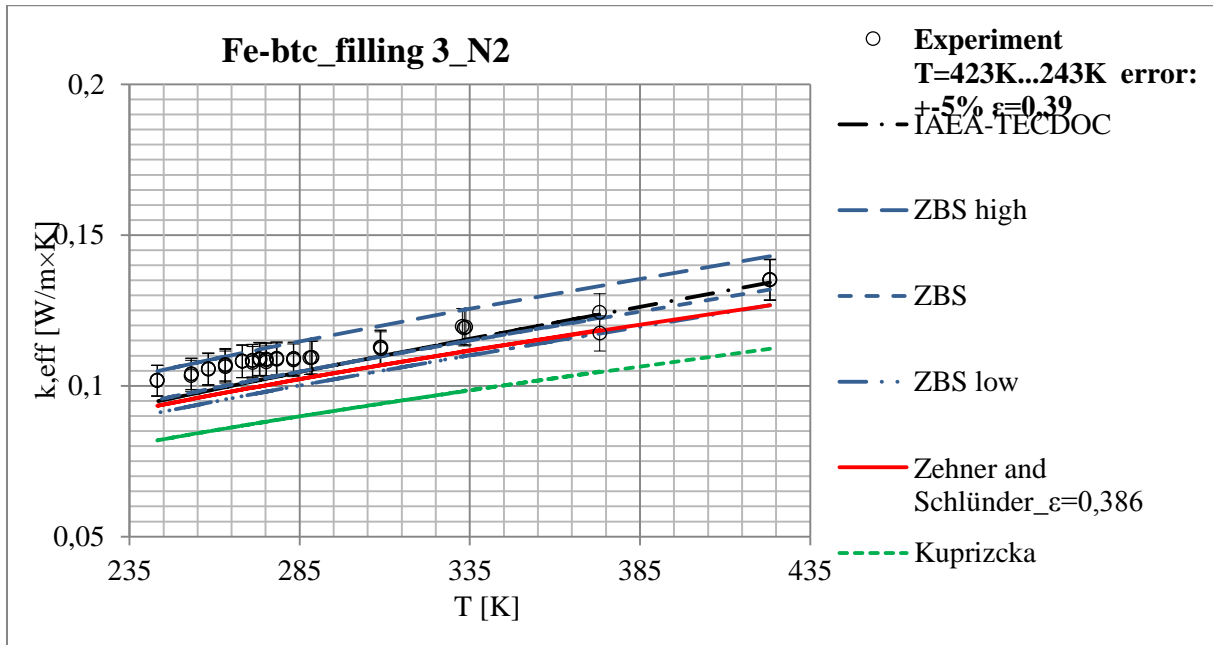
Fe-btc with He, filling 3, measurement error =5%							
$\varepsilon_{\text{bulk}}$	0,386						
ρ_{bulk}	679,72	kg/m ³					
d_p	0,00044	m					
p	1,2	bar					
T [K]	k [W/m×K]	Cp_gas [J/kgK]	k_f [W/m×K]	k_s [W/m×K]	K=k_s/k_f	k_ZBS [W/m×K]	$\Delta k_{\text{ZBS}}/k_{\text{ZBS}}$
423,148	0,230	5196,250	0,196	0,312	1,594	0,265	2 %
423,174	0,228	5196,250	0,196	0,312	1,594	0,265	2 %
423,167	0,227	5196,250	0,196	0,312	1,594	0,265	2 %
332,975	0,223	5196,250	0,166	0,293	1,770	0,238	2 %
333,496	0,223	5196,250	0,166	0,294	1,769	0,239	2 %
332,872	0,223	5196,250	0,166	0,293	1,770	0,238	2 %
288,135	0,218	5196,250	0,150	0,283	1,883	0,224	3 %
288,204	0,218	5196,250	0,150	0,283	1,883	0,224	3 %
288,152	0,218	5196,250	0,150	0,283	1,883	0,224	3 %
278,129	0,219	5196,250	0,147	0,280	1,911	0,221	3 %
278,125	0,220	5196,250	0,147	0,280	1,911	0,221	3 %
278,166	0,220	5196,250	0,147	0,280	1,911	0,221	3 %
273,145	0,220	5196,250	0,145	0,279	1,926	0,219	3 %
273,287	0,220	5196,250	0,145	0,279	1,926	0,219	3 %
273,138	0,220	5196,250	0,145	0,279	1,926	0,219	3 %
268,137	0,219	5196,250	0,143	0,277	1,941	0,217	3 %
268,135	0,219	5196,250	0,143	0,277	1,941	0,217	3 %
268,114	0,219	5196,250	0,143	0,277	1,941	0,217	3 %
258,119	0,215	5196,250	0,139	0,275	1,972	0,214	3 %
258,123	0,215	5196,250	0,139	0,275	1,972	0,214	3 %
258,152	0,215	5196,250	0,139	0,275	1,972	0,214	3 %
243,162	0,208	5196,250	0,134	0,270	2,021	0,209	3 %
243,143	0,209	5196,250	0,134	0,270	2,022	0,209	3 %
243,171	0,209	5196,250	0,134	0,270	2,021	0,209	3 %
253,124	0,213	5196,250	0,137	0,273	1,988	0,212	3 %
253,143	0,213	5196,250	0,137	0,273	1,988	0,212	3 %
253,145	0,213	5196,250	0,137	0,273	1,988	0,212	3 %
263,156	0,218	5196,250	0,141	0,276	1,956	0,216	3 %
263,146	0,218	5196,250	0,141	0,276	1,956	0,216	3 %
263,140	0,218	5196,250	0,141	0,276	1,956	0,216	3 %
271,140	0,220	5196,250	0,144	0,278	1,932	0,218	3 %
271,132	0,220	5196,250	0,144	0,278	1,932	0,218	3 %
271,170	0,220	5196,250	0,144	0,278	1,932	0,218	3 %
275,155	0,220	5196,250	0,145	0,279	1,920	0,220	3 %
275,175	0,220	5196,250	0,145	0,279	1,920	0,220	3 %
275,167	0,220	5196,250	0,145	0,279	1,920	0,220	3 %
283,152	0,219	5196,250	0,148	0,281	1,897	0,222	3 %
283,139	0,219	5196,250	0,148	0,281	1,897	0,222	3 %

283,147	0,219	5196,250	0,148	0,281	1,897	0,222	3 %
307,817	0,221	5196,250	0,157	0,288	1,831	0,230	3 %
308,204	0,220	5196,250	0,157	0,288	1,830	0,231	3 %
308,520	0,220	5196,250	0,157	0,288	1,829	0,231	3 %
373,137	0,229	5196,250	0,179	0,302	1,684	0,250	2 %
373,145	0,229	5196,250	0,179	0,302	1,684	0,250	2 %
373,160	0,230	5196,250	0,179	0,302	1,684	0,250	2 %

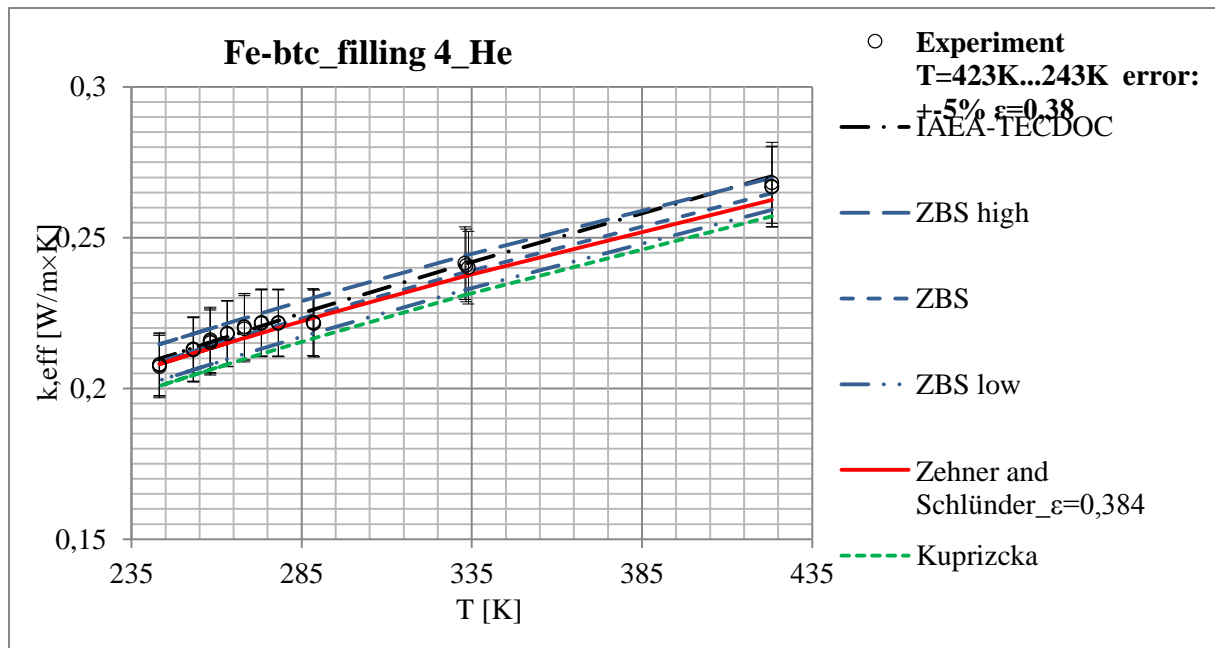


Fe-btc with N2, filling 3 measurement error =5%							
$\varepsilon_{\text{bulk}}$	0,386						
ρ_{bulk}	679,72	kg/m ³					
d_p	0,00044	m					
p	1,2	bar					
T [K]	k [W/m×K]	Cp_gas [J/kgK]	k_f [W/m×K]	k_s [W/m×K]	K=k_s/k_f	k_ZBS [W/m×K]	$\Delta k_{\text{ZBS}}/k_{\text{ZBS}}$
423,135	0,135	1046,357	0,034	0,312	9,168	0,132	6 %
423,164	0,135	1046,360	0,034	0,312	9,168	0,132	6 %
423,149	0,135	1046,358	0,034	0,312	9,168	0,132	6 %
333,348	0,119	1040,036	0,028	0,294	10,502	0,115	7 %
332,779	0,120	1040,016	0,028	0,293	10,512	0,115	7 %
333,785	0,119	1040,051	0,028	0,294	10,494	0,115	7 %
288,469	0,109	1039,106	0,025	0,283	11,441	0,105	7 %
288,680	0,109	1039,107	0,025	0,283	11,436	0,106	7 %
287,981	0,109	1039,102	0,025	0,283	11,453	0,105	7 %
278,286	0,109	1039,056	0,024	0,280	11,692	0,103	7 %
278,157	0,109	1039,056	0,024	0,280	11,695	0,103	7 %
278,305	0,109	1039,056	0,024	0,280	11,691	0,103	7 %
273,188	0,109	1039,049	0,024	0,279	11,823	0,102	7 %
273,381	0,109	1039,049	0,024	0,279	11,818	0,102	7 %
273,161	0,109	1039,049	0,024	0,279	11,824	0,102	7 %
268,115	0,108	1039,053	0,023	0,277	11,959	0,101	7 %
268,149	0,108	1039,053	0,023	0,277	11,958	0,101	7 %
268,181	0,108	1039,052	0,023	0,277	11,957	0,101	7 %
258,175	0,105	1039,086	0,022	0,275	12,238	0,099	7 %
258,119	0,106	1039,086	0,022	0,275	12,240	0,099	7 %
258,132	0,106	1039,086	0,022	0,275	12,240	0,099	7 %
243,148	0,102	1039,188	0,021	0,270	12,700	0,095	7 %
243,139	0,102	1039,188	0,021	0,270	12,700	0,095	7 %
243,145	0,102	1039,188	0,021	0,270	12,700	0,095	7 %
253,109	0,103	1039,114	0,022	0,273	12,388	0,098	7 %
253,146	0,104	1039,114	0,022	0,273	12,387	0,098	7 %
253,163	0,104	1039,114	0,022	0,273	12,387	0,098	7 %
263,140	0,106	1039,065	0,023	0,276	12,097	0,100	7 %
263,127	0,107	1039,065	0,023	0,276	12,097	0,100	7 %
263,143	0,107	1039,065	0,023	0,276	12,096	0,100	7 %
271,177	0,108	1039,049	0,023	0,278	11,877	0,102	7 %
271,154	0,108	1039,049	0,023	0,278	11,877	0,102	7 %
271,072	0,108	1039,049	0,023	0,278	11,879	0,102	7 %
275,191	0,108	1039,051	0,024	0,279	11,771	0,103	7 %
275,160	0,109	1039,051	0,024	0,279	11,772	0,103	7 %
275,161	0,109	1039,051	0,024	0,279	11,772	0,103	7 %
283,141	0,108	1039,074	0,024	0,281	11,570	0,104	7 %
283,186	0,109	1039,074	0,024	0,281	11,569	0,104	7 %

283,253	0,109	1039,074	0,024	0,281	11,567	0,104	7 %
308,833	0,112	1039,371	0,026	0,288	10,985	0,110	7 %
308,648	0,113	1039,367	0,026	0,288	10,988	0,110	7 %
308,830	0,113	1039,371	0,026	0,288	10,985	0,110	7 %
373,179	0,117	1042,054	0,031	0,302	9,840	0,123	6 %
373,133	0,124	1042,051	0,031	0,302	9,840	0,123	6 %

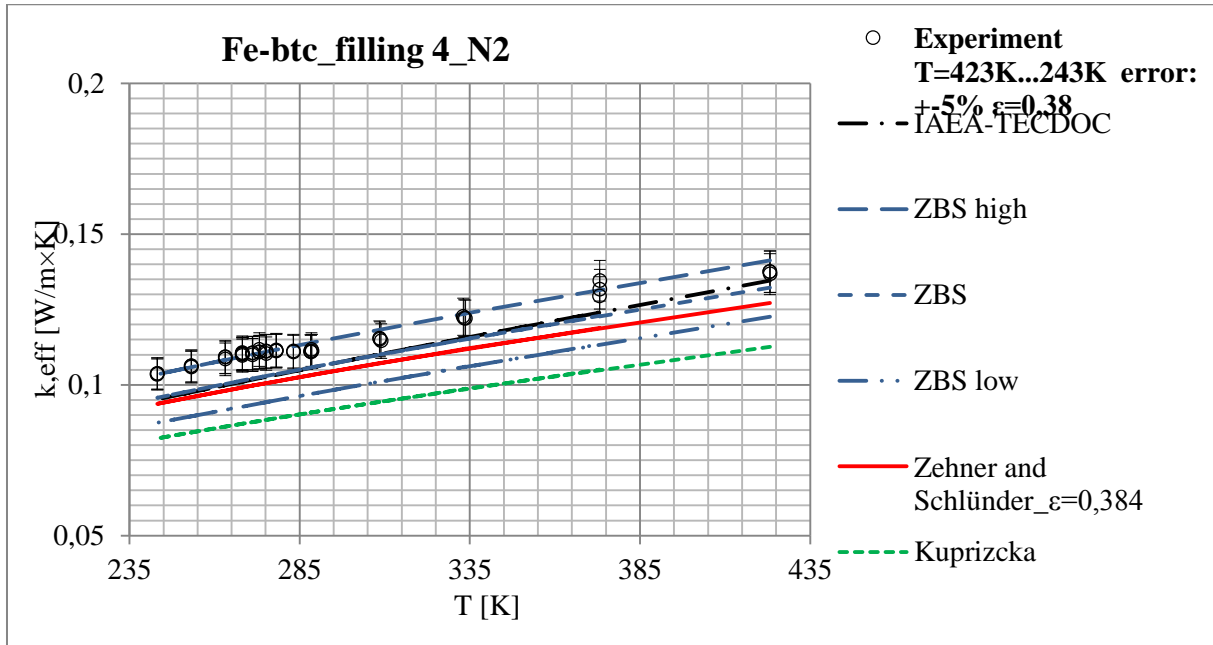


Fe-btc with He, filling 4, measurement error =5%							
$\varepsilon_{\text{bulk}}$	0,384						
ρ_{bulk}	666,68	kg/m ³					
d_p	0,00044	m					
p	1,4	bar					
T [K]	k [W/m×K]	Cp_gas [J/kgK]	k_f [W/m×K]	k_s [W/m×K]	K=k_s/k_f	k_ZBS [W/m×K]	$\Delta k_{\text{ZBS}}/k_{\text{ZBS}}$
423,151	0,268	5196,250	0,196	0,312	1,594	0,265	2 %
423,156	0,267	5196,250	0,196	0,312	1,594	0,265	2 %
423,159	0,267	5196,250	0,196	0,312	1,594	0,265	2 %
332,958	0,242	5196,250	0,166	0,293	1,770	0,239	2 %
333,985	0,240	5196,250	0,166	0,294	1,767	0,239	2 %
333,292	0,241	5196,250	0,166	0,294	1,769	0,239	2 %
288,589	0,222	5196,250	0,150	0,283	1,882	0,224	3 %
288,546	0,222	5196,250	0,150	0,283	1,882	0,224	3 %
288,312	0,222	5196,250	0,150	0,283	1,882	0,224	3 %
278,136	0,222	5196,250	0,147	0,280	1,911	0,221	3 %
278,112	0,222	5196,250	0,147	0,280	1,911	0,221	3 %
278,114	0,222	5196,250	0,147	0,280	1,911	0,221	3 %
273,167	0,222	5196,250	0,145	0,279	1,926	0,219	3 %
273,154	0,222	5196,250	0,145	0,279	1,926	0,219	3 %
273,134	0,222	5196,250	0,145	0,279	1,926	0,219	3 %
268,144	0,220	5196,250	0,143	0,277	1,941	0,218	3 %
268,156	0,220	5196,250	0,143	0,277	1,941	0,218	3 %
268,176	0,220	5196,250	0,143	0,277	1,941	0,218	3 %
258,113	0,216	5196,250	0,139	0,275	1,972	0,214	3 %
258,128	0,216	5196,250	0,139	0,275	1,972	0,214	3 %
258,127	0,215	5196,250	0,139	0,275	1,972	0,214	3 %
243,172	0,207	5196,250	0,134	0,270	2,021	0,209	3 %
243,168	0,208	5196,250	0,134	0,270	2,021	0,209	3 %
243,206	0,208	5196,250	0,134	0,270	2,021	0,209	3 %
253,184	0,213	5196,250	0,137	0,273	1,988	0,212	3 %
253,170	0,213	5196,250	0,137	0,273	1,988	0,212	3 %
253,128	0,213	5196,250	0,137	0,273	1,988	0,212	3 %
263,152	0,218	5196,250	0,141	0,276	1,956	0,216	3 %
263,142	0,218	5196,250	0,141	0,276	1,956	0,216	3 %
263,126	0,218	5196,250	0,141	0,276	1,956	0,216	3 %



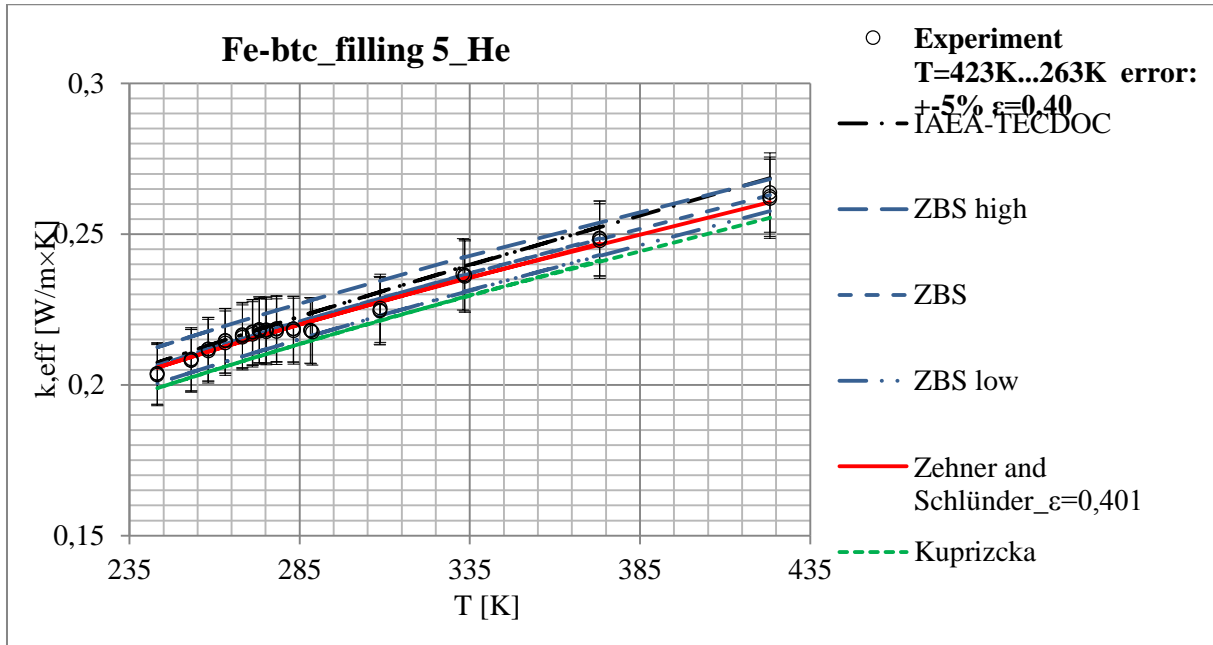
Fe-btc with N2, filling 4, measurement error =5%							
$\varepsilon_{\text{bulk}}$	0,384						
ρ_{bulk}	666,68	kg/m ³					
d_p	0,00044	m					
p	1,2	bar					
T [K]	k [W/m×K]	Cp_gas [J/kgK]	k_f [W/m×K]	k_s [W/m×K]	K=k_s/k_f	k_ZBS [W/m×K]	$\Delta k_{\text{ZBS}}/k_{\text{ZBS}}$
423,161	0,138	1046,360	0,034	0,312	9,168	0,132	7 %
423,181	0,137	1046,362	0,034	0,312	9,168	0,132	7 %
423,151	0,137	1046,358	0,034	0,312	9,168	0,132	7 %
333,063	0,123	1040,026	0,028	0,293	10,507	0,115	8 %
333,299	0,122	1040,034	0,028	0,294	10,503	0,115	8 %
333,700	0,122	1040,048	0,028	0,294	10,495	0,115	8 %
288,441	0,112	1039,106	0,025	0,283	11,442	0,106	8 %
288,203	0,111	1039,104	0,025	0,283	11,447	0,106	8 %
288,310	0,111	1039,105	0,025	0,283	11,445	0,106	8 %
288,596	0,111	1039,107	0,025	0,283	11,438	0,106	8 %
278,134	0,111	1039,056	0,024	0,280	11,696	0,104	8 %
278,145	0,111	1039,056	0,024	0,280	11,695	0,104	8 %
278,100	0,111	1039,056	0,024	0,280	11,696	0,104	8 %
273,149	0,111	1039,049	0,024	0,279	11,824	0,103	8 %
273,152	0,112	1039,049	0,024	0,279	11,824	0,103	8 %
273,131	0,111	1039,049	0,024	0,279	11,825	0,103	8 %
268,147	0,111	1039,053	0,023	0,277	11,958	0,101	8 %
268,159	0,110	1039,053	0,023	0,277	11,958	0,101	8 %
268,157	0,110	1039,053	0,023	0,277	11,958	0,101	8 %
268,174	0,110	1039,053	0,023	0,277	11,957	0,101	8 %
268,164	0,110	1039,053	0,023	0,277	11,958	0,101	8 %
268,161	0,110	1039,053	0,023	0,277	11,958	0,101	8 %
243,157	0,103	1039,188	0,021	0,270	12,699	0,096	8 %
243,164	0,104	1039,188	0,021	0,270	12,699	0,096	8 %
243,172	0,104	1039,188	0,021	0,270	12,699	0,096	8 %
253,148	0,106	1039,114	0,022	0,273	12,387	0,098	8 %
253,133	0,106	1039,114	0,022	0,273	12,388	0,098	8 %
253,191	0,106	1039,114	0,022	0,273	12,386	0,098	8 %
263,145	0,108	1039,065	0,023	0,276	12,096	0,100	8 %
263,131	0,109	1039,065	0,023	0,276	12,097	0,100	8 %
263,170	0,109	1039,065	0,023	0,276	12,096	0,100	8 %
271,145	0,110	1039,049	0,023	0,278	11,877	0,102	8 %
271,187	0,111	1039,049	0,023	0,278	11,876	0,102	8 %
271,125	0,111	1039,049	0,023	0,278	11,878	0,102	8 %
275,163	0,110	1039,051	0,024	0,279	11,772	0,103	8 %
275,159	0,111	1039,051	0,024	0,279	11,772	0,103	8 %
275,140	0,111	1039,051	0,024	0,279	11,772	0,103	8 %
283,143	0,111	1039,074	0,024	0,281	11,570	0,105	8 %

283,140	0,111	1039,074	0,024	0,281	11,570	0,105	8 %
308,947	0,115	1039,373	0,026	0,288	10,982	0,110	8 %
308,585	0,115	1039,366	0,026	0,288	10,990	0,110	8 %
308,442	0,115	1039,363	0,026	0,288	10,993	0,110	8 %
373,176	0,132	1042,053	0,031	0,302	9,840	0,123	7 %
373,176	0,135	1042,053	0,031	0,302	9,840	0,123	7 %
373,137	0,129	1042,051	0,031	0,302	9,840	0,123	7 %



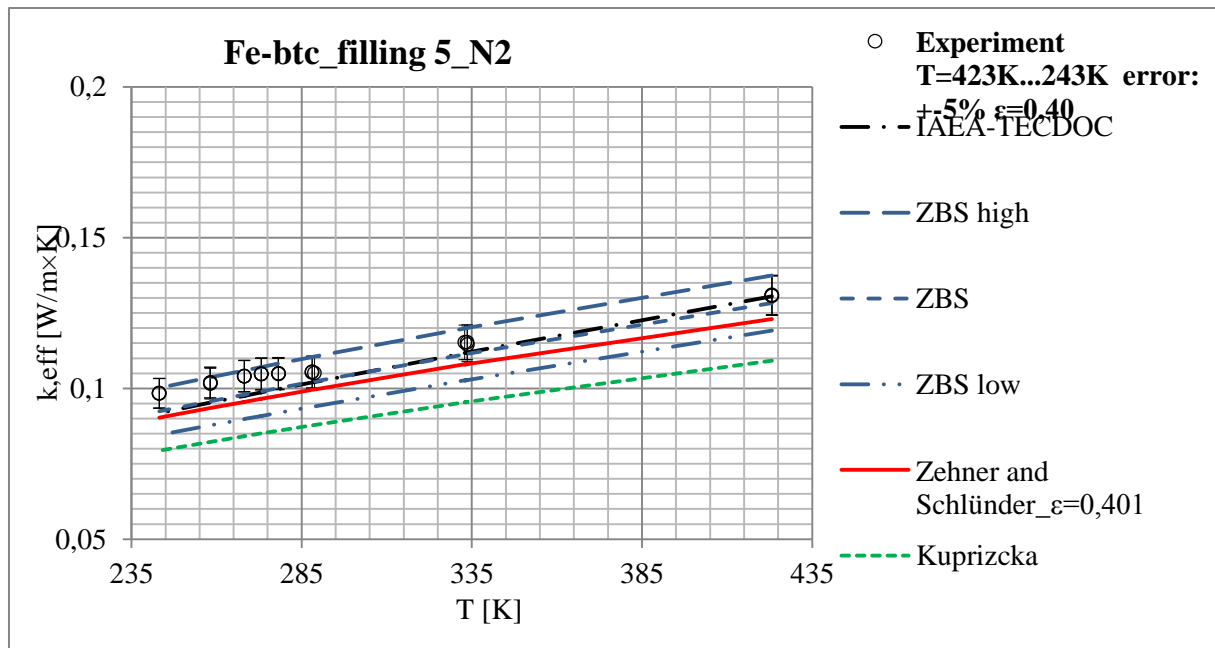
Fe-btc with He, filling 5, measurement error =5%							
$\varepsilon_{\text{bulk}}$	0,401						
ρ_{bulk}	650,52	kg/m ³					
d_p	0,00044	m					
p	1,4	bar					
T [K]	k [W/m×K]	Cp_gas [J/kgK]	k_f [W/m×K]	k_s [W/m×K]	K=k_s/k_f	k_ZBS [W/m×K]	$\Delta k_{\text{ZBS}}/k_{\text{ZBS}}$
423,169	0,264	5196,250	0,196	0,312	1,594	0,263	2 %
423,127	0,262	5196,250	0,196	0,312	1,594	0,263	2 %
423,128	0,262	5196,250	0,196	0,312	1,594	0,263	2 %
333,493	0,236	5196,250	0,166	0,294	1,769	0,237	2 %
332,969	0,237	5196,250	0,166	0,293	1,770	0,236	2 %
333,521	0,236	5196,250	0,166	0,294	1,768	0,237	2 %
288,122	0,218	5196,250	0,150	0,283	1,883	0,222	3 %
288,739	0,217	5196,250	0,150	0,283	1,881	0,222	3 %
288,323	0,218	5196,250	0,150	0,283	1,882	0,222	3 %
278,218	0,218	5196,250	0,147	0,280	1,911	0,219	3 %
278,195	0,218	5196,250	0,147	0,280	1,911	0,219	3 %
278,198	0,219	5196,250	0,147	0,280	1,911	0,219	3 %
273,206	0,218	5196,250	0,145	0,279	1,926	0,217	3 %
273,139	0,218	5196,250	0,145	0,279	1,926	0,217	3 %
273,114	0,218	5196,250	0,145	0,279	1,926	0,217	3 %
268,135	0,216	5196,250	0,143	0,277	1,941	0,215	3 %
268,170	0,217	5196,250	0,143	0,277	1,941	0,215	3 %
268,161	0,216	5196,250	0,143	0,277	1,941	0,215	3 %
258,165	0,212	5196,250	0,139	0,275	1,972	0,212	3 %
258,112	0,212	5196,250	0,139	0,275	1,972	0,212	3 %
258,134	0,211	5196,250	0,139	0,275	1,972	0,212	3 %
243,154	0,204	5196,250	0,134	0,270	2,022	0,206	3 %
243,144	0,203	5196,250	0,134	0,270	2,022	0,206	3 %
243,140	0,204	5196,250	0,134	0,270	2,022	0,206	3 %
253,118	0,208	5196,250	0,137	0,273	1,988	0,210	3 %
253,150	0,209	5196,250	0,137	0,273	1,988	0,210	3 %
253,104	0,208	5196,250	0,137	0,273	1,988	0,210	3 %
263,113	0,215	5196,250	0,141	0,276	1,956	0,214	3 %
263,137	0,214	5196,250	0,141	0,276	1,956	0,214	3 %
263,148	0,215	5196,250	0,141	0,276	1,956	0,214	3 %
271,175	0,217	5196,250	0,144	0,278	1,932	0,216	3 %
271,157	0,217	5196,250	0,144	0,278	1,932	0,216	3 %
271,141	0,217	5196,250	0,144	0,278	1,932	0,216	3 %
275,151	0,218	5196,250	0,145	0,279	1,920	0,218	3 %
275,151	0,218	5196,250	0,145	0,279	1,920	0,218	3 %
275,176	0,218	5196,250	0,145	0,279	1,920	0,218	3 %
283,224	0,218	5196,250	0,148	0,281	1,897	0,220	3 %
283,182	0,218	5196,250	0,148	0,281	1,897	0,220	3 %

283,106	0,219	5196,250	0,148	0,281	1,897	0,220	3 %
308,680	0,225	5196,250	0,157	0,288	1,828	0,229	3 %
308,528	0,225	5196,250	0,157	0,288	1,829	0,229	3 %
308,585	0,224	5196,250	0,157	0,288	1,829	0,229	3 %
373,146	0,248	5196,250	0,179	0,302	1,684	0,249	2 %
373,169	0,248	5196,250	0,179	0,302	1,684	0,249	2 %
373,133	0,249	5196,250	0,179	0,302	1,684	0,249	2 %



Fe-btc with N2, filling 5, measurement error =5%

T [K]	k [W/m×K]	Cp_gas [J/kgK]	k_f [W/m×K]	k_s [W/m×K]	K=k_s/k_f	k_ZBS [W/m×K]	Δk_ZBS/kZBS
ε_bulk	0,401						
ρ_bulk	650,52	kg/m ³					
d_p	0,00044	m					
p	1,2	bar					
423,154	0,131	1046,359	0,034	0,312	9,168	0,128	7 %
423,136	0,131	1046,357	0,034	0,312	9,168	0,128	7 %
423,139	0,131	1046,357	0,034	0,312	9,168	0,128	7 %
332,886	0,115	1040,019	0,028	0,293	10,510	0,111	8 %
333,601	0,115	1040,045	0,028	0,294	10,497	0,111	8 %
333,664	0,115	1040,047	0,028	0,294	10,496	0,111	8 %
288,735	0,105	1039,108	0,025	0,283	11,435	0,102	8 %
288,098	0,106	1039,103	0,025	0,283	11,450	0,102	8 %
288,022	0,105	1039,103	0,025	0,283	11,452	0,102	8 %
278,174	0,105	1039,056	0,024	0,280	11,695	0,100	8 %
278,171	0,105	1039,056	0,024	0,280	11,695	0,100	8 %
278,156	0,105	1039,056	0,024	0,280	11,695	0,100	8 %
273,122	0,105	1039,049	0,024	0,279	11,825	0,099	8 %
273,091	0,105	1039,049	0,024	0,279	11,826	0,099	8 %
273,145	0,105	1039,049	0,024	0,279	11,825	0,099	8 %
268,154	0,104	1039,053	0,023	0,277	11,958	0,098	8 %
268,121	0,104	1039,053	0,023	0,277	11,959	0,098	8 %
268,142	0,104	1039,053	0,023	0,277	11,958	0,098	8 %
258,163	0,102	1039,086	0,022	0,275	12,239	0,096	8 %
258,139	0,102	1039,086	0,022	0,275	12,240	0,096	8 %
258,134	0,102	1039,086	0,022	0,275	12,240	0,096	8 %
243,165	0,098	1039,188	0,021	0,270	12,699	0,092	8 %
243,152	0,098	1039,188	0,021	0,270	12,700	0,092	8 %
243,131	0,098	1039,188	0,021	0,270	12,700	0,092	8 %



Appendix F - Mail from Hot Disk

From: Daniel Cederkrantz [mailto:daniel.cederkrantz@hotdisk.se]
Sent: 30. mai 2013 16:59
To: Christian Schlemminger
Subject: Re: Questions to cryo probe and measurement results

Hello again Christian,

I've been looking at your data, and I see two possible reasons for the discontinuity around 0 C.

1) The silicone oil that seeps into the chamber. However, I find this unlikely unless water joins the silicone oil in finding its way into the chamber. On a side-note here, I've been discussing the silicone oil problem with the manufacturer and they are now considering the problem. As a quick-fix they suggest arranging some kind of simple gasket or lid which prevents the silicone oil leaving the bath.

2) The TCR-values around 0 C could be less than perfect. I plotted the TCR-values (which you find here: C:\HotDiskTPS_7.1\data\Config\TCR-values.tcr) and there is a hint of a "bump" in the data around 0 C. I will investigate this phenomenon, and correct the TCR-data if needed, but I suspect this will take some time. However, you have the equipment necessary to gather TCR-data. If you decide to calibrate TCR on your own, just edit the TCR-file with you new TCR-values. You can even add new temperatures if you want to minimize the interpolation of TCR-values. It is also this file you need to edit when you add the TCR-values for temperatures below -80 C.

Testing of maximum cable-temperature remains to be performed.

Daniel

Appendix G - Foam results

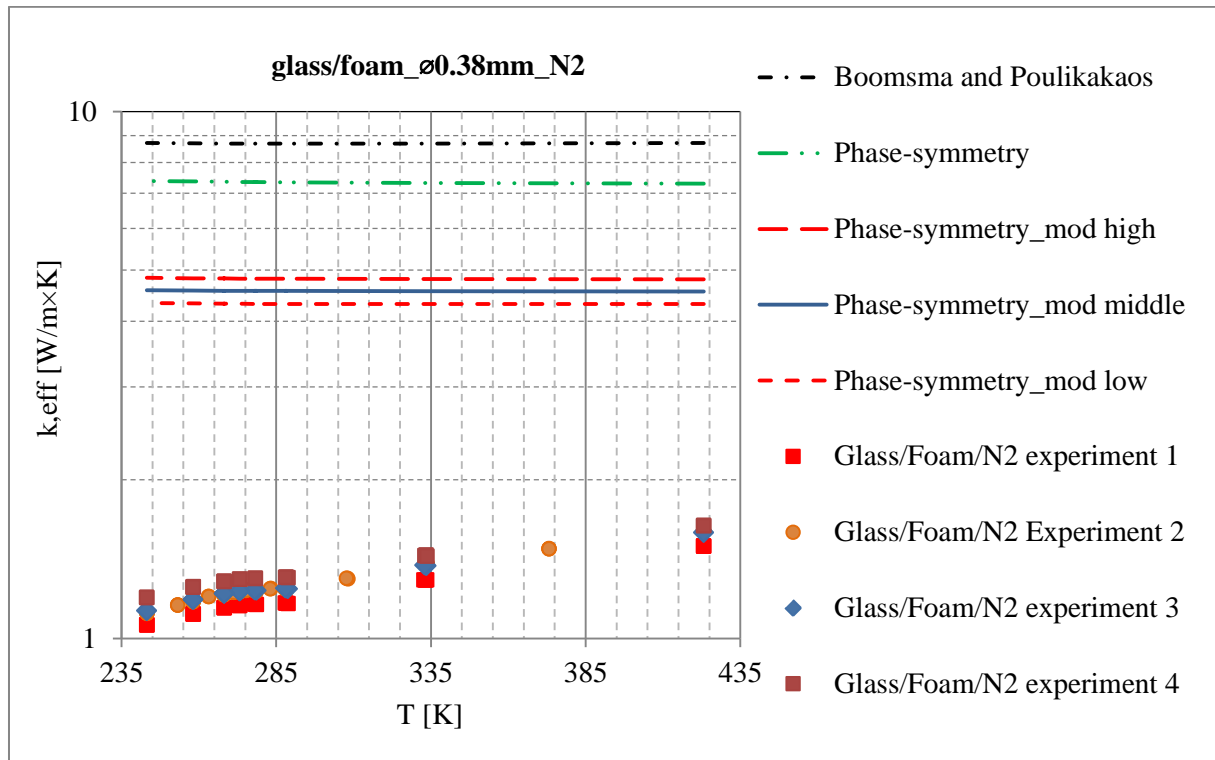
Glass/Foam/N2 experiment 1								
ϵ_{tot}	0,396808		R	8314		e	0,174667	
ϵ_{spec}	0,425047		Cp_gas	1039		η_{high}	0,647214	
ϵ_{foam}	0,933564		dp	0,00038		η_{low}	0,57735	
						η_{middle}	0,612282	
T	k_e	k_f	k_s_glass	k_ZBS	k_s_alu	k_phase-sym_mod		
						High bound	Low Bound	Middle
[K]	[W/m×K]	[W/m×K]	[W/m×K]	[W/m×K]	[W/m×K]	[W/m×K]	[W/m×K]	[W/m×K]
423,14	1,495707	0,034064	1,243263	0,213317	208,8957	4,804016	4,310467	4,557241
423,14	1,497131	0,034064	1,243263	0,213317	208,8957	4,804016	4,310467	4,557241
423,137	1,495335	0,034063	1,243261	0,213316	208,8957	4,804016	4,310466	4,557241
333,602	1,290802	0,027971	1,158053	0,181862	210,665	4,808484	4,310821	4,559653
333,235	1,289158	0,027945	1,157511	0,181719	210,6749	4,808544	4,310858	4,559701
332,739	1,290415	0,02791	1,156777	0,181524	210,6883	4,808625	4,310908	4,559767
288,865	1,163587	0,024742	1,080516	0,16348	211,8803	4,815015	4,314521	4,564768
287,947	1,166929	0,024675	1,078681	0,163084	211,8989	4,81499	4,314452	4,564721
288,225	1,165652	0,024695	1,079238	0,163204	211,8932	4,814994	4,31447	4,564732
277,914	1,161333	0,023931	1,057986	0,158712	212,1877	4,816529	4,315319	4,565924
278,606	1,158105	0,023983	1,059451	0,159016	212,1633	4,81633	4,315176	4,565753
278,299	1,159503	0,02396	1,058802	0,158881	212,1741	4,816417	4,315238	4,565828
273,148	1,153445	0,023575	1,047745	0,156603	212,3694	4,818202	4,316566	4,567384
273,164	1,152823	0,023576	1,04778	0,156611	212,3687	4,818195	4,316561	4,567378
273,144	1,153376	0,023575	1,047737	0,156602	212,3696	4,818203	4,316568	4,567385
268,236	1,142562	0,023207	1,036914	0,15441	212,5785	4,820379	4,318254	4,569316
268,138	1,142635	0,0232	1,036695	0,154366	212,5829	4,820426	4,318291	4,569358
268,167	1,141879	0,023202	1,03676	0,154379	212,5816	4,820412	4,31828	4,569346
258,15	1,112312	0,022445	1,013793	0,149838	213,0531	4,825763	4,322527	4,574145
258,17	1,110462	0,022447	1,01384	0,149847	213,0521	4,825751	4,322518	4,574135
258,158	1,110635	0,022446	1,013812	0,149842	213,0527	4,825758	4,322523	4,574141
243,17	1,058731	0,021299	0,977268	0,142882	213,7914	4,834303	4,329339	4,581821
243,163	1,059883	0,021299	0,97725	0,142879	213,7918	4,834307	4,329342	4,581825
243,123	1,060475	0,021296	0,977149	0,14286	213,7937	4,834329	4,329359	4,581844

Glass/Foam/N2 experiment 2								
ϵ_{tot}	0,378012		R	8314		e	0,174667	
ϵ_{spec}	0,404496		Cp_gas	1039		η_{high}	0,647214	
ϵ_{foam}	0,934526		dp	0,00038		η_{low}	0,57735	
						η_{middle}	0,612282	
T	k_e	k_f	k_s_glass	k_ZBS	k_s_alu	k_phase-sym_mod		
						High bound	Low Bound	Middle
[K]	[W/m×K]	[W/m×K]	[W/m×K]	[W/m×K]	[W/m×K]	[W/m×K]	[W/m×K]	[W/m×K]
423,136	1,601409	0,034063	1,243261	0,225745	208,8957	4,749694	4,263399	4,506553
423,16	1,598644	0,034065	1,243271	0,225752	208,8954	4,749696	4,263401	4,506555
423,158	1,597921	0,034065	1,24327	0,225752	208,8954	4,749696	4,263401	4,506555
333,798	1,383352	0,027985	1,158341	0,192981	210,6597	4,752145	4,261812	4,506984
333,551	1,3814	0,027967	1,157978	0,192879	210,6664	4,752178	4,261829	4,507009
333,108	1,381736	0,027936	1,157324	0,192697	210,6783	4,752238	4,261862	4,507055
287,871	1,242345	0,024669	1,078528	0,173108	211,9005	4,757265	4,264085	4,51068
287,846	1,240873	0,024667	1,078478	0,173096	211,9011	4,757264	4,264083	4,510678
288,444	1,236423	0,024711	1,079676	0,173368	211,8887	4,757293	4,26414	4,510721
278,571	1,227102	0,02398	1,059377	0,168836	212,1645	4,758301	4,264516	4,511413
278,094	1,229075	0,023944	1,058368	0,168615	212,1813	4,758421	4,264597	4,511513
278,205	1,228762	0,023953	1,058603	0,168666	212,1774	4,758392	4,264577	4,51149
273,149	1,22474	0,023575	1,047748	0,166307	212,3694	4,75996	4,265703	4,512836
273,149	1,223047	0,023575	1,047748	0,166307	212,3694	4,75996	4,265703	4,512836
273,127	1,223404	0,023574	1,0477	0,166297	212,3702	4,759968	4,265709	4,512843
268,117	1,210505	0,023198	1,036648	0,163935	212,5838	4,761996	4,267245	4,514625
268,091	1,208131	0,023196	1,03659	0,163922	212,585	4,762008	4,267254	4,514636
268,125	1,208094	0,023199	1,036666	0,163939	212,5834	4,761993	4,267242	4,514622
258,119	1,172856	0,022443	1,01372	0,159149	213,0546	4,766926	4,271089	4,519012
258,167	1,17279	0,022446	1,013833	0,159172	213,0523	4,7669	4,271069	4,518989
258,115	1,173265	0,022442	1,013711	0,159147	213,0548	4,766928	4,271091	4,519014
243,161	1,115929	0,021299	0,977245	0,151807	213,7919	4,774806	4,277269	4,526042
243,166	1,113643	0,021299	0,977257	0,151809	213,7916	4,774803	4,277267	4,526039
243,171	1,11467	0,021299	0,97727	0,151812	213,7914	4,774801	4,277265	4,526037
253,13	1,156673	0,022063	1,001844	0,156724	213,3008	4,769588	4,273183	4,52139
253,148	1,154958	0,022064	1,001887	0,156733	213,2999	4,769578	4,273176	4,521381
253,154	1,155314	0,022065	1,001902	0,156736	213,2996	4,769575	4,273173	4,521378
263,146	1,199547	0,022823	1,025394	0,161567	212,8124	4,764342	4,269064	4,516707
263,091	1,198774	0,022819	1,025268	0,161541	212,815	4,764369	4,269085	4,516731
263,136	1,198776	0,022823	1,025371	0,161562	212,8128	4,764347	4,269067	4,516712
271,162	1,221215	0,023427	1,0434	0,165373	212,4516	4,760715	4,266269	4,513496
271,132	1,221394	0,023424	1,043334	0,165359	212,4529	4,760727	4,266278	4,513507
271,155	1,220988	0,023426	1,043385	0,16537	212,4519	4,760718	4,266271	4,513499
275,105	1,233312	0,023722	1,051983	0,167223	212,2919	4,759289	4,26521	4,512254
275,211	1,232007	0,023729	1,052211	0,167272	212,2878	4,759255	4,265185	4,512225
275,205	1,231066	0,023729	1,052198	0,167269	212,2881	4,759257	4,265187	4,512226

283,114	1,24205	0,024317	1,068858	0,170933	212,0198	4,757467	4,264014	4,510745
283,276	1,241926	0,024329	1,069192	0,171007	212,0152	4,757448	4,264006	4,510732
283,09	1,240256	0,024316	1,068809	0,170922	212,0205	4,75747	4,264015	4,510747
307,98	1,29967	0,026138	1,116496	0,182059	211,4073	4,75638	4,26433	4,51036
308,2	1,296259	0,026154	1,116885	0,182155	211,4005	4,756338	4,264303	4,510325
307,629	1,298313	0,026113	1,115874	0,181906	211,4182	4,756449	4,264373	4,510416
373,138	1,479611	0,030718	1,207184	0,208381	209,7256	4,748741	4,26055	4,504652
373,16	1,47833	0,03072	1,207206	0,208389	209,7251	4,74874	4,26055	4,504651
373,143	1,477543	0,030718	1,207189	0,208383	209,7255	4,748741	4,26055	4,504652

Glass/Foam/N2 experiment 3								
ϵ_{tot}	0,368833		R	8314		e	0,174667	
ϵ_{spec}	0,394674		Cp_gas	1039		η_{high}	0,647214	
ϵ_{foam}	0,934526		dp	0,00038		η_{low}	0,57735	
						η_{middle}	0,612282	
T	k_e	k_f	k_s_glass	k_ZBS	k_s_alu	k_phase-sym_mod		
						High bound	Low Bound	Middle
[K]	[W/m×K]	[W/m×K]	[W/m×K]	[W/m×K]	[W/m×K]	[W/m×K]	[W/m×K]	[W/m×K]
423,157	1,586984	0,034065	1,24327	0,213322	208,8954	4,804017	4,310468	4,557249
423,121	1,587249	0,034062	1,243254	0,213311	208,8959	4,804015	4,310465	4,557246
423,176	1,587353	0,034066	1,243278	0,213328	208,8952	4,804018	4,31047	4,55725
333,276	1,374061	0,027948	1,157572	0,181735	210,6738	4,808537	4,310854	4,559701
333,537	1,372245	0,027966	1,157957	0,181837	210,6667	4,808495	4,310828	4,559667
332,913	1,375093	0,027922	1,157035	0,181593	210,6836	4,808597	4,310891	4,559749
288,494	1,242644	0,024715	1,079775	0,16332	211,8877	4,815001	4,31449	4,56475
288,746	1,240326	0,024733	1,080279	0,163428	211,8827	4,81501	4,31451	4,564765
287,906	1,243214	0,024672	1,078599	0,163066	211,8998	4,81499	4,31445	4,564724
278,569	1,232047	0,02398	1,059373	0,159	212,1646	4,81634	4,315184	4,565766
278,087	1,234315	0,023944	1,058353	0,158788	212,1815	4,816478	4,315282	4,565885
278,092	1,234265	0,023944	1,058364	0,15879	212,1813	4,816477	4,315281	4,565884
273,192	1,228913	0,023579	1,047841	0,156623	212,3676	4,818184	4,316553	4,567373
273,203	1,228172	0,023579	1,047865	0,156628	212,3672	4,81818	4,31655	4,567369
273,102	1,228605	0,023572	1,047645	0,156583	212,3713	4,81822	4,31658	4,567405
268,119	1,21562	0,023198	1,036653	0,154357	212,5837	4,820435	4,318298	4,569371
268,1	1,217149	0,023197	1,03661	0,154349	212,5846	4,820444	4,318305	4,569379
268,187	1,215822	0,023203	1,036805	0,154388	212,5807	4,820402	4,318273	4,569342
258,085	1,184314	0,02244	1,01364	0,149809	213,0563	4,8258	4,322557	4,574183
258,152	1,184025	0,022445	1,013798	0,149839	213,053	4,825762	4,322526	4,574148
258,123	1,183569	0,022443	1,013729	0,149826	213,0544	4,825778	4,322539	4,574163
243,141	1,127817	0,021297	0,977194	0,142868	213,7928	4,834319	4,329351	4,581839
243,144	1,128659	0,021297	0,977202	0,14287	213,7927	4,834318	4,32935	4,581838
243,143	1,128118	0,021297	0,977199	0,142869	213,7927	4,834318	4,32935	4,581838
253,155	1,162237	0,022065	1,001904	0,147541	213,2996	4,828642	4,324829	4,57674
253,175	1,162855	0,022066	1,001952	0,14755	213,2986	4,828631	4,32482	4,576729
253,138	1,163668	0,022064	1,001863	0,147533	213,3004	4,828652	4,324837	4,576749

Glass/Foam/N2 experiment 4								
ε_{tot}	0,389464	R	8314	e	0,174667			
ε_{fspec}	0,416333	Cp_gas	1039	η_{high}	0,647214			
ε_{foam}	0,935462	dp	0,00038	η_{low}	0,57735			
				η_{middle}	0,612282			
T	k_e	k_f	k_s_glass	k_ZBS	k_s_alu	k_phase-sym_mod		
						High bound	Low Bound	Middle
[K]	[W/m×K]	[W/m×K]	[W/m×K]	[W/m×K]	[W/m×K]	[W/m×K]	[W/m×K]	[W/m×K]
423,15	1,636716	0,034064	1,243267	0,218492	208,8955	4,675974	4,196761	4,436374
423,154	1,637426	0,034065	1,243269	0,218493	208,8955	4,675975	4,196762	4,436374
423,152	1,635095	0,034064	1,243268	0,218492	208,8955	4,675975	4,196761	4,436374
333,428	1,438211	0,027959	1,157796	0,186385	210,6697	4,678838	4,195621	4,437234
333,06	1,435379	0,027933	1,157253	0,186237	210,6796	4,678889	4,195649	4,437274
333,723	1,431661	0,027979	1,158231	0,186502	210,6617	4,678797	4,195598	4,437203
288,239	1,307131	0,024696	1,079266	0,167396	211,8929	4,68418	4,198196	4,441193
288,816	1,302173	0,024739	1,080418	0,167651	211,8813	4,684211	4,198253	4,441237
288,023	1,305473	0,02468	1,078833	0,167301	211,8973	4,684172	4,198177	4,441179
278,223	1,299067	0,023954	1,058641	0,162935	212,1767	4,685354	4,198728	4,442046
278,133	1,298212	0,023947	1,058451	0,162894	212,1799	4,685378	4,198744	4,442065
278,31	1,299013	0,023961	1,058825	0,162974	212,1737	4,685332	4,198713	4,442027
273,138	1,294658	0,023575	1,047724	0,160635	212,3698	4,686952	4,199887	4,443424
273,164	1,292856	0,023576	1,04778	0,160646	212,3687	4,686942	4,19988	4,443416
273,172	1,293754	0,023577	1,047798	0,16065	212,3684	4,686939	4,199878	4,443413
268,097	1,283389	0,023196	1,036603	0,158331	212,5847	4,689008	4,201455	4,445236
268,124	1,281708	0,023199	1,036664	0,158343	212,5835	4,688996	4,201446	4,445225
268,149	1,281034	0,0232	1,03672	0,158355	212,5824	4,688985	4,201437	4,445215
258,177	1,252357	0,022447	1,013856	0,153729	213,0518	4,693918	4,205303	4,449615
258,137	1,250687	0,022444	1,013762	0,153711	213,0537	4,693939	4,20532	4,449634
258,114	1,250016	0,022442	1,013708	0,1537	213,0549	4,693951	4,20533	4,449644
243,143	1,195376	0,021297	0,977199	0,146583	213,7927	4,701867	4,211568	4,456721
243,15	1,194642	0,021298	0,977217	0,146586	213,7924	4,701863	4,211565	4,456718
243,15	1,194623	0,021298	0,977217	0,146586	213,7924	4,701863	4,211565	4,456718



Appendix H - Risk Assessment Report

Risk Assessment Report

Termisk konduktivitetsrigg: måling av termisk konduktivitet i porøse medier.

[Thermal conductivity rig: measurements of thermal conductivity in porous media]

Prosjekttittel	Conductivity rig: thermal conductivity measurements in porous media
Prosjektleder	Erling Næss/Christian Schlemminger
Enhet	NTNU
HMS-koordinator	Erik Langørgen
Linjeleder	Olav Bolland
Plassering	VATlab
Romnummer	Finlab
Riggansvarlig	Jan Georg Henriksen/Christian Schlemminger
Risikovurdering utført av	Erik Langørgen/Christian Schlemminger/Jan Georg Henriksen

TABLE OF CONTENTS

1	INTRODUCTION	1
2	ORGANISATION	1
3	RISK MANAGEMENT IN THE PROJECT	1
4	DRAWINGS, PHOTOS, DESCRIPTIONS OF TEST SETUP	1
5	EVACUATION FROM THE EXPERIMENT AREA	8
6	WARNING	8
6.1	Before experiments.....	8
6.2	Nonconformance.....	8
7	ASSESSMENT OF TECHNICAL SAFETY	9
7.1	HAZOP.....	9
7.2	Flammable, reactive and pressurized substances and gas	9
7.3	Pressurized equipment.....	9
7.4	Effects on the environment (emissions, noise, temperature, vibration, smell)	10
7.5	Radiation	10
7.6	Usage and handling of chemicals.....	10
7.7	EI safety (need to deviate from the current regulations and standards.)	10
8	ASSESSMENT OF OPERATIONAL SAFETY	10
8.1	Procedure HAZOP.....	10
8.2	Operation and emergency shutdown procedure.....	10
8.3	Training of operators.....	11
8.4	Technical modifications.....	11
8.5	Personal protective equipment.....	11
8.6	General Safety	11
8.7	Safety equipment	11
8.8	Special actions.....	11
9	QUANTIFYING OF RISK - RISK MATRIX.....	11
10	CONCLUSJON	12
11	REGULATIONS AND GUIDELINES	13
12	DOCUMENTATION.....	14
13	GUIDANCE TO RISK ASSESSMENT TEMPLATE	14

1 INTRODUCTION

The experiment is about measuring the thermal conductivity in a packed bed of porous and non porous media, in order to calculate the respective conductivity's of the sample media.

The rig is located in the FinLab in floor 1B, inside the VATlab.

2 ORGANISATION

Rolle	NTNU	Sintef
Lab Ansvarlig:	Morten Grønli	Harald Mæhlum
Linjeleder:	Olav Bolland	Mona Mølsvik
HMS ansvarlig:	Olav Bolland	Mona Mølsvik
HMS koordinator	Erik Langørgen	Harald Mæhlum
HMS koordinator	Bård Brandåstrø	
Romansvarlig:	Jan Georg Henriksen	
Prosjektleder:	Erling Næss/Christian Schlemminger	
Ansvarlig riggoperatører:	Jan Georg Henriksen	

3 RISK MANAGEMENT IN THE PROJECT

Hovedaktiviteter risikostyring	Nødvendige tiltak, dokumentasjon	DATE
Prosjekt initiering	Prosjekt initiering mal	15.01.2013
Veiledningsmøte Guidance Meeting	Skjema for Veiledningsmøte med pre-risikovurdering	n.a
Innledende risikovurdering Initial Assessment	Fareidentifikasjon – HAZID Skjema grovanalyse	20.02.2013
Vurdering av teknisk sikkerhet Evaluation of technical security	Prosess-HAZOP Tekniske dokumentasjoner	15.05.2013
Vurdering av operasjonell sikkerhet Evaluation of operational safety	Prosedyre-HAZOP Opplæringsplan for operatører	15.05.2013
Sluttvurdering, kvalitetssikring Final assessment, quality assurance	Uavhengig kontroll Utstedelse av apparaturkort Utstedelse av forsøk pågår kort	15.05.2013

4 DRAWINGS, PHOTOS, DESCRIPTIONS OF TEST SETUP

Test setup description/location of equipment

The thermal conductivity measurement rig is located in the FinLab in the VATLab. The HotDisk TPS 2500S is supplied by the Swedish company Hot Disc AB. It utilizes a small electrical power (<2W) to heat up a special shaped resistance, which is used as a temperature sensor simultaneously. The transient temperature rise of the sensor is recorded and analyzed by the TPS2500S. As result the material thermal diffusivity, specific heat capacity and thermal conductivity are determined. Different material

types e.g. solid materials or powders can be measured. In the particular case different sorts of powders are used for the measurements.

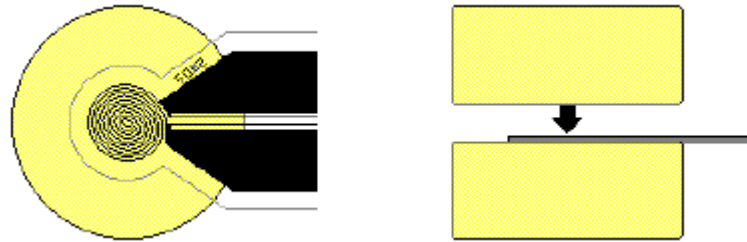


Figure 1 Sensor position between sample pieces

. Porous media is poured in to a sample holder, and a HotDisk sensor is placed in between the samples, as shown in Figure. 1.

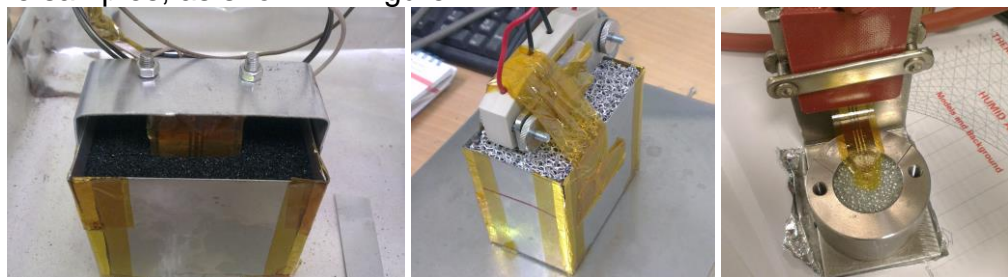


Figure 2 Sample holders

Different sample holders are used for different types of porous media. Graphic examples are given in Fig. 2. If room-temperature measurements with air are conducted, measurements can start as soon as the wires are connected to the sensor.



Figure 3 Vacuum cell

Most measurements however, are conducted at a range of $-30\text{ }^{\circ}\text{C} < T < 150\text{ }^{\circ}\text{C}$ with pressurized gas (He/N₂, at 0.1 ...0.4 bar relative). In order to do this, the sample holder, or sometimes the porous media itself, is lowered into the vacuum / pressure cell. This pressure cell is provided by HotDisk AB as well and can withstand pressures of 1 bar relative and 200°C, see attachment B. Wires are then connected to the vacuum / pressure cell itself (from inside and outside), as shown in Figure 3. The lid is then sealed with a silicone gasket and if necessary with silicon vacuum grease and lowered into a thermal bath. The oil bath can stabilize at any given temperature between -35 and +200 degrees Celsius. After connecting the vacuum suction line with pressure sensors and the gas supply (Figure 4 or 5, next page) a

final leakage test is necessary to guaranty safe and reliable measurements. Once thermal bath has stabilized, measurements can start.

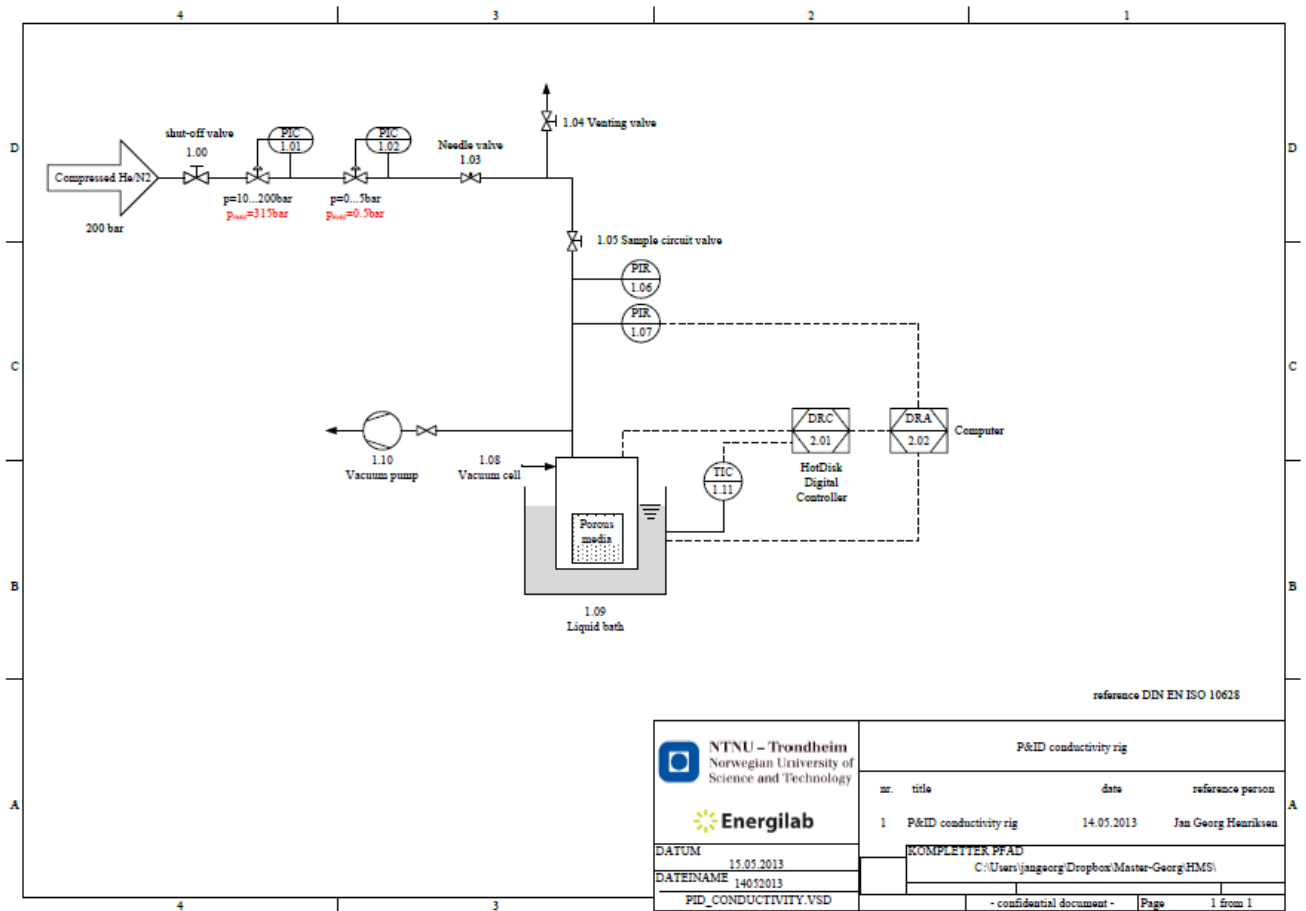


Figure 4 flow schematic conductivity rig (larger version attached at the very end of the report)

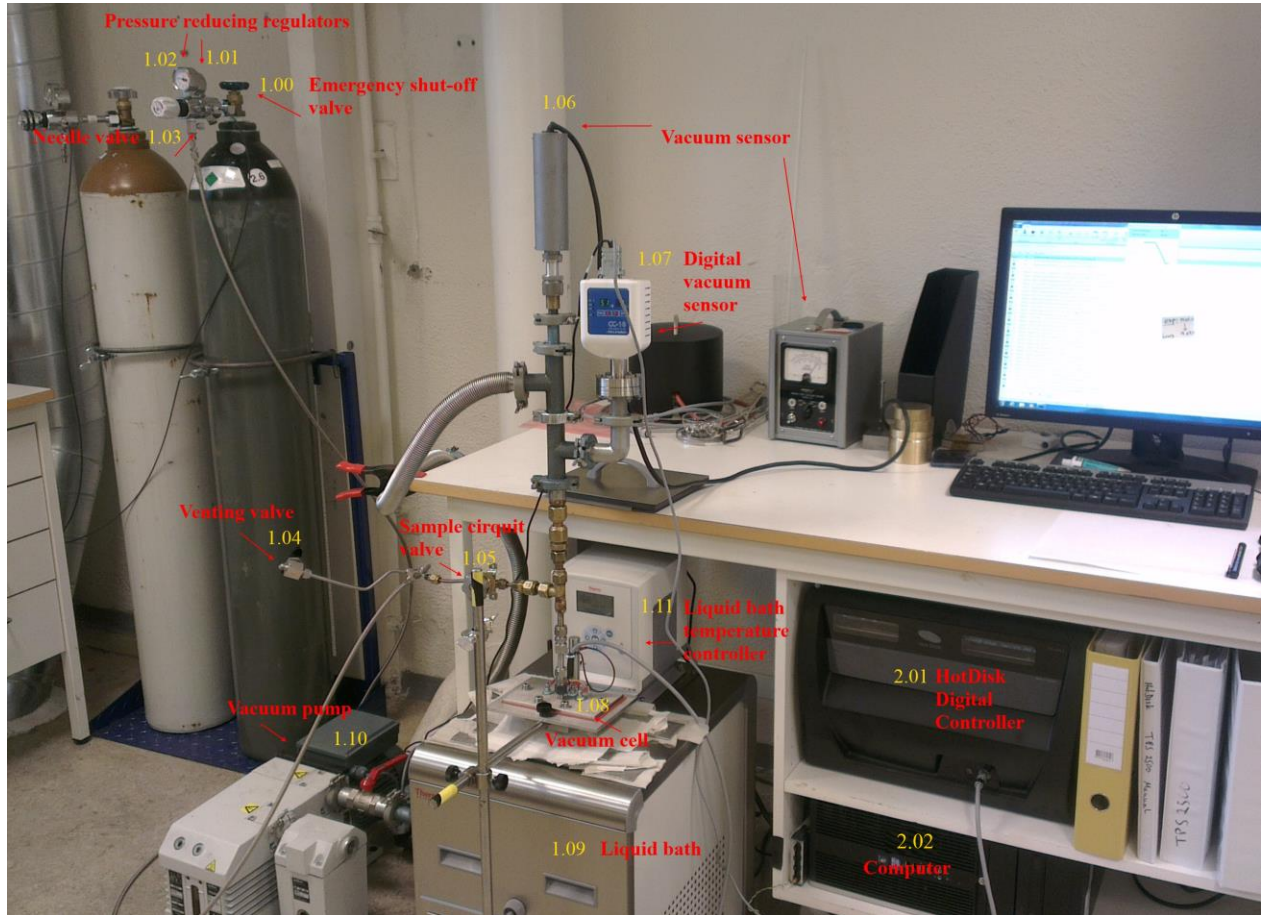


Figure 5- Thermal conductivity setup with gas supply, vacuum sensors and computer analyser. Location: Finlab.

As shown in Figure 4 and Figure 5, compressed gas (N₂ or He at approximately 200 bar) from a gas bottle is supplied after opening the shut-off valve (1.00). A maximal allowed pressure is set with the pressure regulators (max 1.4 bar (absolute)) (1.01) and (1.02). Experiments are performed usually at 1.2...1.4 bar (absolute). Next follows a needle valve (1.03) for extra security, and a venting valve (1.04). The venting valve is there in order to ensure that pressure can be released if it is too high, or for venting before gas change. By turning the pressure regulator (1.02) up, or turning it down and venting through (1.04) one can regulate the pressure. By opening up the sample circuit valve (1.05) the system is supplied with gas.

The porous medium is located inside the pressure cell (1.08), which again is lowered in the liquid bath (1.09). Before one starts any measurements the porous medium must be evacuated. This is because the porous powder contains humid air which can interfere with the measurement. Evacuation is monitored through the vacuum pressure indicators (1.06) and (1.07). In order to evacuate, the sample circuit valve (1.05) is closed, the vacuum pump (1.10) is started and its valve is opened. When vacuum reaches 10^{-2} torr (0.13 bar), the valve on the vacuum pump (1.10) is closed and the sample circuit valve (1.05) is opened. Gas is then purged into the system.

To ensure that all humidity is gone, the porous medium must also be activated. In order to heat it, the liquid bath controller (1.11) is then set to 150 degrees Celsius. The evacuation process is then repeated five times over.

The HotDisk Digital Controller TPS2500S (2.01) governs the measurements together with a timetable set up in the software on the computer (2.02).

The filling and emptying procedure is explained short further down. An additional “Procedure for running experiments” summarizes all important steps for carrying out safe measurements and is added in Appendix G.

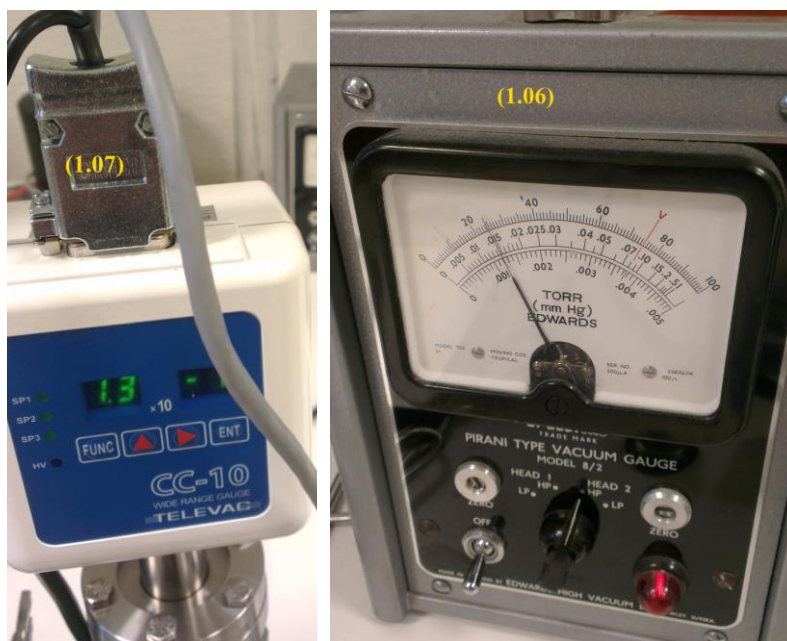


Figure 6 Vacuum pressure indicators

The components installed at the conductivity rig are listed in Table 1 below. The list can be used to identify the main instrument parameters.

Table 1 Sensor actor list conductivity rig

Sensoric und Actoric Permeability Rig											
Lfd. P&ID		measurement position		measure-/actuating variable			device specification			signal	comments
Nr.	Nr.	medium	position	sensor / device	S/A	EMSR	device typ	measure-/control value	U / I / P	range	
							(z.B. producer, name (typ).)		[V, A, W]		
1	1.00	compressed N2/He	gas bottle	shut-off valve	A		Yara Praxair	200bar	bar		
2	1.01	compressed N2/He	gas bottle	Pressure reducing regulator	A/S	PIC	Yara Praxair	200bar	bar	p_max=315 bar	
3	1.02	compressed N2/He	gas bottle	Pressure reducing regulator	A/S	PIC	Yara Praxair	operating @ 0.5 bar	< bar	p_max=5 bar	
4	1.03	compressed N2/He	gas bottle	Needle valve	A		Yara Praxair	operating @ 0.2,0.4 bar	bar	p_max= 60 bar	
5	1.04	compressed N2/He	between gas bottle/sample circuit	Venting valve	A		Swagelok SS 43GS 6mm	operating @ 0.2,0.4 bar	bar	0.5bar	
6	1.05	compressed or evacuated N2/He	between venting valve/sample holder	Sample circuit valve	A		Danfoss	operating @ 0.2,0.4 bar	bar	0.5bar	
7	1.06	compressed or evacuated N2/He	above sample holder	Vacuum pressure indicator	S	PIR	SPEEDIVAC	0.005...1 torr	torr	0.005...1 torr	1 torr =0.013 bar
8	1.07	compressed or evacuated N2/He	above sample holder	Vacuum pressure indicator	S	PIR	TELEVAC CC-10	10 ⁹ ...10 ³ torr 10 ³ ...10 ¹ torr 10 ¹ ...10 ⁰ torr 10 ⁰ ...10 ² torr	torr	10 ⁹ ...10 ³ torr	can log to pc
9	1.08	compressed or evacuated N2/He	in liquid bath	Vacuum pressure cell (sample inside)	-		HotDisk Vacuum cell 11502	operating @ 0.2,0.4 bar	bar	Tmax =200°C p_max=2.5 bar	
10	1.09	Oil	floor	Liquid bath	-		AC200				
11	1.10	compressed or evacuated N2/He	floor next to liquid bath	Vacuum pump	A		Oerlikon AF-16-25	p=10 ³ ...5·10 ⁻³	torr	p=10 ³ ...5·10 ⁻³ torr	<=10 ⁻⁴ mbar (given from producer)
12	1.11		on top of liquid bath	liquid bath temperature controller	A/S	TIC	Thermo Scientific AC 200	T=243...423	K	T=238...473K	
13	2.01		in desk next to liquid bath	Hotdisk digital measurement controller	A/S	DRC	HotDisk Th. Const. Analyser TPS 2500S				Bridge: Keithley 2400, Off balance: Keithley 2700 (6.5 digits resolution)
14	2.02		in desk next to liquid bath	Computer	A/S	DRA	HotDisk Th. Const. Ana. Version 7.0.16	Thermal conductivity k	W/mK	0.005-500 W/mK	Repeatability +0.5%, Thermal conductivity uncertainty=+5%

Filling of new powder

1. If rig is running, set liquid bath to 22 degrees and close shut-off and needle valve. Open the sample circuit valve and vent the system to ambient pressure.
2. When liquid bath has been at 22 degrees for 10 minutes, shut of the bath.
3. Remove wires from pressure cell.
4. Then remove the pressure cell from the bath.
5. Remove the pressure cell lid and disconnect the inner wires.
6. Control possible leakages and damages at the gasket
7. Wear glasses, hand gloves and dusk mask for protection.
8. Remove silicone gasket and take out the sample/sample holder.
9. Weigh the sample holder and measure sample height.
10. Empty sample holder and remove sensor.
11. Clean vacuum pressure cell, sensor, rubber sealing, and sample holder.
12. Weigh the sample holder without any powder in it. One can now tell how much mass the powder has lost during evacuation.
13. Pour in a new powder sample using a funnel.
14. Weigh new powder and measure filling height.
15. If the powder consists of small light grains, tape aluminum foil over the sample in order to prevent powder loss during evacuation.
16. Put sample holder back into the pressure cell.
17. Lubricate the sample holder and its lid with vacuum grease if necessary.
18. Connect wires and close the lid.
19. Mount the pressure cell into the liquid bath.
20. Cover the gap between pressure cell and bath to prevent oil vaporization.
21. Then start new experiment (described below)

The dismantling, emptying and filling of the cylinder, which contains the powder sample is shown more in detail in figure 7.

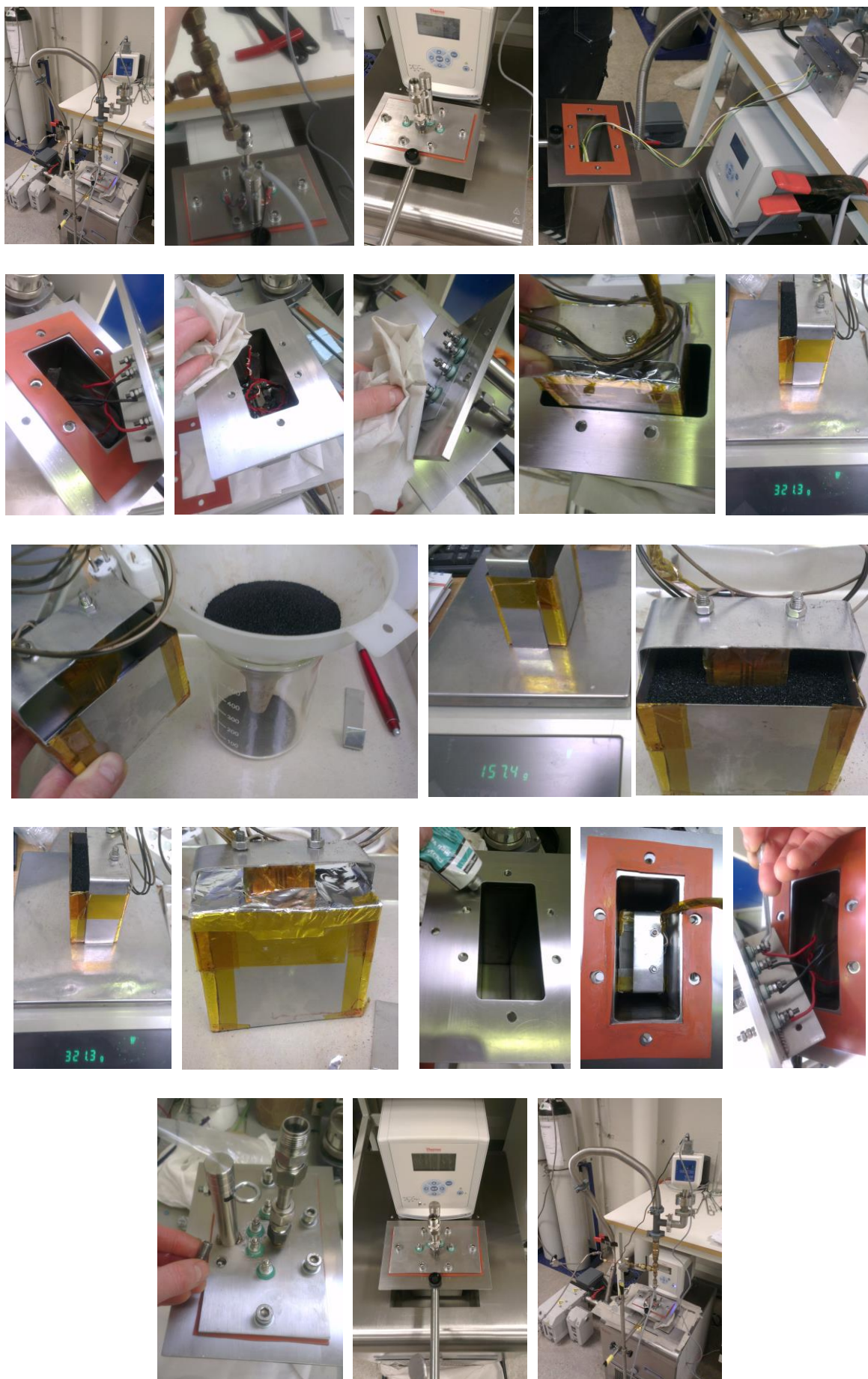


Figure 7 Dismantling, emptying filling and mantling.

Experimental procedure

1. Restart liquid bath and computer.
2. Use glasses and gloves.
3. All valves are closed.
4. Set liquid bath (1.09) to 150 degrees and start vacuum pump (1.10).
5. Open the shut-off valve.
6. Adjust pressure with the pressure regulator (1.02). Pressure must be <0.5bar.
7. Open needle valve (1.03).
8. Open venting valve (1.04) and regulate (1.02) to desired pressure (0.4 or 0.2 bar). Then close the venting valve (1.04).
9. Open sample circuit valve (1.05). Gas now flows into the pressure cell (1.08).
10. Wait 10 seconds and close sample circuit valve (1.05)
11. Open valve on the vacuum pump (1.10).
12. When vacuum is below 10^{-2} torr (0.13 bar), close vacuum pump valve (1.10).
13. Repeat point 9-12 six times.
14. Open sample circuit valve (1.05) and turn off vacuum pump (1.10).
15. Close needle valve (1.03) and wait one hour before starting the experiment.

5 EVACUATION FROM THE EXPERIMENT AREA

Evacuate at signal from the alarm system or local gas alarms with its own local alert with sound and light outside the room in question, see 6.2

Evacuation from the rigging area takes place through the marked emergency exits to the assembly point, (corner of Old Chemistry Kjelhuset or parking 1a-b.)

Action on rig before evacuation:

1. Shut off the gas (N₂ or He) supply (1.00) marked with sign "Emergency shut-off valve"
2. Power off the electrical supply.

6 WARNING

6.1 Before experiments

E-mail with information about the planned experiment to: iept-experiments@ivt.ntnu.no

The e-mail should contain the following items:

- Name of responsible person:
- Experimental setup/rig:
- Start Experiments: (date and time)
- Stop Experiments: (date and time)

You should get the approval back from the laboratory management before start up. All running experiments are notified in the activity calendar for the lab to be sure they are coordinated with other activity.

6.2 Nonconformance

FIRE

For fires which you are not able to put out with locally available fire extinguishers, activate the nearest fire alarm and evacuate area. Be then available for fire brigade

and building caretaker to detect fire place.

If possible, notify:

NTNU	SINTEF
Labsjef Morten Grønli, tlf: 918 97 515	Labsjef Harald Mæhlum tlf 930 149 86
HMS: Erik Langørgen, tlf: 91897160 HMS: Bård Brandåstrø, tlf918 97 257	Forskningssjef Mona Mølsvik 93008868
Instituttleder: Olav Bolland: 91897209	
NTNU Sintef Beredskapstelefon	800 80 388

GASALARM

At a gas alarm, close gas bottles immediately and ventilated the area. If the level of gas concentration does not decrease within a reasonable time, activate the fire alarm and evacuate the lab. Designated personnel or fire department checks the leak to determine whether it is possible to seal the leak and ventilate the area in a responsible manner.

Alert Order in the above paragraph.

PERSONAL INJURY

- First aid kit in the fire / first aid stations
- Shout for help
- Start life-saving first aid•

CALL 113 if there is any doubt whether there is a serious injury

Other Nonconformance (AVVIK)

NTNU:

Reporting nonconformance, Innsida, avviksmelding:

https://innsida.ntnu.no/lenkesamling_vis.php?katid=1398

SINTEF:

Synergi

7 ASSESSMENT OF TECHNICAL SAFETY

7.1 HAZOP

The experiment set up is divided into the following nodes:

Node 1	Sections filled with pressurized N2/He.
--------	---

Attachments: skjema: Hazop_mal

Conclusion: Safety taken care of

7.2 Flammable, reactive and pressurized substances and gas

Contains the experiments Flammable, reactive and pressurized substances and gas

NO	YES. Explosion document have to be made and or documented pressure test, (See 7.3)
-----------	--

Attachments: n.a.

Conclusion: n.a.

7.3 Pressurized equipment

Contain the set up pressurized equipment?

YES	but working at a total pressure of max 1.5 bar
------------	--

Attachments: YES. Attachment B Instructions TPS Vacuum /Backfilled insert Cell for Circulation Bath 11502 (2013/02/25)

Pressure in rig never exceeds 1,5 bar_{absolute} respective 0,5 bar_{relative}, and will therefore cause no risk, since the working medium is only N₂ or He @ -30...150 °C.

Conclusion: all devices downstream from valve (1.02) are working around ambient pressure

7.4 Effects on the environment (emissions, noise, temperature, vibration, smell)

NEI	YES
-----	-----

Conclusion: n.a.

7.5 Radiation

NEI	JA, Radiation source need to have an own risk assessment
-----	--

Attachments: n.a.

Conclusion: n.a.

7.6 Usage and handling of chemicals.

NEI	JA, Do a risk assessment of the use
-----	-------------------------------------

Attachments: MSDS

Conclusion: The operator needs to use during **filling and emptying of material:**

Protection glasses

Laboratory hand gloves

Dust mask

The operator needs to use during **experiments:**

Glasses and laboratory hand gloves.

7.7 El safety (need to deviate from the current regulations and standards.)

NEI	JA, El safety have to be evaluated
-----	------------------------------------

Attachments: none

Conclusion: only regular devices with 220V are used

8 ASSESSMENT OF OPERATIONAL SAFETY

For ensuring that established procedures cover all identified risk factors that must be taken care of through procedures and ensure that the operators and technical performance have sufficient expertise.

8.1 Prosedure HAZOP

The method is a procedure to identify causes and sources of danger to operational problems.

Attachments: HAZOP_MAL_Proseedyre

Conclusion: procedure is uncomplicated and easy to understand → Safety taken care of

8.2 Operation and emergency shutdown procedure

The operating procedure is a checklist that must be filled out for each experiment.

Emergency procedure should attempt to set the experiment set up in a harmless state by unforeseen events.

Attachments: Procedure for running experiments

Emergency shutdown procedure:

1. Shut off the gas (He or N₂) supply by closing valve (1.00) marked with sign "Emergency shut-off valve".
2. Power off the liquid bath.

8.3 Training of operators

A Document showing training plan for operators

What are the requirements for the training of operators?

- *What it takes to be an independent operator*
- *Job Description for operators*

Attachments: Training program for operators

8.4 Technical modifications

- Technical modifications made by the Operator
 - Yes
- What technical modifications give a need for a new risk assessment; (by changing the risk picture)?
 - If more pressure is needed (>1,5 bar), or other types of samples with higher safety requirements than already described is used.

Conclusion: All modifications can be made by the operator

8.5 Personal protective equipment

- It is mandatory use of eye protection when handling fine powder.
- Use gloves when handling fine powder.
- Use of respiratory protection apparatus when handling fine powder.

Conclusion: always glasses, dust mask and gloves nearby during powder handling.

8.6 General Safety

- Monitoring: operator must start the experiment. After start: experiment can execute itself without operator presence.

Conclusion: The operator is allowed to leave during the experiment.

8.7 Safety equipment

- Warning signs, see the Regulations on Safety signs and signaling in the workplace

8.8 Special actions.

none

9 QUANTIFYING OF RISK - RISK MATRIX

See Chapter 13 "Guide to the report template".

The risk matrix will provide visualization and an overview of activity risks so that management and users get the most complete picture of risk factors.

IDnr	Aktivitet-hendelse	Frekv-Sans	Kons	RV
Xx	<i>Pipes are torn; N₂ or He@<0,5 bar stream out</i>	1	B2	B2
	<i>Liquid bath not covered; water is spilled into it</i>	1	B1	B1

Conclusion : *Participants will make a comprehensive assessment to determine whether the remaining risks of the activity / process is acceptable. Barriers and driving outside working hours e.g.*

10 CONCLUSJON

The rig is built in good laboratory practice (GLP).

Experiment unit card get a period of **24 months**

Experiment in progress card get a period of **24 months**

11 REGULATIONS AND GUIDELINES

Se <http://www.arbeidstilsynet.no/regelverk/index.html>

- Lov om tilsyn med elektriske anlegg og elektrisk utstyr (1929)
- Arbeidsmiljøloven
- Forskrift om systematisk helse-, miljø- og sikkerhetsarbeid (HMS Internkontrollforskrift)
- Forskrift om sikkerhet ved arbeid og drift av elektriske anlegg (FSE 2006)
- Forskrift om elektriske forsyningsanlegg (FEF 2006)
- Forskrift om utstyr og sikkerhetssystem til bruk i eksplosjonsfarlig område NEK 420
- Forskrift om håndtering av brannfarlig, reaksjonsfarlig og trykksatt stoff samt utstyr og anlegg som benyttes ved håndteringen
- Forskrift om Håndtering av eksplosjonsfarlig stoff
- Forskrift om bruk av arbeidsutstyr.
- Forskrift om Arbeidsplasser og arbeidslokaler
- Forskrift om Bruk av personlig verneutstyr på arbeidsplassen
- Forskrift om Helse og sikkerhet i eksplosjonsfarlige atmosfærer
- Forskrift om Høytrykksspyling
- Forskrift om Maskiner
- Forskrift om Sikkerhetsskilting og signalgivning på arbeidsplassen
- Forskrift om Stillaser, stiger og arbeid på tak m.m.
- Forskrift om Sveising, termisk skjæring, termisk sprøyting, kullbuemeisling, lodding og sliping (varmt arbeid)
- Forskrift om Tekniske innretninger
- Forskrift om Tungt og ensformig arbeid
- Forskrift om Vern mot eksponering for kjemikalier på arbeidsplassen (Kjemikalieforskriften)
- Forskrift om Vern mot kunstig optisk stråling på arbeidsplassen
- Forskrift om Vern mot mekaniske vibrasjoner
- Forskrift om Vern mot støy på arbeidsplassen

Veiledninger fra arbeidstilsynet

se: <http://www.arbeidstilsynet.no/regelverk/veiledninger.html>

12 DOCUMENTATION

- Tegninger, foto, beskrivelser av forsøksoppsetningen
- Hazop_mal
- Sertifikat for trykkpåkjent utstyr
- Håndtering avfall i NTNU
- Sikker bruk av LASERE, retningslinje
- HAZOP_MAL_Prosedyre
- Forsøksprosedyre
- Opplæringsplan for operatører
- Skjema for sikker jobb analyse, (SJA)
- Apparatorkortet
- Forsøk pågår kort

13 GUIDANCE TO RISK ASSESSMENT TEMPLATE

Kap 7 Assessment of technical safety.

Ensure that the design of the experiment set up is optimized in terms of technical safety.

Identifying risk factors related to the selected design, and possibly to initiate re-design to ensure that risk is eliminated as much as possible through technical security.

This should describe what the experimental setup actually are able to manage and acceptance for emission.

7.1 HAZOP

The experimental set up is divided into nodes (eg motor unit, pump unit, cooling unit.). By using guidewords to identify causes, consequences and safeguards, recommendations and conclusions are made according to if necessary safety is obtained. When actions are performed the HAZOP is completed.

(e.g. "No flow", cause: the pipe is deformed, consequence: pump runs hot, precaution: measurement of flow with a link to the emergency or if the consequence is not critical used manual monitoring and are written into the operational procedure.)

7.2 Flammable, reactive and pressurized substances and gas.

According to the Regulations for handling of flammable, reactive and pressurized substances and equipment and facilities used for this:

<p>Flammable material: Solid, liquid or gaseous substance, preparation, and substance with occurrence or combination of these conditions, by its flash point, contact with other substances, pressure, temperature or other chemical properties represent a danger of fire.</p>
--

<p>Reactive substances: Solid, liquid, or gaseous substances, preparations and substances that occur in combinations of these conditions, which on contact with water, by its pressure, temperature or chemical conditions, represents a potentially dangerous reaction, explosion or release of hazardous gas, steam, dust or fog.</p>
--

<p>Pressurized : Other solid, liquid or gaseous substance or mixes having fire or hazardous material response, when under pressure, and thus may represent a risk of uncontrolled emissions</p>
--

Further criteria for the classification of flammable, reactive and pressurized substances are set out in Annex 1 of the Guide to the Regulations "Flammable, reactive and pressurized substances"

<http://www.dsb.no/Global/Publikasjoner/2009/Veiledning/Generell%20veiledning.pdf>

http://www.dsb.no/Global/Publikasjoner/2010/Tema/Temaveiledning_bruk_av_farlig_stoff_Del_1.pdf

Experiment setup area should be reviewed with respect to the assessment of Ex zone

- Zone 0: Always explosive atmosphere, such as inside the tank with gas, flammable liquid.
- Zone 1: Primary zone, sometimes explosive atmosphere such as a complete drain point
- Zone 2: secondary discharge could cause an explosive atmosphere by accident, such as flanges, valves and connection points

7.4 Effects on the environment

With pollution means: bringing solids, liquid or gas to air, water or ground, noise and vibrations, influence of temperature that may cause damage or inconvenience effect to the environment.

Regulations: <http://www.lovdatab.no/all/hl-19810313-006.html#6>

NTNU guidance to handling of waste: <http://www.ntnu.no/hms/retningslinjer/HMSR18B.pdf>

7.5 Radiation

Definition of radiation

Ionizing radiation: Electromagnetic radiation (in radiation issues with wavelength <100 nm) or rapid atomic particles (e.g. alpha and beta particles) with the ability to stream ionized atoms or molecules.

Non ionizing radiation: Electromagnetic radiation (wavelength >100 nm), og ultrasound₁ with small or no capability to ionize.

Radiation sources: All ionizing and powerful non-ionizing radiation sources.

Ionizing radiation sources: Sources giving ionizing radiation e.g. all types of radiation sources, x-ray, and electron microscopes.

Powerful non ionizing radiation sources: Sources giving powerful non ionizing radiation which can harm health and/or environment, e.g. class 3B and 4. MR₂ systems, UVC₃ sources, powerful IR sources₄.

₁Ultrasound is an acoustic radiation ("sound") over the audible frequency range (> 20 kHz). In radiation protection regulations are referred to ultrasound with electromagnetic non-ionizing radiation.

₂MR (e.g. NMR) - nuclear magnetic resonance method that is used to "depict" inner structures of different materials.

₃UVC is electromagnetic radiation in the wavelength range 100-280 nm.

₄IR is electromagnetic radiation in the wavelength range 700 nm - 1 mm.

For each laser there should be an information binder (HMSRV3404B) which shall include:

- General information
- Name of the instrument manager, deputy, and local radiation protection coordinator
- Key data on the apparatus
- Instrument-specific documentation
- References to (or copies of) data sheets, radiation protection regulations, etc.
- Assessments of risk factors
- Instructions for users

- Instructions for practical use, startup, operation, shutdown, safety precautions, logging, locking, or use of radiation sensor, etc.
- Emergency procedures

See NTNU for laser: <http://www.ntnu.no/hms/retningslinjer/HMSR34B.pdf>

7.6 Usage and handling of chemicals.

In the meaning chemicals, a element that can pose a danger to employee safety and health

See: <http://www.lovdatab.no/cgi-wift/ldles?doc=/sf/sf/sf-20010430-0443.html>

Safety datasheet is to be kept in the HSE binder for the experiment set up and registered in the database for chemicals.

Kap 8 Assessment of operational procedures.

Ensures that established procedures meet all identified risk factors that must be taken care of through operational barriers and that the operators and technical performance have sufficient expertise.

8.1 Procedure Hazop

Procedural HAZOP is a systematic review of the current procedure, using the fixed HAZOP methodology and defined guidewords. The procedure is broken into individual operations (nodes) and analyzed using guidewords to identify possible nonconformity, confusion or sources of inadequate performance and failure.

8.2 Procedure for running experiments and emergency shutdown.

Have to be prepared for all experiment setups.

The operating procedure has to describe stepwise preparation, startup, during and ending conditions of an experiment. The procedure should describe the assumptions and conditions for starting, operating parameters with the deviation allowed before aborting the experiment and the condition of the rig to be abandoned.

Emergency procedure describes how an emergency shutdown have to be done, (conducted by the uninitiated),

what happens when emergency shutdown, is activated. (electricity / gas supply) and which events will activate the emergency shutdown (fire, leakage).

Kap 9 Quantifying of RISK

Quantifying of the residue hazards, Risk matrix

To illustrate the overall risk, compared to the risk assessment, each activity is plotted with values for the probability and consequence into the matrix. Use task IDnr.

Example: If activity IDnr. 1 has been given a probability 3 and D for consequence the risk value become D3, red. This is done for all activities giving them risk values.

In the matrix are different degrees of risk highlighted in red, yellow or green. When an activity ends up on a red risk (= unacceptable risk), risk reducing action has to be taken

CONSEQUENCES	Svært alvorlig	E1	E2	E3	E4	E5
	Alvorlig	D1	D2	D3	D4	D5
	Moderat	C1	C2	C3	C4	C5
	Liten	B1	B2	B3	B4	B5
	Svært liten	A1	A2	A3	A4	A5
		Svært liten	Liten	Middels	Stor	Svært Stor
		PROBABILITY				

The principle of the acceptance criterion. Explanation of the colors used in the matrix

Farge	Beskrivelse
Rød	Unacceptable risk Action has to be taken to reduce risk
Gul	Assessment area. Actions has to be considered
Grønn	Acceptable risk. Action can be taken based on other criteria

Attachment to Risk Assessment report

[Conductivity rig: thermal conductivity measurements of porous media in a packed bed]

Project name	Conductivity rig: conductivity measurements in porous media
Project leader	Erling Næss/Christian Schlemminger
Organization	NTNU
HSE-koordinator	Erik Langørgen
Head of Department	Olav Bolland
Rig name	Conductivity rig
Plassering	VATlab
Room number	FinLab
Rig responsible	Jan Georg Henriksen/Christian Schlemminger

TABLE OF CONTENTS

- ATTACHMENT A HAZOP MAL 1
- ATTACHMENT B – PRESSURE TESTING CERTIFICATE 1
- ATTACHMENT C - GLASS BEADS SPECIFICATIONS..... 2
- ATTACHMENT D - MOF-SPECIFICATIONS..... 3
- ATTACHMENT F HAZOP MAL PROSEDURE 1
- ATTACHMENT G PROCEDURE FOR RUNNING EXPERIMENTS 1
- ATTACHMENT H TRAINING OF OPERATORS 3
- ATTACHMENT I FORM FOR SAFE JOB ANALYSIS 4
- ATTACHMENT J APPARATURKORT UNITCARD 1
- ATTACHMENT K FORSØK PÅGÅR KORT..... 1

• ATTACHMENT A HAZOP MAL

Project: Node: 1 Sections filled with pressurized N2 or He, vacuum, and liquid bath containing hot/cold oil.							Page
Ref	Guideword	Causes	Consequences	Safeguards	Recommendations	Action	Date/Sign
1	No flow	valves closed /Pipes blocked etc. Gas bottle is empty.	Can't conduct experiment/wrong measurement values No safety hazards	Always conduct experiment according to procedure		Check all valves. If not ok; dismantle & check for blockage	
2	Reverse flow	n.a.					
3	More flow	High pressure <5bar	Torn pipes (most likely not)	Always check pressure before starting experiment. Keep sample circuit valve closed. Close Needle Valve (1.03)	Check if instruments states zero before exp. Open venting valve.	Close (if not already) sample circuit valve). Adjust pressure regulator and vent out pressure	
4	Less flow	Blockage in pipes or leakage.	Pressure chamber not flushed → Air and moist may still be inside. No safety hazards.	Clean pipes regularly. Make sure everything is tight and sealed.	Set pressure to the system and spray sealing's with soap water	Check for leaks. If not ok → Dismantle and check for blockage.	
5	More level	Amount of filled powder is too much	Powder floats out of sample holder → could be evacuated/ plug the pipes.	Make sure to fill the proper height. Have filter inside piping system.		Dismantle setup and refill powder	
6	Less level	Amount of filled powder is too less	Wrong measurements	Make sure to measure probing depth.	Put in the correct probing depth in	Dismantle setup and refill powder	

Project: Node: 1 Sections filled with pressurized N2 or He, vacuum, and liquid bath containing hot/cold oil.							Page
Ref	Guideword	Causes	Consequences	Safeguards	Recommendations	Action	Date/Sign
					Analyser software.		
7	No vacuum when evacuating.	Vacuum pump valve not open/Sample circuit valve not closed/leakage.	Wrong measurement values (moist still inside powder) No safety hazards	Conducti experiment according to procedure. Always close the sample circuit valve during evacuation.	Always check pressure before and after valves are turned on	Check valves. Check for leaks with soap water. If not ok→dismantle and clean setup and start over.	
8	Some vacuum (but not enough	leakage	Wrong measurement values (moist still inside powder) No safety hazards	Screw the pressure cell lid on firm (but not too firm). Use vacuum grease.	Always check pressure before and after valves are turned on	Stop the leakage. Clean setup and screw sealing's tighter together.	
9	More temperature	Oil in liquid bath increases in volume→high-level warning.	Measurement stops. Slippery floor. Evaporated oil.	Make sure no warning comes during evacuation. If also no oil is evaporated it is a good sign. Cover bath.	Test @ 150 degrees: if high level warning not sho within an hour it is ok.	Raise the pressure cell.	
10	Less temperature	Oil in liquid bath decreases in volume→/low-level warning.	Measurement stops	Have enough oil in the bath/lower the pressure cell far enough.	Test @ 150 degrees: if high level warning not sho within an hour it is ok.	Lower pressure cell.	
11	More viscosity	n.a.					
12	Less viscosity	n.a.					
13	Composition	Spilling water into	Boiling water, oil	Cover bath. Keep bath at		Put lid on.	

Project:							Page
Node: 1 Sections filled with pressurized N2 or He, vacuum, and liquid bath containing hot/cold oil.							
Ref	Guideword	Causes	Consequences	Safeguards	Recommendations	Action	Date/Sign
	Change	the oil.	bursts out.	room temperature between experiments.			
14	Contamination	n.a.					
15	Relief	n.a.					
16	Instrumentation	Damage or failure zeroing	See 1;3;4;5;6;7;8;9;10	See 1;3;4;5;6;7;8;9;10	See 1;3;4;5;6;7;8;9;10	See 1;3;4;5;6;7;8;9;10	
17	Sampling	See 5 and 6	See 5 and 6	See 5 and 6	See 5 and 6	See 5 and 6	
18	Corrosion/erosion	n.a.					
19	Service failure	n.a.					
20	Abnormal Operation	See 1;3;4;5;6;7;8	Can't use values	Always conduct according to same procedure – no shortcuts	Take your time	Turn off and recalibrate instruments. Go through checklist	
21	Maintenance	Rig not run properly	maintenance	Always follow same procedure		Change whatever needs to be changed	
22	Ignition	Non-flammable oil/gas.	-	-	-	-	
23	Spare equipment	Not used				Store in C165	
24	Safety						

- **ATTACHMENT B – PRESSURE TESTING CERTIFICATE**

Pressure testing certificate: mail from vacuum cell supplier.

From: Daniel Cederkrantz [<mailto:daniel.cederkrantz@hotdisk.se>]

Sent: 15. februar 2013 11:04

To: Erling Næss

Cc: Henrik Otterberg

Subject: Re: NTNUs HotDisk system

Hi Erling,

Thank you for this information. Regarding point 1: The bottom will most likely be welded on the new design. Regarding point 2: The plan is to have two glide connection with a the space in-between them filled with vacuum grease to keep them lubricated and vacuum tight. I will investigate the possibility to use a electrical heater, but this would increase the complexity of the device. I'll see what the workshop thinks about this.

The requested dome for reducing the icing of the cryo probe is now integrated in the design, with a flange diameter in the range of 120-150 mm, matching the ISO flange. The N2 and vacuum connections will be extended and standard 3/8" tubs will be used for easy Swagelok integration.

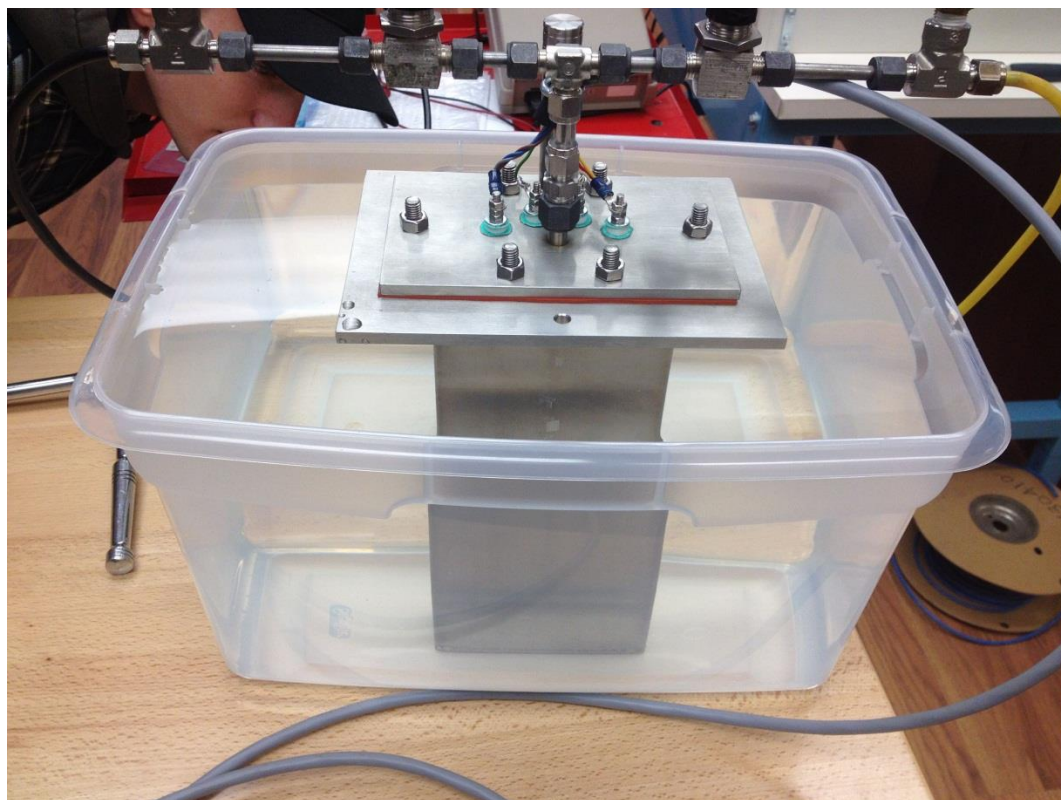
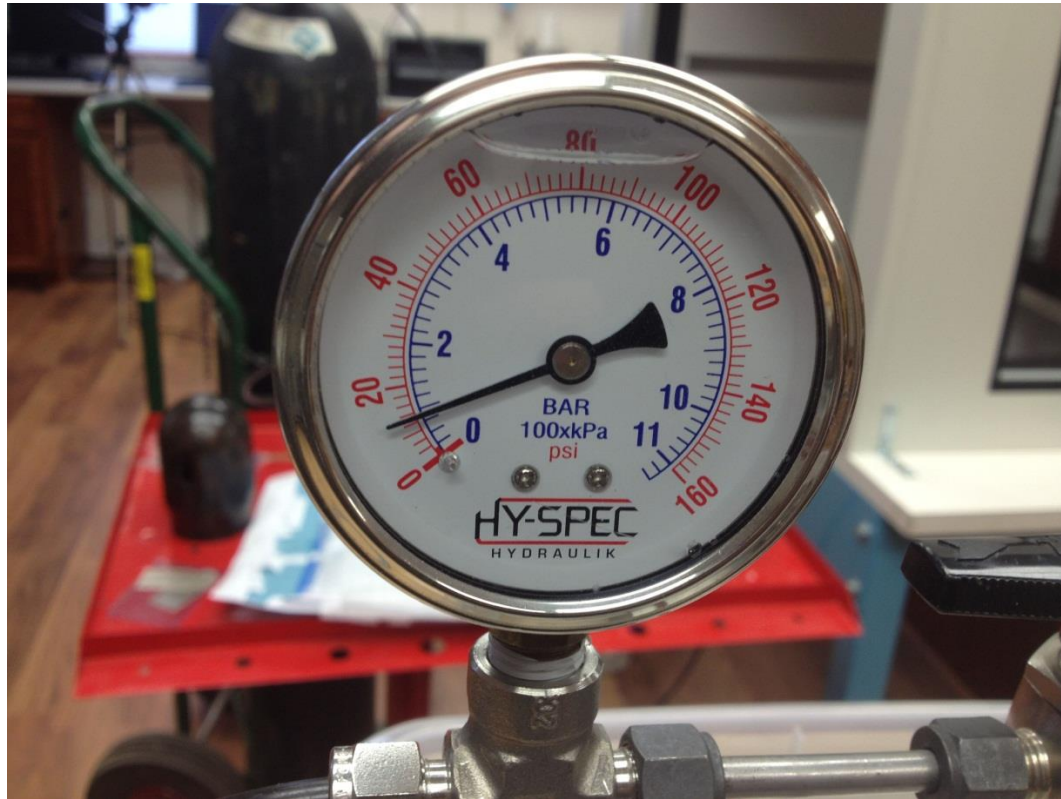
I have also confirmed the inner diameter of the powder sample holder to 60 mm and the inner tube for cables and suspension of the copper cell will likely be made of stainless steel and have an outer diameter of 20 mm and a wall thickness of 1,5 mm.

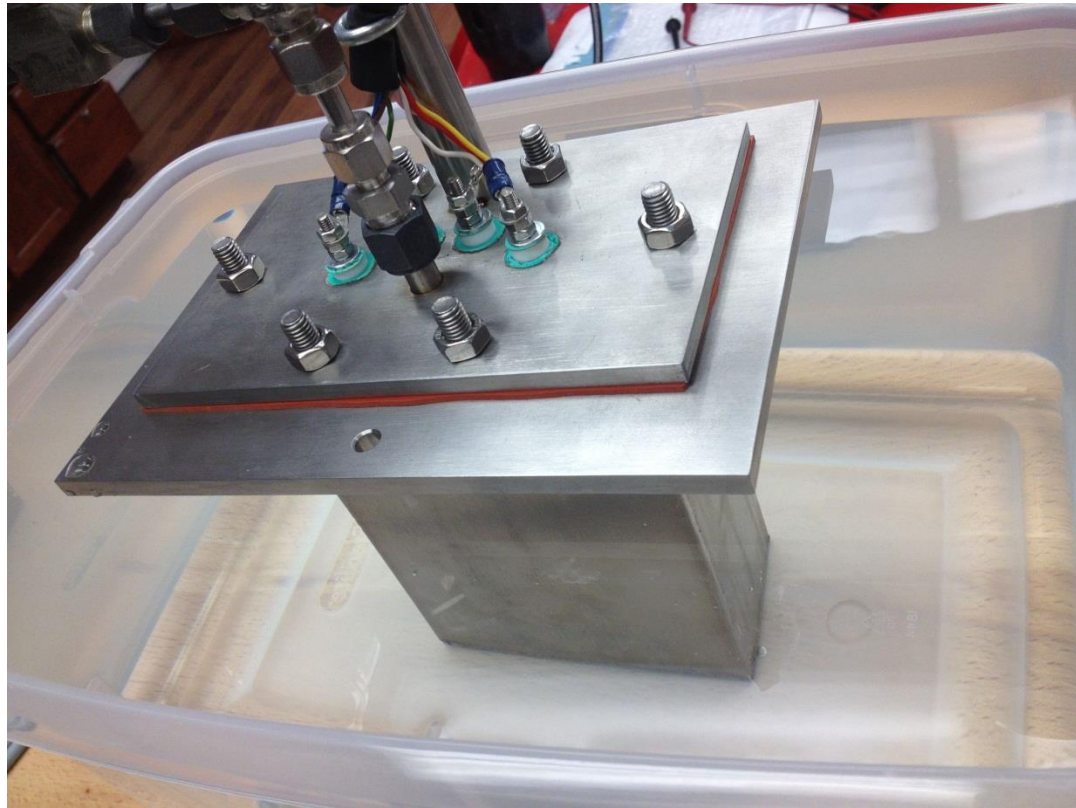
I've also been in further contact with our Canadian supplier of the vacuum cell to use with the oil bath, and I got the attached photos showing their testing of the device. As you can see on the pictures the type of sealing has been changed to silicone gasket, which they claim to be superior to the old gasket.

Regarding maximum pressure they say the following: "It is designed to our local max pressure, which does not require certification of "15 PSI" (1 bar). You may recommend to confirm what the non-certified max pressure is for the clients country."

You mention 5 bar, but I have no recollection or mentioning this, but I certainly remember promising to determine the maximum pressure, which according to the above should be 1 bar above ambient without any special certifications.

Sincerely,
Daniel





TPS Vacuum / Backfilled Insert Cell for Circulating Bath 11502

Maximum temperature: 200°C

Written by: Dale Hume

Last Reviewed: 2013/02/25

TPS Vacuum / Backfilled Insert Cell for Circulating Bath

Instructions for Setup and Use

Summary

TPS Vacuum / Backfilled Insert Cell for Circulating Bath for measuring thermal properties up to 200°C.

Required Materials

- Insert Sample Holder, with integrated PEEK High Temperature Adaptor
- Mica Board Insulation
- Clamping Bar for the TPS sensor
- Clamping Bar Knurled Knobs
- TPS Sensor (*not included*)
- Top / Bottom Sample Plates
- Top / Bottom Sample Plates Knurled Knobs
- Circulating Insert
- Valves and Gauges (*not included*)



Figure 1a. Required Materials

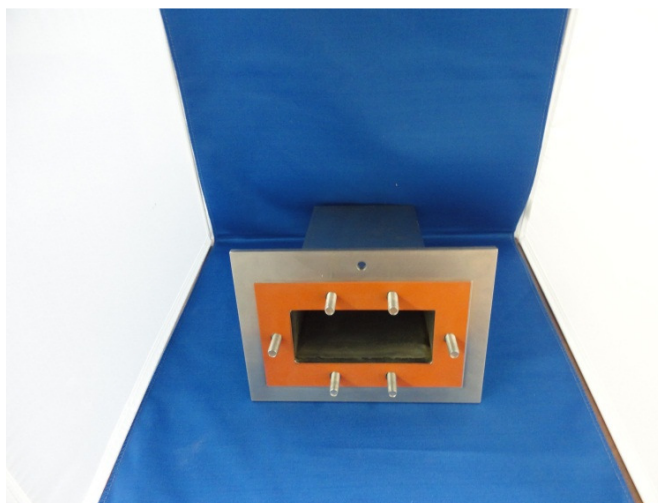


Figure 1b. Required Materials

Insert Procedure

1. The TPS sensor / sample insert comes pre-assembled with the PEEK High Temperature Adaptor (see *Figure 2a*). The electrically insulating Mica Board Insulation is placed on top of the PEEK Adaptor first and then the Clamping Bar is placed on top of the Mica and the PEEK Adaptor (see *Figure 2b*).



Figure 2a. TPS PEEK High Temperature Adaptor positioned on sample / sensor insert

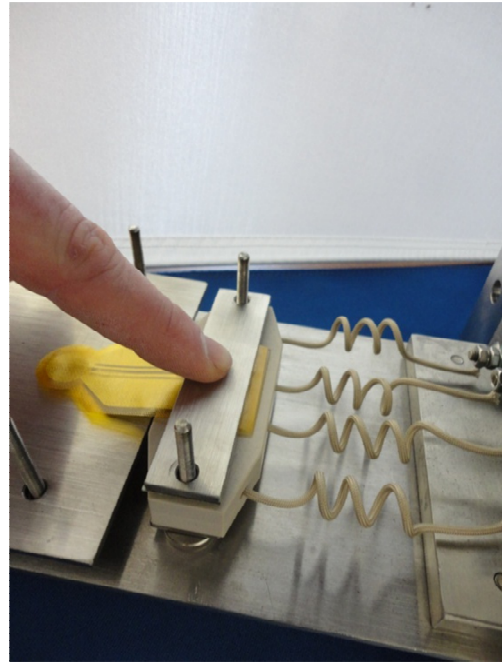


Figure 2b. Positioning of TPS Sensor, Mica Board Insulation and Clamping Bar

2. To position the TPS sensor in the final stage of assembly of the High Temperature TPS Sensor Holder, align the four metal contact pads of the TPS sensor with the metal contact pads (*screws*) of the TPS PEEK High Temperature Adaptor.

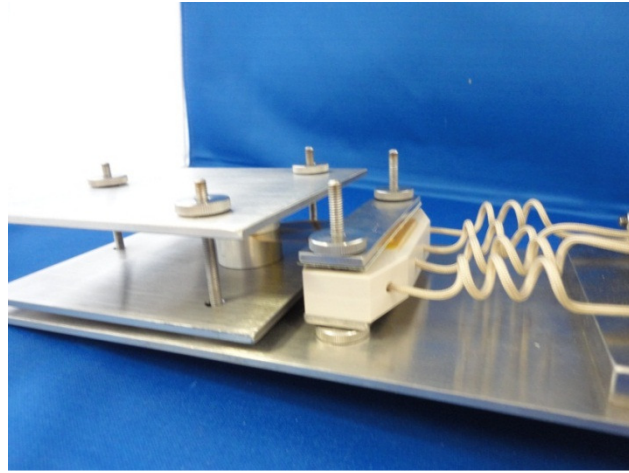
To assist with TPS sensor alignment, a positioning guide has been conveniently machined into the Adaptor surface. The TPS sensor should be positioned within the guide boundaries with the sensor contact pads facing down toward the contact pads of the PEEK adaptor.

To ensure best contact, position the TPS sensor and using your finger press firmly on the middle of the Clamping Bar and tighten each knurled knob included with the Clamping Bar.

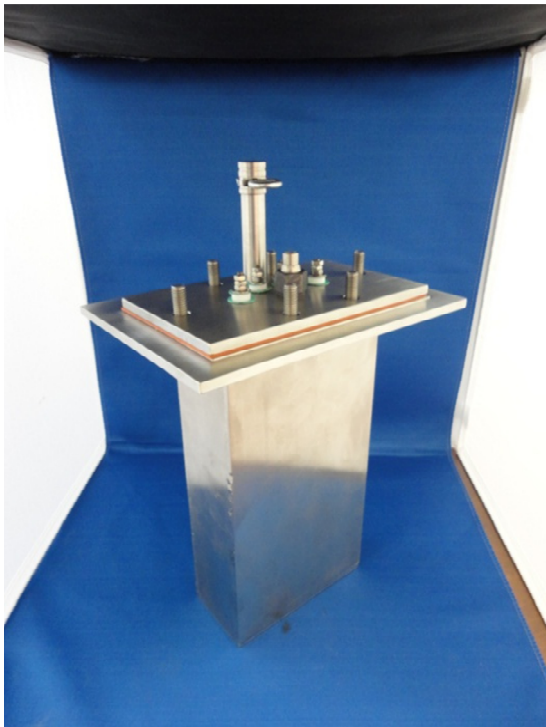


Figure 3. Positioning the TPS Sensor

3. For optimal horizontal alignment of the sensor holder and the upper and lower sample plates, the knurled knobs can be adjusted for the best horizontal testing position of TPS Sensor, based on available sample thickness.



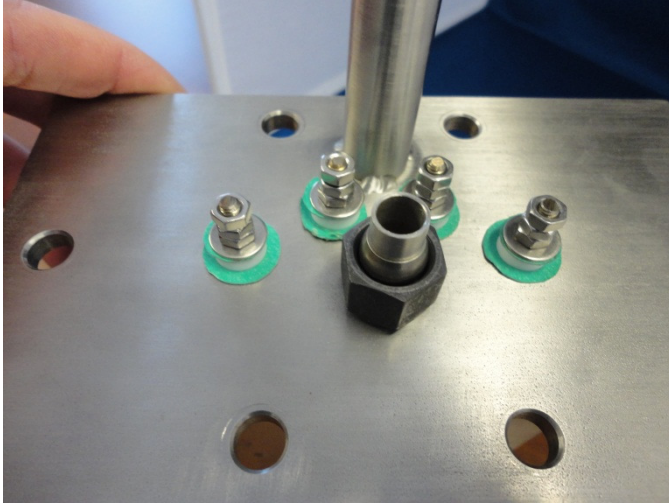
4. Once the sample is set, the testing insert can be positioned inside the circulator insert; the silicone gasket must be in place between the sample insert and circulator insert for sealing. The assembly is then evenly tightened with bolts.



5. Once the assembly is sealed, vacuum and pressure (*maximum pressure of 15 PSI*) can be applied as needed with the use of the included tube nut (*Parker CPI 6BZ, Tube O.D. 3/8*).

6. Your insert will arrive with TPS controller wires already attached; for reference the controller wires are attached as follows (*referencing the figure below*):

- Post (*Far Left*): **Brown/Grey/Blue**
- Post (*Inside Left*): **Green**
- Post (*Inside Right*): **Pink**
- Post (*Far Right*): **White/Red/Yellow**



***Suggestion**

Prior to making measurements on an unknown sample, first measure the Stainless Steel training materials first included with your TPS System to verify that everything is properly connected.

Circulator Procedure

1. The assembled circulator insert is now ready to be attached to the assembly stand.



2. By adjustment of the assembly stand, the insert can now be positioned and lowered into the fluid bath of the circulator. Ensure that there is space left between the insert and the bottom of the fluid bath to isolate any vibrations that could affect thermal property measurements.



***Notes**

- ***It is recommended that a small hole be drilled into the HD Liquid Sample Holder block to allow for the TPS HD Thermocouple Sensor to be used. If this is undertaken, care should be taken to ensure that the hole is drilled into the block away from the sample fill area of the Holder.***

- **ATTACHMENT C - GLASS BEADS SPECIFICATIONS.**

Cleaning, Care, Aids / Aids / Glass beads



Glass beads

Reflex beads made of soda-lime glass. Specific weight approx. 2.5 g/cm³.

Technical Specifications:

Apparent density depending on size 1.46-1.51 kg/l. Refraction index 1.5188. Chemical composition: SiO₂ 72.5 %; Na₂O 13.0 %; K₂O 0.2 %; CaO 9.6 %; MgO 4.22 %; Al₂O₃ 0.58 % Fe₂O₃ 0.11 %.

Article	Ø (mm)	Pack Qty.	Price
●A553.1	0,25-0,5	1 kg	19.80 €
●A554.1	0,75-1,0	1 kg	19.80 €
●A555.1	1,25-1,65	1 kg	19.80 €
●A556.1	1,7-2,1	1 kg	19.80 €
●A557.1	2,85-3,45	1 kg	19.80 €

Accessories

Glass beads

● PRODUCT AVAILABILITY: IN STOCK ■ ARTICLE SOON AVAILABLE ▲ ARTICLE NOT AVAILABLE

Additional information

- Tables



Add this page to service-bookmarks

- **ATTACHMENT D – MOF SPECIFICATIONS.**

SAFETY DATA SHEET

according to Regulation (EC) No. 1907/2006

Version 5.0 Revision Date 16.11.2012

Print Date 22.05.2013

GENERIC EU MSDS - NO COUNTRY SPECIFIC DATA - NO OEL DATA

1. IDENTIFICATION OF THE SUBSTANCE/MIXTURE AND OF THE COMPANY/UNDERTAKING**1.1 Product identifiers**

Product name : Basolite® F300

Product Number : 690872

Brand : Aldrich

CAS-No. : 1195763-37-1

1.2 Relevant identified uses of the substance or mixture and uses advised against

Identified uses : Laboratory chemicals, Manufacture of substances

1.3 Details of the supplier of the safety data sheetCompany : Sigma-Aldrich Norway AS
Filipstad Brygge 1
N-0252 OSLO

Telephone : +47 23 176000

Fax : +47 23 176010

E-mail address : eurtechserv@sial.com

1.4 Emergency telephone number

Emergency Phone # : Giftinformasjonssentralen 22 59 13 00

2. HAZARDS IDENTIFICATION**2.1 Classification of the substance or mixture****Classification according to Regulation (EC) No 1272/2008 [EU-GHS/CLP]**

Acute toxicity, Oral (Category 4)

Skin irritation (Category 2)

Eye irritation (Category 2)

Specific target organ toxicity - single exposure (Category 2)

Classification according to EU Directives 67/548/EEC or 1999/45/EC

Harmful by inhalation, in contact with skin and if swallowed. Harmful: possible risk of irreversible effects through inhalation, in contact with skin and if swallowed. Irritating to eyes and skin.

2.2 Label elements**Labelling according Regulation (EC) No 1272/2008 [CLP]**

Pictogram



Signal word

Warning

Hazard statement(s)

H302

Harmful if swallowed.

H315

Causes skin irritation.

H319

Causes serious eye irritation.

H371

May cause damage to organs.

Precautionary statement(s)

P260

Do not breathe dust/ fume/ gas/ mist/ vapours/ spray.

P305 + P351 + P338

IF IN EYES: Rinse cautiously with water for several minutes. Remove contact lenses, if present and easy to do. Continue rinsing.

Supplemental Hazard Statements none

According to European Directive 67/548/EEC as amended.

Hazard symbol(s)



R-phrase(s)

R20/21/22

R36/38

R68/20/21/22

Harmful by inhalation, in contact with skin and if swallowed.

Irritating to eyes and skin.

Harmful: possible risk of irreversible effects through inhalation, in contact with skin and if swallowed.

S-phrase(s)

S26

In case of contact with eyes, rinse immediately with plenty of water and seek medical advice.

S36/37

Wear suitable protective clothing and gloves.

Caution - this mixture contains a substance not yet fully tested.

2.3 Other hazards - none

3. COMPOSITION/INFORMATION ON INGREDIENTS

3.2 Mixtures

Synonyms : Iron 1,3,5-benzenetricarboxylate
Fe-BTC

Formula : $C_9H_3FeO_6$

Molecular Weight : 262,96 g/mol

Component	Classification	Concentration
Iron-1,3,5-benzenetricarboxylate		
	Acute Tox. 4; Skin Irrit. 2; Eye Irrit. 2; H302, H315, H319 Xn, R22 - R36/38	-
Methanol		
CAS-No. 67-56-1	Flam. Liq. 2; Acute Tox. 3; STOT SE 1; H225, H301 + H311 + H331, H370 F, T, R11 - R23/24/25 - R39/23/24/25	3 - 10 %
EC-No. 200-659-6		
Index-No. 603-001-00-X		
Registration number 01-2119433307-44-XXXX		
Diiron trioxide		
CAS-No. 1309-37-1	Skin Irrit. 2; Eye Irrit. 2; STOT SE 3; H315, H319, H335 Xi, R36/37/38	< 10 %
EC-No. 215-168-2		

For the full text of the H-Statements and R-Phrases mentioned in this Section, see Section 16

4. FIRST AID MEASURES

4.1 Description of first aid measures

General advice

Consult a physician. Show this safety data sheet to the doctor in attendance.

If inhaled

If breathed in, move person into fresh air. If not breathing, give artificial respiration. Consult a physician.

In case of skin contact

Wash off with soap and plenty of water. Take victim immediately to hospital. Consult a physician.

In case of eye contact

Rinse thoroughly with plenty of water for at least 15 minutes and consult a physician.

If swallowed

Never give anything by mouth to an unconscious person. Rinse mouth with water. Consult a physician.

4.2 Most important symptoms and effects, both acute and delayed

To the best of our knowledge, the chemical, physical, and toxicological properties have not been thoroughly investigated.

4.3 Indication of any immediate medical attention and special treatment needed

no data available

5. FIREFIGHTING MEASURES**5.1 Extinguishing media****Suitable extinguishing media**

Use water spray, alcohol-resistant foam, dry chemical or carbon dioxide.

5.2 Special hazards arising from the substance or mixture

Carbon oxides, Iron oxides

5.3 Advice for firefighters

Wear self contained breathing apparatus for fire fighting if necessary.

5.4 Further information

no data available

6. ACCIDENTAL RELEASE MEASURES**6.1 Personal precautions, protective equipment and emergency procedures**

Use personal protective equipment. Avoid dust formation. Avoid breathing vapors, mist or gas. Ensure adequate ventilation. Evacuate personnel to safe areas. Avoid breathing dust.

6.2 Environmental precautions

Prevent further leakage or spillage if safe to do so. Do not let product enter drains.

6.3 Methods and materials for containment and cleaning up

Pick up and arrange disposal without creating dust. Sweep up and shovel. Keep in suitable, closed containers for disposal.

6.4 Reference to other sections

For disposal see section 13.

7. HANDLING AND STORAGE**7.1 Precautions for safe handling**

Avoid contact with skin and eyes. Avoid formation of dust and aerosols. Provide appropriate exhaust ventilation at places where dust is formed.

7.2 Conditions for safe storage, including any incompatibilities

Store in cool place. Keep container tightly closed in a dry and well-ventilated place.

7.3 Specific end uses

no data available

8. EXPOSURE CONTROLS/PERSONAL PROTECTION**8.1 Control parameters****Components with workplace control parameters****8.2 Exposure controls****Appropriate engineering controls**

Handle in accordance with good industrial hygiene and safety practice. Wash hands before breaks and at the end of workday.

Personal protective equipment

Eye/face protection

Face shield and safety glasses Use equipment for eye protection tested and approved under appropriate government standards such as NIOSH (US) or EN 166(EU).

Skin protection

Handle with gloves. Gloves must be inspected prior to use. Use proper glove removal technique (without touching glove's outer surface) to avoid skin contact with this product. Dispose of contaminated gloves after use in accordance with applicable laws and good laboratory practices. Wash and dry hands.

The selected protective gloves have to satisfy the specifications of EU Directive 89/686/EEC and the standard EN 374 derived from it.

Body Protection

Complete suit protecting against chemicals, The type of protective equipment must be selected according to the concentration and amount of the dangerous substance at the specific workplace.

Respiratory protection

Where risk assessment shows air-purifying respirators are appropriate use a full-face particle respirator type N99 (US) or type P2 (EN 143) respirator cartridges as a backup to engineering controls. If the respirator is the sole means of protection, use a full-face supplied air respirator. Use respirators and components tested and approved under appropriate government standards such as NIOSH (US) or CEN (EU).

9. PHYSICAL AND CHEMICAL PROPERTIES

9.1 Information on basic physical and chemical properties

a) Appearance	Form: solid Colour: brown
b) Odour	odourless
c) Odour Threshold	no data available
d) pH	no data available
e) Melting point/freezing point	no data available
f) Initial boiling point and boiling range	no data available
g) Flash point	no data available
h) Evaporation rate	no data available
i) Flammability (solid, gas)	no data available
j) Upper/lower flammability or explosive limits	no data available
k) Vapour pressure	no data available
l) Vapour density	no data available
m) Relative density	no data available
n) Water solubility	no data available
o) Partition coefficient: n-octanol/water	no data available
p) Autoignition temperature	no data available
q) Decomposition temperature	no data available
r) Viscosity	no data available

- s) Explosive properties no data available
- t) Oxidizing properties no data available

9.2 Other safety information

Bulk density 160 - 350 kg/m³

10. STABILITY AND REACTIVITY

10.1 Reactivity

no data available

10.2 Chemical stability

no data available

10.3 Possibility of hazardous reactions

no data available

10.4 Conditions to avoid

no data available

10.5 Incompatible materials

Strong oxidizing agents

10.6 Hazardous decomposition products

Other decomposition products - no data available

11. TOXICOLOGICAL INFORMATION

11.1 Information on toxicological effects

Acute toxicity

no data available

Skin corrosion/irritation

no data available

Serious eye damage/eye irritation

no data available

Respiratory or skin sensitization

no data available

Germ cell mutagenicity

no data available

Carcinogenicity

IARC: 3 - Group 3: Not classifiable as to its carcinogenicity to humans (Diiron trioxide)

Reproductive toxicity

no data available

Specific target organ toxicity - single exposure

no data available

Specific target organ toxicity - repeated exposure

no data available

Aspiration hazard

no data available

Potential health effects

Inhalation

Toxic if inhaled. Causes respiratory tract irritation.

Ingestion

Toxic if swallowed.

Skin

Toxic if absorbed through skin. Causes skin irritation.

Eyes

Causes serious eye irritation.

Signs and Symptoms of Exposure

To the best of our knowledge, the chemical, physical, and toxicological properties have not been thoroughly investigated.

Additional Information

RTECS: Not available

12. ECOLOGICAL INFORMATION

12.1 Toxicity

no data available

12.2 Persistence and degradability

no data available

12.3 Bioaccumulative potential

no data available

12.4 Mobility in soil

no data available

12.5 Results of PBT and vPvB assessment

no data available

12.6 Other adverse effects

no data available

13. DISPOSAL CONSIDERATIONS

13.1 Waste treatment methods

Product

Offer surplus and non-recyclable solutions to a licensed disposal company. Dissolve or mix the material with a combustible solvent and burn in a chemical incinerator equipped with an afterburner and scrubber.

Contaminated packaging

Dispose of as unused product.

14. TRANSPORT INFORMATION

14.1 UN number

ADR/RID: -

IMDG: -

IATA: -

14.2 UN proper shipping name

ADR/RID: Not dangerous goods

IMDG: Not dangerous goods

IATA: Not dangerous goods

14.3 Transport hazard class(es)

ADR/RID: -

IMDG: -

IATA: -

14.4 Packaging group

ADR/RID: -

IMDG: -

IATA: -

14.5 Environmental hazards

ADR/RID: no

IMDG Marine pollutant: no

IATA: no

14.6 Special precautions for user

no data available

15. REGULATORY INFORMATION

This safety datasheet complies with the requirements of Regulation (EC) No. 1907/2006.

15.1 Safety, health and environmental regulations/legislation specific for the substance or mixture

no data available

15.2 Chemical Safety Assessment

no data available

16. OTHER INFORMATION**Text of H-code(s) and R-phrase(s) mentioned in Section 3**

Acute Tox.	Acute toxicity
Eye Irrit.	Eye irritation
Flam. Liq.	Flammable liquids
H225	Highly flammable liquid and vapour.
H301 + H311 + H331	Toxic if swallowed, in contact with skin or if inhaled
H302	Harmful if swallowed.
H315	Causes skin irritation.
H319	Causes serious eye irritation.
H335	May cause respiratory irritation.
H370	Causes damage to organs.
Skin Irrit.	Skin irritation
STOT SE	Specific target organ toxicity - single exposure
F	Highly flammable
R11	Highly flammable.
R22	Harmful if swallowed.
R23/24/25	Toxic by inhalation, in contact with skin and if swallowed.
R36/37/38	Irritating to eyes, respiratory system and skin.
T	Toxic
Xi	Irritant
R36/38	Irritating to eyes and skin.
R39/23/24/25	Toxic: danger of very serious irreversible effects through inhalation, in contact with skin and if swallowed.
Xn	Harmful

Further information

Copyright 2012 Sigma-Aldrich Co. LLC. License granted to make unlimited paper copies for internal use only.

The above information is believed to be correct but does not purport to be all inclusive and shall be used only as a guide. The information in this document is based on the present state of our knowledge and is applicable to the product with regard to appropriate safety precautions. It does not represent any guarantee of the properties of the product. Sigma-Aldrich Corporation and its Affiliates shall not be held liable for any damage resulting from handling or from contact with the above product. See www.sigma-aldrich.com and/or the reverse side of invoice or packing slip for additional terms and conditions of sale.

• ATTACHMENT F HAZOP MAL PROSEDURE

Project: Node: 1							Page
Ref#	Guideword	Causes	Consequences	Safeguards	Recommendations	Action	Date/Sign
	Not clear procedure	Procedure is to ambitious, or confusingly	Fail in measurement point	Simple procedure Note: already applied			
	Step in the wrong place	The procedure can lead to actions done in the wrong pattern or sequence	Pressurized N2 or He <5 bar can leak out.	no parts can be connected in wrong direction and fail positions Note: already applied			
	Wrong actions	Procedure improperly specified	Fail in measurement point; Pressurized N2 or He <5 bar can leak out.	Marks at setup sign clearly the actions, linked to the procedure steps, Note: already applied			
	Incorrect information	Information provided in advance of the specified action is wrong	Fail in measurement point; Pressurized N2 or He <5 bar can leak out.	Procedure is written clearly and prevents misunderstanding. Contact to project leaders is accessible. Note: already			

Project: Node: 1							Page
Ref#	Guideword	Causes	Consequences	Safeguards	Recommendations	Action	Date/Sign
				applied			
	Step missing	Missing step, or step requires too much of operator	Fail in measurement point; Pressurized N2 or He <5 bar can leak out.	Proven procedure is applied and Operator training in necessary Note: already applied			
	Step unsuccessful	Step has a high probability of failure	Fail in measurement point; Pressurized N2 or He <5 bar can leak out.	Operator training Note: already applied			
	Influence and effects from other	Procedure's performance can be affected by other sources	Fail in measurement point;	Notification of measurements to responsible person Note: clear mention in procedure			

• **ATTACHMENT G PROCEDURE FOR RUNNING EXPERIMENTS**

Experiment, name, number: Conductivity rig: measuring conductivity in porous media	Date/ Sign
Project Leader: Erling Næss/Christian Schlemminger	
Experiment Leader: Jan Georg Henriksen/Christian Schlemminger	
Operator, Duties: Jan Georg Henriksen/Christian Schlemminger	

	Conditions for the experiment:	Completed
1	Experiments should be run in normal working hours, 08:00-16:00 during winter time and 08.00-15.00 during summer time. Experiments outside normal working hours shall be approved.	
2	The operator must start the experiment. After start operator may leave and experiment will run itself.	
3	An early warning is given according to the lab rules, and accepted by authorized personnel.	
4	Be sure that everyone taking part of the experiment is wearing the necessary protecting equipment and is aware of the shut down procedure and escape routes.	
		Carried out
	Filling of new powder	
5	If rig is running, set liquid bath to 22 degrees and close shut-off and needle valve. Open the sample circuit valve and vent the system to ambient pressure.	
6	When liquid bath has been at 22 degrees for 10 minutes, shut of the bath.	
7	Remove wires from pressure cell.	
8	Then remove the pressure cell from the bath.	
9	Remove the pressure cell lid and disconnect the inner wires.	
10	Remove rubber sealing and take out the sample/sample holder.	
11	Use glasses eye protection, gloves and dusk mask	
12	Weigh the sample holder and measure sample height.	
13	Empty sample holder and remove sensor.	
14	Clean vacuum pressure cell, sensor, rubber sealing, and sample holder.	
15	Weigh the sample holder without any powder in it. One can now tell how much mass the powder has lost during evacuation.	
16	Pour in a new powder sample using a funnel.	
17	Weigh new powder and measure filling height.	
18	If the powder consists of small light grains, tape aluminum foil over the sample in order to prevent powder loss during evacuation.	
19	Put sample holder back into the pressure cell.	
20	Lubricate the sample holder and its lid with vacuum grease.	
21	Connect wires and close the lid. Connect to computer.	

22	Mount the pressure cell into the liquid bath.	
23	Cover the gap between pressure cell and bath to prevent oil vaporization.	
24	Then start new experiment (described below)	

	Experimental procedure	
25	Restart liquid bath and computer.	
26	Use glasses and gloves.	
27	All valves are closed.	
28	Set liquid bath (1.09) to 150 degrees and start vacuum pump (1.10).	
29	Open the shut-off valve.	
30	Adjust pressure with the pressure regulator (1.02). Pressure must be <0.5bar.	
31	Open needle valve (1.03).	
32	Open venting valve (1.04) and regulate (1.02) to desired pressure (0.4 or 0.2 bar). Then close the venting valve (1.04).	
33	Open sample circuit valve (1.05). Gas now flows into the pressure cell (1.08).	
34	Wait 10 seconds and close sample circuit valve (1.05)	
35	Open valve on the vacuum pump (1.10).	
36	When vacuum is below 10^{-2} torr (0.13 bar), close vacuum pump valve (1.10).	
37	Repeat point 37-40 six times.	
38	Open sample circuit valve (1.05) and turn off vacuum pump (1.10).	
39	Close the needle valve (1.03) and wait 1 hour before starting the experiment.	
	End of experiment	
40	Close all valves starting with the shut-off valve (1.00)	
41	Open venting valve (1.04) and sample circuit valve (1.05) and vent the system to ambient pressure.	
42	Turn of liquid bath (1.09)	
43	Empty sample holder (if not used afterwards) and cover liquid bath.	
	Also:	
44	Remove all obstructions/barriers/signs around the experiment.	
45	Tide up and return all tools and equipment.	
46	Tidy and clean work areas.	
47	Return equipment and systems back to their normal operation settings	
48	To reflect on before the next experiment and experience useful for others	
49	Was the experiment completed as planned and on scheduled in professional terms?	
50	Was the competence which was needed for security and completion of the experiment available to you?	
51	Do you have any information/ knowledge from the experiment that you should document and share with fellow colleagues?	

• ATTACHMENT H TRAINING OF OPERATORS

Experiment, name, number: Thermal conductivity measurements in porous media	
Project Leader: Christian Schlemminger / Erling Næss	22-05-2013 <i>Ch. Sc.</i> Date/Sign
Operator Jan Georg Henriksen	

	Knowledge to EPT LAB in general	
	Lab	
	- Access	
	- Routines and rules	
	- Working hour	
	Knowledge about the evacuation procedures.	
	Activity calendar for the Lab	
	Early warning, iept-experiments@ivt.ntnu.no	
	Knowledge to the experiments	
	MSDS	✓
	Use of personal safety equipment	✓
	Procedures for the experiments	✓
	Emergency shutdown	✓
	Nearest fire and first aid station	✓
	Practical training with project leader	✓

I hereby declare by my signing, that I have reviewed and understood the HSE regulations, have been given appropriate training for running this experiment and am aware of my personal responsibility by working in EPT laboratories.

Operatør

Dato 22/5-2013

Signert *Jan Georg Henriksen*

- ATTACHMENT I FORM FOR SAFE JOB ANALYSIS**

SJA name:	
Date:	Location:
Mark for completed checklist:	

Participators:		
SJA-responsible:		

Specification of work (What and how?):
Risks associated with the work:
Safeguards: (plan for actions, see next page):
Conclusions/comments:

Recommended/approved	Date/Signature:	Recommended/approved	Date/Signature:
SJA-responsible:		HSE responsible:	
Responsible for work:		Other, (position):	

HSE aspect	Yes	No	NA	Comments / actions	Resp.
Documentation, experience, qualifications					
Known operation or work?					
Knowledge of experiences / incidents from similar operations?					
Necessary personnel?					
Communication and coordinating					
Potential conflicts with other operations?					
Handling of an eventually incident (alarm, evacuation)?					
Need for extra assistance / watch?					
Working area					
Unusual working position					
Work in tanks, manhole?					
Work in ditch, shaft or pit?					
Clean and tidy?					
Protective equipment beyond the personal?					
Weather, wind, visibility, lighting, ventilation?					
Usage of scaffolding/lifts/belts/ straps, anti-falling device?					
Work at heights?					
Ionizing radiation?					
Influence of escape routes?					
Chemical hazards					
Usage of hazardous/toxic/corrosive chemicals?					
Usage of flammable or explosive chemicals?					
Risk assessment of usage?					
Biological materials/substances?					
Dust/asbestos/dust from insulation?					
Mechanical hazards					
Stability/strength/tension?					
Crush/clamp/cut/hit?					
Dust/pressure/temperature?					
Handling of waste disposal?					
Need of special tools?					
Electrical hazards					
Current/Voltage/over 1000V?					
Current surge, short circuit?					
Loss of current supply?					
Area					
Need for inspection?					
Marking/system of signs/rope off?					
Environmental consequences?					
Key physical security systems					
Work on or demounting of safety systems?					
Other					

• **ATTACHMENT J APPARATURKORT UNITCARD**

Apparatur/unit

Dette kortet SKAL henges godt synlig på apparaturen! *This card MUST be posted on a visible place on the unit!*

Faglig Ansvarlig (Scientific Responsible) Christian Schlemminger / Erling Næss	Telefon mobil/privat (Phone no. mobile/private) 41063418 / 91897970
Apparaturansvarlig (Unit Responsible) Christian Schlemminger/ Jan Georg Henriksen	Telefon mobil/privat (Phone no. mobile/private) 41063418 / 994 32 522
NTNU – Sintef Beredskapstelefon	800 80 388
Sikkerhetsrisikoer (Safety hazards)	
<ul style="list-style-type: none"> • Pressurized He/N2 • Hot/cold liquid bath 	
Sikkerhetsregler (Safety rules)	
Use eye protection glasses.	
Do not touch liquid bath and/or nearby components.	
Nødstopp prosedyre (Emergency shutdown) <i>Close gas shut-off valve signed as "Emergency shut-off valve"</i>	
<i>Disable power supply to liquid bath</i>	

Her finner du (Here you will find):

Prosedyrer (Procedures)	above computer screen , in FinLab.
Bruksanvisning (User's manual)	in computer desk in the FinLab.

Nærmeste (nearest)

Brannslukningsapparat (fire extinguisher)	beside elevator
Førstehjelpsskap (first aid cabinet)	beside elevator

NTNU
Institutt for energi og prosessteknikk

SINTEF Energi
Avdeling energiprosesser

Dato

Dato

Signert

Signert

• ATTACHMENT K FORSØK PÅGÅR KORT

Forsøk pågår! Experiment in progress!

Dette kort skal settes opp før forsøk kan påbegynnes This card has to be posted before an experiment can start

Ansvarlig / Responsible Christian Schlemminger / Erling Næss	Telefon work/mobile/home 41063418 / 91897970
Operatører/Operators Jan Georg Henriksen / Christian Schlemminger 994 32 522 / 41063418	Forsøksperiode/Experiment time(start – slutt)
Project leaders signature	Project Thermal conductivity measurements.
NTNU – Sintef Beredskapstelefon	800 80 388
Kort beskrivelse av forsøket / Short description of the experiment There is a new conductivity rig located in the FinLab in the VATLab. It is a swedish HotDisk setup and utilizes a small power (<2W) to heat up a sample of porous material and then measure the temperature transient. From the measured temperature differences the HotDisk Software then calculates the thermal conductivity. Thermal conductivity's for various porous media are then found. These values can be used to verify theoretical models. Relaterte farer / related hazards Hot/cold liquid bath and nearby components → do not touch! Liquid bath may evaporate oil → be aware of slippery floor! Vacuum pump causes noise. Pressurized Helium or Nitrogen can cause noise Pressurized Helium or Nitrogen may cause tubes to crack Don't eat and drink in the area	

NTNU
 Institutt for energi og prosessteknikk

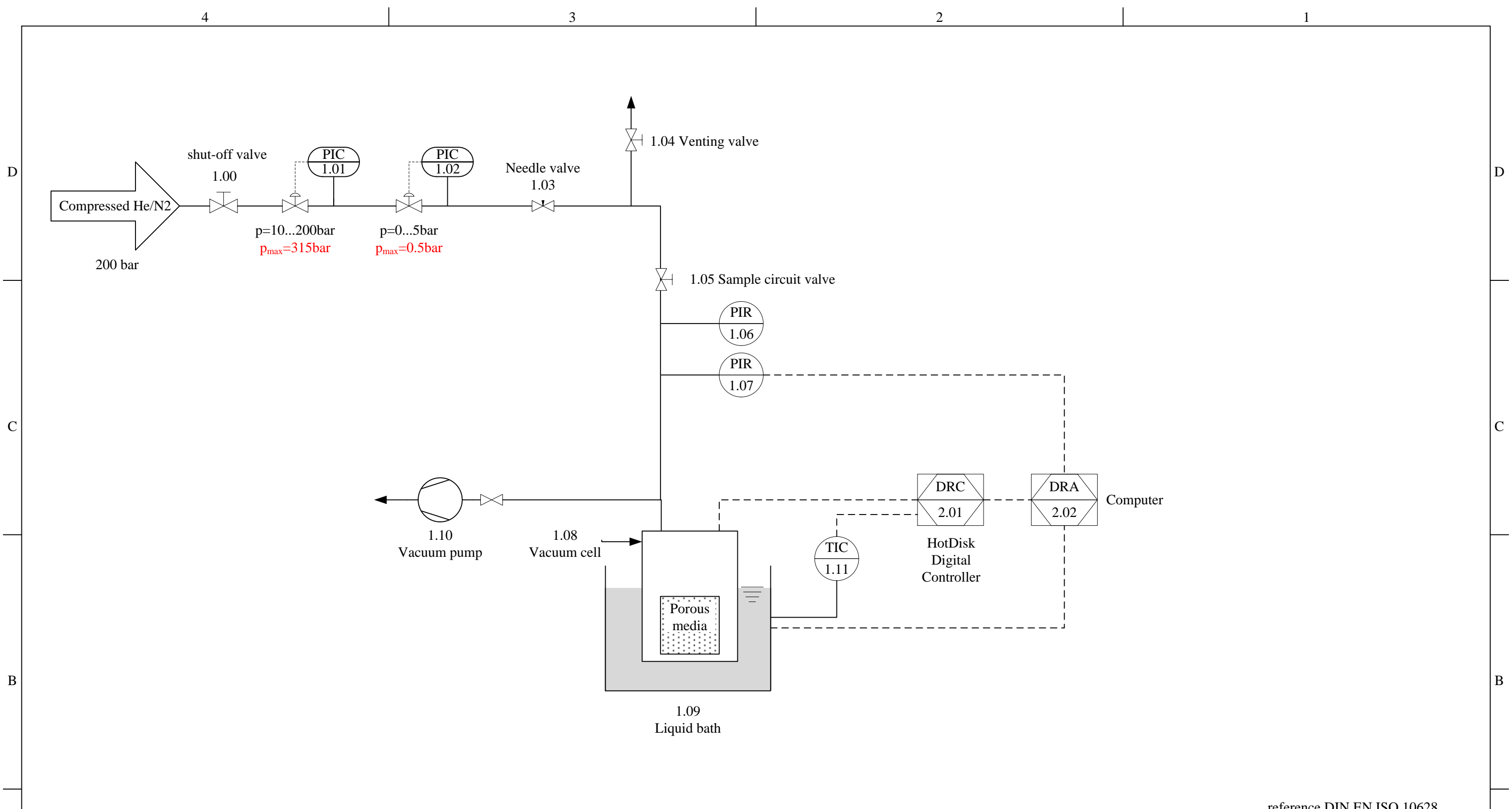
SINTEF Energi
 Avdeling energiprosesser

Dato



Dato

Signert

Signert



reference DIN EN ISO 10628

 NTNU - Trondheim Norwegian University of Science and Technology 	P&ID conductivity rig			
	nr.	title	date	reference person
	1	P&ID conductivity rig	14.05.2013	Jan Georg Henriksen
	DATUM		KOMPLETTER PFAD	
15.05.2013		C:\Users\jangeorg\Dropbox\Master-Georg\HMS\		
DATEINAME 14052013				
PID_CONDUCTIVITY.VSD				
		- confidential document -	Page	1 from 1

FORSØK PÅGÅR

Enhet (unit) og bygg/romnr. (building/room no.):

NTNU-E 302

C165C

1. etg

Laboratorium

Finlab 1

Dette kortet SKAL henges opp før forsøk kan starte!

This card MUST be posted on the unit before the experiment startup!

Apparatur (Unit) Thermal conductivity rig	Dato godkjent (Date Approved) 31. mai 2013		
Prosjektleder (Project Leader) Erling Næss	Telefon mobil/privat (Phone no. mobile/private) 918 97 970		
Apparaturansvarlig (Unit Responsible) Erling Næss	Telefon mobil/privat (Phone no. mobile/private) 918 97 970		
Godkjente operatører (Approved Operators)	Navn/Name	Telefon/Phone	Mobil
	Schlemminger, Christian		410 63 418
	Henriksen, Jan Georg		99432522
Prosjekt (Project) Thermal conductivity measurements in porous media			
Forsøksstid / Experimental time (start - stop) 31.05.2013 - 31.05.2014			
Kort beskrivelse av forsøket og relaterte farer (Short description of the experiment and related hazards) <ul style="list-style-type: none">• Hot/cold liquid bath and nearby componets do not touch!• Liquid bath may evaporate il, be aware of slippery floor!• Vacuum pump causes noise.• Pressurized Helium or Nitrogen can cause noise• Pressurized Helium or Nitrogen may cause tubes to crack• Don't eat and drink in the area			

NTNU

Institutt for energi og prosessteknikk

Dato

4/6 - 2013

Signert

Olav Ballan

APPARATURKORT

Enhet (unit) og bygg/romnr. (building/room no.):

NTNU-E 302

C165C

1. etg

Laboratorium

Finlab 1

Dette kortet SKAL henges godt synlig ved maskinen!
This card MUST be posted on a visible place on the unit!

Apparatur (Unit) Thermal conductivity rig	Dato Godkjent (Date Approved) 31. mai 2013
Prosjektleder (Project Leader) Erling Næss	Telefon mobil/privat (Phone no. mobile/private) 918 97 970
Apparaturansvarlig (Unit Responsible) Erling Næss	Telefon mobil/privat (Phone no. mobile/private) 918 97 970
Sikkerhetsrisikoer (Safety hazards) <ul style="list-style-type: none">• Pressurized He/N₂• Hot/cold liquid bath	
Sikkerhetsregler (Safety rules) <ul style="list-style-type: none">• Use eye protection glasses.• Do not touch liquid bath and/or nearby components	
Nødstop prosedyre (Emergency shutdown) <ul style="list-style-type: none">• Close gas shut-off valve signed as "Emergency shut-off valve"• Disable power supply to liquid bath	
Her finner du (Here you will find):	
Prosedyrer (Procedures)	At the control desk
Bruksanvisning (User manual)	At the control desk
Brannslukningsapparat (Fire extinguisher)	1. etasje TermiskLab (nord)
Førsthjelpsskap (First aid cabinet)	1. etasje TermiskLab (nord)

NTNU

Institutt for energi og prosessteknikk

Dato

4/6 - 2013

Signert

Olav Ball